Unified Tractable Model for Large-Scale Networks Using Stochastic Geometry: Analysis and Design

Dissertation by

Laila Hesham Abd El-Aziz Fouad Afify

In Partial Fulfillment of the Requirements

For the Degree of

Doctor of Philosophy

King Abdullah University of Science and Technology

Thuwal, Kingdom of Saudi Arabia

December, 2016

EXAMINATION COMMITTEE PAGE

The dissertation of Laila Hesham Afify is approved by the examination committee

Committee Chairperson: Professor Tareq Y. Al-Naffouri
External Committee Member: Professor Wei Yu
Committee Members: Professor Mohamed-Slim Alouini, Professor Basem Shihada, Professor Taous-Meriem Laleg-Kirati

DEDICATION

to my precious daughter, Nada, and my parents

ABSTRACT

Unified Tractable Model for Large-Scale Networks Using Stochastic Geometry: Analysis and Design

Laila Hesham Afify

The ever-growing demands for wireless technologies necessitate the evolution of next-generation wireless networks that fulfill the diverse wireless users requirements. However, upscaling existing wireless networks implies upscaling an intrinsic component in the wireless domain; the aggregate network interference. Being the main performance-limiting factor, it becomes crucial to develop a rigorous analytical framework to accurately characterize the out-of-cell interference, to reap the benefits of emerging networks. Due to the different network setups and key performance indicators, it is essential to conduct a comprehensive study that unifies the various network configurations together with the different tangible performance metrics. In that regard, the focus of this thesis is to present a unified mathematical paradigm, based on Stochastic Geometry, for large-scale networks with different antenna/network configurations. By exploiting such a unified study, we propose an efficient automated network design strategy to satisfy the desired network objectives. First, this thesis studies the exact aggregate network interference characterization, by accounting for each of the interferers signals in the large-scale network. Second, we show that the information about the interferers symbols can be approximated via the Gaussian signaling approach. The developed mathematical model presents twofold analysis unification for uplink and downlink cellular networks literature. It aligns the tangible decoding error probability analysis with the abstract outage probability and ergodic rate analysis. Furthermore, it unifies the analysis for different antenna configurations, i.e., various multiple-input-multiple-output (MIMO) systems. Accordingly, we propose a novel reliable network

design strategy that is capable of appropriately adjusting the network parameters to meet desired design criteria. In addition, we discuss the diversity-multiplexing tradeoffs imposed by differently flavored MIMO schemes, describe the relation between the diverse network parameters and configurations, and study the impact of temporal interference correlation on the performance of large-scale networks. Finally, we investigate some interference management techniques by exploiting the proposed framework. The proposed framework is compared to the exact analysis as well as intensive Monte Carlo simulations to demonstrate the model accuracy. The developed work casts a thorough inclusive study that is beneficial to deepen the understanding of the stochastic deployment of the next-generation large-scale wireless networks and predict their performance.

ACKNOWLEDGEMENTS

In the name of Allah, the Most gracious and the Most merciful. All praise is for Allah for His blessings to complete this thesis. Without His guidance, my accomplishments would never have been possible.

First of all, I am most indebted to my thesis advisor Prof. Tareq Y. Al-Naffouri. Without his continuous support, guidance, encouragement, and belief in me, this work would not have been possible. I consider myself to be truly fortunate to work under his excellent academic supervision, and learn from his profound intuition. I would like to extend my gratitude to Dr. Hesham ElSawy who has been a brilliant teacher from whom I learned tremendously throughout this work. His passion for knowledge and dedication to research have provided me with an excellent role model that I hope to emulate in my future career. I am also thankful to Prof. Mohamed-Slim Alouini for his support which contributed in many ways to the success of this study.

I would like to express my gratitude to my thesis committee members, Prof. Wei Yu, Prof. Basem Shihada, and Prof. Taous-Meriem Laleg-Kirati, for their careful reading of this thesis and their invaluable comments. I also wish to thank Prof. Giuseppe Caire, Dr. Fadel Digham, Dr. Abla Kammoun, and Prof. Ahmed Sultan. I also would like to thank my colleagues at KAUST, Emna Zedini, Konpal Ali, Rabe Arshad, Mudassir Masood, and Amal Hyadi. I am really grateful to my dear friends at KAUST, Dalal Nour El Dine, Mai Omar, Eva Barankova, and Sally Mamdouh. This thesis has been kept on track with the support of my lifetime friends in my hardest days, Yarah, Ahmedin, Ahmad ElMoslimany, Toka, Sara, and Zeinab. Special thanks are due to Aicha and Lenylyn for the great help and assistance. I thank Dr. Mohammad Khafagy for his help at the start of my PhD.

Finally, my sincere gratitude goes to my parents, Prof. Soad Bashandy and Eng. Hesham Afify, and my sister Eng. Nada Hesham, whose selfless sacrifices, and efforts with unceasing prayers has enabled me to complete this thesis. I am indebted to my daughter, Nada, for being the brightest light in the darkest nights of this journey.

TABLE OF CONTENTS

Examination Committee Page **2**

Copyright **3**

Dedication **4**

Abstract **5**

Acknowledgements **7**

List of Abbreviations **13**

List of Symbols **15**

List of Figures **19**

List of Tables **20**

1 Introduction and Overview **21**
1.1 Motivation and Contribution of the Thesis 27
1.2 Thesis Outline 29

2 Stochastic Geometry Background **32**
2.1 Introduction 32
2.2 Stochastic Geometry Preliminaries 33
2.2.1 Poisson Point Processes (PPPs) 34
2.2.1.1 Functionals of Poisson Point Processes 36
2.2.2 Interference Modeling via Poisson Point Processes 37
2.3 SINR Model for Cellular Networks in Stochastic Geometry Literature 39

3 Baseline System Model **45**
3.1 Network Model 45
3.1.1 Transmitter and Receiver characteristics 46
3.2 Complex Received signal model 47

3.2.1 Downlink Scenario 47
3.2.2 Uplink Scenario 48

4 Error Performance Analysis in Uplink Cellular Networks via the EiD Approach 50
4.1 Introduction 50
4.2 System Model 51
4.2.1 K-tier Network Model 51
4.2.2 Complex received signal 54
4.2.3 Methodology of Analysis 55
4.3 ASEP in Single-Tier Uplink Cellular network 56
4.3.1 Interference Characterization 56
4.3.2 Gaussian Representation 57
4.3.3 Conditional Performance Analysis 59
4.3.4 Deconditioning 60
4.4 ASEP in Multi-Tier Uplink Cellular network 61
4.4.1 Interference Characterization 62
4.4.2 Gaussian Representation 63
4.4.3 Conditional Performance Analysis 63
4.4.4 Deconditioning 64
4.5 Simulation Results 66
4.5.1 Simulation Setup 67
4.6 Chapter Summary 69
4.6.1 EiD Approach outline 69
4.6.2 Conclusion and Future work 70

5 The Influence of Gaussian Signaling Approximation on the SINR Model 72
5.1 Introduction 72
5.2 Proposed ASEP Analysis 73
5.2.1 ASEP in the Downlink Scenario 75
5.2.2 ASEP in the Uplink Scenario 77
5.3 Numerical Results 79
5.4 Chapter Summary and Conclusions 80

6 Unified Performance Analysis for Downlink MIMO networks 84
6.1 Introduction 84

6.2 Downlink MIMO System Model 85
6.2.1 Downlink MIMO Received Signal Model 85
6.3 Equivalent Downlink SISO-SINR Representation 86
6.4 A Unified Downlink Performance Analysis 90
6.5 Characterizing Downlink MIMO Configurations 95
6.5.1 **Single-Input-Multiple-Output (SIMO) systems** 96
6.5.2 **Orthogonal Space-Time Block Coding (OSTBC)** 96
6.5.3 **Zero-Forcing beamforming with MLR (ZF-Rx)** 97
6.5.4 **Space-Division Multiple Access (SDMA)** 97
6.5.5 **Spatially Multiplexed MIMO (SM-MIMO) systems** . . 98
6.6 Numerical and Simulation Results 99
6.6.1 Proposed model validation 99
6.6.2 Diversity-Multiplexing Tradeoffs & Design Guidelines 100
6.7 Chapter Summary and Conclusions 108

7 Unified Performance Analysis for Uplink MIMO networks 109
7.1 Introduction 109
7.2 Uplink MIMO System Model 109
7.2.1 Uplink MIMO Received Signal Model 111
7.3 Equivalent Uplink SISO-SINR Representation 112
7.4 A Unified Uplink Performance Analysis 113
7.5 Characterizing Uplink MIMO Configurations 116
7.5.1 **Maximum-Ratio-Combining (MRC) receivers** 116
7.5.2 **Orthogonal Space-Time Block Coding (OSTBC)** 117
7.5.3 **Zero-Forcing beamforming with MLR (ZF-Rx)** 117
7.6 Numerical and Simulations Results 117
7.7 Chapter Summary and Conclusions 119

8 Effect of Interference Temporal Correlation 122
8.1 Introduction 122
8.2 Temporal Correlation in the Downlink 123
8.2.1 Downlink Coverage Probability Analysis 126
8.2.2 Numerical and Simulation Results 127
8.3 Temporal Correlation in the Uplink 127
8.3.1 System Model 129
8.3.2 Uplink Coverage Probability Analysis for Retransmissions . . 131
8.4 Non-binding Transmit Power Constraint 138

8.5 Numerical and Simulations Results 141
8.6 Chapter Summary and Conclusions 142

9 Interference Management **143**
9.1 Introduction 143
9.2 System Model 143
9.3 Impact of Interference Management on ASEP performance 144
9.3.1 Random Frequency Reuse 145
9.3.2 Coordinated Frequency Reuse 145
9.4 Simulation Results 147
9.5 Chapter Summary and Conclusions 152

10 Concluding Remarks and Future Directions **153**
10.1 Conclusion 153
10.2 Future Directions 155
10.2.1 Impact of imperfect Channel state information (CSI) 155
10.2.2 Extension to Massive MIMO Setup 156

References **157**
A.1 Proof of Lemma 4.1 172
A.2 Proof of Lemma 4.2 174
A.3 Proof of Theorem 4.1 174
A.4 Proof of Lemma 4.3 175

Appendix B **178**
B.1 Proof of Lemma 5.1 178
B.2 Proof of Lemma 5.2 178

Appendix C **180**
C.1 Proof of Theorem 6.1 180
C.2 Equivalent SISO model for different MIMO configurations 181
C.2.1 Proof of Lemma 6.2 181
C.2.2 Proof of Lemma 6.3 182
C.2.3 Proof of Lemma 6.4 184
C.2.4 Proof of Lemma 6.5 185
C.2.5 Proof of Lemma 6.6 186

Appendix E **190**
E.1 Proof of Lemma 9.1 190
E.2 Proof of Lemma 9.2 191
F.1 Journal Publications 192

ABBREVIATIONS

Symbol	Definition
ABEP	Average Bit Error Probability
APEP	Average Pairwise Error Probability
ASEP	Average Symbol Error Probability
AWGN	Additive White Gaussian Noise
BEP	Bit Error Probability
BS	Base Station
CDF	Cumulative distribution function
CF	Characteristic Function
CFR	Coordinated Frequency Reuse
CLT	Central Limit Theorem
CSI	Channel State Information
DL	Downlink Transmission
EiD	Equivalent-in-Distribution
FPC	Fractional Power Control
i.i.d.	Independent and identically distributed
KPI	Key Performance Indicator
LT	Laplace Transform
MGF	Moment Generating Function
MIMO	Multiple-input-multiple-output
MISO	Multiple-input-single-output
MLR	Maximum-likelihood Receiver
MPSK	M-ary Phase Shift Keying
MRC	Maximum Ratio Combining
MU-MIMO	Multi-User MIMO
OSTBC	Orthogonal Space-Time Block Codes
PC	Power Control

Symbol	Definition

PDF	Probability density function
PEP	Pairwise Error Probability
PGFL	Probability Generating Functional
PPP	Poisson point process
QAM	Quadrature Amplitude Modulation
QoS	Quality-of-Service
RFR	Random Frequency Reuse
RSS	Radio Signal Strength
SDMA	Space-Division Multiple Access
SEP	Symbol Error Probability
SIMO	Single-input-multiple-output
SINR	Signal-to-interference-and-noise ratio
SIR	Signal-to-interference ratio
SISO	Single-input-single-output
SNR	Signal-to-noise ratio
SM-MIMO	Spatially Multiplexed MIMO
SS	Spherically Symmetric
UE	User Equipment
UL	Uplink Transmission
ZF-Rx	Zero-Forcing Receiver

LIST OF SYMBOLS

Symbol	Definition
$1\{.\}$	The indicator function
$f_X(\cdot)$	PDF of the random variable X
$F_X(\cdot)$	CDF of the random variable X
$\mathbb{P}[\cdot]$	The probability of the event $[\cdot]$
$\mathbb{E}_X[\cdot]$	Expectation with respect to the random variable X
λ_B	Intensity of Base Stations
λ_u	Intensity of Users
λ	Effective intensity of interferers
Ψ	Poisson point process
Ψ^o	Poisson point process excluding the origin point o
P_U	Maximum transmit power for users
N_r	Number of receive antennas
N_t	Number of transmit antennas
$\mathcal{K}$	Number of single-antenna users
K	Number of heterogeneous tiers
g	channel impulse response
$\tilde{g}$	channel power gain $\lvert g\rvert^2$
$\tilde{g}^{(j)}$	channel power gain at instant j
$\tilde{g}_o$	Intended channel power gain
$\tilde{g}_i$	Interfering channel power gain
$\mathbf{H}_o$	Intended MIMO channel impulse response matrix
$\mathbf{H}_i$	Interfering MIMO channel impulse response matrix
m_o	Gamma shape parameter of $\tilde{g}_o$
m_i	Gamma shape parameter of $\tilde{g}_i$
Ω_o	Gamma scale parameter of $\tilde{g}_o$
Ω_i	Gamma scale parameter of $\tilde{g}_i$

Symbol	Definition
$\mathscr{M}$	Modulation scheme
M	Constellation size
I_{agg}	Aggregate interference complex signal
$\mathcal{I}$	Interference power
$\mathcal{N}_o$	Noise power
$\mathcal{S}$	Desired signal power
η	Path-loss exponent
Υ	Signal-to-interference-and-noise ratio
$\bar{\Upsilon}$	Signal-to-interference ratio
$\bar{\Upsilon}^{(j)}$	Signal-to-interference ratio at instant j
$\mathcal{L}_X(\cdot)$	The Laplace transform of the PDF of the random variable X
$\mathcal{L}_X^{(1,2)}(\cdot,\cdot)$	Joint LT of PDF of correlated samples of random variable X at instants $1,2$
θ	SIR threshold defined for correct reception
$\mathcal{O}(\theta)$	Outage probability at threshold θ
$\mathcal{P}_{\text{cov}}(\theta)$	Average Coverage Probability at threshold θ
$\mathcal{P}_{c^{(j)}}(\theta)$	Coverage Probability at time slot j at threshold θ
$\mathcal{R}$	Ergodic Capacity
$\Gamma(\cdot)$	The gamma function
$\Gamma(a,b)$	The upper incomplete gamma function defined as $\Gamma(a,b)=\int_x^\infty t^{a-1}e^{-1}db$
$\gamma(a,b)$	The lower incomplete gamma function defined as $\gamma(a,b)=\int_0^b t^{a-1}e^{-t}dt$
$\text{erfc}(\cdot)$	The Complementary Error Function
${}_2F_1(\cdot,\cdot;\cdot;\cdot)$	Gauss hypergeometric function
${}_1F_1(\cdot;\cdot;\cdot)$	Kummer confluent hypergeometric function
p	Independent activity prbability
$\epsilon^{(j)}$	FPC compensation factor of desired signal at instant j
ϵ_i	Interference FPC compensation factor
$\|.\|_F$	Frobenious norm
$\|.\|$	Euclidean norm
$\forall$	for all

LIST OF FIGURES

1.1 Ratio between the number of connected smart devices to the world human population over the past few decades upto 2020. Data source [1,2]. 22
1.2 Anticipated 5G future wireless networks applications. 23
1.3 Hexagonal Deterministic Grid model for base stations. 26
1.4 Possion distributed base stations forming Voronoi tessellations. . . . 27

4.1 Uplink (dotted-red) vs. downlink (solid-blue) association regions for a three-tier cellular network. Squares are macro BSs, triangles are micro BSs, and circles are pico BSs. 52
4.2 The set of simultaneously active UEs per channel resource over 4000 km^2 area. The black squares are the BSs and the red dots are their associated UEs. Each BS serves only one UE per channel, such that a UE is associated with the nearest BS. 53
4.3 Average symbol error probability for 4-QAM and 16-QAM modulated signals versus the Signal-to-Noise ratio (SNR) at the receiving BS. . . 66
4.4 Average symbol error probability for 4-QAM modulated signals versus the Signal-to-Noise ratio (SNR) at the receiving BS for Gaussian distributed aggregate interference and that characterized via the adopted EiD approach. 67

5.1 ASEP versus the received Signal-to-Noise ratio (SNR) for 4-QAM modulated signals in the downlink. 80
5.2 ASEP versus the received Signal-to-Noise ratio (SNR) for 16-QAM modulated signals in the downlink. 81
5.3 ASEP versus the received Signal-to-Noise ratio (SNR) for 4-QAM modulated signals in the uplink. 82
5.4 ASEP versus the received Signal-to-Noise ratio (SNR) fo 16-QAM modulated signals in the uplink. 83

6.1 ASEP performance against $\frac{P}{\mathcal{N}_o}$ for different MIMO setups. 100

6.2 ASEP for 4-QAM modulation, for the different MIMO setups using the same number of antennas $N_t = 2$ and $N_r = 2$, at $p = 1$. 101
6.3 ASEP for 16-QAM modulation, for the different MIMO setups using the same number of antennas $N_t = 2$ and $N_r = 2$, at $p = 1$. 102
6.4 Outage Probability versus SIR threshold θ, for the different MIMO setups using the same number of antennas $N_t = 2$ and $N_r = 2$, at $p = 1$.103
6.5 Unified Outage performance versus the ratio $\frac{m_o}{m_i}$ for an arbitrary MIMO setup, for $\theta = 0, 5, 10$ dB at $\frac{P}{\mathcal{N}_o} = 90$dB. 104
6.6 Unified ASEP performance versus the ratio $\frac{m_o}{m_i}$ for an arbitrary MIMO setup, for 4-QAM and 16-QAM at $\frac{P}{\mathcal{N}_o} = 90$dB. 105
6.7 Unified Outage Probability performance for $\frac{m_o}{m_i} = \frac{1}{2}$ at $\theta = 5$ dB at $\frac{P}{\mathcal{N}_o} = 90$dB. 106
6.8 Flowchart for MIMO selection in cellular networks 107

7.1 ASEP for 4-QAM modulation, for the different MIMO setups using the same number of antennas $N_t = 2$ and $N_r = 2$, at $p = 1$. 118
7.2 ASEP for 16-QAM modulation, for the different MIMO setups using the same number of antennas $N_t = 2$ and $N_r = 2$, at $p = 1$. 119
7.3 Unified Outage performance versus the ratio $\frac{m_o}{m_i}$ for an arbitrary uplink MIMO setup, for $\theta = 0, 5, 10$ dB at $\rho = -70$ dBm. 120
7.4 Unified ASEP performance versus the ratio $\frac{m_o}{m_i}$ for an arbitrary uplink MIMO setup, for 4-QAM and 16-QAM. 121

8.1 The effect of interference correlation for different m_o and m_i. 128
8.2 Incremental diversity for the same inter-cell interference. 129
8.3 Variation of the average received power for the different ϵ values together with the CDF of the serving distance against the serving distance r_o. 130
8.4 Coverage probability for $\epsilon = 1$. 132
8.5 Coverage probability for $\epsilon = 0.5$. 133
8.6 Coverage probability for $\epsilon = 0$. 134
8.7 Coverage probability for hybrid compensation factors. 138
8.8 Analytic coverage probability versus $\epsilon^{(2)}$ employing power-ramping scheme at $\theta = 10$ dB. 139
8.9 Analytic coverage probability versus ϵ employing for $P_U = \infty$ at $\theta = 0, 10$ dB. 140

9.1 The effect of coordinated frequency reuse on the average symbol error probability in the downlink scenario for 4-QAM modulated signals. . 148
9.2 The effect of coordinated frequency reuse on the average symbol error probability in the downlink scenario for 16-QAM modulated signals. . 149
9.3 The effect of coordination and frequency reuse on average symbol error probability in the downlink scenario for 4-QAM modulated signals with $\Delta = 8$. 150
9.4 The effect of coordination and frequency reuse on average symbol error probability in the downlink scenario for 4-QAM modulated signals with $\Delta = 4$. 151

LIST OF TABLES

5.1 Runtime for the EiD and Gaussian Signaling approaches 79

6.1 SISO-equivalent gamma distribution parameters for various MIMO settings. 90

6.2 Overall achievable and actual rates gains per cell, with respect to SISO networks, for the different MIMO setups, in an interference-limited scenario for $M = 4, 16$-QAM modulation scheme. 103

7.1 SISO-equivalent gamma distribution parameters for various uplink MIMO settings. 116

Chapter 1

Introduction and Overview

Over the past few decades, the world has experienced an exponential growth and rapid evolution in the wireless telecommunications industry. With the emerging wireless technologies being an essential part of the everyday life, both academia and industry have witnessed tremendous advances to support practical implementations and satisfy the ever-growing demands. It has already been officially declared that the number of smart connected devices has outgrown the humans population over the world [1, 2] as elaborated in Fig. 1.1. Clearly, the world is about to witness a huge evolution in the information technology a few years from now. Going far beyond the existing wireless networks, which were not designed to support the new evolving experiences that users are expecting, with a thousand-fold increase in numbers of smartphones, tablets and personal smart devices, is thus a must. Future networks are expected to handle and accommodate smart personal devices, high mobility users, machine-to-machine (M2M) connections, home automation, self-driving cars, robots, medical monitoring, etc. Furthermore, there have been hundrends of reserach attempts to address these fundamental paradigm shifts in wireless networks operation recently. For instance, the emergence of new multi-tiered hetereogenous wireless networks (HetNets), that support unplanned deployment of access points, and can also operate over cellular bands, has been suggested [3]. In other words, the deployment of macro base stations (BSs) is to be complemented with different types of low-cost access points known as small cells (femto-, pico- and micro-cells) [3]. Overlaying macro BSs with user-deployed small cells is a promising strategy that will

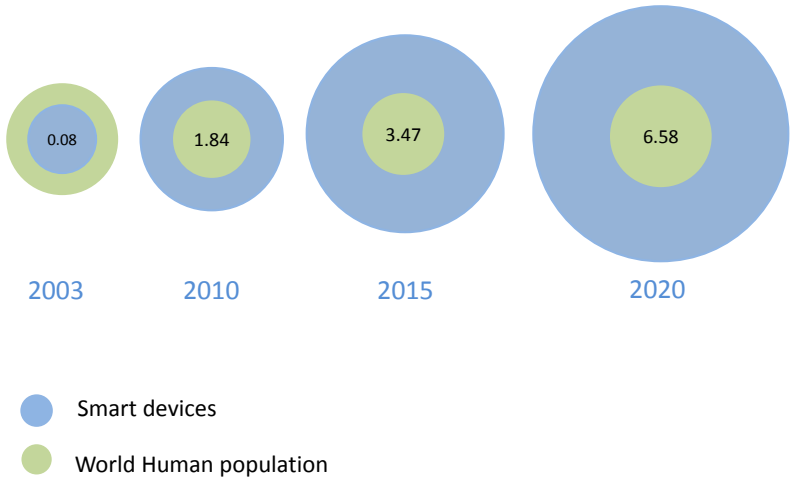

Figure 1.1: Ratio between the number of connected smart devices to the world human population over the past few decades upto 2020. Data source [1, 2].

significantly help to cope with the growing traffic requirements by providing enhanced capacity and improved network coverage, especially in dead zones [3–5]. In addition to HetNets, multiple-input-multiple-output (MIMO) transmission offers diverse options for antenna configurations that can lead to different diversity and multiplexing tradeoffs, which can be exploited to improve several aspects in the wireless networks performance [6–8]. For instance, link capacity gains can be harvested by multiplexing several data streams into the same channel via MIMO spatial multiplexing. Enhanced link reliability can be obtained by transmit and/or receive diversity. The network capacity can be improved by accommodating more user equipment (UEs) per channel via multi-user MIMO techniques. Motivated by its potential gains, MIMO is considered an essential ingredient in the future cellular networks to accommodate the novel features and capacity demands.

The unprecedented number of connected devices with such diverse requirements is expected to dramatically increase the traffic volume whilst imposing very strict

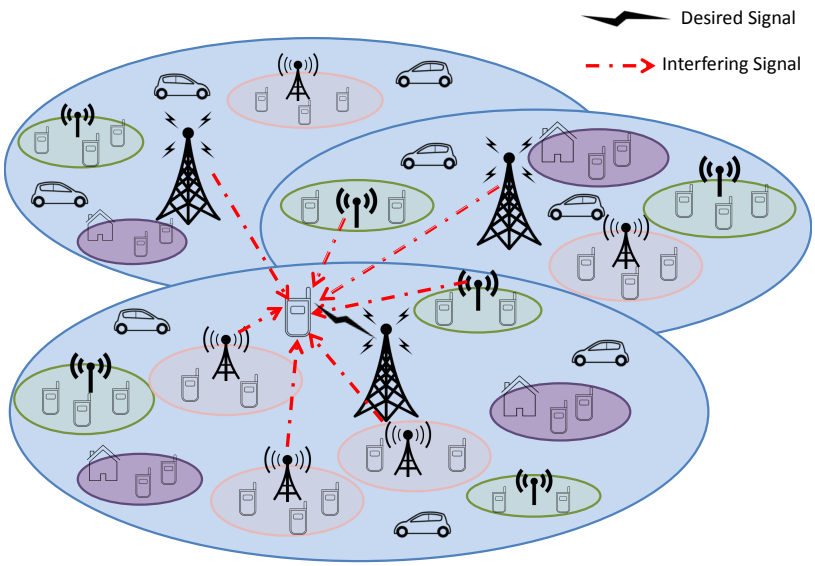

Figure 1.2: Anticipated 5G future wireless networks applications.

constraints on the quality of service (QoS) performance. To name a few of the encountered challenges, future wireless networks are required to provide very high data rates, enhanced reliability, energy efficient operation, seamless coverage and most importantly, provide a fusion of all the current wireless technologies under one seamless unified network [9,10]. Driven by all these requirements and challenges, the fifth generation of cellular networks (5G) has received immense attention from researchers and operators. It is expected to supersede the fourth generation (4G) cellular networks by 2020, while supporting integrated operation of the current technologies [9–11].

Such massive growth in the number of antennas, accommodated users, radio access technologies, applications, in addition to the network size, implies a significant increase in the intrinsic component of the novel wireless networks; namely, the aggregate network interference, as shown in Fig. 1.2. Therefore, as the emerging cellular networks grow denser, it becomes crucial to effeciently develop accurate and rigorous analytical models to guarantee accommodating such inevitably exploding growth, and quantify the various system performance measures with respect to the

key performance-limiting factors in realistic environments.

The key pillar and the most commonly studied model in the analysis of wireless networks is the received signal-to-interference-plus-noise ratio (SINR) model, or the signal-to-interference ratio (SIR) model in interference-limited environments. In fact, the SINR/SIR model has the ability to abtsract the overall network performance. Typically, the received signal strength is affected by several factors, e.g., the distance from the transmitter, the properties of the propagation channels, path-loss model, transmit power, and most importantly the inevitable concurrent transmissions, i.e., the aggregate network interference. Therefore, the captured information in the SINR model is fundamental for studying the dynamics of wireless networks. To this end, the SINR model has been the most informative metric of interest in the literature to derive tangible and representative performance indicators. In particular, some key performance indicators (KPIs) that govern the performance of wireless networks and how they relate to the SINR are defined as follows.

- Outage Probability ($\mathcal{O}(\theta)$): One of the most commonly studied performance metrics in wireless networks. It is defined as the probability that the received SINR falls below a certain threshold θ, such that

$$\mathcal{O}(\theta) = \mathbb{P}\left(\text{SINR} < \theta\right). \tag{1.1}$$

- Ergodic Capacity ($\mathcal{R}$): According to Shannon's theorem, it is defined as the maximum number of successfully transmitted bits over a point-to-point link, normalized to the link bandwidth such that

$$\mathcal{R} = \log_2\left(1 + \text{SINR}\right) \qquad \text{bits/s/Hz}. \tag{1.2}$$

- Bit/Symbol Error Probability (BEP/SEP): The probability that the demodu-

later incorrectly decodes the received bit/symbol. The definition of the BEP/SEP with respect to the SINR basically depends on the adopted modulation scheme.

- Pairwise Error Probability (PEP): It is the probability that the demodulator incorrectly chooses between a pair of arbitrary codewords without considering all other possibilities.

Obviously, the SINR is a basic and essential ingredient required to study different KPIs in the network. Therefore, accurate modeling and efficient analysis of the SINR allows for direct inspection of the provided QoS parameters as well as adjusting the network operation to tackle the faced challenges. However, it is not generally straightforward to derive the probability distribution function (PDF) of the receive SINR. Moreover, the interfering transmissions are highly governed by the network topology and interferers spatial distribution, in addition to the various system parameters, which renders the statistical charcterization of realistic aggregate network interference a challenging task. The network geometry can be assumed to follow a deterministic structure [12] or a stochastic nodal distribution. Nevertheless, recent studies have shown that for actual deployments of cellular networks, the spatial locations of BSs deviate from being regular to a more randomzied structure [13, 14]. Fig. 1.3 shows the classical representation of BSs service area adopting the grid-based model, which has been shown to be too optimistic, and underestimates the actual aggregate interference. Therefore, two decades ago, it has been suggested that the service cell in the two-dimensional plane be represented by a convex Voronoi cell formed from the intersection of half-planes [15]. Fig. 1.4 demonstrates the Poisson-Voronoi tessellations constituted by the convex Voronoi cells of the spatial domain, forming a cellular network of Poisson distributed BSs and UEs [16]. Although Fig. 1.4 shows completely random Poisson distributed BSs, to the contrary of practical scenarios, this random model has surprisingly proven to be a realistic and accurate representation of actual cellular networks architecture [13, 14]. Furthermore, it provides notably tractable

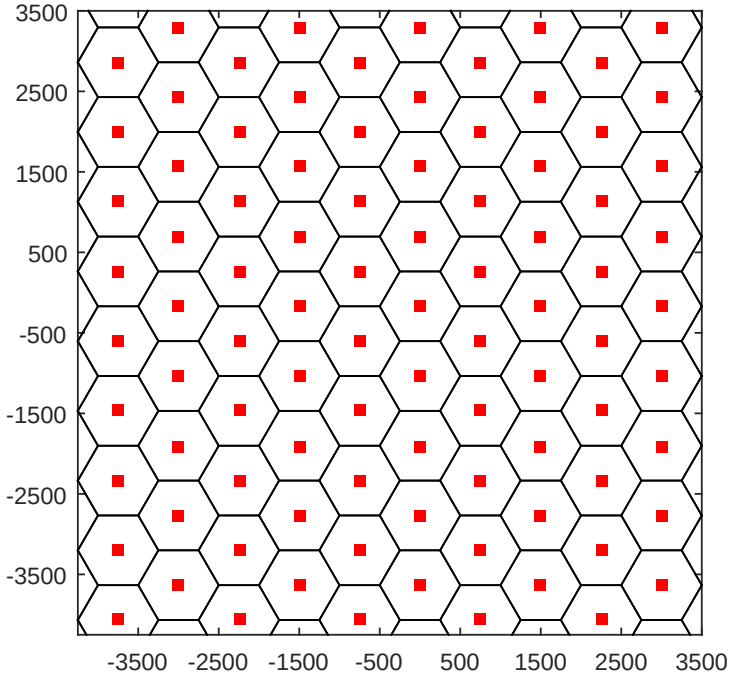

Figure 1.3: Hexagonal Deterministic Grid model for base stations.

analytic results for highly rigorous assessment of the network. Nevertheless, adopting the randomized BSs model introduces challenging uncertainties to the inherent randomness in cellular topology and renders exact interference characterization, and accordingly exact SINR characterization, more involved. That is, the SINR model is required to capture the dynamic network realizations and provide topology-aware performance indicators. In the context of large-scale networks with topological randomness, Stochastic Geometry has been shown to provide an elegant and systematic mathematical framework that naturally accounts for the involved uncertainties and enables spatially averaged SINR characterization [13, 17–21].

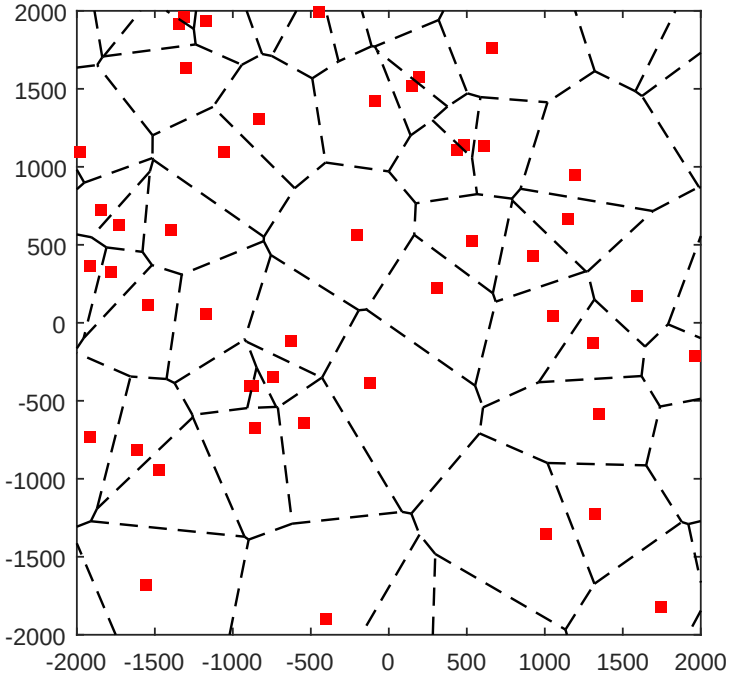

Figure 1.4: Possion distributed base stations forming Voronoi tessellations.

1.1 Motivation and Contribution of the Thesis

Stochastic Geometry analysis succeeded to model realistic interference environments taking into consideration the interferers locations building on the notion of typicality [13,17,22] using two largely disjoint approaches. The first approach, which is more common in the literature, is to abstract SINR models in terms of the statistics of the aggregate interference power only, for the purpose of studying outage probability and ergodic capacity [13, 23–35]. Despite being very crucial metrics that highly affect the network performance, they are not sufficient for rigorous performance characterization as this approach overlooks the effect of important communication design factors on the network performance. On the other hand, the second approach characterizes interference at the signal baseband level in order to be able to delve into fine communication systems details, such as the modulation scheme, constellation type, and signal recovery techniques [36–38]. The analytical paradigm proposed in [36,37] based

on the latter technique, referred to as *Equivalent-in-Distribution* (EiD) approach, is therefore able to capture the impact of network parameters on tangible and practical performance metrics; such as the average BEP (ABEP) and the average SEP (ASEP), in realistic interference environments. Nevertheless, this is achieved at the expense of significantly complicated analysis that is highly dependent on the employed network configuration. Specifically, the complexity of the EiD analysis can be attributed to the necessity to model the aggregate interference signal at the complex baseband level and statistically account for the transmitted symbols from each interferer.

This thesis presents an approximate, yet highly accurate, framework that is able to capture detailed communication system aspects as the EiD approach, but with much simpler analysis that likewise relies on the Poisson point process (PPP) abstraction model [13, 17, 19, 20, 39]. The main idea, which is inspired by the work in [40, 41] is to approximate the interferers transmitted symbols by Gaussian codebooks. This approximation alleviates the baseband analysis of the EiD and only requires the computation of the Laplace Transform of the probability density functions (LT) of the interference power. Hence, it facilitates the analysis steps and results in less computationally intensive expressions than the EiD approach. Moreover, the work developed in this dissertation focuses on unifying both aforementioned approaches in order to conduct a single comprehensive and inclusive study that brings outage probability, ergodic rate, and error probability analyses together. Such study is critically important in order to rigorously model and design the emerging large-scale cellular networks. This thesis is the first to present a unified study that can be used to investigate the different tangible performance metrics and provide guidelines for efficient cellular networks design. Particularly, we propose an automated reliable strategy to achieve a desired network objective under various performance constraints.

The main contributions of the developed framework can be summarized in the following points:

- Developing a unified mathematical paradigm based on the single-input-single-output (SISO) SINR model that is able to bridge the gap between error probability, outage probability, and ergodic rate analysis. Hence, it is possible to look at all three performance metrics within a single study.

- Extending the SISO-SINR model to evaluate outage probability, ergodic rate and decoding error probability for different MIMO schemes. Note that the decoding error probability model based on the EiD approach presented in [37] differs across the MIMO configurations due to the different effect of the precoding/combining matrices on the aggregate interference when accounting for modulation type and constellation size.

- Bypassing the complex baseband interference analysis, which simplifies the decoding error probability analysis and reduces the computational complexity of the final expressions, when compared to [37], without compromising the model accuracy.

- Revealing the cost of multiplexing, in terms of outage probability and decoding error, in large-scale cellular networks. We also show the appropriate diversity compensation for such cost.

- Accounting for the signal retransmission upon decoding failure in downlink and uplink scenarios. SINR temporal correlation among the original and retransmitted signals is captured and the resulting diversity loss is quantified.

- Utilizing the developed unified framework to quantify the effect of interference management on the ASEP performance in cellular networks.

1.2 Thesis Outline

The rest of the dissertation is organized as follows.

1. Chapter 2 presents some Stochastic Geometry preliminaries that are employed throughout the thesis. In addition, it provides an overview of the SINR model using Stochastic Geometry analysis in the literature.

2. Chapter 3 describes the baseline system model that is adopted throughout the thesis, with slight modifications that are detailed in each chapter according to the desired network setup.

3. Chapter 4 studys the exact interfererence characterization and investigates the error probability performance in uplink cellular networks with full inversion power control, by utilizing the exact EiD approach proposed in [36]. The performance of the depicted system is analyzed via Monte Carlo simulations, and compared to the common Gaussian interference power approximation. The derived expressions are computationally involved and not straightforward to be extendible to more complex system setups.

4. Chapter 5 develops a unified framework by exploiting the Gaussian signaling approximation in a single-tier SISO cellular network, for both the downlink and uplink transmissions. General Nakagami-m fading environments are studied, and patterns of variations of error performance versus the fading parameters are investigated. The derived expressions for the decoding error probability were verified via numerical results.

5. In Chapter 6, the framework developed in Chapter 5 is extended to study MIMO downlink cellular networks via a unified model with SISO-equivalent SINR model. A novel design methodology is proposed and several diversity-multiplexing tradeoffs are discussed.

6. Chapter 7 extends the proposed model for the analysis of uplink cellular networks employing power control. Similar to Chapter 6, the unified mathematical

model is exploited for proposing a reliable design strategy.

7. Chapter 8, shows the effect of temporal correlation of the aggregate network interference on different network setups, such that time diversity loss is quantified. In the downlink scenario, the effect of signals retransmissions on the coverage performance is studied. Incremental diversity is proven to compensate for the temporal correlation, and achieves the optimistic independent retransmissions performance. On the other hand, the uplink setting under fractional power control is investigated, where the impact of the power control compensation factor on the retransmissions performance is studied.

8. Interference management techniques and their effect on the average error probability performance are investigated in Chapter 9.

9. Chapter 10 provides a brief summary of this thesis dissertation and concludes its contributions. It also discuss potential reserach directions for future work.

Chapter 2

Stochastic Geometry Background

2.1 Introduction

Stochastic Geometry tools have emerged for the purpose of studying collections of randomly distributed point patterns, which are known in the literature as point processes [19]. The branch of Stochastic Geometry theory that aims at mathematically modeling a probabilistic process generating points in time or space is known as Stochastic Point Process theory. Specifically, in the emerging large-scale wireless networks, point processes are used to abstract the spatial distributions of the transmitting and receiving wireless nodes [17]. Such abstraction allows for incorporating the various network uncertainties, e.g., topological randomness, channels fading/shadowing characteristics, and channel access schemes, in one analytically tractable framework to provide performance spatial averages. Therefore, Stochastic Geometry analysis has recently received remarkable attention in the wireless communications community due to its ability to adequately characterize location-dependent interference in wireless networks [17,19,20,42,43]. In the context of large-scale cellular networks, the Stochastic Geometry framework is substantially beneficial to efficiently model and design the future generations of cellular networks. For tractability, the BSs' locations are typically assumed to follow a spatial homogeneous Poisson point process (PPP). Although the PPP implies no correlation among the BSs' locations, the PPP assumption has been proven to provide simple, yet accurate models, for cellular networks [13, 44]. Hence, the PPP assumption is widely accepted to model

cellular networks and has been adopted in [14, 23, 36, 38, 45–47]. In this dissertation, we express the aggregate network interference in terms of the set of interferers that constitute a point process (specifically a PPP, for tractability). Stochastic Geometry techniques are hence exploited for studying and characterizing the aggregate network interference and the SINR models.

In this chapter we will introduce some mathematical preliminaries from the Stochastic Geometry toolset and give an overview on the Stochastic Geometry analysis in the literature.

2.2 Stochastic Geometry Preliminaries

Stochastic Geometry provides location-independent evaluation of various performance metrics, which is achieved via the point process abstraction of the randomly deployed wireless nodes. Accordingly, using Stochastic Geometry analysis, averaging over all possible network realizations is feasible. The structural randomness of wireless networks and its impact on the network-wide performance can be described using probabilistic and statistical functionals of the random sets, i.e., point processes, that abstract the random locations and numbers of wireless nodes [17, 19, 20]. Formal definitions, properties and functionals of the adopted Poisson point processes in this thesis will be shown next.

Definition 2.1. Point Process: A point process is defined as the locally finite random subset Ψ described over the $\mathtt{d}$-dimensional space $\mathbb{R}^{\mathtt{d}}$, with a random counting measure N. such that the set $\{r_o, r_1, r_2, \cdots\}$ where r_i for $i = o, 1, 2, \cdots$, are the locations of the points constituting Ψ. Its intensity measure, defined as the average number of points, in a Borel set $\mathtt{B} \subset \mathbb{R}^d$ is given as $\Lambda(\mathtt{B}) = \mathbb{E}[\Psi(\mathtt{B})]$.

Definition 2.2. Stationarity of a point process:

A point process is said to be stationary if its distribution is invariant under transla-

tions, where

$$\mathbb{P}\{\Psi \in \mathcal{X}\} = \mathbb{P}\{x + \Psi \in \mathcal{X}\}. \tag{2.1}$$

Definition 2.3. Homogeneous point process:
A homogoeneous point process is characterized by a constant intensity measure, independent of the points locations, such that

$$\Lambda(\mathtt{B}) = \Lambda. \tag{2.2}$$

Otherwise, the point process is said to be inhomogeneous, where its intensity is a function of the point location r_i such that

$$\Lambda(\mathtt{B}) = \Lambda\left(r_i\right). \tag{2.3}$$

2.2.1 Poisson Point Processes (PPPs)

The most convenient and most popular point process for statistically modeling wireless nodes with no interaction, i.e., complete spatial randomness, is the PPP [13, 17, 39, 48]. For instance, [49–51] adopt the PPP abstraction model for ad hoc networks and since then the PPP assumption has been verified and well studied [44, 52, 53]. Furthermore, the Poisson deployment is considered as the baseline deployment for evaluating the performance of other diverse, possibly more practical, deployments from that of the PPP model [54–56]. Thus, the focus in this thesis will be on the PPP abstraction model to yield insightful trends that can be further exploited for other models or deployments.

Definition 2.4. Poisson Point Process (PPP):
A stationary point process Ψ, with intensity measure λ, is said to be Poisson, if the number of points in the bounded set $\mathtt{B} \subset \mathbb{R}^{\mathtt{d}}$ is a discrete Poisson random variable

such that

$$\mathbb{P}\left(\mathrm{N}\left(\mathtt{B}\right)=j\right)=\exp\left\{-\lambda\mathbf{L}\left(\mathtt{B}\right)\right\}\frac{\left(\lambda\mathbf{L}\left(\mathtt{B}\right)\right)^{j}}{j!} \tag{2.4}$$

where $\mathbf{L}\left(\mathtt{B}\right)$ is the Lebesgue measure (generally, the $\mathtt{d}$-dimensional volume) of the set $\mathtt{B}$. In addition, PPPs are characterized by complete independence among the distinct points. That is, for mutually disjoint subsets $\mathtt{B}_j \subset \mathbb{R}^{\mathtt{d}}$, wher $\mathtt{B}=\cup_j \mathtt{B}_j$, the random variables $\Psi\left(\mathtt{B}_j\right)$ are independent. This property is known as independent scattering, which is highly useful in modeling completely random wireless nodes in a two-dimensional network.

Furthermore, PPPs exhibit important features that facilitate the performance analysis of wireless networks:

Property 1. Thinning:
Some points can be retained or excluded from the point process under investigation according to some retention probability $p\left(x\right)$ [17, 19]. There are two types of random inclusion and exclusion of points in a point process:

1. Independent Thinning: The retention function is independent for all points in the point process, i.e., $p\left(x\right)=p$. For a homogeneous PPP Ψ with intensity Λ, that is independently thinned with retention function p, then Ψ is thinned into the PPPs; Ψ_1 with intensity $p\Lambda$ and Ψ_2 with intensity $\left(1-p\right)\Lambda$. In addition, Ψ_1 and Ψ_2 are independent point processes.

2. Dependent Thinning: A point is retained or excluded from the point process according to a probabilistic event that depends on the location of the point (or another property that marks this point in the point process). If point process Ψ has an intensity measure Λ, then thinning Ψ with retention probability $p\left(x\right)$ will result in the point process $\bar{\Psi}$ with intesnity measure $\Lambda\left(\mathtt{B}\right)=\int_{\mathtt{B}} p\left(x\right)\Lambda\left(dx\right)$.

Property 2. Superposition: The infinite superposition of independent Poisson point processes Ψ_{κ} with intensities λ_{κ} is also a Poisson point process $\Psi = \sum_{\kappa}^{\infty} \Psi_{\kappa}$ with intensity $\lambda = \sum_{\kappa} \lambda_{\kappa}$. Note that the superposition property holds as well for the finite case.

2.2.1.1 Functionals of Poisson Point Processes

Theorem A. Slivnyak's Theorem:
Addition or removal of a point (or set of points) to/from the PPP maintains the same distribution of the other points in the point process. That is, the reduced Palm distribution of a homogeneous PPP Ψ, which is denoted by $\mathbf{P}^{\mathtt{x}}(\mathtt{B})$, is equal to that of Ψ. In other words, $\mathbf{P}^{\mathtt{x}}(\mathtt{B}) = \mathbf{P}(\Psi^{\mathtt{x}} \cup \{\mathtt{x}\} \in \mathtt{B})$, such that $\Psi^{\mathtt{x}} = \Psi \setminus \mathtt{x}$, is the PPP excluding the point with spatial coordinates $\mathtt{x}$. Therefore, it is straightforward to condition on a point in the point process (i.e., the test node), which does not contribute to the network-wide performance but still belongs to the network under study.

Theorem B. Probability Generating Functional:
The probability generating functional (PGFL) of a point process Ψ with intensity $\Lambda(x)$ is given by

$$\begin{aligned} \mathcal{PG}_{\Psi}(\mathbf{U}) &= \mathbb{E}\left[\prod_{x \in \Psi} \mathbf{U}(x)\right] \\ &= \exp\left\{-\int_{\mathbb{R}^{\mathtt{d}}} (1 - \mathbf{U}(x))\, \Lambda(x)\, \mathrm{d}x\right\} \end{aligned} \tag{2.5}$$

where $\mathbf{U}(x) : \mathbb{R}^{\mathtt{d}} \to [0, 1]$ is a mapping function from the $\mathtt{d}$-dimensional space to the probability space.

Theorem C. Lalpace Functional:

The Lalpace Functional of a Poisson point process Ψ with intensity $\Lambda(x)$ is given by

$$\mathcal{L}_{\Psi}(\mathbf{U}) = \exp\left\{-\int_{\mathbb{R}^{\mathtt{d}}} \left(1 - e^{\mathbf{U}(x)}\right) \Lambda(x)\, \mathrm{d}x\right\} \tag{2.6}$$

where $\mathbf{U}(x) : \mathbb{R}^{\mathtt{d}} \to [0,1]$ is a mapping function from the $\mathtt{d}$-dimensional space to the probability space.

2.2.2 Interference Modeling via Poisson Point Processes

Definition 2.5. Shot Noise Process:

For a stationary PPP Ψ, concurrent transmitted signals received at an arbitrary point generate random fields that can be modeled by a shot noise process [17, 19, 57]. Specifically, aggregate wireless networks interference, at an arbitrary point $\mathtt{x}$, resulting from a Poisson field of interferers Ψ, has been modeled in the literature by a shot noise process such that

$$I(\mathtt{x}) = \sum_{\mathtt{x}_i \in \Psi} \mathcal{V}(\mathtt{x}_i)\, \ell(\mathtt{x}_i - \mathtt{x}) \tag{2.7}$$

where $\ell(\cdot)$ is the path-loss function, and the function $\mathcal{V}(\cdot)$ incorporates various wireless network propagation and transmission characteristics, such as transmit powers, fading and shadowing functions. The form of (2.7) can be exploited for expressing aggregate interfering signals I_{agg} or aggregate interference powers $\mathcal{I}_{\text{agg}}$, measured at an arbitrary point in the network according to Slivnyak's theorem [17, 19, 20, 42]. It is highly important to highlight that the aggregate interference at an arbitrary point is a representative for the aggregate interference experienced by any other point in the network. Note that, the Laplace functional of a PPP will be used in the rest of this thesis as the Laplace Transform of the probability distribution function of the interference power, which is a function of a PPP.

Definition 2.6. Symmetric α-Stable (SαS) Distribution: Stable distributions

represent a notably useful family of heavy-tailed distributions in modeling interference and impulsive noise [58]. Moreover, the Gaussian distribution is in fact a special case of stable distributions family. The univariate SαS distribution is characterized by its characteristic function (CF) given by

$$\Phi_{S\alpha S}\left(\omega\right)=\exp\left\{-\mathcal{Q}\left|\omega\right|^{q}\right\} \tag{2.8}$$

where $\mathcal{Q}$ is the distribution dispersion, and q is the characteristic exponent. For multivariate spherically symmetric (SS) α-stable distributions, the characteristic function is expressed as

$$\Phi_{S\alpha S}\left(\boldsymbol{\omega}\right)=\exp\left\{-\mathcal{Q}\left|\sum_{j=1}^{J}\omega_{j}^{2}\right|^{\frac{q}{2}}\right\} \tag{2.9}$$

where $\boldsymbol{\omega}=(\omega_1,\omega_2,\cdots,\omega_J)$. The bivariate S$\alpha$S distributions, with $\boldsymbol{\omega}=(\omega_1,\omega_2)$ where

$$\Phi_{S\alpha S}\left(\left|\boldsymbol{\omega}\right|\right)=\exp\left\{-\mathcal{Q}\left|\boldsymbol{\omega}\right|^{2q}\right\} \tag{2.10}$$

We next delve into the the Signal-to-interference-and-noise ratio model notion.

Definition 2.7. Signal-to-interference-and-noise ratio (SINR):
The receive signal-to-interference-and-noise ratio (SINR) at a test user is expressed as

$$\Upsilon^{(j)}=\frac{\mathcal{S}^{(j)}}{\mathcal{N}_o+\mathcal{I}_{\text{agg}}^{(j)}} \tag{2.11}$$

where $\mathcal{S}^{(j)}$ is the signal power at a generic measurement instant j, $\mathcal{N}_o$ is the noise power and $\mathcal{I}_{\text{agg}}^{(j)}$ is the aggregate interference power at generic time j. Note that, $\mathcal{S}^{(j)}$ incorporates multi-path fading, shadowing and the distance decay represented by the path-loss function $\ell\left(\mathtt{x}\right)$. In this dissertation, we adopt the unbounded path-loss model

$\ell(\mathtt{x}) = \|\mathtt{x}_i - \mathtt{x}\|^{-\eta}$, with $\eta \geq 2$ as the path-loss exponent. That is to say, the SINR model accounts for the various uncertainties in the netwrok including the random topology. In other words, the SINR, $\Upsilon^{(j)}$, is indeed a random variable that captures several crucial factors, namely; network geometry, test receiver location, propagation characteristics, transmit powers, path-loss attenuation, measurement time instant and consequently network parameters that accordingly vary with the time j.

Building on the aforementioned properties and characteristics of PPPs, and exploiting the notion of aggregate network interference as a PPP functional together with the SINR model, we next give an overview of the SINR model in the the context of large-scale cellular networks literature, employing Sotchastic Geometry analysis.

2.3 SINR Model for Cellular Networks in Stochastic Geometry Literature

The use of the Stochastic Geometry powerful toolset in cellular networks has been considered in the literature as early as 1997 [15, 59]. Exploiting recent advances in Stochastic Geometry analysis, several mathematical frameworks have been developed, over the past two decades, to study different network operation in cellular networks in a Poisson field of interferers [13,23–35,37–39,43,45,46,52,60–64]. Stochastic Geometry does not only provide systematic and tractable framework to model spatially averaged cellular networks operation in interference environments, it also captures the behavior of realistic cellular networks as reported in [13, 14, 44]. The most common and simple approach used in the Stochastic Geometry literature for SINR characterization is to account only for the coherent sum of the interferers' signal powers at the test receiver [13, 39]. This technique is proven to be highly accurate and useful to model outage probability and ergodic rate in different types of networks [23, 46]. For instance, [23] models SINR coverage probability and ergodic rate in multi-tier downlink cellular networks. Characterization of downlink SINR and achievable rate for cellular HetNets

has been investigated in [65–70]. Ergodic rate and outage in uplink cellular networks are studied in [47, 71–74]. Cognitive cellular networks are modeled in [46, 64]. In [75], the aggregate interference has been asympototically analyzed, and closed-form expressions were derived for approximate outage probability. SINR association was characterized in [76]. In [77], perfect successive interference cancellation (SIC) has been proposed in uplink cellular networks based on the SIR model to quantify the outage probability of the network. Device-to-deice (D2D) communication in two-tier heterogeneous cellular networks has been studied in [78] via SIR coverage and network throughput under dynamic time-division duplexing (TDD) systems. Further tradeoffs between traffic offloading and energy consumption have been revealed in mutli-tier cellular networks, and tractable expressions have been derived for local cell capacity in [79]. The work in [63] derives the asymptotic spectral efficiency for uplink multi-antenna cellular networks. For MIMO cellualr networks, the authors in [24] study the SINR coverage probability of orthogonal space-time block codes (OSTBC). Studies for the outage probability and ergodic rate for space-division-multiple-access (SDMA) MIMO, also known as multi-user MIMO (MU-MIMO), are available in [34, 35] for single-tier cellular networks and in [80] for multi-tier cellular networks. Coverage probability improvement via maximum-ratio-combining (MRC) with spatial interference correlation is quantified in [25, 81, 82]. The potential gains of beamforming and interference alignment in terms of SINR coverage and network throughput are quantified in [26–28]. Coverage probability and rate for MRC and optimum combining in uplink MIMO cellular networks are studied in [83]. Network MIMO via BS cooperation performance in terms of outage probability and ergodic rate are studied in [29–33, 84, 85]. Distributed antenna systems (DAS) in cellular networks are analyzed in [86]. Joint optimization of the optimal frequency resue factor and network bias in a heterogeneous cellular network is analyzed in [87]. A general framework that can compare outage probability and rate for different MIMO

schemes in advanced cellular network models is developed in [88].

Although the mathematical models presented in [24–35, 37, 38, 63] are all based on Stochastic Geometry, there are significant differences in terms of the analysis steps as well as the level of details provided by each model. The majority of the models focus on the outage probability and ergodic capacity for simplicity [24–35]. Nevertheless, it is highly improtant to note that the adopted SINR model for outage and ergodic rate analysis available in the literature are typically restricted to interference power statsitics, which is implicitly assumed to be complex Gaussian. Thus, interference power is lumped with the noise variance, and the SINR model is directly applied to study network-wide outage and rate performance.

While both outage probability and ergodic rate are fundamental KPIs in wireless communications, they convey no information about the underlying modulation scheme, constellation size, or receiver type. Considering more tangible KPIs, such as decoding error probability and average throughput[1], requires alternative and more involved analysis. Treating interference as noise, the average decoding performance of a symbol conveyed in the received signal is characterized through the following two steps:

(i) conditionally averaging over the transmitted symbols and noise (while conditioning on the network geometry and channel gains),

(ii) then averaging over the channel gains and network geometry.

The averaging in step (i) is done based on the modulation scheme, constellation size, and receiver type. Then, in step (ii), the averaging is done using stochastic geometry analysis.

However, the exploited Gaussianity holds for specific scenarios as demonstrated in [89, 90]. That is, the second-order statistics of the aggregate interference may

[1]Throughput is defined as the number of successfully transmitted bits per channel use.

not be well approximated by Gaussian distribution in realistic interference environments [39, 42, 43, 91]. In fact, [18, 39, 43, 51, 58, 62, 92, 93] have shown that heavy-tailed stable distributions, specifically symmetric α-stable (SαS) distributions [94, 95], are the most convenient to accurately characterize the aggregate network interference from a homogeneous Poisson field of interferers under specific conditions. [93, 96, 97] discuss the applicability of the SαS distributions in wireless networks with Poisson field of interferers. Nevertheless, in cellular networks, an interference protection region is imposed which renders the aggregate network interference inaccurately modeled by neither Gaussian nor SαS distributions [36, 39]. Therefore, accurate and exact statistical descriptions of the aggregate network interference in realistic environments have not been well formulated yet. Moreover, the average decoding error performance in step (i) is only characterized for certain distributions of additive noise channels (e.g., Gaussian [98], Laplacian [99, 100], and Generalized Gaussian [101]), in which the additive white Gaussian noise (AWGN) channel represents the simplest case. Accounting for the exact distribution of the interfering symbols, the interference-plus-noise distribution does not directly fit into any of the distributions where the average decoding error performance is known. Hence, the averaging step (i) cannot be directly conducted unless the interference-plus-noise term is expressed or approximated via one of the inaccurate distributions where the average decoding error performance is legitimate. The authors in [37] thus proposed the *Equivalent-in-Distribution* (EiD) approach where an exact conditional Gaussian representation for the coherent sum of interfering baseband signals is achieved. Hence, the conditional error probability analysis (i.e., step (i)) is conducted via error probability expressions for AWGN channels, followed by the deconditioning step in (ii). The main drawback of the EiD approach is the analytic and computational complexity that can be attributed to the necessity to model the aggregate interference signal at the complex baseband level and statistically account for the transmitted symbols from each interferer [43, 91]. This

complicates both averaging steps (i), (ii) specially in more complicated setups (e.g., MIMO networks). Furthermore, the EiD approach for the error probability analysis in [37] is completely disjoint from the outage probability and ergodic rate analysis in [24–35]. Following the same analysis methodology as the EiD approach, which relies on the conditional Gaussian representation of the interfering signals, we propose abstracting the unnecessary information conveyed within the interfering symbols by Gaussian signals. That is, we assume that the interfering signals are drawn from Gaussian codebooks. Gaussian signaling approximation directly implies Gaussianity of the aggregate interfering signals, conditioned on other network parameters (i.e., network geometry, fading channels).

In addition, the analysis in each of the mathematical models presented in [24–35, 37, 38] is highly dependent on the considered MIMO configuration. Having mathematical models that are significantly different in the analysis steps from one KPI to another and from one antenna configuration to another makes it challenging to conduct comprehensive studies that include different antenna configurations and compare their performances in terms of different KPIs. Therefore, the main focus of this dissertation is to present a unified mathematical paradigm, based on Stochastic Geometry, to study the average error probability, outage probability, and ergodic rates for cellular networks with different network settings. The proposed framework in this thesis develops an equivalent SISO-SINR representation that can be directly applied to different network/antenna configurations [102–104]. It is worth noting that the SISO-SINR representation used in this paper was used in the context of ad-hoc networks to study the outage probability and transmission capacity in [105]. In the context of cellular networks, it was also used to study OSTBC in [24,106,107], receive diversity in [25], and MU-MIMO in [34]. Moreover, the Gaussian signaling approximation simplifies the decoding error analysis without sacrificing the model accuracy and aligns the decoding error analysis with the outage probability and ergodic rate

analysis.

In the next chapter, we demonstrate the baseline system model, based on Stochastic Geometry, that represents the core of the various settings studied in this thesis.

Chapter 3

Baseline System Model

In this chapter, we provide the baseline system model for this thesis, such that extensions to this model are highlighted in the following chapters as needed.

3.1 Network Model

We will consider a single-tier cellular network such that extension to a multi-tier network is straightforward by following [23, 47] as will be shown in Chapter 4. Single-antenna BSs are modeled via a homogeneous PPP ψ_B with intensity λ_B. The locations of the user equipments (UEs) are modeled via an independent PPP ψ_u with intensity λ_u, and each UE is equipped with a single antenna. A distance-dependent power-law path-loss attenuation is employed, in which the signal power attenuates at the rate $r^{-\eta}$ with the distance r, where $\eta > 2$ is the path-loss exponent. Without loss of generality, we assume that the set $\Psi_B = \{r_o, r_1, r_2, \cdots\}$ contains the ascending ordered distances of the BSs from the origin (i.e., $r_o < r_1 < r_2$). We assume i.i.d. Nakagmai-m channel gains, where m is assumed to be an integer. Therefore, the analysis is valid for various fading environments, as Nakagami-m can approximate several fading models [66]. Saturation conditions are assumed where all BSs will always have UEs to serve and all BSs and UEs always have saturated buffers. According to Slivnyak's Theorem [17], there is no loss in generality to study the performance for a test link in which the test receiver is located at the origin, o [91]. Let p be the independent transmission probability for each BS. Note that p can be calculated as in [108], and setting $p = 1$

gives the traditional saturation condition (i.e., $\lambda_u \gg \lambda$) where all BSs are active. Moreover, universal frequency reuse scheme with no intra-cell interference is employed across the network. That is, each BS will be serving only one user per channel resource and all channels are reused by all BSs. Let the distance between a transmitter and its intended receiver be denoted as D_i. Note that the distance between the test receiver and its intended transmitter has the PDF

$$f_{D_i}(x) = 2\pi\tilde{\lambda}\, x\, e^{-\pi\lambda x^2}, \qquad x > 0 \tag{3.1}$$

where $\tilde{\lambda}$ is the intensity of the PPP constituted by the set of interferers and represented via the set $\tilde{\Psi}$ that contains the distances of the interferers to the origin.

It is worth emphasizing that for a certain network realization, an averaged performance metric is obtained with respect to all other sources of randomness that are not related to the network geographical distribution. Next, a spatially averaged performance is derived for the slowly varying network topology, or to account for all the possible network realizations.

3.1.1 Transmitter and Receiver characteristics

At the transmitter side, data is mapped to a general bi-dimensional constellation $\mathbf{S}$ with M equiprobable symbols denoted as $s^{(\kappa)} = a^{(\kappa)} \exp\{\jmath\varphi^{(\kappa)}\}$, where $\jmath = \sqrt{-1}$, and $\kappa = 1, 2, \cdots, M$. Moreover, the symbols have unit power such that, $\mathbb{E}\left[|s^{(\kappa)}|^2\right] = 1$. Let the desired symbol and the interferering symbols be denoted by s_o and s_i, respectively. For the EiD approach, both $s_o, s_i \in s^{(\kappa)}$, such that the interferers' transmitted symbols are accounted for. On the other hand, by applying the Gaussian signaling approximation, the interferers' symbols are abstracted and approximated by a Gaussian signal $s_i \approx \tilde{s}_i$, with unit-power spectral density. Note that, the developed framework can be extended to different symbol generation probabilities. At the test

receiver side, the intended symbol is recovered via a Maximum-likelihood receiver (MLR) with perfect Channel State Information (CSI). Further, it is assumed that the test receiver has perfect intended link CSI and is unaware of the inter-cell interference. Beside simplifying the analysis, interference unawareness assumption enables us to quantify the performance degradation due to aggregate interference. In addition, it sets the stage to study more realistic receiver designs that are able to operate in such interference environments, and/or develop more advanced interference coordination techniques that improve the system performance.

3.2 Complex Received signal model

Typically, the received complex signal at the test receiver in a SISO network is given by

$$y = \sqrt{P_o}\, r_o^{-\frac{\eta}{2}}\, g_o\, s_o\, + \sum_{r_i \in \tilde{\Psi}} \sqrt{P_i}\, r_i^{-\frac{\eta}{2}}\, g_i\, s_i\, + n, \tag{3.2}$$

where P_o is the transmit power of the intended transmitter, P_i is the transmit power of the interferers, g_o and g_i are independent random variables representing the intended and interfering channel impulse responses. r_i is the distance between the interferer and the test receiver at the origin o. Finally, $n \sim \mathcal{CN}(0, \mathcal{N}_o)$ denotes the circularly symmetric complex Gaussian noise at the receiver.

3.2.1 Downlink Scenario

In the downlink scenario, all BSs transmit with a constant power $P_o = P_i = P$. Assuming nearest BS association, the test user is subject to interference from the BSs in $\Psi^o = \Psi_B \setminus r_o$, thus $\tilde{\Psi} = \Psi^o$ and $\tilde{\lambda} = \lambda_B$. Building on the notion of p, then, the point process of the active interfering BSs in the set $\tilde{\Psi}^o \subseteq \Psi^o$ after independent thinning is also a PPP but with intensity $\lambda = p\lambda_B$ [17]. This assumption is used

to reflect load awareness and/or frequency reuse as discussed in [37, 109]. Thus, the received complex signal at the test UE is represented as

$$y = \sqrt{P}\, r_o^{-\frac{\eta}{2}}\, g_o s_o + \sum_{r_i \in \tilde{\Psi}^o} \sqrt{P}\, r_i^{-\frac{\eta}{2}}\, g_i s_i + n, \tag{3.3}$$

3.2.2 Uplink Scenario

Considering the uplink data transmission, we assume truncated channel inversion power control. That is, each UE adjusts its transmit power such that its signal is received with an average value of ρ at its serving BS. Under average radio signal strength (RSS) based association, each user is associated to its nearest BS if and only if (a) it can invert its path-loss to its nearest BS, and (b) its nearest BS is not serving another user. Therefore, the transmit power at a generic UE, denoted as $P_i = P_{u_i} = \rho d_i^{\eta}$, where $0 \leq P_{u_i} \leq P_U$, such that P_U is the maximum transmit power for the UE. The UEs that cannot invert their channels are kept silent. Employing the channel inversion power control (i.e., $P_o r_o^{-\eta} = \rho$), (3.2) can be re-written as

$$y = \sqrt{\rho} g_o s_o + \sum_{r_i \in \tilde{\Psi}_u} \sqrt{P_{u_i}} g_i s_i r_i^{-\frac{\eta}{2}} + n, \tag{3.4}$$

such that $\tilde{\Psi}_u$ is the set of interfering users. Since we have one active user per BS per channel resource, the intensity of interfering UEs is $\lambda = p\lambda_B$, i.e., the intensity of active BSs. However, the interfering UEs do not constitute a PPP [47, 110]. Nevertheless, we assume that users whose distances from the test receiver are represented by the set $\tilde{\Psi}_u$ constitute a PPP and that the users' transmit powers are independent despite the fact that according to the considered system model, the locations of interfering UEs are correlated due to the no intra-tier interference assumption. That is, given that an active UE is present in a specific cell on a specific channel, no other user can be using the same channel within that cell. Furthermore, the transmit powers

of the active users are identically distributed but are not generally independent due to the correlation among adjacent Voronoi cells. However, for analytical tractability, the correlations among the active users location as well as their transmit powers are ignored. The accuracy of this assumption has been validated in [47, 110]. We will further confirm the validity of this assumption in the results. Further, P_{u_i} is the random variable representing the adaptive transmit power of the i^{th} UE under the assumed truncated channel inversion power control [47].

Next, we present the framework developed in this thesis, that investigates the performance of celullar networks setup described above. We start with the exact error probability analysis using the EiD approach as will be discussed in the next chapter.

Chapter 4

Error Performance Analysis in Uplink Cellular Networks via the EiD Approach

4.1 Introduction

Based on stochastic geometry analysis, an analytical paradigm has been recently developed in [36], that is able to delve into fine communication systems details. Applying this framework, the impact of network parameters on tangible and practical performance metrics; such as average ABEP and ASEP, in realistic interference environments is captured. The model proposed in [36], referred to as *Equivalent-in-Distribution* (EiD) approach, treats the aggregate network interference at the signal level instead of the power level. Hence, it is able to include fine communication aspects (such as the modulation scheme, constellation type, signal recovery method, etc.) into the analysis. The authors then extend this model for multiple-input-multiple-output (MIMO) systems in [38, 45] and are able to characterize and compare the performance of different MIMO setups in realistic interference environments. Nevertheless, the models in [36, 38, 45] focus on downlink cellular systems. Note that, as discussed in [47, 110], uplink modeling is quite different from its downlink counterpart due to the per user power control, the limited transmit power of user equipments (UEs), and the correlation among the set of active users per channel. In this chapter, we extend the EiD approach to model the ASEP in uplink networks. Additionally, we exploit the heterogeneity trends in future wireless networks. That is to say, user-oriented deployment of small cells is investigated in a multi-tier cellular network setting. Such

randomized deployment, which randomly varies over the spatial domain, together with the geographical constraints, increases the entailed spatial uncertainty. This inherent spatial randomness involves numerous uncertainties to the network model, which makes modeling and understanding the basic performance-limiting factor, i.e., the SINR, more challenging. Moreover, this network structure gives rise to different types of interference, namely the intra-tier and inter-tier interference, which substantially deteriorate the system performance. In this chapter, we develop a mathematical framework based on the EiD approach to characterize the inter-tier and intra-tier interference in an uplink K-tier cellular network.

4.2 System Model

In this section we extend the baseline system model described in Chapter 3 to study single-tier as well as multi-tier cellular networks in a Rayleigh fading environment as elaborated in what follows.

4.2.1 K-tier Network Model

We consider the uplink traffic in a K-tier cellular network. The locations of the BSs of tier k, where $k \in \{1, 2, \cdots, K\}$, are modeled via an independent homogeneous PPP, denoted as ψ_k, with intensity λ_k. Also, the locations of the UEs are distributed over $\mathbb{R}^2$ according to an independent PPP, denoted in the sequel as ψ_u, with intensity λ_u. Let the set Ψ_u contain the distances between the interfering users to the test receiving BS. It is assumed that users have saturated buffers and that $\lambda_u \gg \Lambda$, where $\Lambda = \sum_{k=1}^{K} \lambda_k$, such that each BS will always have users to serve (i.e., saturation condition). As shown in Fig 4.1, the LTE standard allows decoupled downlink and uplink association [111, Chapter 13]. That is, in contrast to downlink which imposes a weighted Voronoi coverage due to the heterogeneous transmit power limits of the BSs, the uplink imposes a homogeneous Voronoi coverage due to the homogeneous

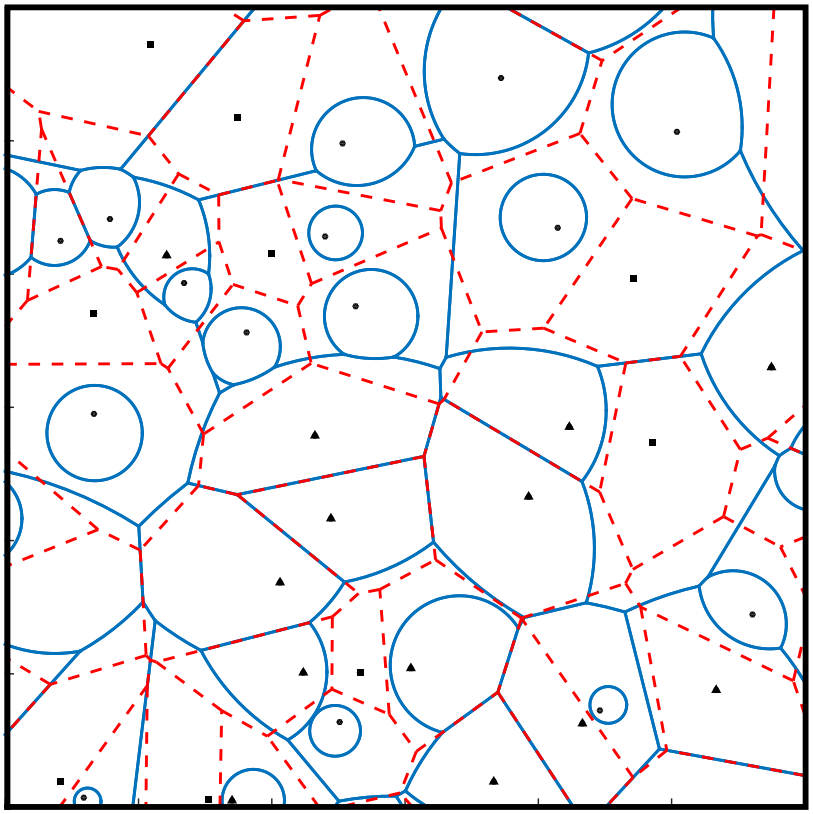

Figure 4.1: Uplink (dotted-red) vs. downlink (solid-blue) association regions for a three-tier cellular network. Squares are macro BSs, triangles are micro BSs, and circles are pico BSs.

transmit power limits of the UEs. Therefore, the distribution of the distance between a typical user and its serving BS in the uplink in tier k, denoted by D_k, is $f_{D_k}(x) = 2\pi\Lambda x \exp\{-\Lambda\pi x^2\}$, $x \geq 0$. Finally, the activity factor $p = 1$. The environment-dependent path-loss exponent, η, is assumed to be common among all the K-tiers. Note that, generalization to different path-loss exponents is straightforward as in [47], however it comes at the expense of more involved analysis. UEs employ a truncated channel inversion power control scheme, where each UE adapts its transmit power in order to compensate for the distance decay rate such that the average received power at its serving BS in tier k is equal to ρ_k, which is the same for all BSs belonging to the same tier. Since the transmit powers of UEs is constrained by a maximum value of P_U, users with high path-loss such that P_U is not sufficient to maintain ρ_k

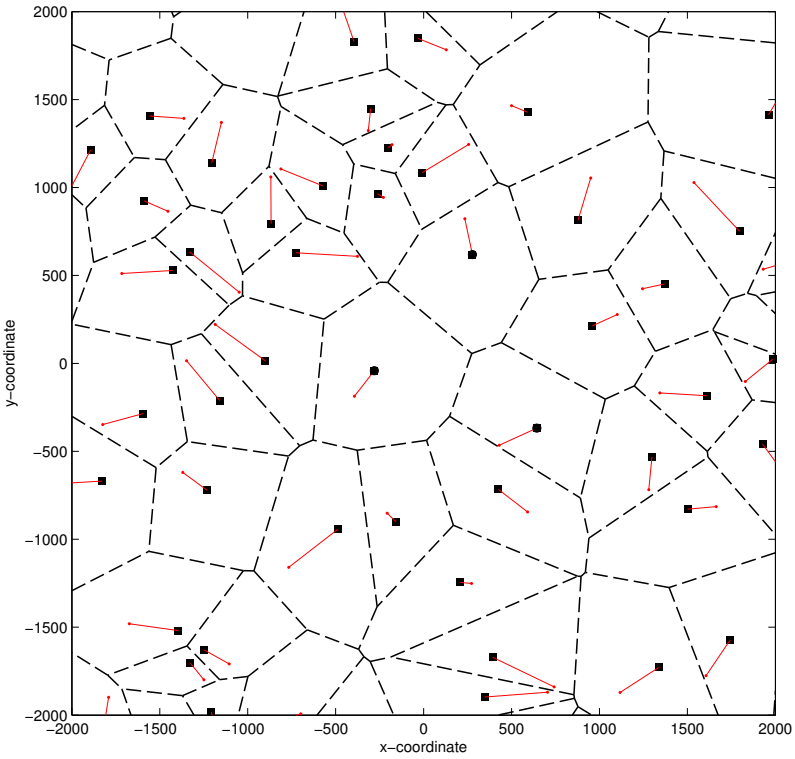

Figure 4.2: The set of simultaneously active UEs per channel resource over 4000 km^2 area. The black squares are the BSs and the red dots are their associated UEs. Each BS serves only one UE per channel, such that a UE is associated with the nearest BS.

at the corresponding BS do not transmit and go into outage. Our main focus is to characterize the ASEP for active users (i.e., users who can invert their path-loss). We study the ASEP at a test BS receiver from tier j and located at the origin, o. From Slivnyak's Theorem [17], there is no loss in generality to study the ASEP at that test BS.

4.2.2 Complex received signal

Based on the aforementioned system model, the complex signal received at the test BS in the j^{th} tier can be represented as

$$y_j = \sqrt{P_{o,j}}\, r_{o,j}^{-\frac{\eta}{2}} g_{o,j} s_{o,j} + \underbrace{\sum_{k=1}^{K} \sum_{r_i \in \tilde{\Psi}_{u,k}} \sqrt{P_{u_i,k}}\, r_{i,k}^{-\frac{\eta}{2}} g_{i,k} s_{i,k}}_{I_{\text{agg}}} + n, \tag{4.1}$$

where $\tilde{\Psi}_{u,k}$ is the set of distances of interfering users associated to tier k BSs. Although the interfering UEs do not constitute a PPP, we assume that the point process formed by the interferers is a PPP with intensity λ_k [47, 110]. $r_{o,j} \sim f_{D_j}(x)$ is the distance between the test BS and intended user, $r_{i,k}$ is the distance between the i^{th} interfering UE associated to tier k and the receiving BS at the origin, $P_{o,j}$ and $P_{u_i,k}$ respectively denote the transmit power of the scheduled UE and the i^{th} interfering UE from the k^{th} tier, $s_{o,j}, s_{i,k} \in \mathbf{S}$ are the transmitted and interfering symbols, respectively. In (4.1), $g_{o,j} = \alpha_j e^{\jmath\phi_j}$ and $g_{i,k} = \alpha_{i,k} e^{\jmath\phi_{i,k}}$ are the intended and interfering channels impulse responses, respectively, where α_j and $\alpha_{i,k}$ are independent Rayleigh distributed random variables modeling the small-scale channel fading, with $\mathbb{E}[\alpha_j^2] = \Omega_j$ and $\mathbb{E}[\alpha_{i,k}^2] = \Omega_k \; \forall i$. The phases ϕ_j and $\phi_{i,k}$ are assumed to be independent uniformly distributed random variables in the range $[0, 2\pi)$. Let $I_{\text{agg}} = \sum_{k=1}^{K} I_k$ be the aggregate network interference complex signal, where $I_k = \sum_{i \in \tilde{\Psi}_{u,k}} \sqrt{P_{u_i,k}}\; r_{i,k}^{-\frac{\eta}{2}} g_{i,k} s_{i,k}$ is the interference from tier k. By employing the channel inversion power control (i.e., $P_{o,j} r_{o,j}^{-\eta} = \rho_j$), (4.1) is re-written as

$$y_j = \sqrt{\rho_j} g_{o,j} s_{o,j} + I_{\text{agg}} + n. \tag{4.2}$$

4.2.3 Methodology of Analysis

The main goal is to extend the well known ASEP expressions available for AWGN channel to characterize ASEP in realistic uplink interference environment. Note that the ASEP expressions for AWGN are usually in terms of the average SNR (i.e., averaged over the Gaussian noise) [98, chapter 8]. In the developed framework, we mathematically express the interference signal strength as a zero-mean conditionally complex Gaussian random variable and obtain the conditional average SINR. Hence, the ASEP expressions based on the AWGN assumption are legitimate. Then, we decondition on the used ASEP expressions to obtain the uplink cellular network performance. As discussed in [36], the conditional Gaussian representation of the interference can be obtained by exploiting the fact that if two random variables have equivalent characteristic functions then they have equivalent distributions. The analysis in the presented framework is divided into the following steps:

1. Interference Characterization: Use stochastic geometry to obtain the characteristic function of the inter-tier interference I_k, and consequently, I_{agg}.

2. Gaussian Representation: Use the characteristic function (CF) of I_k to represent the interference as a function containing Gaussian and non-Gaussian random variables.

3. Conditional Analysis: Calculate the conditional average SINR, i.e., conditioned on the non-Gaussian random variables, and obtain the conditional ASEP using the AWGN setting framework.

4. Deconditioning: Decondition over the non-Gaussian random variables to obtain unconditional parametric ASEP expressions.

4.3 ASEP in Single-Tier Uplink Cellular network

We first start with the analysis of an uplink single-tier cellular network depicted in Fig. 4.2, where the subscript for the correpsonding k^{th} tier is dropped. For clarity of presentation, this section is further divided into four subsections corresponding to the four aforementioned modeling steps enumerated in Section 4.2.3.

4.3.1 Interference Characterization

Characterizing the transmit powers of the interfering UEs is the first step to characterize their interference at the test BS. Due to channel inversion power control and the random service distance D_i following the Rayleigh distribution, the transmit power of a typical UE $P_{u_i} = \rho D_i^{\eta}$, where $P_{u_i} \leq P_U$, is a random variable with probability density function (PDF) [47]

$$f_{P_{u_i}}(p) = \frac{2\pi\lambda p^{\frac{1}{b}-1} e^{-\pi\lambda\left(\frac{p}{\rho}\right)^{\frac{1}{b}}}}{2b\left(1 - e^{-\pi\lambda\left(\frac{P_U}{\rho}\right)^{\frac{1}{b}}}\right)}, \tag{4.3}$$

and j^{th} moment given by

$$\mathbb{E}_{P_{u_i}}\left[P_{u_i}^{\mathrm{j}}\right] = \frac{\rho^{\mathrm{j}}\ \gamma\left(\mathrm{j}b+1, \pi\lambda\left[\frac{P_U}{\rho}\right]^{\frac{1}{b}}\right)}{(\pi\lambda)^{\mathrm{j}b}\left(1 - e^{-\pi\lambda\left(\frac{P_U}{\rho}\right)^{\frac{1}{b}}}\right)}, \tag{4.4}$$

where $b = \frac{\eta}{2}$, $\gamma(\mathrm{a}, \mathrm{b}) = \int_0^{\mathrm{b}} t^{\mathrm{a}-1} e^{-t} \mathrm{d}t$ is the lower incomplete gamma function [112].

Next, we characterize the aggregate interference I_{agg} in (4.1) for the special case of single-tier (i.e., K=1) dropping the index $j = 1$ for notational convenience. It is well known that there is no explicit expression for the PDF of the aggregate interference even for the simple PPP, except for very special cases which are not valid for cellular networks [13]. Hence, the aggregate interference is usually characterized via its char-

acteristic function instead. It is worth mentioning that, contrary to [47] and other stochastic geometry analyses which handle interference at the power level, I_{agg} here is the complex superposition of all interfering signals. The aggregate interference is characterized in the following lemma.

Lemma 4.1. *In an uplink single-tier cellular network under the system model presented in Section 9.2, with $K = 1$, $\rho_k = \rho$, and $\Omega_k = \Omega_i$, the CF of the aggregate interference can be approximated by*

$$\Phi_{I_{\text{agg}}}(|\boldsymbol{\omega}|) \approx \exp\left\{-\nu(\rho,\lambda)\sum_{q=1}^{\infty}\left[\tau_q\left(|\boldsymbol{\omega}|^2\rho\Omega_i\right)^q\sum_{\kappa=1}^{M}\frac{1}{M}\left|s^{(\kappa)}\right|^{2q}\right]\right\}, \tag{4.5}$$

where $\boldsymbol{\omega} = (\omega_1, \omega_2)$ and

$$\nu(\rho,\lambda) = \frac{\gamma\left(2, \pi\lambda\left[\frac{P_U}{\rho}\right]^{\frac{1}{b}}\right)}{1 - e^{-\pi\lambda\left(\frac{P_U}{\rho}\right)^{\frac{1}{b}}}}, \tag{4.6}$$

and

$$\tau_q = \frac{\left(-\frac{1}{b}\right)_q\left(-\frac{1}{4}\right)^q}{q!\left(1-\frac{1}{b}\right)_q}. \tag{4.7}$$

Proof. See Appendix A.1. □

It is worth mentioning that the approximation in Lemma 4.1 is due to the assumption that $\tilde{\Psi}_u$ constitutes a PPP.

4.3.2 Gaussian Representation

The second step in the EiD approach is to represent the aggregate network interference I_{agg} as a conditionally Gaussian random variable. Following [36], the Gaussian representation can be achieved by defining two sets of independent random variables

$\mathcal{B}_q$ and G_q such that $\mathcal{B}_q$ is a real random variable with moment generating function (MGF) $\mathcal{M}_{\mathcal{B}_q}(z) = e^{z^q}$ and G_q is a complex Gaussian random variable with zero-mean and variance

$$\sigma_q^2 = 4\left[\nu(\rho,\lambda)\,\tau_q \rho^q \Omega_i^q \sum_{\kappa=1}^{M} \frac{1}{M} |s^{(\kappa)}|^{2q}\right]^{\frac{1}{q}}. \tag{4.8}$$

We claim that

$$I_{\text{agg}} \overset{d}{=} \underbrace{\sum_{q=1}^{\infty} \sqrt{\mathcal{B}_q} G_q}_{i_{\text{agg}}}. \tag{4.9}$$

The equivalence in distribution between i_{agg} and I_{agg} can be easily verified by noting that the characteristic function of i_{agg} is given by

$$\begin{aligned}
\mathbb{E}\left[e^{\jmath\boldsymbol{\omega} i_{\text{agg}}}\right] &= \mathbb{E}_{B_q}\left[\mathbb{E}_{G_q}\left[e^{\jmath\boldsymbol{\omega}\sum_{q=1}^{\infty}\sqrt{B_q}G_q}\right]\right] \\
&= \prod_{q=1}^{\infty} e^{-\left(\frac{\sigma_q^2|\boldsymbol{\omega}|^2}{4}\right)^q} \\
&= \exp\left\{-\sum_{q=1}^{\infty}\left(\frac{\sigma_q^2|\boldsymbol{\omega}|^2}{4}\right)^q\right\},
\end{aligned} \tag{4.10}$$

substituting σ_q^2 from (4.8) in (4.10) gives a matching characteristic function as in Lemma 4.1, which proves the equivalence in distribution between I_{agg} and i_{agg}. Now, conditioned on $\{\mathcal{B}_q\}_{q=1}^{\infty}$, i_{agg} is a weighted sum of Gaussian random variables and hence is conditionally Gaussian.

4.3.3 Conditional Performance Analysis

According to the Gaussian representation of i_{agg}, the received signal at the intended BS can be expressed as

$$y \overset{d}{=} \sqrt{\rho}\, g_o\, s_o + \underbrace{\sum_{q=1}^{\infty} \sqrt{\mathcal{B}_q} G_q}_{i_{\text{agg}}} + n. \tag{4.11}$$

Since $\{G_q\}_{q=1}^{\infty}$ are independent zero-mean Gaussian random variables, conditioning on $\mathcal{B}_q$, the interference plus noise $(i_{\text{agg}} + n)$ is a zero-mean complex Gaussian random variable. This representation is the key that merges stochastic geometry analysis and the rich literature on the performance analysis in additive white Gaussian noise. That is, since the interference is conditionally Gaussian, the SNR formulas in AWGN channels can be extended to realistic interference environments by deriving the conditional average SINR. In that regard, conditioned on s_o, g_o, and $\{\mathcal{B}_q\}_{q=1}^{\infty}$, the conditionally averaged SINR at the receiving BS is given by

$$\begin{aligned}\Upsilon\left(g_o, \mathcal{B}_q\right) &= \frac{\mathbb{E}_{s_o}\left[\left|\mathbb{E}\left[y \mid g_o, \mathcal{B}_q\right]\right|^2\right]}{\mathbb{E}_{s_o}\left[\mathbb{E}\left(\left|y\right|^2 \mid g_o, \mathcal{B}_q\right) - \left|\mathbb{E}\left(y \mid g_o, \mathcal{B}_q\right)\right|^2\right]} \\ &= \frac{\rho \alpha_o^2}{\mathcal{N}_o}\left[1 + \sum_{q=1}^{\infty} \frac{\mathcal{B}_q \sigma_q^2}{\mathcal{N}_o}\right]^{-1}. \end{aligned} \tag{4.12}$$

Thus, following [98, chapter 9], for any modulation scheme $\mathscr{M}$, the ASEP conditioned on the SINR random vaiable for MLR can be expressed in the form

$$\text{ASEP}(\mathscr{M}|\Upsilon) = \sum_{c=1}^{\mathcal{C}(\mathscr{M})} w_c \int_0^{\mu_c} e^{-\Upsilon \frac{\beta_c}{\sin^2 \vartheta}} \mathrm{d}\vartheta, \tag{4.13}$$

where $\mathcal{C}(\mathscr{M})$ is the number of terms that constitute the ASEP expression for the modulation scheme $\mathscr{M}$, w_c is a modulation-dependent weighting factor, and μ_c and β_c are

modulation-specific parameters. For instance, for M-QAM modulation, $\mathcal{C}(M\text{-QAM}) = 2$, $w_1 = \frac{4}{\pi}\frac{\sqrt{M}-1}{\sqrt{M}}$, $w_2 = -\frac{4}{\pi}\left(\frac{\sqrt{M}-1}{\sqrt{M}}\right)^2$, $\mu_1 = \frac{\pi}{2}$, $\mu_2 = \frac{\pi}{4}$, and $\beta_1 = \beta_2 = \beta = \frac{3}{2(M-1)}$. The unconditional ASEP for single-tier uplink cellular network is obtained via the deconditioning steps detailed in the next subsection.

4.3.4 Deconditioning

By deconditioning (4.13) using the SINR PDF, the resulting expression becomes a function of the SINR MGF which cannot be directly derived. Instead, we use the following identity to express the MGF of the SINR in terms of its CDF [98]

$$\mathcal{M}_{\Upsilon}\left(-z\right) = z\int_0^{\infty} e^{-z\mathrm{y}} F_{\Upsilon}\left(\mathrm{y}\right)\mathrm{dy}. \tag{4.14}$$

The unconditional SINR CDF can be obtained from the following lemma.

Lemma 4.2. *Considering the conditional SINR expressed by (4.12), the unconditional SINR CDF can be written as*

$$F_{\Upsilon}\left(\mathrm{y}\right) = 1 - e^{-\frac{\mathrm{y}\mathcal{N}_o}{\Omega_i \rho}} e^{-\Delta(\mathrm{y})}, \tag{4.15}$$

with

$$\Delta(\mathrm{y}) \;=\; \sum_{\kappa=1}^{M} \frac{\nu\left(\rho,\lambda\right)}{M}\left[{}_1F_1\left(-\frac{1}{b};1-\frac{1}{b};-\mathrm{y}\left|s^{(\kappa)}\right|^2\right)-1\right], \tag{4.16}$$

where ${}_1F_1(a;c;z) = \sum_{q=0}^{\infty}\frac{(a)_q}{(c)_q q!}z^q$ *is the Kummer confluent hypergeometric function [112].*

Proof. See Appendix A.2 □

For the sake of notational convenience, we follow the approach used in [36] and define the integral function $\mathcal{J}_{\Upsilon}(\mu,\beta) = \int_0^{\mu}\frac{\beta}{\sin^2\vartheta}\int_0^{\infty} e^{-\frac{\beta \mathrm{y}}{\sin^2\vartheta}} F_{\Upsilon}\left(y\right)\mathrm{dyd}\vartheta$. Hence, the

ASEP for uplink cellular networks can be characterized from the following theorem.

Theorem 4.1. *Under the assumption of truncated channel inversion power control, and for an arbitrary modulation technique, the ASEP for MLR in the single-tier uplink cellular network depicted in Fig. 4.2 can be expressed in the form*

$$ASEP(\mathscr{M}) = \sum_{c=1}^{\mathcal{C}(\mathscr{M})} w_c \mathcal{J}_{\Upsilon}(\mu_c, \beta_c), \tag{4.17}$$

where $\mathcal{C}(\mathscr{M})$, w_c, μ_c, and β_c are modulation-specific parameters defined in Section 4.3.3. The integral function $\mathcal{J}_{\Upsilon}(\mu, \beta)$ is given by

$$\mathcal{J}_{\Upsilon}(\mu, \beta) = \mu - \int_0^{\infty} \beta \mathcal{Y}(\beta y) \left[e^{-\frac{y\mathcal{N}_o}{\Omega_i \rho}} e^{-\Delta(y)} \right] \mathrm{d}y, \tag{4.18}$$

where $\Delta(y)$ is defined in (4.16) and

$$\mathcal{Y}(\beta y) = \begin{cases} \dfrac{1}{2} e^{-\beta y} \sqrt{\dfrac{\pi}{\beta y}} \left(1 - erf\left(\sqrt{\beta y} \cot \mu \right) \right), & 0 \leq \mu < \dfrac{\pi}{2}, \\ \dfrac{1}{2} e^{-\beta y} \sqrt{\dfrac{\pi}{\beta y}} \left(1 + erf\left(\sqrt{\beta y} \cot \mu \right) \right), & \dfrac{\pi}{2} \leq \mu < \pi. \end{cases} \tag{4.19}$$

Proof. See Appendix A.3. □

4.4 ASEP in Multi-Tier Uplink Cellular network

In this section we extend the above analysis to multi-tier uplink cellular network. Just as in the single-tier case, we will start by characterizing the transmit powers of the interfering UEs from the k^{th} tier with transmit power denoted by $P_{u_i,k} = \rho_k r_{i,k}^{\eta}$,

where $P_{u_i,k} \leq P_U$. The transmit power will have the PDF [47]

$$f_{P_{u_i,k}}(p) = \frac{2\pi\Lambda p^{\frac{1}{b}-1} e^{-\pi\Lambda\left(\frac{p}{\rho_k}\right)^{\frac{1}{b}}}}{2b\left(1 - e^{-\pi\Lambda\left(\frac{P_U}{\rho_k}\right)^{\frac{1}{b}}}\right)}, \tag{4.20}$$

and j^{th} moment

$$\mathbb{E}_{P_{u_i,k}}\left[P_{u_i,k}^{\mathrm{j}}\right] = \frac{\rho_k^{\mathrm{j}}\ \gamma\left(\mathrm{j}b+1, \pi\Lambda\left[\frac{P_U}{\rho_k}\right]^{\frac{1}{b}}\right)}{(\pi\Lambda)^{\mathrm{j}b}\left(1 - e^{-\pi\Lambda\left(\frac{P_U}{\rho_k}\right)^{\frac{1}{b}}}\right)}. \tag{4.21}$$

4.4.1 Interference Characterization

Next, we study the superposition of the interfering signals from the network tiers, denoted by $I_{\text{agg}} = \sum_{k=1}^{K} I_k$. The aggregate interference is a sum of independent interferences and so its characteristic function is given by $\Phi_{I_{\text{agg}}}(|\omega|) = \prod_{k=1}^{K} \Phi_{I_k}(|\omega|)$. The intra-tier (i.e., $k = j$) and inter-tier (i.e., $k \neq j$) interference CF $\Phi_{I_k}(|\omega|)$ are characterized in the following lemma.

Lemma 4.3. *In a multi-tier uplink cellular network under the system model described in Section 4.2, for a Rayleigh fading environment, the CF of the aggregate interference from the k^{th} tier is approximatly given by*

$$\Phi_{I_k}(|\boldsymbol{\omega}|) \approx \exp\left\{-\nu(\rho_k, \lambda_k) \sum_{q=1}^{\infty}\left[\tau_q\left(\left|\boldsymbol{\omega}\right|^2 \rho_k \Omega_k\right)^q \sum_{\kappa=1}^{M} \frac{1}{M}\left|s^{(\kappa)}\right|^{2q}\right]\right\}. \tag{4.22}$$

where, similar to (4.6),

$$\nu(\rho_k, \lambda_k) = \frac{\lambda_k \gamma\left(2, \pi\Lambda\left[\frac{P_U}{\rho_k}\right]^{\frac{1}{b}}\right)}{\Lambda\left(1 - e^{-\pi\Lambda\left(\frac{P_U}{\rho_k}\right)^{\frac{1}{b}}}\right)}, \tag{4.23}$$

and τ_q is the same as in (4.7).

Proof. See Appendix A.4. □

4.4.2 Gaussian Representation

Following the steps of Section 4.3.2, we can represent the inter-tier interference as

$$I_k \overset{d}{=} \underbrace{\sum_{q=1}^{\infty} \sqrt{\mathcal{B}_{q,k}} G_{q,k}}_{i_k}, \tag{4.24}$$

such that $G_{q,k} \sim \mathcal{N}\left(0, \sigma_{q,k}^2\right)$ and $\sigma_{q,k}^2$ is given by

$$\sigma_{q,k}^2 = 4\left[\nu\left(\rho_k, \lambda_k\right) \tau_q \rho_k^q \Omega_k^q \sum_{\kappa=1}^{M} \frac{1}{M} |s^{(\kappa)}|^{2q}\right]^{\frac{1}{q}}. \tag{4.25}$$

By conditioning on $\{\mathcal{B}_{q,k}\}_{q=1}^{\infty}$, i_k is a conditionally Gausian random variable. Consequently, $i_{\text{agg}} = \sum_{k=1}^{K} i_k$ is also conditionally Gaussian.

4.4.3 Conditional Performance Analysis

The received signal at the intended BS can be expressed as

$$y_j \overset{d}{=} \sqrt{\rho_j} s_{o,j} g_{o,j} + \underbrace{\sum_{k=1}^{K} \sum_{q=1}^{\infty} \sqrt{\mathcal{B}_{q,k}} G_{q,k}}_{i_{\text{agg}}} + n. \tag{4.26}$$

We can now lump interference and noise ($i_{\text{agg}} + n$) and represent them as a conditionally complex Gaussian random variable with zero-mean as i_{agg} is a weighted sum of indepenent Gaussian random variables ($G_{q,k}$) when conditioned on $\mathcal{B}_{q,k}$. Then, the

conditionally averaged SINR at the typical receiving BS from tier j is given by

$$\Upsilon_j\left(g_{o,j},\mathcal{B}_{q,k}\right)=\frac{\mathbb{E}_{s_{o,j}}\left[\left|\mathbb{E}\left[y_j\mid g_{o,j},\mathcal{B}_{q,K}\right]\right|^2\right]}{\mathbb{E}_{s_{o,j}}\left[\mathbb{E}\left(\left|y\right|^2\mid g_{o,j},\mathcal{B}_{q,k}\right)-\left|\mathbb{E}\left(y_j\mid g_{o,j},\mathcal{B}_{q,k}\right)\right|^2\right]}$$
$$=\frac{\rho_j\alpha_j^2}{\mathcal{N}_o}\left[1+\sum_{q=1}^{K}\sum_{k=1}^{\infty}\frac{\mathcal{B}_{q,k}\sigma_{q,k}^2}{\mathcal{N}_o}\right]^{-1}. \tag{4.27}$$

From [98, chapter 8], and similar to the single-tier scenario, the ASEP, in the j^{th} tier, conditioned on the SINR random variable for any modulation scheme $\mathscr{M}$, and employing a MLR, can be represented by

$$\text{ASEP}_j(\mathscr{M}|\Upsilon_j)=\sum_{c=1}^{\mathcal{C}(\mathscr{M})}w_c\int_0^{\mu_c}e^{-\Upsilon_j\frac{\beta_c}{\sin^2\vartheta}}\mathrm{d}\vartheta, \tag{4.28}$$

where $\mathcal{C}(\mathscr{M})$, w_c, and μ_c and β_c are defined in subsection 4.3.3. Next, we carry out the deconditioning step to obtain the unconditional ASEP for the multi-tier uplink cellular network.

4.4.4 Deconditioning

By exploiting the relationship (4.14) transforming the MGF to the CDF, we obtain the unconditional SINR CDF in the following lemma.

Lemma 4.4. *Considering the conditional SINR expressed by (4.12), the unconditional SINR CDF can be written as*

$$F_{\Upsilon_j}\left(\mathrm{y}\right)=1-e^{-\frac{\mathrm{y}\mathcal{N}_o}{\Omega_j\rho_j}}e^{-\sum_{k=1}^{K}\Delta(y,k)}, \tag{4.29}$$

where

$$\Delta(\mathrm{y},k)=\sum_{\kappa=1}^{M}\frac{\nu\left(\rho_k,\lambda_k\right)}{M}\left[{}_1F_1\left(-\frac{1}{b};1-\frac{1}{b};-\mathrm{y}\left|s^{(\kappa)}\right|^2\right)-1\right], \tag{4.30}$$

Proof. See Appendix A.3. □

The following theorem characterizes the ASEP in multi-tier uplink cellular networks.

Theorem 4.2. *In a multi-tier cellular network, assuming truncated channel inversion power control, and for an arbitrary modulation technique, the ASEP for MLR for a generic user in tier j, using an arbitrary modulation scheme $\mathscr{M}$, can be expressed in the form*

$$ASEP_j(\mathscr{M}) = \sum_{c=1}^{\mathcal{C}(\mathscr{M})} w_c \mathcal{J}_{\Upsilon_j}(\mu_c, \beta_c). \tag{4.31}$$

The integral function $\mathcal{J}_{\Upsilon_j}(\mu, \beta)$ is given by

$$\mathcal{J}_{\Upsilon_j}(\mu, \beta) = \mu - \int_0^{\infty} \beta \mathcal{Y}(\beta \mathrm{y}) \left[e^{-\frac{\mathrm{y}\mathcal{N}_o}{\Omega_j \rho_j}} e^{-\sum_{k=1}^{K} \Delta(\mathrm{y},k)} \right] \mathrm{dy}. \tag{4.32}$$

As a consequence, the ASEP for a generic user in a generic tier is given by

$$ASEP(\mathscr{M}) = \sum_{j=1}^{K} \frac{\lambda_j}{\Lambda} ASEP_j(\mathscr{M}) \tag{4.33}$$

Proof. See Appendix A.6 □

The ASEP result in (4.33) has the following alternative interpretations;

(i) the SEP averaged over all UEs in all tiers;

(ii) the ASEP achieved by a randomly selected UE in the network;

(iii) the average error probability of all symbols communicated within the cellular network.

The validity of the proposed analytical model is verified in the next section via Monte Carlo simulations.

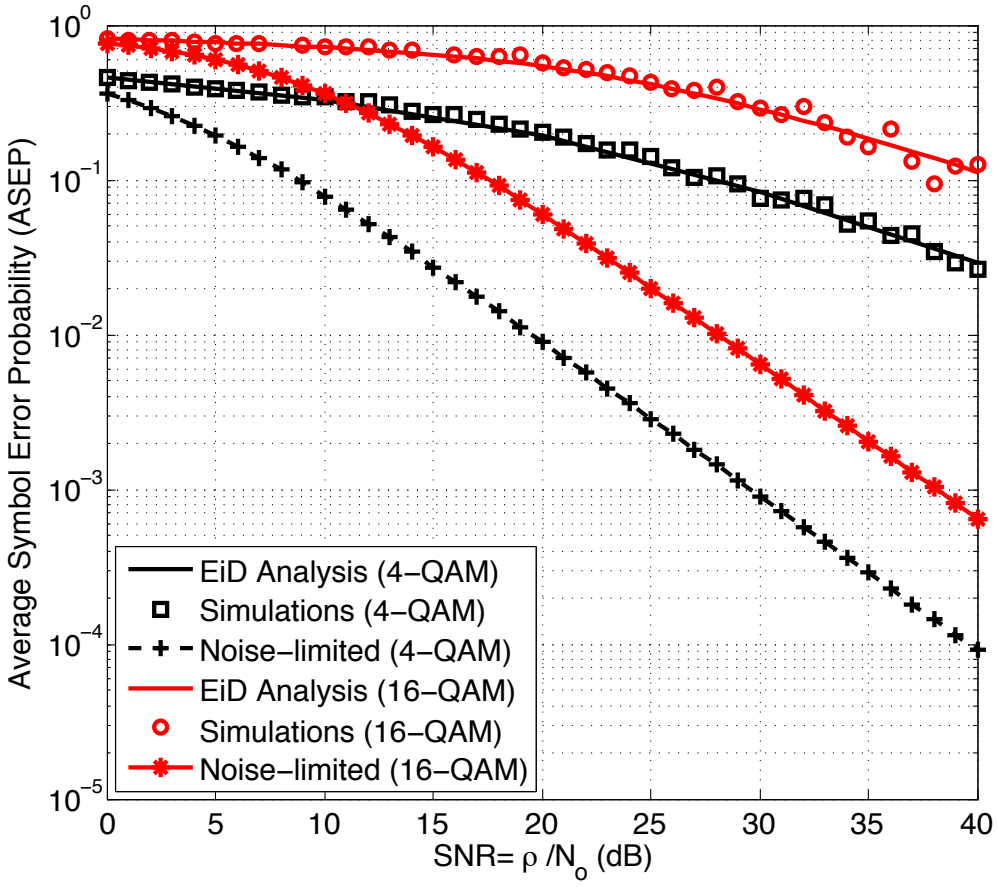

Figure 4.3: Average symbol error probability for 4-QAM and 16-QAM modulated signals versus the Signal-to-Noise ratio (SNR) at the receiving BS.

4.5 Simulation Results

In this section, we verify via Monte Carlo simulations the validity of the proposed EiD approach in the depicted uplink scenario with truncated channel inversion power control. For simplicity, we assume that all tiers have the same average received power threshold $\rho_k = \rho, \forall k$. Analytically, such scenario is equivalent to a single-tier cellular network, which is the numerically simulated case.

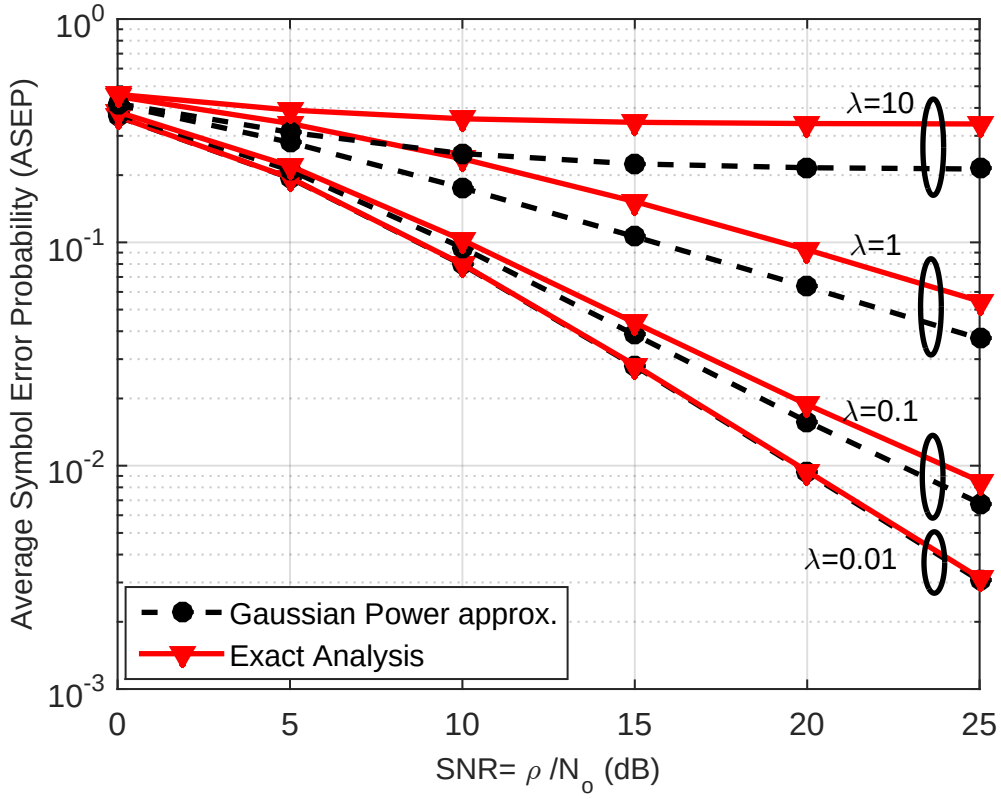

Figure 4.4: Average symbol error probability for 4-QAM modulated signals versus the Signal-to-Noise ratio (SNR) at the receiving BS for Gaussian distributed aggregate interference and that characterized via the adopted EiD approach.

4.5.1 Simulation Setup

The simulation parameters are as follows. The path-loss exponent $\eta = 4$, the noise power $\mathcal{N}_o = -90$ dBm, the users intensity $\lambda_u = 10$ UEs/km^2, the BSs intensity $\lambda_1 = \lambda = 3$ BSs/km^2, the mean channel (power) gain $\Omega_k = \Omega = 1$, $\forall k$ and the maximum transmit power $P_U = 1$ W. The symbols are modulated using square quadrature amplitude modulation (QAM), with a constellation size $M \in \{4, 16\}$. Without loss of generality, we assume that both the desired and interfering signals are modulated by the same modulation technique. However, the framework presented holds for interfering UEs using different modulation schemes. In each simulation run, we realize the cellular network by distributing the BSs and users according to two independent

PPPs with intensities λ and λ_u, respectively. Each user is associated to its nearest BS if and only if (a) it can invert its path-loss to its nearest BS, and (b) its nearest BS is not serving another user. Hence, we end up with a maximum of one active user per BS. In each network realization, each active user sends 1000 symbols to its serving BS over independent Rayleigh channels, where the channel gain remains fixed over the symbol duration but changes from one symbol to another. We then compute the average symbol error probability for the test BS and repeat the simulation for 10000 times. Note that, there are two different time scales for the system setup variations. The first time scale is for the fast variation of the fading channels that are averaged over for the same (fixed) network realization. The second time scale is for the variation of the network topology, and by averaging over the randomized network topology, a spatially averaged performance is obtained. Therefore, by considering only the first time scale, a realization-dependent performance is computed, which can also be beneficial for fixed network realizations.

Fig. 4.3 shows the ASEP versus the received SNR, in which we change ρ while keeping $\mathcal{N}_o$ constant to vary the SNR, for 4-QAM and 16-QAM modulation schemes. The figure validates our analysis as the simulation results match the analytic expressions derived for the uplink cellular network. Furthermore, we show the noise-limited (i.e., interference-free) ASEP curves in order to visualize the interference effect on the MLR performance. The performance gap between the noise-limited and the derived expressions for the ASEP represents the performance degradation of the MLR due to uplink aggregate interference. It also shows that the ASEP has a lower decay rate with ρ in the depicted scenario when compared to the noise-limited regime. This is due to the fact that increasing ρ does not only improve the intended received signal strength at the test BS, but also aggravates the uplink aggregate interference. That is, a higher ρ requires a higher transmit power from the UEs, due to the employed truncated channel inversion power control, which increases the inter-cell interference.

In Fig. 4.4 we compare the performance of the developed interference characterization with that of Gaussian interference with variance $\sigma^2_{I_{\text{agg}}} = -\Phi''_{I_{\text{agg}}}(|\boldsymbol{\omega}| = 0) = \frac{\nu(\rho,\lambda)\rho\Omega}{2b-2}$, where $\Phi''_{I_{\text{agg}}}(|\boldsymbol{\omega}|)$ is the second derivative of the interference characteristic function in (4.5). The reported results show that as the intensity of interferers increases, the performance of the Gaussian approximation deviates from the proposed unconditional interference characterization. This is owing to the fact that few interferers, which are close to the test BS, dominate the aggregate interference, which renders the central limit theorem (CLT) approximation inapplicable and violates the Gaussian assumption. Note that for low intensity of BSs, the ASEP performance is dominated by the noise power and the performance gap is unnoticeable. However, as the intensity of BSs increases, the interference becomes more prominent and the gap becomes more distinguishable.

4.6 Chapter Summary

4.6.1 EiD Approach outline

This section summarizes the outline of the EiD approach. In this approach, the complex aggregate interference signal I_{agg} is first characterized by its CF, which is then exploited to obtain the conditional Gaussian representation of I_{agg}. This is achieved via an infinite sum of randomly scaled zero-mean Gaussian random variables. Matching CFs directly implies EiD, since two random variables are said to be equal in distribution if they have the same CFs. The Gaussian representation of I_{agg} enables the legitimate use of performance expressions available in the AWGN channel literature. However, these expressions have to be deconditioned over the infinite series of random variables $\mathcal{B}_q$. Further, as the EiD approach accounts for every transmitted symbol by each interferer, the expression for the CF of I_{agg} contains $\mathbb{E}[f(\mathcal{Z})]$, where $f(\cdot)$ is a function that depends on the network parameters (e.g., path loss exponent, MIMO setup) and $\mathcal{Z}$ is a random variable denoting the symbol transmitted by a

generic interferer.

4.6.2 Conclusion and Future work

In this chapter we develop an analytical paradigm to analyze the average symbol error probability performance of uplink traffic in a single and multi-tier cellular network with power control. The developed EiD approach is critically beneficial for studying network performance in realistic interference environments as it utilizes stochastic geometric tools to account for the network geometry in the performance characterization. Contrary to other stochastic geometry models adopted in the literature, the developed analysis accounts for important communication system parameters and goes beyond signal-to-interference-plus-noise ratio characterization. That is, the presented model accounts for the modulation scheme, constellation type, and signal recovery techniques to model the ASEP. To this end, we derive single integral expressions for the ASEP for different modulation schemes due to aggregate network interference. Finally, Monte Carlo simulation results demonstrate the accuracy of the analytic error probability parametric expressions for square M-QAM modulated signals and under maximum average received signal power BS association policy. We also compare the performance of the interference characterization derived herein to that of the commonly used Gaussian interference power approximation.

In this chapter, the developed model statistically accounts for the transmitted symbols from each interferer, which highly complicates the analysis. In the next chapter, we present an approximate framework that is able to capture detailed communication system aspects as the EiD model, but with much simpler analysis. The proposed model in the next chapter neither has infinite random variable series to decondition on (i.e., $\mathcal{B}_q$) nor does it need to evaluate the expectation $\mathbb{E}\left[f(\mathcal{Z})\right]$, which significantly simplifies the analysis, while maintaining the model accuracy. We next focus on the Gaussian signaling approach to study the approximate ASEP perfor-

mance in downlink and uplink cellular networks, and investigate the accuracy of such approximation.

Chapter 5

The Influence of Gaussian Signaling Approximation on the SINR Model

5.1 Introduction

Chapter 4, extended the new EiD paradigm developed in [36,37,113], to capture more system details and extend the stochastic geometry analysis for cellular networks to tangible error performance metrics (e.g., symbol error probability). However, the analysis associated with the EiD approach is involved as it statistically accounts for the transmitted symbol from each interferer, which can be a BS in the downlink or user equipment (UE) in the uplink. Further, the EiD approach requires baseband signal analysis to calculate the characteristic function of the probability density function (CF) of the complex interference amplitude, which is non-trivial to compute in advanced system models [37].

This chapter presents an approximate framework that is able to capture detailed communication system aspects just like the EiD, but with much simpler analysis. This is achieved by approximating the interferers' transmitted symbols by Gaussian codebooks [40, 41, 114]. Such approximation alleviates the baseband analysis of the EiD approach and thus facilitates the analysis steps. Further, it results in less computationally intensive expressions than the EiD approach and it only requires the computation of the LT of the interference power[1]. The accuracy of the proposed approximation is verified against the exact EiD approach. It is worth mentioning that

[1]The LT of the interference is equivalent to the moment generating function but with a negative argument.

the proposed approximation aligns the error performance analysis with the outage and ergodic rate calculation in the literature, as all require the LT of the interference power only. As discussed earlier in Chpater 4, the main problem is that the ASEP expressions available in the literature are only legitimate for AWGN or Gaussian interference channels [98, chapter 8], which is not the case in cellular networks [13]. Therefore, both the EiD and the proposed analysis rely on the conditionally Gaussian interference representation, in order to utilize the conventional SINR model.

Interferers' symbols are hereafter abstracted and approximated by a Gaussian signal $\tilde{s}_i$ with unit power spectral density. Note that the Gaussian interfering symbols are the core assumption that discriminates the proposed framework in this chapter from the EiD approach, which accounts for the interferers' transmitted symbols.

5.2 Proposed ASEP Analysis

In order to derive the ASEP expressions via the porposed framework, we follow the baseline system model described in Chapter 3 for a single-tier SISO cellular network. Due to the Gaussian codebook assumption for the interfering signals (i.e., $\tilde{s}_i \sim \mathcal{CN}(0,1)$), the aggregate interference in (3.2) is conditionally Gaussian (i.e., conditioned on r_o, P_i, g_i and r_i $\forall i$). Note that, in the uplink scenario, $P_i = P_{u_i}$ is the random variable representing the adaptive transmit power of the i^{th} UE under the assumed truncated channel inversion power control [47], as explained in Chapters 3 and 4. On the other hand, $P_i = P$ is constant in the downlink model, and thus we no longer need to condition the SINR on the transmit power. The general received signal model is expressed as

$$y \approx \sqrt{P_o}\, r_o^{-\frac{\eta}{2}} g_o s_o + \sum_{r_i \in \tilde{\Psi}} \sqrt{P_i} r_i^{-\frac{\eta}{2}} g_i \tilde{s}_i + n, \tag{5.1}$$

Let $\tilde{g}_o = |g_o|^2$ and $\tilde{g}_i = |g_i|^2$. For a Nakagami-m fading environment, with integer m, then $\tilde{g}_o$ and $\tilde{g}_i$ follow the gamma distributions $\tilde{g}_o \sim \text{Gamma}\,(m_o, \Omega_o)$ and $\tilde{g}_i \sim \text{Gamma}\,(m_i, \Omega_i)$. Accordingly, the conditionally averaged SISO-SINR model is represented as

$$\Upsilon\left(\tilde{g}_o, r_o, P_i, \tilde{g}_i, r_i\right) = \frac{P_o r_o^{-\eta} \tilde{g}_o}{\sum_{r_i \in \tilde{\Psi}} P_i r_i^{-\eta} \tilde{g}_i + \mathcal{N}_o}, \tag{5.2}$$

where $\sum_{r_i \in \tilde{\Psi}} P_i r_i^{-\eta} \tilde{g}_i$ represents the aggregate network interference power which we hereafter denote as $\mathcal{I}_D$ and $\mathcal{I}_U$ for the downlink and uplink scenarios, respectively, resulting from the set of interferers $\tilde{\Psi}$.

Since Υ is averaged over a zero-mean conditionally Gaussian aggregate interference signal, we can utilize the ASEP performance in AWGN channels expressions. In this case, following [98, chapter 8], for square quadrature amplitude modulation scheme, i.e., M-QAM, the conditional ASEP is written as

$$\text{ASEP}(M\text{-QAM}|\Upsilon) = w_1 \text{erfc}\left(\sqrt{\beta\Upsilon}\right) + w_2 \text{erfc}^2\left(\sqrt{\beta\Upsilon}\right), \tag{5.3}$$

where $w_1 = 2\frac{\sqrt{M}-1}{\sqrt{M}}$, $w_2 = -\left(\frac{\sqrt{M}-1}{\sqrt{M}}\right)^2$, and $\beta = \frac{3}{2(M-1)}$. The unconditional ASEP is then obtained by averaging over the random variables $\{\tilde{g}_o, r_o, P_i, \tilde{g}_i, r_i\}$.

To facilitate the deconditioning step, we utilize the folowing expressions derived in [40]

$$\mathbb{E}\left[\text{erfc}\left(\sqrt{\frac{\text{aY}}{X+C}}\right)\right] = 1 - \frac{\Gamma(m_o+\frac{1}{2})}{\Gamma(m_o)}\frac{2}{\pi}\int_0^\infty \frac{1}{\sqrt{z}}\, e^{-z\left(1+\frac{m_o C}{\text{a}\Omega_\text{o}}\right)}{}_1F_1\left(1-m_o; \frac{3}{2}, z\right)\mathcal{L}_X\left(\frac{m_o z}{\text{a}\Omega_\text{o}}\right)\text{d}z, \tag{5.4}$$

and

$$\mathbb{E}\left[\mathrm{erfc}^2\left(\sqrt{\frac{\mathrm{aY}}{X+C}}\right)\right] = 1 - \frac{4m_o}{\pi}\int_0^{\infty} e^{-z\frac{m_o C}{\mathrm{a}\Omega_\mathrm{o}}}\mathcal{L}_X\left(\frac{m_o z}{\mathrm{a}\Omega_\mathrm{o}}\right)\int_0^{\frac{\pi}{4}} {}_1F_1\left(m_o+1;2,\frac{-z}{\sin^2\vartheta}\right)\frac{\mathrm{d}\vartheta}{\sin^2\vartheta}\mathrm{d}\vartheta\mathrm{d}z, \tag{5.5}$$

where $Y \sim \mathrm{Gamma}(m_o, \Omega_o)$ follows a Gamma distribution, X has an arbitrary distribution with LT $\mathcal{L}_X(\cdot)$, C is constant, a is a scaling factor, and ${}_1F_1(a;c;z) = \sum_{q=0}^{\infty}\frac{(a)_q z^q}{(c)_q q!}$ is the Kummer confluent hypergeometric function [112]. Note that (5.4) and (5.5) are only valid for integer m_o. Projecting back to the SINR expressions in (5.3), we can see that $Y = \tilde{g}_o$, $X = \mathcal{I}$ (whether $\mathcal{I}_D$ for the downlink or $\mathcal{I}_U$ for the uplink) and $C = \mathcal{N}_o$. Next, it is essential to characterize the LT of the aggregate interference for both the downlink and uplink cases. Generally, the LT of the interference from a PPP can be written as [17]

$$\mathcal{L}_X(z) = \exp\left\{-2\pi\lambda\int_t^{\infty}\mathbb{E}\left[1-e^{-zx^{-\eta}\tilde{g}}\right]x\mathrm{d}x\right\} \tag{5.6}$$

such that (5.6) is obtained by utilizing the probability generating functional (PGFL) of the interfering PPP [17]. The above analysis is unified for both the downlink and uplink scenarios. In what follows we discuss in details the analysis steps for each case separately.

5.2.1 ASEP in the Downlink Scenario

In order to derive the LT of the aggregate interference given in (5.6), we first let the limit of the integral $t = r_o$, since $r_i > r_o, \forall i$. Then, the LT of the aggregate network interfernce in the downlink $\mathcal{I}_D$, is characterized by the following lemma.

Lemma 5.1. *Conditioned on r_o, the aggregate interference power affecting a receiver located r_o meters away in a downlink cellular network under Nakagami-m fading has*

the LT given by

$$\mathcal{L}_{\mathcal{I}_D|r_o}(z) = \exp\left\{-\pi\lambda r_o^2\left[\left({}_2F_1\left(\frac{-1}{b}, m_i; 1-\frac{1}{b}; -z\Omega_i P r_o^{-\eta}\right)-1\right)\right]\right\}, \tag{5.7}$$

where ${}_2F_1(\cdot,\cdot;\cdot;\cdot)$ *is the Gauss hypergeometric function [112].*

Proof. See Appendix B.1 □

By using the above lemma, we can derive the ASEP expression for the downlink scenario, which is summarized in the following theorem.

Theorem 5.1. *For the described system model, under Nakagami-m fading environment and arbitrary path-loss exponent η, for M-QAM modulated signals in the downlink, the ASEP expression is approximated by*

$$\begin{aligned}\mathrm{ASEP}_{\mathrm{DL}} \approx w_1\Bigg[1-\frac{\Gamma\left(m_o+\frac{1}{2}\right)}{\Gamma(m_o)}\frac{2}{\pi}\int_0^\infty\int_0^\infty 2\pi\lambda_B x e^{-\pi\lambda_B x^2}\frac{1}{\sqrt{z}}e^{-z\left(1+\frac{m_o\mathcal{N}_o x^\eta}{\Omega_o\beta P}\right)} \\ \times {}_1F_1\left(1-m_o;\frac{3}{2};z\right)\cdot\mathcal{L}_{\mathcal{I}_D|x}\left(\frac{m_o z x^\eta}{\Omega_o\beta P}\right)\mathrm{d}x\mathrm{d}z\Bigg] \\ + w_2\Bigg[1-\frac{4m_o}{\pi}\int_0^\infty\int_0^\infty 2\pi\lambda_B x e^{-\pi\lambda_B x^2}e^{-z\left(\frac{m_o\mathcal{N}_o x^\eta}{\Omega_o\beta P}\right)} \\ \times\int_0^{\frac{\pi}{4}} {}_1F_1\left(m_o+1;2;\frac{-z}{sin^2\vartheta}\right)\frac{1}{sin^2\vartheta}\cdot\mathcal{L}_{\mathcal{I}_D|x}\left(\frac{m_o z x^\eta}{\Omega_o\beta P}\right)\mathrm{d}\vartheta\mathrm{d}x\mathrm{d}z\Bigg].\end{aligned} \tag{5.8}$$

Corollary 5.1. *The* ASEP *expressions in a Rayleigh fading environment, (i.e., $m_o = 1, m_i = 1$), with a path-loss exponent $\eta = 4$, is further simplified into*

$$\mathrm{ASEP}_{\mathrm{DL}} \approx \sum_{c=1}^{2} w_c\left(1-\int_0^\infty \Xi(z)\frac{\lambda_B c\,\mathrm{erfc}\left(\sqrt{z}1_{\{c=2\}}\right)e^{-z}}{\sqrt{\pi z}}\mathrm{d}z\right) \tag{5.9}$$

such that $\Xi(z) = \frac{1}{2}\sqrt{\frac{\pi}{\mathfrak{v}}}\exp\left\{\frac{\mathfrak{u}^2}{4\mathfrak{v}}\right\}erfc\left(\frac{\mathfrak{u}}{2\sqrt{\mathfrak{v}}}\right)$, $\mathfrak{u} = \pi\lambda\left[\sqrt{\frac{z}{\beta}}\arctan\left(\sqrt{\frac{z}{\beta}}\right)+1\right]$ *and* $\mathfrak{v} = \frac{z\mathcal{N}_o}{P\beta}$.

Proof. With the aid of the integral

$$\int_0^\infty e^{-\mathfrak{u}k} e^{-\mathfrak{v}k^2} \mathrm{d}k = \frac{1}{2}\sqrt{\frac{\pi}{\mathfrak{v}}} \exp\left(\frac{\mathfrak{u}^2}{4\mathfrak{v}}\right) \operatorname{erfc}\left(\frac{\mathfrak{u}}{2\sqrt{\mathfrak{v}}}\right), \tag{5.10}$$

we can obtain the unconditional $\mathrm{ASEP}_{\mathrm{DL}}$ in (5.9) by inserting (5.4), (5.5) and (5.7) into (5.3) and averaging over the aforementioned Rayleigh distance distribution. □

5.2.2 ASEP in the Uplink Scenario

To derive the ASEP for the uplink scenario, we start first from the LT expression in (5.6)which is an approximation as the set of interfering UEs does not constitute a PPP. Under the truncated channel inversion power control, the lower limit of the integral from (5.6) is given by $t = \left(\frac{P_{u_i}}{\rho}\right)^{\frac{1}{\eta}}$ since $r_i > r_o \left(\frac{P_{u_i}}{P_o}\right)^{\frac{1}{\eta}}$. The aggregate interference power in the uplink denoted by $\mathcal{I}_U$ has the LT characterized via the following lemma.

Lemma 5.2. *In a single-tier SISO uplink cellular network, the aggregate interference power LT in Nakagami-m fading environment can be approximated by*

$$\mathcal{L}_{\mathcal{I}_U}(z) \approx \exp\left\{-\nu(\rho,\lambda)\left[\left({}_2F_1\left(\frac{-1}{b}, m_i; 1-\frac{1}{b}; -z\rho\Omega_i\right) - 1\right)\right]\right\}, \tag{5.11}$$

where $\nu(\rho,\lambda) = \frac{\gamma\left(2,\pi\lambda\left[\frac{P_u}{\rho}\right]^{\frac{1}{b}}\right)}{1-e^{-\pi\lambda\left(\frac{P_u}{\rho}\right)^{\frac{1}{b}}}}$, *and* $\gamma(a,c) = \int_0^c t^{a-1}e^{-t}\mathrm{d}t$ *is the lower incomplete gamma function [112].*

Proof. See Appendix B.2 □

We can now state the following theorem about the ASEP of the uplink scenario.

Theorem 5.2. *Under the system model being studied, in Nakagami-m fading environment and M-QAM modulated signals in an uplink transmission scenario employing*

truncated channel inversion power control, the ASEP expression is approximated by

$$\begin{aligned}\mathrm{ASEP}_{\mathrm{UL}} \approx w_1 \left[1 - \frac{\Gamma\left(m_o + \frac{1}{2}\right)}{\Gamma\left(m_o\right)} \frac{2}{\pi} \int_0^{\infty} \frac{1}{\sqrt{z}} e^{-z\left(1+\frac{m_o \mathcal{N}_o}{\Omega_o \beta \rho}\right)} \, {}_1F_1\left(1 - m_o; \frac{3}{2}; z\right) \cdot \mathcal{L}_{\mathcal{I}_U}\left(\frac{m_o z}{\Omega_o \beta \rho}\right) \mathrm{d}z\right] \\ + w_2 \left[1 - \frac{4m_o}{\pi} \int_0^{\infty} e^{-z\left(\frac{m_o \mathcal{N}_o}{\Omega_o \beta \rho}\right)} \int_0^{\frac{\pi}{4}} {}_1F_1\left(m_o + 1; 2; \frac{-z}{sin^2\vartheta}\right) \frac{1}{sin^2\vartheta} \cdot \mathcal{L}_{\mathcal{I}_U}\left(\frac{m_o z}{\Omega_o \beta \rho}\right) \mathrm{d}\vartheta \mathrm{d}z\right].\end{aligned} \tag{5.12}$$

Corollary 5.2. *In a Rayleigh fading environment, with $m_o = m_i = 1$, and for the special case of $\eta = 4$, the uplink ASEP expressions are simplified to*

$$\mathrm{ASEP}_{\mathrm{UL}} \approx \sum_{c=1}^{2} w_c \left(1 - \int_0^{\infty} \frac{c \, \mathrm{erfc}\left(\sqrt{z} 1_{\{c=2\}}\right) e^{-z\left(1+\frac{\mathcal{N}_o}{\rho\beta}\right)}}{\sqrt{\pi z}} \exp\left\{-\nu\left(\rho, \lambda\right) \sqrt{\frac{z}{\beta}} \arctan\left(\sqrt{\frac{z}{\beta}}\right)\right\} \mathrm{d}z\right) \tag{5.13}$$

Proof. We directly plug (5.4), (5.5), and (5.11) into (5.3) to obtain $\mathrm{ASEP}_{\mathrm{UL}}$. □

A noteworthy observation to be highlighted is that the Gaussian approximation does not reduce the number of integrals required to calculate the ASEP when compared to the EiD approach in [36, 113]. Nevertheless, it reduces the number of hypergeometric functions inside the exponential function to only one hypergeometric function for any constellation size (c.f. (5.8) and (5.12)) for M-QAM modulation, which significantly reduces the computational complexity. As evident from Table 5.1, the proposed Gaussian codebooks anaylsis significantly decreases the computational complexity of the EiD appraoch. Particularly, the proposed analysis, for the special case of $\eta = 4$ and Rayleigh fading environments, the ASEP expressions give a single-integral of some elementary functions (i.e., $\arctan(\cdot)$) which substantially reduces the computational complexity. Even for the case of general path-loss and Nakagami-m fading, the ASEP expressions by the proposed approach still take a simpler form. Note that, in some cases (e.g., phase-shift-keying (PSK)) the EiD-based ASEP expressions

Adopted Approach	Uplink Transmission	Downlink Transmission
EiD	156.92 (secs)	7327.374 (secs)
Gaussian Signaling ($m_o = m_i = 1$)	0.005245 (secs)	0.3369 (secs)

Table 5.1: Runtime for the EiD and Gaussian Signaling approaches

already have only one hypergeometric function. Though the Gaussian approximation has no effect on the number of hypergeometric functions in this case, it still represents a unified framework and provides a consistent methodology for studying more complex setups.

5.3 Numerical Results

In this section, we verify the proposed analysis against the exact EiD approach in the depicted downlink and uplink scenarios. For the downlink, we vary the BS transmit powers (P) while keeping $\mathcal{N}_o$ constant to vary the transmit SNR, while for the uplink we change ρ against $\mathcal{N}_o$. The network parameters are selected as follows, the path-loss exponent $\eta = 4$, the noise power $\mathcal{N}_o = -90$ dBm, the UEs intensity $\lambda_u = 10$ UEs/km^2, the BSs intensity $\lambda_B = \lambda = 3$ BSs/km^2, and the maximum transmit power $P_U = 1$ W. Note that the effective intensity of the interfering UEs is that of the serving BSs in the resource block of interest, i.e. λ. The desired symbols are modulated using square quadrature amplitude modulation (QAM) scheme, with a constellation size $M \in \{4, 16\}$.

Figs. 5.1 and 5.2 show the ASEP versus $\frac{P}{\mathcal{N}_o}$, for various Nakagami-m fading environments in the downlink scenario under 4-QAM and 16-QAM modulated signals, respectively. In Figs. 5.3 and 5.4, we plot the ASEP performance for the uplink transmission versus the received SNR for different Nakagami-m fading environments, for 4-QAM and 16-QAM modulation, respectively. Indeed, the proposed Gaussian approximation yields very accurate error performance for the system model under

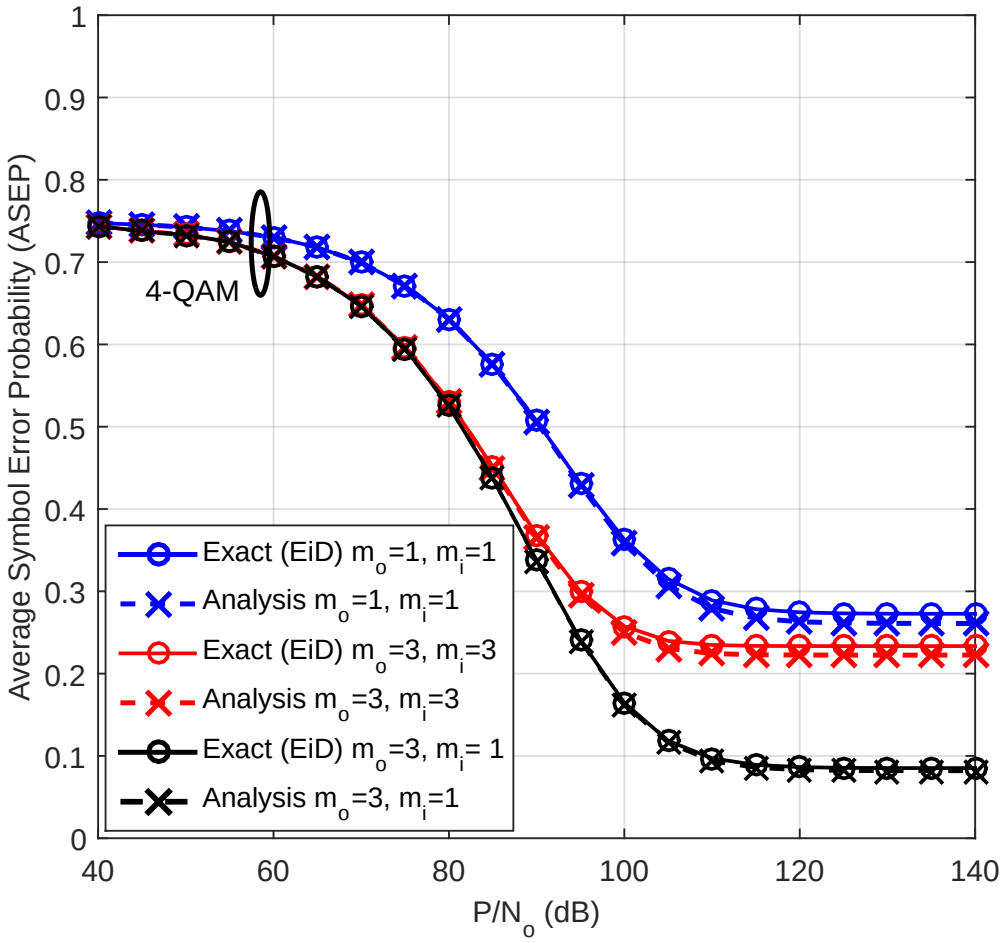

Figure 5.1: ASEP versus the received Signal-to-Noise ratio (SNR) for 4-QAM modulated signals in the downlink.

study when compared to the exact EiD analysis. Therefore, the numerical results are in favor of the proposed approach in terms of accuracy while being computationally much less complex than the EiD approach.

5.4 Chapter Summary and Conclusions

This chapter presents a simple unified framework for the average symbol error performance in cellular networks. The proposed model provides an approximate, yet accurate, framework, that is also able to capture fine wireless communication details

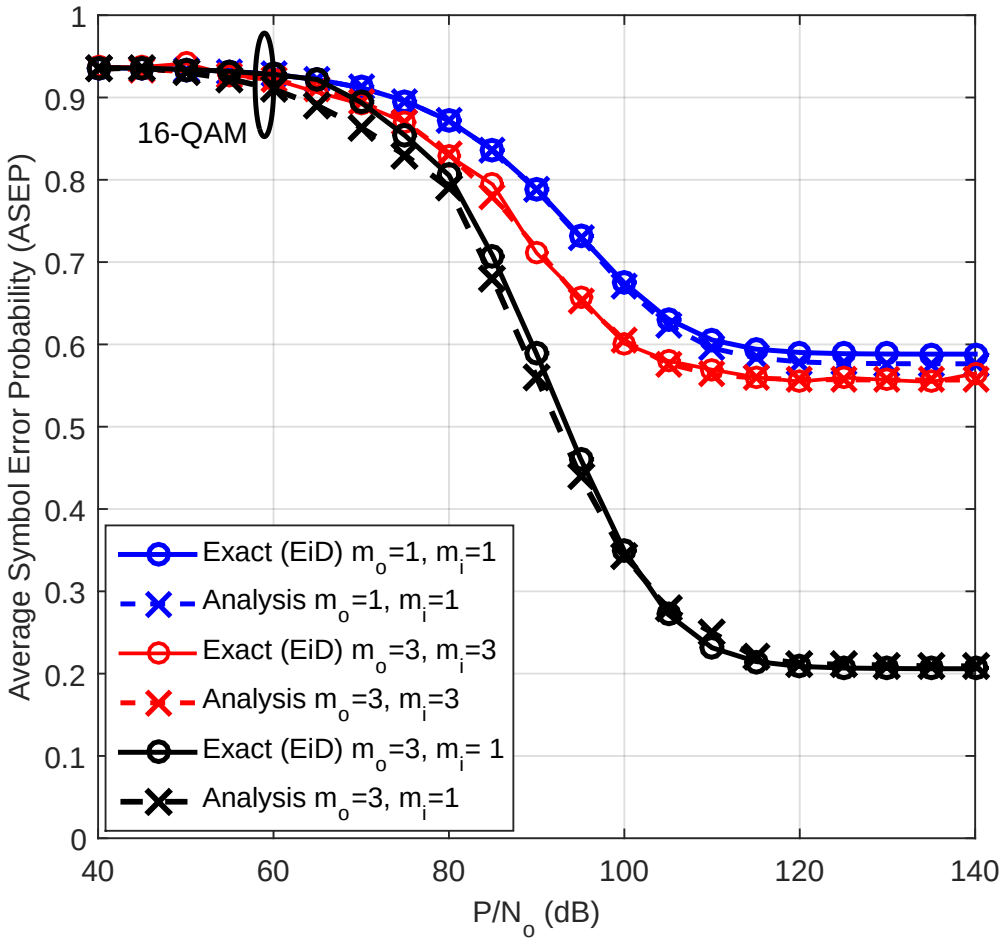

Figure 5.2: ASEP versus the received Signal-to-Noise ratio (SNR) for 16-QAM modulated signals in the downlink.

similar to the EiD approach, but with much simpler analysis. Moreover, the proposed approach is critically beneficial for studying network performance in realistic interference environments. Although the number of integrals in the ASEP expressions is not reduced when compared to the EiD approach, this approach alleviates the baseband analysis and aligns it with the stochastic geometry literature. The analytic and computational complexity is substantially reduced while maintaining the accuracy and generality of the EiD framework. The presented model is applied to downlink and uplink scenarios of single-tier cellular SISO networks.

In the next chapter, we extend the developed model to arbitrary MIMO antenna

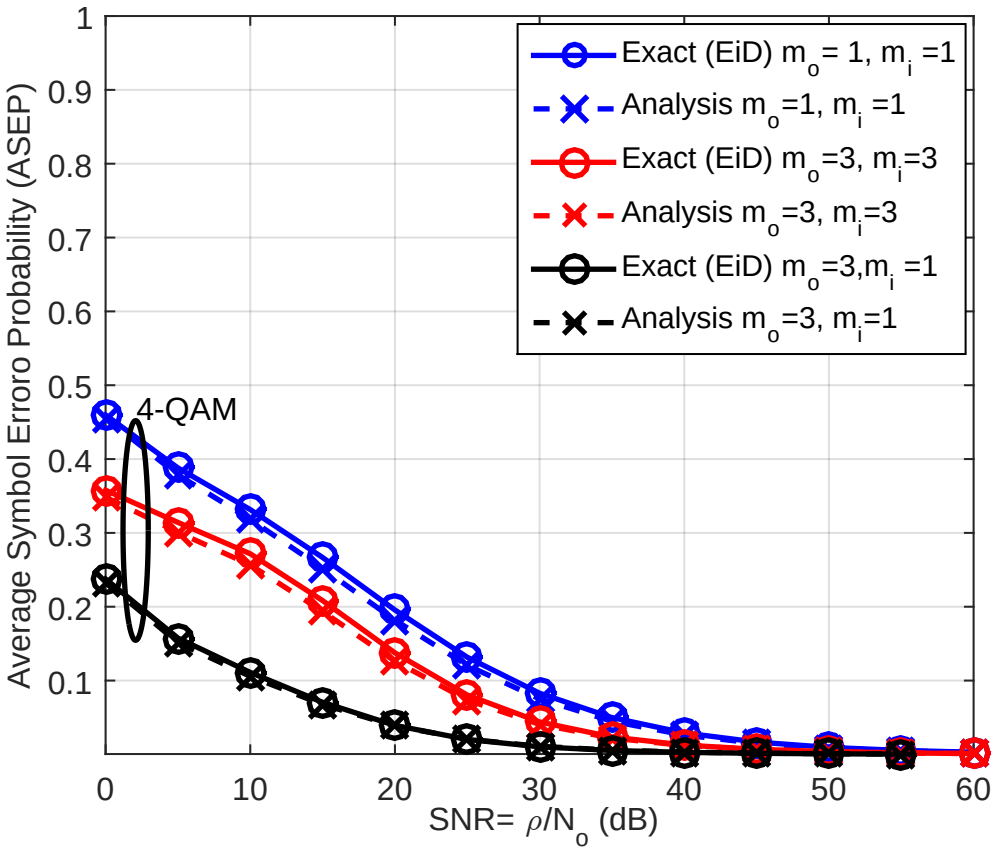

Figure 5.3: ASEP versus the received Signal-to-Noise ratio (SNR) for 4-QAM modulated signals in the uplink.

configurations in more complex setups.

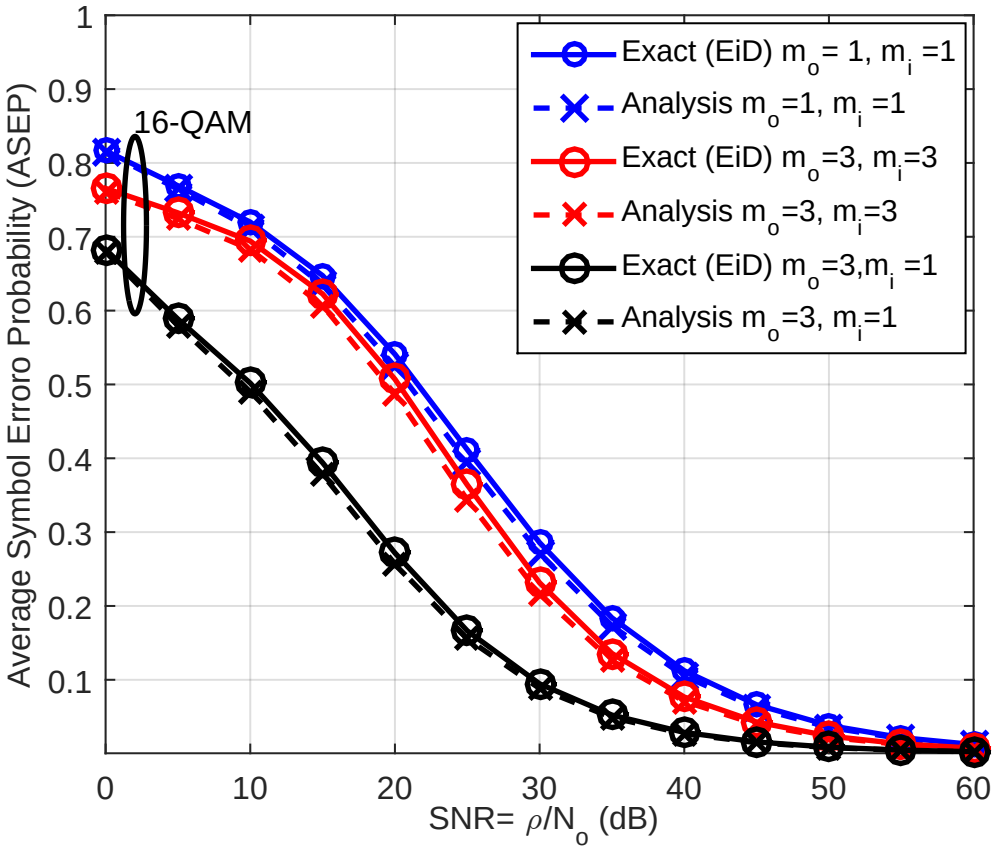

Figure 5.4: ASEP versus the received Signal-to-Noise ratio (SNR) fo 16-QAM modulated signals in the uplink.

Chapter 6

Unified Performance Analysis for Downlink MIMO networks

6.1 Introduction

This chapter presents a unified mathematical paradigm, based on Stochastic Geometry, for downlink cellular networks with multiple-input-multiple-output (MIMO) BSs. The developed paradigm presents twofold analysis unification for MIMO cellular networks literature. First, it integrates the tangible decoding error probability and the abstracted (i.e., modulation scheme and receiver type agnostic) outage probability analysis, which are largely disjoint in the literature. Second, it unifies the analysis for different MIMO configurations. The unified MIMO analysis provides an equivalent SISO representation for the per-data stream SINR in MIMO cellular networks. To this end, we discuss the diversity-multiplexing tradeoff imposed by different MIMO schemes. Moroever, several design insights are highlighted based on the proposed unified framework.

It is worth noting that the SISO-SINR representation used in this chapter is used to study OSTBC in [24, 106, 107], receive diversity in [25], and MU-MIMO in [34]. However, the analysis in [24, 25, 34, 106, 107] is confined to outage probability and ergodic rate only. Also, the OSTBC studies in [24, 106, 107] use the SISO-SINR model as an approximation for the outage probblity characterization. In this chapter, we extend the equivalent SISO-SINR model to evaluate decoding error probability, outage probability, ergodic rate, and throughput in MIMO cellular networks with transmit diversity (MISO), receive diversity (SIMO), OSTBC, MU-MIMO, and spatial

multiplexing with zero-forcing receivers (ZF-Rx). Furthermore, we prove that the equivalent SISO-SINR model is exact in the case of OSTBC MIMO scheme.

6.2 Downlink MIMO System Model

We build the analysis for this chapter on the system model described in Chapter 3, with some extensions to be detailed as follows. BSs and UEs are equipped with N_t and N_r colocated antennas, respectively. The colocated antennas assumption is common in MIMO models based on Stochastic Geometry analysis to maintain the model tractability [24–28,34,35,37,38,63]. Conditions on the relation between N_r and N_t depend on the MIMO setup under study, as will be shown later. In addition to path-loss attenuation, we consider a Rayleigh multi-path fading environment between transmitting and receiving antennas, such that fading channels are independent from each other. That is, the channel gain matrix from a transmitting BS to a generic UE, denoted as $\mathbf{H} \in \mathbb{C}^{N_r \times N_t}$, has independent zero-mean unit variance complex Gaussian entries, i.e., $\mathbf{H} \sim \mathcal{CN}(0, \mathbf{I})$, where $\mathbf{I}$ is the identity matrix. By expressing the received signal model, differences between the SISO and the MIMO models will be elaborated as shown in what follows.

6.2.1 Downlink MIMO Received Signal Model

For a general MIMO setup in a Rayleigh fading environment, with arbitrary precoding/combining schemes, the complex baseband received signal vector accounting for the precoding matrices is denoted as $\mathbf{y}$, and after applying combining matrices is expressed as $\tilde{\mathbf{y}}$, and we can write

$$\begin{aligned}\tilde{\mathbf{y}} &= \mathbf{W}_o\, \mathbf{y} \\ &= \sqrt{\frac{P}{r_o^{\eta}}}\mathbf{W}_o\mathbf{H}_o\mathbf{V}_o\mathbf{s} + \sum_{r_i \in \tilde{\Psi}^o} \sqrt{\frac{P}{r_i^{\eta}}}\mathbf{W}_o\mathbf{H}_i\mathbf{V}_i\mathbf{s}_i + \mathbf{W}_o\mathbf{n}, \end{aligned} \tag{6.1}$$

where $\tilde{\Psi}^o$ is the set of distances between the test receiver and the actively interfering BSs, such that $\Psi^o = \Psi \setminus r_o$. The interfering BSs constitute a PPP $\tilde{\psi}^o = \psi \setminus o$ with intensity $\lambda = p\lambda_B$, such that p is the activity factor. $P = \frac{E_s}{N_t}$ is the transmit power per antenna at the BSs as E_s is the energy per symbol, $\mathbf{H}_o \in \mathbb{C}^{N_r \times N_t}$ is the useful channel matrix from the serving BS, and $\mathbf{H}_i \in \mathbb{C}^{N_r \times N_t}$ is the interfering channel matrix from the i^{th} interfering BS, $\mathbf{H}_o$ and $\mathbf{H}_i$, have independent and identically distributed (i.i.d.) $\mathcal{CN}(0,1)$ entries, $\mathbf{s} \in \mathbb{C}^{L \times 1}$ and $\mathbf{s}_i \in \mathbb{C}^{L \times 1}$ are, respectively, the intended and interfering symbols vector, where L represents the number of multiplexed data streams. [1]. The symbols in $\mathbf{s}$ and $\mathbf{s}_i$ are independently drawn from an equiprobable two dimensional unit-energy constellations. The matrices $\mathbf{V}_o \in \mathbb{C}^{N_t \times L}$ and $\mathbf{V}_i \in \mathbb{C}^{N_t \times L}$ are the intended and interfering precoding matrices at the intended BS and the i^{th} interfering BS, respectively, while $\mathbf{W}_o \in \mathbb{C}^{L \times N_r}$ is the combining matrix at the test receiver. Note that $\mathbf{W}_o$ and $\mathbf{V}_o$ are tailored to each realization of $\mathbf{H}_o$ and are determined based on the employed MIMO scheme at the serving BS. On the other hand, $\mathbf{V}_i$ depends on the employed MIMO scheme at the i^{th} interfering BS and is independent from the interfering channel matrix $\mathbf{H}_i$ as we assume no inter-BS interference management. The noise $\mathbf{n} \in \mathbb{C}^{N_r \times 1}$ is the zero-mean additive white Gaussian noise vector with covariance matrix $\mathcal{N}_o \mathbf{I}_{N_r}$, where $\mathbf{I}_{N_r}$ is the identity matrix of size N_r. Finally, we assume a per-symbol maximum likelihood (ML) receiver at the test UE to decode the symbols in $\mathbf{s}$.

6.3 Equivalent Downlink SISO-SINR Representation

Assuming per-stream symbol-by-symbol ML receiver, the employed precoding, combining, and equalization techniques decouple symbols belonging to different streams

[1] According to the employed MIMO setup, we might need to introduce a slight abuse of notation to preserve the convention used in (6.1). For instance, in multi-user MIMO setup with $\mathcal{K}$ single-antenna users, the parameter N_r should be replaced with $\mathcal{K}$ so that the signal model in (6.1) remains valid.

(i.e., in case of multiplexing) and/or combine symbols belonging to the same stream (i.e., in case of diversity) at the decoder to allow disjoint and independent symbol detection across the multiplexed data streams. Hence, the precoding and combining matrices ($\mathbf{W}_o$ and $\mathbf{V}_o$) are tailored to each realization of $\mathbf{H}_o$ such that the product $\mathbf{W}_o\mathbf{H}_o\mathbf{V}_o$ always gives a diagonal matrix of size L, with the appropriate, possibly different, diagonal values that correspond to the stream being decoded. Without loss of generality, let us focus on the decoding performance of a generic symbol in the l^{th} stream, in which the instantaneous received signal after applying combining/precoding techniques is given by

$$\tilde{y}_l = \sqrt{\frac{P}{r_o^{\eta}}} \underbrace{\sum_{k=1}^{L} \overbrace{\bar{\mathbf{w}}_{o,l}^T \mathbf{H}_o \mathbf{v}_{o,k}}^{[0\ 0 \ldots g_{o,k} \ldots 0\ 0]} s_k}_{g_{o,l} s_l} + \sum_{r_i \in \tilde{\Psi}^o} \underbrace{\sqrt{\frac{P}{r_i^{\eta}}} \sum_{k=1}^{L} \overbrace{\bar{\mathbf{w}}_{o,l}^T \mathbf{H}_i \mathbf{v}_{i,k}}^{a_{l,k}^{(i)}} s_{i,k}}_{I_i} + \bar{\mathbf{w}}_{o,l}^T \mathbf{n}, \tag{6.2}$$

such that $l \in \{1, \cdots, L\}$, $\bar{\mathbf{w}}_{o,l}$ is the l^{th} column of matrix $\mathbf{W}_o^T$, and $\mathbf{v}_{i,k}$ is the k^{th} column of matrix $\mathbf{V}_i$ which is designed based on the channel matrix between the i^{th} interfering BS and its associated users, denoted as $\tilde{\mathbf{H}}_i$. Further, $g_{o,l}$ is a real random scaling factor that appears in the intended signal due to the equalization applied to detect the l^{th} desired symbol, and $a_{l,k}^{(i)}$, $\forall k$ are the complex random coefficients combining the interfering symbols from the antennas of the i^{th} interfering BS. As shown in (6.2), the coefficients $a_{l,k}^{(i)}$ are generated from the product $\bar{\mathbf{w}}_{o,l}^T \mathbf{H}_i \mathbf{v}_{i,k}$, and they capture the per-BS precoding and test receiver combining effects on the aggregate interference. As discussed earlier, $\bar{\mathbf{W}}_o$ and $\mathbf{V}_i$ are designed independently from each other and neither of them accounts for the realization of the interfering channel matrix $\mathbf{H}_i$. Therefore, the coefficients $a_{l,k}^{(i)}$ randomly change with each realization of $\mathbf{H}_o$, $\mathbf{H}_i$, and $\tilde{\mathbf{H}}_i$.

It is clear from (6.2) that the aggregate interference seen at the decoder of the test UE is highly affected by the per-interfering BS precoding scheme ($\mathbf{v}_{i,k}$), the number of

streams transmitted by each interfering BS (L), the per-stream transmitted symbol ($s_{i,k}$), and the employed combining technique ($\bar{\mathbf{w}}_{o,l}$) at the test UE. Therefore, characterizing the aggregate interference in (6.2) is essential to characterize and quantify the MIMO operation in cellular networks. The aggregate interference term contains three main sources of randomness, namely, the network geometry, the channel gains[2], and the interfering symbols.

To facilitate the error probability analysis and achieve a unified error probability, outage probability and ergodic rate analysis, we only account for the entries in the intended symbol vector $\mathbf{s}$ of (6.1) and abstract the entries in $\mathbf{s}_i$ by i.i.d. zero-mean Gaussian signals $\tilde{\mathbf{s}}_i$ with unit-variance as shown in Chapter 5. Such abstraction ignores the unnecessary and usually unavailable information of the interfering signals. Assuming Gaussian signaling for the interfering symbols (i.e., the entries in $\tilde{\mathbf{s}}_i$ are Gaussian), (6.2) can be rewritten as

$$y_l = \sqrt{P} r_o^{-\frac{\eta}{2}} g_{o,l} s_l + \sum_{r_i \in \tilde{\Psi}^o} \underbrace{\sqrt{P} r_i^{-\frac{\eta}{2}} \sum_{k=1}^{L} a_{l,k}^{(i)} \tilde{s}_{i,k}}_{I_i} + \bar{\mathbf{w}}_{o,l}^T \mathbf{n}. \tag{6.3}$$

It is important to note that the random variables $g_{o,l} \ \ \forall l$ are i.i.d, and hence, there is no loss in generality in dropping the index l and studying an arbitrary stream. Conditioned on r_i and $a_{l,k}^{(i)} \ \forall \{i,k,l\}$, the lumped interference-plus-noise term in (6.3) is Gaussian because of the Gaussianity of $\tilde{s}_{i,k}, \ \forall i,k$. This renders the well-known AWGN error probability expressions legitimate to conduct the averaging over the transmitted symbols and noise, since the noise variance used in the AWGN-based expressions is replaced by the variance of the lumped interference and noise terms in (6.3). That is, the decoding error can be studied by using the AWGN expressions with the conditional SINR (i.e., conditioned on the channel gains and network geometry), followed by averaging over the different communication aspects using the Stochastic

[2]Note that the precoding and combining matrices are functions of the channel gains.

Geometry analysis. The Gaussian signaling approximation leads to the following proposition.

Proposition 6.1. *Consider a downlink MIMO cellular network with N_t antennas at each BS and N_r antennas at each UE in a Rayleigh fading environment with i.i.d. unit-mean channel power gains and Gaussian signaling approximation to the interfering symbols, then the per-data stream conditional SINR at the decoder of a generic UE after combining/equalization can be represented by the following equivalent SISO-SINR*

$$\Upsilon = \frac{Pr_o^{-\eta}\tilde{g}_o}{\sum_{r_i \in \tilde{\Psi}^o} Pr_i^{-\eta}\tilde{g}_i + \mathcal{N}_o}, \tag{6.4}$$

where the random variables $\tilde{g}_o \sim Gamma(m_o, 1)$ and $\tilde{g}_i \sim Gamma(m_i, 1)$ capture the effect of MIMO precoding, combining, and equalization. The values of m_o and m_i are determined based on the number of antennas (N_t and N_r), the number of multiplexed data streams per BS (L) and the employed MIMO configuration as shown in Table 6.1.

Proof. The detailed discussion and proof for each MIMO setup is given in Section 6.5 (see Table 6.1). Here, we just sketch a high-level proof of the proposition. The equivalent channel gains in (6.4) are $\tilde{g}_o = |g_o|^2$ and $\tilde{g}_i = |g_i|^2 = \sum_{k=1}^{L} |a_{l,k}^{(i)}|^2$, where g_o is the random scale for the intended symbol due to precoding and combining/equalization as shown in (6.2). Since precoding and combining/equalization are usually in the form of linear combination of the channel power gains and that the channel gains have independent Gaussian distributions, the random variables $\tilde{g}_o$ and $\tilde{g}_i$ $\forall i$ are independent χ^2-distributed with degrees of freedom equal to the number of linearly combined random variables, which depends on the number of antennas, precoding technique, and number of multiplexed data streams per BS. Note that the χ^2 distribution for interfering channel gains $\tilde{g}_i$ is exact only if the precoding vectors in each BS are independent. In the case of dependent precoding vectors, the correlation is

ignored and the χ^2 distribution for $\tilde{g}_i$ is an approximation. Such approximation is commonly used in the literature for tractability [24, 26–31, 34, 35, 37, 38], and is verified in Section 6.6. Exploiting the one-to-one mapping between the χ^2 distribution and the gamma distribution, we follow the convention in [24, 26–31, 34, 35, 37, 38] and use the gamma distribution, instead of the χ^2 distribution, for $\tilde{g}_o$ and $\tilde{g}_i$. □

It is important to note that, the proposed SISO-SINR model relies on the assumption of independent Rayleigh fading channels. While spatially correlated fading channels model provides more realistic fading environment [115], however, such correlation is ignored for tractability as in [24, 26–31, 34, 35, 37, 38].

MIMO Setup	L	$\boldsymbol{m_o}$	$\boldsymbol{m_i}$	Accuracy	Proof
SIMO	1	N_r	1	Exact	Lemma 6.2
OSTBC	N_s	$N_s N_r$	N_s	Exact	Lemma 6.3
ZF-Rx	N_t	$N_r - N_t + 1$	N_t	Exact	Lemma 6.4
SDMA	$\mathcal{K}$	$N_t - \mathcal{K} + 1$	$\mathcal{K}$	Approx.	Lemma 6.5
MISO	1	N_t	1	Exact	Corollary 6.1
SM-MIMO	N_t	N_r	N_t	Approx.	Lemma 6.6

Table 6.1: SISO-equivalent gamma distribution parameters for various MIMO settings.

Proposition 6.1 gives the equivalent SISO representation for the MIMO cellular network in which the effect of precoding, combining, and equalization of the employed MIMO scheme is abstracted by the random variables $\tilde{g}_o$ and $\tilde{g}_i$ in (6.4). Hence, unified analysis and expressions for different KPIs and MIMO configurations, respectively, are viable as will be shown in the next section.

6.4 A Unified Downlink Performance Analysis

Based on the Gaussian signaling approximation, interference-plus-noise in (6.3) is conditionally Gaussian. Hence, the decoding error performance of the MIMO scheme is studied by plugging the conditional SINR in (6.4) with the appropriate channel

gains (i.e., $\tilde{g}_o$ and $\tilde{g}_i$) in the corresponding AWGN-based decoding error expression, followed by averaging over the channel gains and network geometry. Using the AWGN expression for the SEP for M-QAM modulation scheme given in [98], the ASEP in MIMO cellular networks can be expressed as

$$\text{ASEP}\left(\Upsilon\right) = w_1 \mathbb{E}\left[\text{erfc}\left(\sqrt{\beta\Upsilon}\right)\right] + w_2 \mathbb{E}\left[\text{erfc}^2\left(\sqrt{\beta\Upsilon}\right)\right], \tag{6.5}$$

where $w_1 = 2\frac{\sqrt{M}-1}{\sqrt{M}}, w_2 = -\left(\frac{\sqrt{M}-1}{\sqrt{M}}\right)^2$, and $\beta = \frac{3}{2(M-1)}$ are constellation-size specific constants. It is worth mentioning that the error probability expression in (6.5) can model other modulation schemes by just changing the modulation-specific parameters as detailed in [98]. The Gaussian signaling approximation is also the key that unifies the ASEP, outage probability, and ergodic rate analysis. This is because both outage and capacity are information theoretic KPIs that implicitly assume Gaussian codebooks, which directly lead to the conditional SINR in the form given by Proposition 6.1. Consequently, both the outage probability and ergodic capacity are also functions of the SINR in the form of (6.4), and are given by

$$\mathcal{O}(\theta) = \mathbb{P}\left\{\Upsilon < \theta\right\}, \tag{6.6}$$

and

$$\mathcal{R} = \mathbb{E}\left[\ln\left(1+\Upsilon\right)\right]. \tag{6.7}$$

As discussed earlier, the expectations in (6.5), (6.6), and (6.7) are with respect to the network geometry and channel gains, which are evaluated via Stochastic Geometry analysis. Such expectations are usually expressed in terms of the Laplace transform of the aggregate interference power in (6.4), denoted as $\mathcal{I}_D = \sum_{r_i \in \tilde{\Psi}^o} P r_i^{-\eta} \tilde{g}_i$. The LT of the interference power in the SISO-equivalent SINR given in (6.4) is characterized by the following lemma.

Lemma 6.1. *Consider a cellular network with a MIMO transmission scheme that can be represented via the equivalent SISO-SINR in* (6.4) *and BSs modeled via a PPP with intensity* λ*. Assume that each BS transmits a symbol vector of length* L *per channel use (pcu) with symbols drawn from a zero-mean unit-variance Gaussian distribution. The LT of the interference power affecting an arbitrary symbol at a receiver located* r_o *meters away from its serving BS is given by*

$$\mathcal{L}_{\mathcal{I}_D|r_o}(z) = \exp\left\{-\pi\lambda r_o^2\left[\left({}_2F_1\left(\frac{-1}{b}, m_i; 1-\frac{1}{b}; -zPr_o^{-\eta}\right)-1\right)\right]\right\}, \tag{6.8}$$

where ${}_2F_1(\cdot,\cdot;\cdot;\cdot)$ *is the Gauss hypergeometric function [112].*

Proof. Starting from the definition of the LT, we have

$$\begin{aligned}\mathcal{L}_{\mathcal{I}_D|r_o}(z) &= \mathbb{E}\left[\exp\left\{-z\sum_{r_i\in\tilde{\Psi}^o} Pr_i^{-\eta}\tilde{g}_i\right\}\right]\\ &\overset{(a)}{=} \exp\left\{-2\pi\lambda\int_{r_o}^{\infty}\mathbb{E}\left[1-e^{-zPx^{-\eta}\tilde{g}}\right]x\mathrm{d}x\right\}\\ &\overset{(b)}{=} \exp\left\{-2\pi\lambda\int_{r_o}^{\infty}\left[1-\frac{1}{(1+zPx^{-\eta})^{m_i}}\right]x\mathrm{d}x\right\},\end{aligned} \tag{6.9}$$

where (a) follows from the probability generating functional (PGFL) of the homogeneous PPP [17] constituted by the interferers lying outside a disk of radius r_o, i.e. $r_i > r_o$, with intensity λ, and (b) follows from the LT of the gamma distributed channel gains with shape parameter m_i and unity scale parameter. Evaluating the integral yields the LT in (6.8). □

Using Proposition 6.1 and Lemma 6.1, we arrive to the unified MIMO expressions for the ASEP, outage probability, and ergodic rate in the following theorem.

Theorem 6.1. ***Unified Analysis:*** *Consider a cellular network with MIMO transmission scheme that can be represented via the equivalent SISO-SINR in* (6.4) *and BSs modeled via a PPP with intensity* λ*, in which each BS transmits a symbol vector*

of length L pcu with symbols drawn from an equiprobable unit-power square quadrature amplitude modulation (M-QAM) scheme, then the ASEP for an arbitrary symbol is approximated by

$$\begin{aligned}\mathrm{ASEP}_{\mathrm{DL}} \approx w_1 \Bigg[1 - \frac{\Gamma\left(m_o+\frac{1}{2}\right)}{\Gamma\left(m_o\right)}\frac{2}{\pi}\int_0^\infty\int_0^\infty 2\pi\lambda_B x e^{-\pi\lambda_B x^2}\frac{1}{\sqrt{z}}e^{-z\left(1+\frac{m_o\mathcal{N}_o x^\eta}{\beta P}\right)} \\ \times {}_1F_1\left(1-m_o;\frac{3}{2};z\right)\cdot\mathcal{L}_{\mathcal{I}_D|x}\left(\frac{m_o z x^\eta}{\beta P}\right)\mathrm{d}x\mathrm{d}z\Bigg] \\ + w_2\Bigg[1-\frac{4m_o}{\pi}\int_0^\infty\int_0^\infty 2\pi\lambda_B x e^{-\pi\lambda_B x^2}e^{-z\left(\frac{m_o\mathcal{N}_o x^\eta}{\beta P}\right)} \\ \times\int_0^{\frac{\pi}{4}} {}_1F_1\left(m_o+1;2;\frac{-z}{sin^2\vartheta}\right)\frac{1}{sin^2\vartheta}\cdot\mathcal{L}_{\mathcal{I}_D|x}\left(\frac{m_o z x^\eta}{\beta P}\right)\mathrm{d}\vartheta\mathrm{d}x\mathrm{d}z\Bigg],\end{aligned} \tag{6.10}$$

where ${}_1F_1(\cdot;\cdot;\cdot)$ is the Kummer confluent hypergeometric function [112].

For an interference-limited scenario, the probability that the SIR for an arbitrary symbol goes below a threshold θ is given by

$$\mathcal{O}_{\mathrm{DL}}\left(\theta\right) = 1 - \int_0^\infty 2\pi\lambda_B\, x e^{-\pi\lambda_B x^2}\sum_{j=0}^{m_o-1}\frac{(-1)^j}{j!}\frac{\mathrm{d}^j}{\mathrm{d}z^j}\left(\frac{\theta r_o^\eta}{P}\right)^j\mathcal{L}_{\mathcal{I}_D|x}\left(z\right)\Big|_{z=\frac{\theta x^\eta}{P}}\mathrm{d}x, \tag{6.11}$$

and the ergodic rate for an arbitrary data stream is given by

$$\mathcal{R}_{\mathrm{DL}} = \int_0^\infty\int_0^\infty 2\pi\lambda_B\, x e^{-\pi\lambda_B x^2}\mathcal{L}_{\mathcal{I}_D|x}\left(\frac{z x^\eta}{P}\right)\left(\frac{1-(1+z)^{-m_o}}{z}\right)\mathrm{d}z\mathrm{d}x, \tag{6.12}$$

where $\mathcal{L}_{\mathcal{I}_D|x}\left(z\right)$ in (6.10), (6.11), *and* (6.12) *is the LT given in Lemma 6.1.*

Proof. See Appendix C.1. □

The ASEP given in (6.10) is an approximation due to the Gaussian signaling approximation used in (6.3). However, the outage probability and ergodic rate are both exact because both are typically derived based on the Gaussian codebooks. The

outage probability in (6.11) is given for interference-limited networks for tractability, which is a common assumption in cellular network because the interference term usually dominates the noise. Both equations (6.11) and (6.12) are approximations in cases of SDMA and SM-MIMO due to the approximate characterization of the interference as shown in Table 6.1. Note that different exact/approximate forms for the outage probability and ergodic rate, shown in (6.11) and (6.12), respectively, can be derived via Gil-Pelaez inversion theorem as in [88, 116] and Alzer's inequality as in [117, 118]. Nevertheless, both approaches are based on the Gaussian signaling approximation and equivalent SISO representation given in Proposition 6.1.

The ASEP expression given in (6.10) presents three advantages over the ASEP expressions given in [37] derived using the EiD approach. First, (6.10) provides a unified ASEP expression for all considered MIMO schemes. Second, the ASEP is characterized based on the LT given in Lemma 6.1, which is the same LT used for characterizing the outage probability and ergodic rate. Third, the computational complexity to evaluate (6.10) is less than the complexity of the ASEP expressions in [37]. The reduced complexity of (6.10) stems from the fact that it includes a single hypergeometric function in the exponential term while the expressions for the ASEP in [37] include summations of hypergeometric functions inside the exponential term. It should be highlighted that the EiD approach leads to the same computational complexity as in (6.10) for some modulation schemes, e.g., phase-shift-keying (M-PSK) [37]. Nevertheless, the proposed Gaussian approximation and equivalent SISO representation simplifies the ASEP analysis and unifies it with outage and ergodic rate results when compared to the EiD approach which always involves the complex baseband interference analysis.

In Section 6.6, we show that the advantages presented by (6.10) do not sacrifice the model accuracy when compared to the ASEP in [37], specially that the ASEP in [37] is also approximate in case of SDMA and SM-MIMO schemes.

Before giving numerical results and insights obtained from the developed mathematical model, we first illustrate how the equivalent SISO-SINR model given in Proposition 6.1 holds for the considered MIMO schemes.

6.5 Characterizing Downlink MIMO Configurations

This section details the methodology to abstract different MIMO configuration via the equivalent SISO model given in Proposition 6.1 with parameters given in Table 6.1. In order to conduct the analysis for the different MIMO setups, we first need to define the set $\left\{\breve{\mathbf{H}}\right\}$ as the set of channel matrices that affect the aggregate interference signals due to precoding and/or combining. For instance, due to precoding, combining, and equalization, the interference from the i^{th} interfering BS is multiplied by $\mathbf{W}_o\mathbf{H}_i\mathbf{V}_i$, and hence, $\left\{\breve{\mathbf{H}}\right\} = \{\mathbf{H}_o, \tilde{\mathbf{H}}_i\}$, where $\mathbf{H}_o$, and $\tilde{\mathbf{H}}_i$ are the channel matrices between, respectively, the intended BS and the test user, and the i^{th} interfering BSs and its associated users. The methodology to characterize the distribution of the equivalent channel gains are given in the following steps:

1. SNR characterization: $\tilde{g}_o$ is first characterized by projecting the signal of the intended data-stream on the null-space of the signals of the other data streams that are multiplexed by the intended BSs. Note that we may manipulate the resultant SNR such that the noise variance is not affected by any random variable as in (6.4) and the projection effect is contained in $\tilde{g}_o$ and $\tilde{g}_i$ only.

2. Per-stream equivalent channel gain representation: $\tilde{g}_i$ from each interfering BS is characterized based on the manipulation done in the SNR characterization in the previous step and characterizing $|a_{l,k}^{(i)}|^2$ given in (6.3). Note that $|a_{l,k}^{(i)}|^2$ is characterized based on $\left\{\breve{\mathbf{H}}\right\}$ which captures the channel gain matrices involved in precoding the signal at the i^{th} BS and combining the interfering symbols at the test UE.

Based on these two steps, the equivalent SISO-SINR given in Proposition 6.1 for the MIMO schemes given in Table 6.1 is illustrated in this section.

6.5.1 Single-Input-Multiple-Output (SIMO) systems

For a SIMO system, receive diversity is achieved using one transmit antenna (i.e., $L = N_t = 1$) and N_r receive antennas. Since $N_t = 1$, then the intended and interfering channel vectors are denoted by $\mathbf{h}_o$ and $\mathbf{h}_i \in \mathbb{C}^{N_r \times 1}$, respectively. By employing Maximum Ratio-Combining (MRC) strategy to combine the received signals, then $\bar{\mathbf{w}}_o^T = \mathbf{h}_o^H$. The equivalent SISO channel gains are given by the following lemma.

Lemma 6.2. *For a receive diversity SIMO setup technique, the Gamma distribution parameters for the equivalent intended and interfering channel gains are given by* $\boldsymbol{m_o = N_r}$ *and* $\boldsymbol{m_i = 1}$*, respectively.*

Proof. See Appendix C.2. □

6.5.2 Orthogonal Space-Time Block Coding (OSTBC)

Let the orthogonal space-time block codes be transmitted over T time instants, and only $N_s \leq N_t$ transmit antennas are active per time instant. The received signal is equalized via the equalizer $\mathbf{W}_o = \frac{\mathbf{H}_{\text{eff}}^H}{\|\mathbf{H}_o\|_{\text{F}}}$, where $\mathbf{H}_{\text{eff}}$ is the effective intended channel matrix depending on the employed orthogonal code [24, 37]. Since no precoding is applied then $\mathbf{V}_o = \mathbf{V}_i = \mathbf{I}_{N_t}$. The equivalent SISO channel gains are given by the following lemma.

Lemma 6.3. *A space-time encoder is employed at the network BSs. Then, the Gamma distribution parameters are given as* $\boldsymbol{m_o = N_s N_r}$ *and* $\boldsymbol{m_i = N_s}$*.*

Proof. See Appendix C.2. □

6.5.3 Zero-Forcing beamforming with MLR (ZF-Rx)

Zero-forcing is a low-complexity suboptimal, yet efficient, technique to suppress interference from other transmitted symbols in the network. In order to recover the distinct transmitted streams, the received signal is multiplied by the equalizing matrix $\mathbf{W}_o = \left(\mathbf{H}_o^H \mathbf{H}_o\right)^{-1} \mathbf{H}_o^H$ representing the pseudo-inverse of the intended channel matrix $\mathbf{H}_o$, whereas we assume no precoding at the transmitters side, i.e., $\mathbf{V}_o = \mathbf{V}_i = \mathbf{I}_{N_t}$. The equivalent SISO channel gains are given by the following lemma.

Lemma 6.4. *By employing a ZF-Rx such that $L = N_t$ distinct streams are being transmitted from the BSs, it can be shown that $\boldsymbol{m_o = N_r - N_t + 1}$ and $\boldsymbol{m_i = N_t}$.*

Proof. See Appendix C.2. □

6.5.4 Space-Division Multiple Access (SDMA)

SDMA is used to accommodate more users on the same resources to increase the network capacity. In this case, we consider that each BS is equipped by N_t transmit antennas and applies ZF transmission to simultaneously serve $\mathcal{K}$ single-antenna UEs that are independently and randomly distributed within its coverage area. To avoid rank-deficiency, we let $N_t \geq \mathcal{K}$, and hence, the number of data streams $L = \mathcal{K}$. A ZF-precoding in the form of $\mathbf{V}_o = [\mathbf{v}_1, \mathbf{v}_2 \cdots \mathbf{v}_{\mathcal{K}}]$ such that $\mathbf{v}_l = \frac{\mathbf{q}_l}{\|\mathbf{q}_l\|}$ and $\mathbf{q}_l$ is defined as the l^{th} column of $\mathbf{Q} = \mathbf{H}_o^H \left(\mathbf{H}_o \mathbf{H}_o^H\right)^{-1}$ is applied by the test BS and no combining is applied at the single antenna test UE, and hence, $\mathbf{W}_o = \mathbf{I}_{\mathcal{K}}$. The interfering BSs apply the same precoding and combining strategy, and hence, the interfering precoding matrices are in the form $\mathbf{V}_i = [\mathbf{v}_{i,1}, \mathbf{v}_{i,2} \cdots \mathbf{v}_{i,\mathcal{K}}]$ such that $\mathbf{v}_{i,k} = \frac{\tilde{\mathbf{q}}_k}{\|\tilde{\mathbf{q}}_k\|}$ and $\tilde{\mathbf{q}}_k$ is the k^{th} column of $\tilde{\mathbf{Q}}_i = \tilde{\mathbf{H}}_i^H \left(\tilde{\mathbf{H}}_i \tilde{\mathbf{H}}_i^H\right)^{-1}$, note that $\tilde{\mathbf{H}}_i \neq \mathbf{H}_i$ is the interfering channel matrix towards the corresponding intended users. The equivalent SISO channel gains are given by the following lemma.

Lemma 6.5. *In a multi-user MIMO setup, the corresponding Gamma distributions parameters are given by* $\boldsymbol{m_o = N_t - \mathcal{K} + 1}$*, and* $\boldsymbol{m_i \approx \mathcal{K}}$*.*

Proof. See Appendix C.2. □

Corollary 6.1. Single-User Beamforming (SU-BF):

The SDMA scenario reduces to SU-MISO setting if the number of served users in the network is $\mathcal{K} = 1$*. Hence,* $m_o = N_t$ *and* $m_i = 1$*.*

6.5.5 Spatially Multiplexed MIMO (SM-MIMO) systems

For the sake of completeness, we also consider a spatially multiplexed MIMO setup with optimum joint maximum-likelihood receiver. This case is important because it represents the benchmark for ZF decoding. Note that the analysis in this case is slightly different from the aforementioned schemes since joint detection is employed. Nevertheless, it can be represented via the equivalent SISO-SINR given in Proposition 6.1. Due to joint detection, no precoding/combining is applied such that $\mathbf{W}_o = \mathbf{V}_o = \mathbf{V}_i = \mathbf{I}_{N_t}$. To analyze this case, we define the error vector $\mathbf{e}(\mathbf{s}, \hat{\mathbf{s}}) = \mathbf{s} - \hat{\mathbf{s}}$ as the distance between $\mathbf{s}$ and $\hat{\mathbf{s}}$ and hence we derive the APEP, which is then used to approximate the ASEP as shown in the following lemma.

Lemma 6.6. *For a SM-MIMO transmission, the Gamma distribution parameter for the equivalent intended channel gains is given by* $\boldsymbol{m_o = N_r}$*, while for the equivalent interfering links is given by* $\boldsymbol{m_i = N_t}$*. Furthermore, the averaged PEP over the distance distribution of* r_o *is*

$$\mathrm{APEP}(\|\boldsymbol{e}\|) \approx 1 - \frac{\Gamma\left(m_o + \frac{1}{2}\right)}{\Gamma(m_o)} \frac{2}{\pi} \int_0^\infty \int_0^\infty 2\pi\lambda_B x e^{-\pi\lambda_B x^2} \frac{1}{\sqrt{z}} e^{-z\left(1 + \frac{m_o \mathcal{N}_o x^\eta}{4\|\boldsymbol{e}\|^2 P}\right)} \times {}_1F_1\left(1 - m_o; \frac{3}{2}; z\right) \mathcal{L}_{\mathcal{I}_D|x}\left(\frac{m_o z}{4\|\boldsymbol{e}\|^2 P x^{-\eta}}\right) \mathrm{d}x\mathrm{d}z. \tag{6.13}$$

Consequently, using the Nearest Neighbor approximation [119], where there are M equiprobable symbols, then

$$\mathrm{ASEP}_{\mathrm{DL}} \approx N_{\|\mathrm{e}\|_{min}} \, \mathrm{APEP}\left(\|\boldsymbol{e}\|_{min}\right), \tag{6.14}$$

where $N_{\|\boldsymbol{e}\|_{min}}$ is the number of constellation points having the minimum Euclidean distance denoted by $\min_{\boldsymbol{s},\hat{\boldsymbol{s}}} \|\boldsymbol{e}(\boldsymbol{s},\hat{\boldsymbol{s}})\|$ among all possible pairs of transmitted symbols, and hence, is a modulation-specific parameter.

Proof. See Appendix C.2. □

6.6 Numerical and Simulation Results

In this section, we verify the validity and accuracy of the proposed unified model and discuss the potential of such unified framework for designing cellular networks.

6.6.1 Proposed model validation

The BSs transmit powers (P) vary while $\mathcal{N}_o$ is kept constant to vary the transmit SNR, the path-loss exponent $\eta = 4$, the noise power $\mathcal{N}_o = -90$ dBm, the BSs intensity $\lambda_B = 10$ BSs/km^2, $\lambda_u = 20$ users/km^2. The desired symbols are modulated using square quadrature amplitude modulation (QAM) scheme, with a constellation size M.

We validate the derived ASEP for the proposed model via Monte Carlo simulations, in Fig. 6.1, for the network setup detailed as: activity factor $p = 1$ and (a) SIMO: $N_t = 1$ and $N_r = 3$, (b) the OSTBC: we consider a 2×2 Alamouti code, (c) zero-forcing with MLR with $N_t = 2, N_r = 5$, (d) the SDMA multi-user setting using a zero-forcing precoder at the transmitters side with $\mathcal{K} = 3$ single-antenna users to be served by BSs equipped with $N_t = 5$ antennas. Lines represent the proposed analytic results, and markers represent Monte Carlo simulations. The figure further veri-

fies the accuracy of the Gaussian signaling approximation and the developed ASEP model, in which the analytic ASEP expressions perfectly match the simulations that generate the exact QAM-modulated interfering symbols. Also, as evident from the figure, SIMO transmissions, OSTBC, ZF-Rx, and SDMA transmissions have the same performance up to SNR = 80 dB, i.e., noise-limited network, whereas the ASEP performance starts to be distinguishable when the network becomes interference-limited.

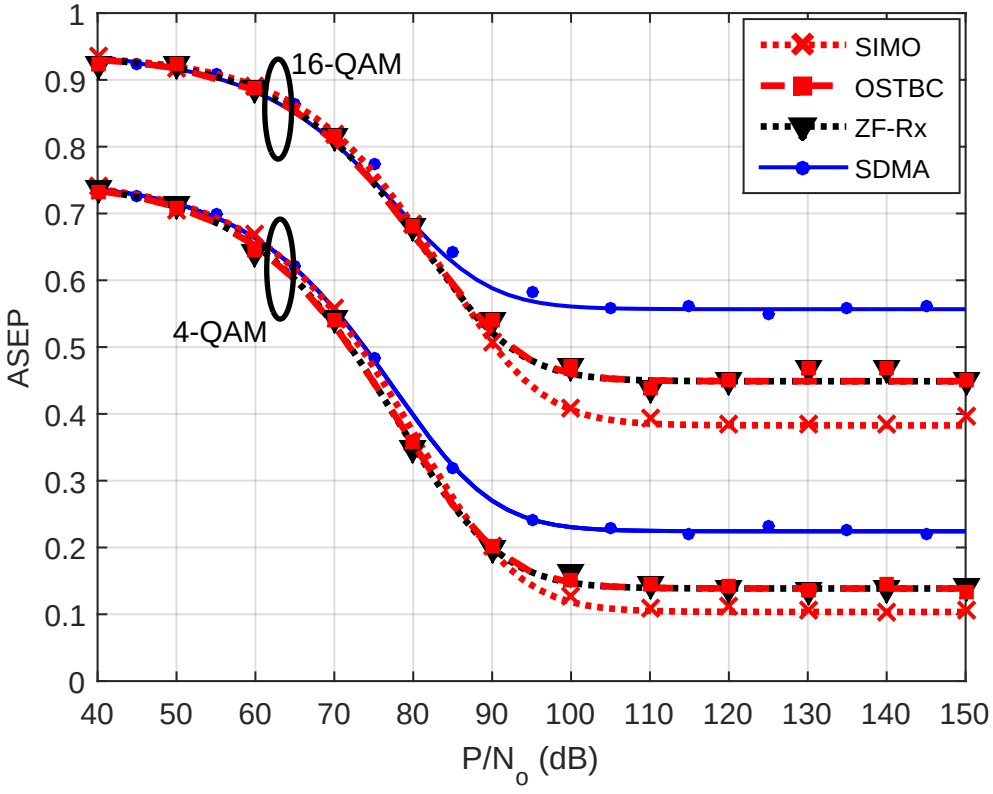

Figure 6.1: ASEP performance against $\frac{P}{N_o}$ for different MIMO setups.

6.6.2 Diversity-Multiplexing Tradeoffs & Design Guidelines

For a fixed number of antennas $N_t = 2$ and $N_r = 2$, Figs. 6.2, 6.3 and 6.4 together with Table 6.2 compare the performance of the considered MIMO configurations in

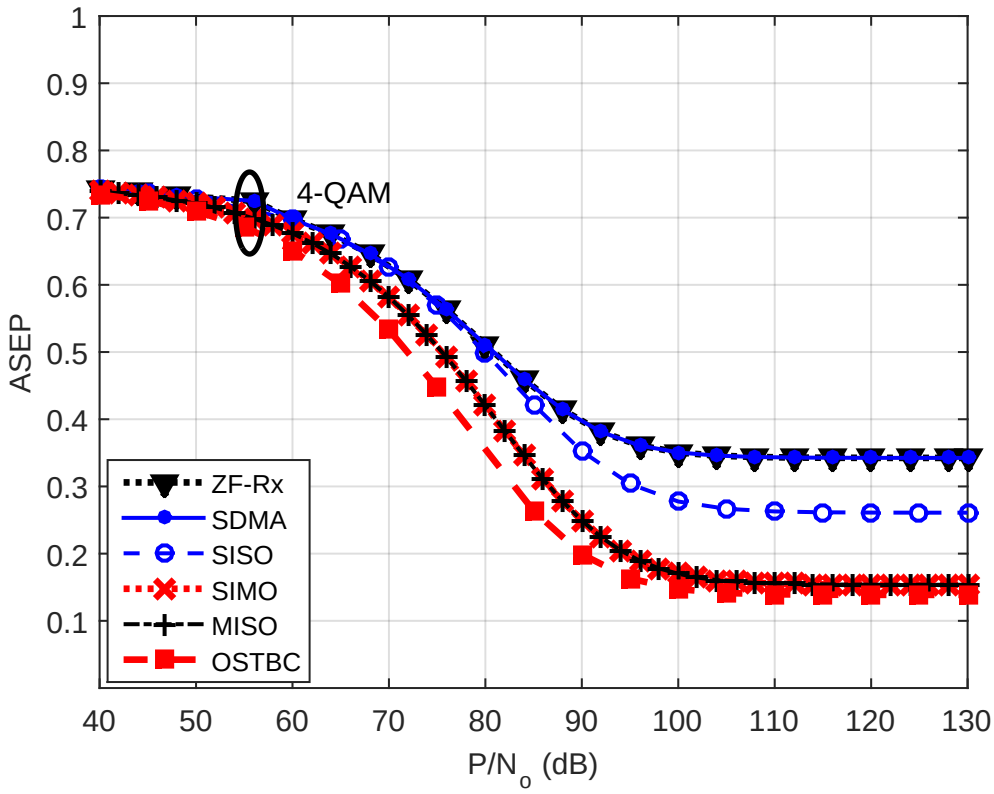

Figure 6.2: ASEP for 4-QAM modulation, for the different MIMO setups using the same number of antennas $N_t = 2$ and $N_r = 2$, at $p = 1$.

terms of error probability, outage probability, ergodic rate, and throughput[3], and quantify the achievable gains with respect to the SISO configuration. Note that, for SIMO and MISO, N_t and N_r are set to 1, respectively. Further, in SDMA scenario, the number of single-antenna users served in the network is $\mathcal{K} = 2$. Figs. 6.2, 6.3, and 6.4 as well as Table 6.2 clearly show the diversity-multiplexing tradeoff in cellular networks. Fig. 6.4 shows the outage probability improvement due to diversity, in which the OSTBC achieves the highest outage probability reduction. This is because OSTBC provides both transmit and receive diversity while MISO and SIMO provide either transmit or receive diversity. Note that despite that MISO and SIMO have the

[3]The throughput is defined as the number of successfully transmitted bits pcu and is given by $\log_2(M)(1 - \text{ASEP})$.

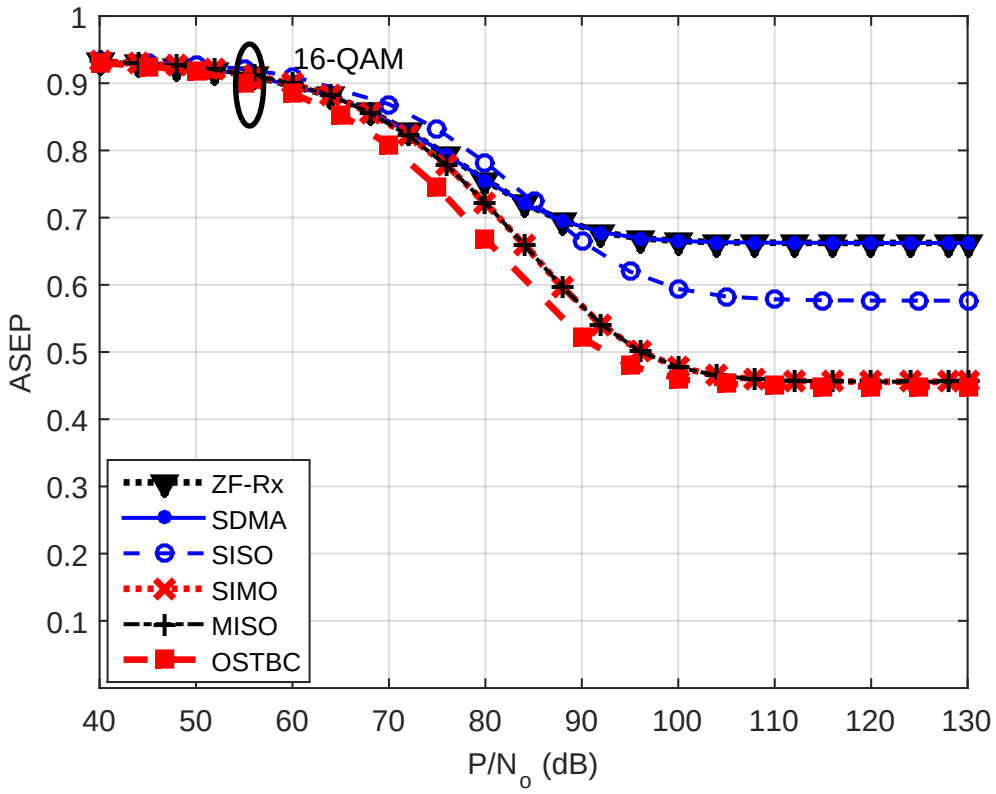

Figure 6.3: ASEP for 16-QAM modulation, for the different MIMO setups using the same number of antennas $N_t = 2$ and $N_r = 2$, at $p = 1$.

same performance, the SIMO is preferred because it relies on the receive CSI which is easier to obtain than the transmit CSI. The figure also shows the negative impact of multiplexing on the per-stream ASEP and outage probability in ZF-Rx and MU-MIMO schemes. However, multiplexing several streams per BS improves the overall ergodic rate and per-cell throughput as shown in Table 6.2.

The results in Figs. 6.2, 6.3 and 6.4, and Table 6.2 show the diversity-multiplexing tradeoffs that can be achieved for a 2×2 MIMO setting. However, as N_t and N_r grow, several diversity and multiplexing tradeoffs are no longer straightforward to compare. Hence, it is beneficial to have a unified methodology to select the appropriate diversity, multiplexing, and number of antennas to meet a certain design objective. From Proposition 6.1 and the subsequent results we noticed two important insights:

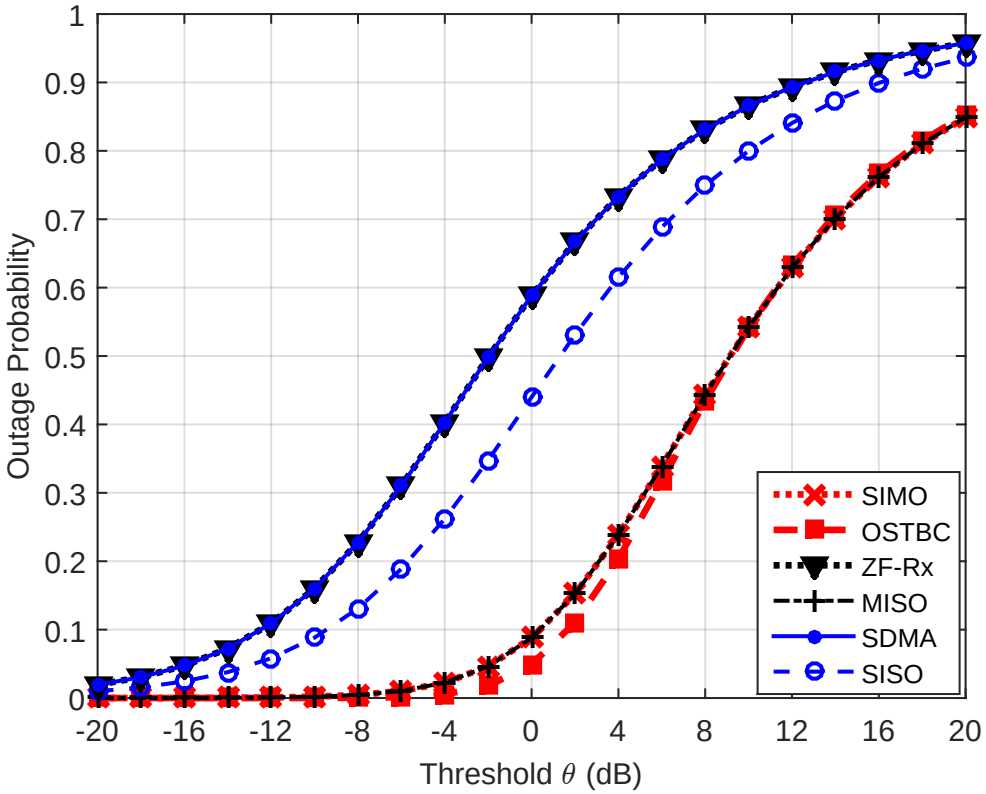

Figure 6.4: Outage Probability versus SIR threshold θ, for the different MIMO setups using the same number of antennas $N_t = 2$ and $N_r = 2$, at $p = 1$.

MIMO Setup	m_o	m_i	Ergodic Rate (bits/sec/Hz)	No. of bits pcu 4-QAM	16-QAM
SIMO	2	1	2.9523	1.6926	2.1772
OSTBC	4	2	2.9771	1.7228	2.2044
ZF-Rx	1	2	3.1644	2.6300	2.7008
SDMA	1	2	3.1644	2.6300	2.7008
MISO	2	1	2.9523	1.6926	2.1772
SISO	1	1	1.48899	1.4780	1.6936

Table 6.2: Overall achievable and actual rates gains per cell, with respect to SISO networks, for the different MIMO setups, in an interference-limited scenario for $M = 4$, 16-QAM modulation scheme.

- The performances of MIMO schemes differ according to their relative m_o and m_i values. In other words, MIMO configurations with equal $\frac{m_o}{m_i}$ ratio have ap-

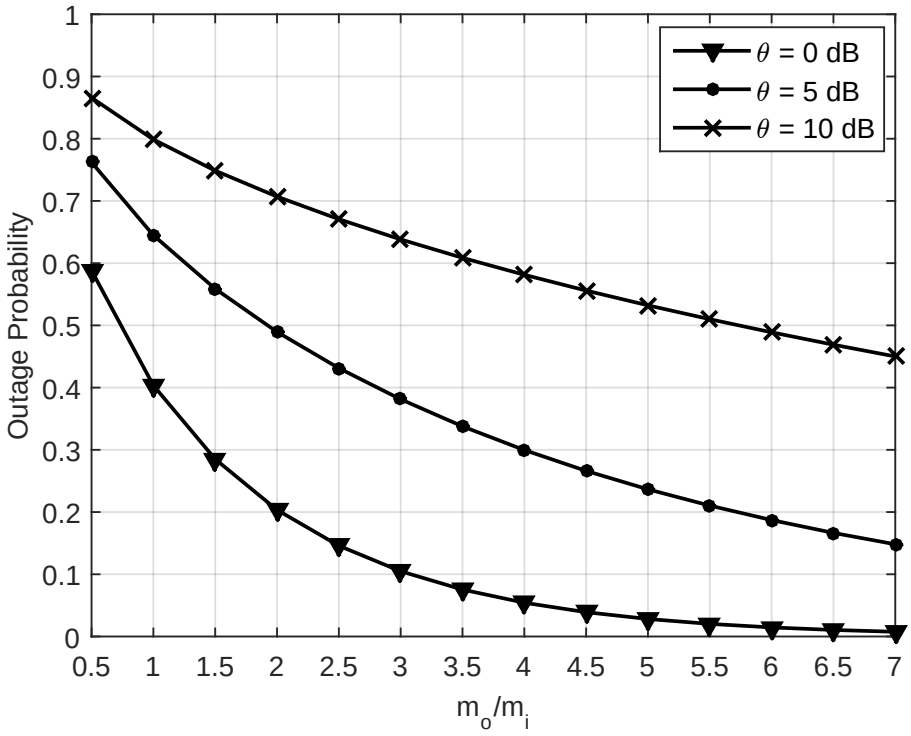

Figure 6.5: Unified Outage performance versus the ratio $\frac{m_o}{m_i}$ for an arbitrary MIMO setup, for $\theta = 0, 5, 10$ dB at $\frac{P}{\mathcal{N}_o} = 90$dB.

proximately equivalent per-stream performance as shown in Fig. 6.7. Moreover, such equivalence in performance can be further verified by the numerical results of [37] where similar ASEP performance among different MIMO schemes having the same fading parameters has been reported.

- Multiplexing more data streams increases m_i and does not affect m_o. On the other hand, diversity increases m_o and does not affect m_i. In other words, m_o represents the diversity gain and m_i represents the number of independently multiplexed data streams per BS (i.e., multiplexing gain).

Based on the aforementioned insights, we plot the unified MIMO outage probability and ASEP performance results in Figs. 6.5 and 6.6, respectively, which show the outage probability and ASEP performance for a varying ratio of $\frac{m_o}{m_i}$ that can

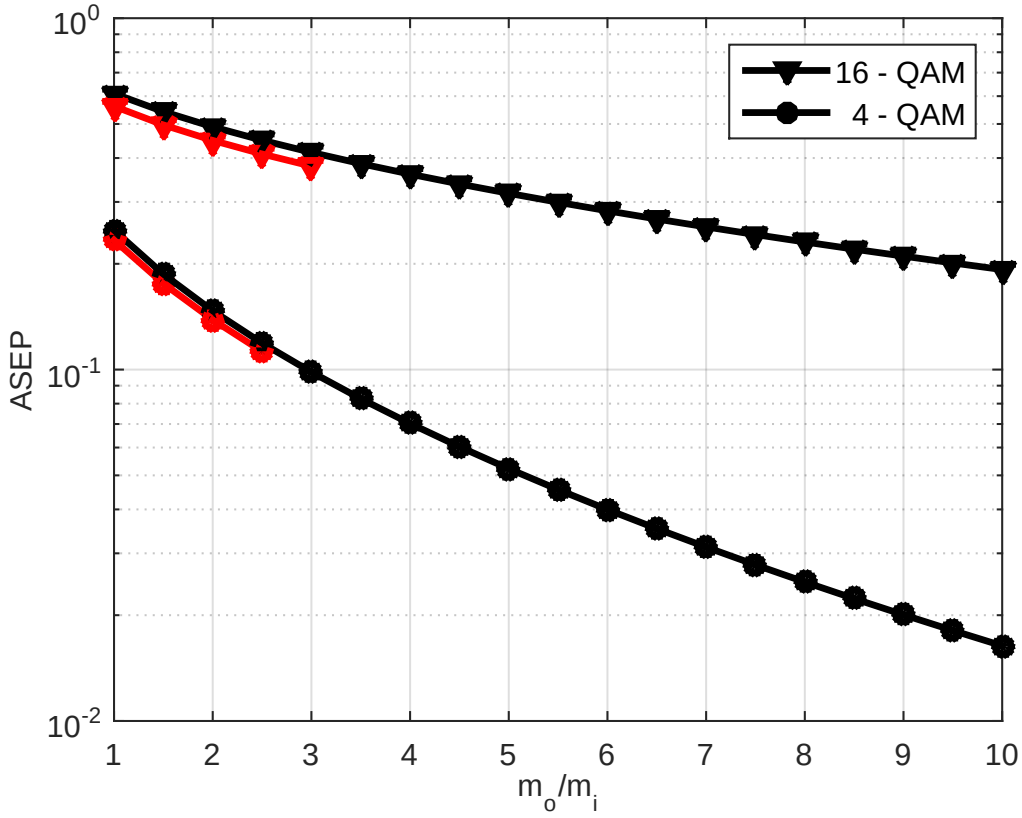

Figure 6.6: Unified ASEP performance versus the ratio $\frac{m_o}{m_i}$ for an arbitrary MIMO setup, for 4-QAM and 16-QAM at $\frac{P}{\mathcal{N}_o} = 90$dB.

be used for all considered MIMO schemes. Conversely, Figs. 6.5 and 6.6 present a unified design methodology for MIMO cellular networks as shown in Fig. 6.8. Such unified design provides reliable guidelines for network designers and defines the different flavors of the considered MIMO configurations in terms of achievable diversity and/or multiplexing gains. For instance, for an ASEP or outage probability constraint, the corresponding ratio $\frac{m_o}{m_i}$ and modulation scheme are determined. Then, the network designer can determine the MIMO technique depending on the number of data streams (or number of users) that need to be simultaneously served (i.e., determine L or $\mathcal{K}$). Finally, the number of transmit and receive antennas for the selected MIMO scheme can be determined from Table 6.1.

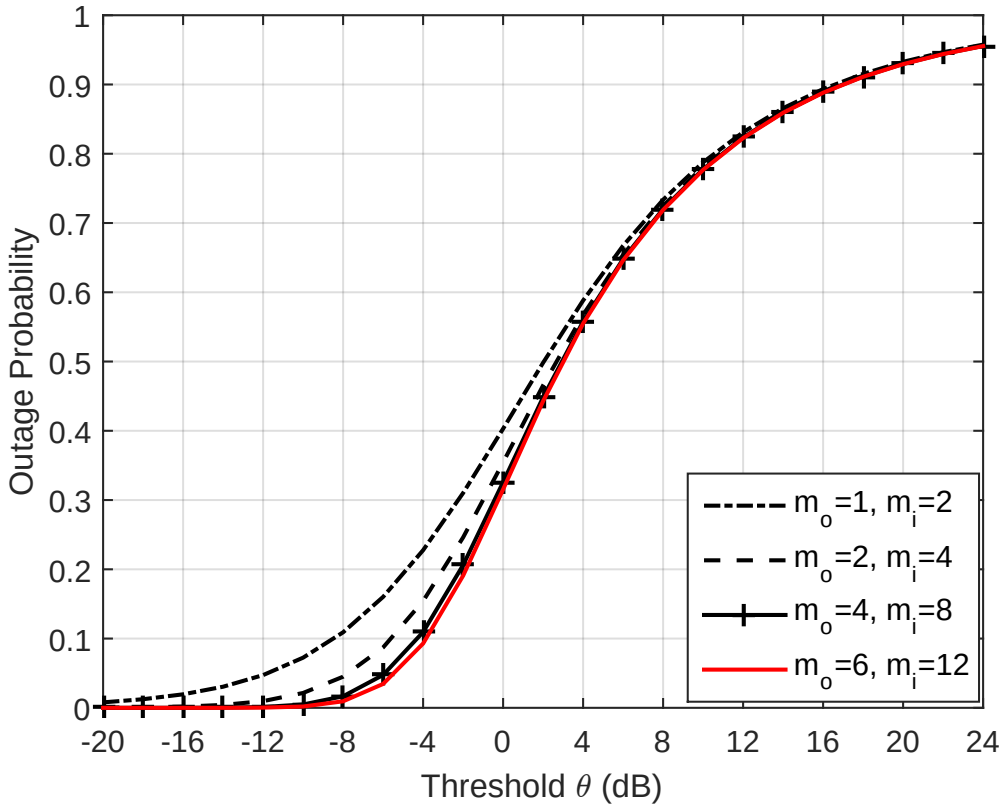

Figure 6.7: Unified Outage Probability performance for $\frac{m_o}{m_i} = \frac{1}{2}$ at $\theta = 5$ dB at $\frac{P}{\mathcal{N}_o} = 90$dB.

Figs. 6.5 and 6.6 clearly show that incrementing the ratio $\frac{m_o}{m_i}$ enhances the diversity gain whereas decrementing it provides a higher multiplexing gain. That is, network designers are able to maintain the same per-stream ASEP/outage probability by appropriately adjusting the operational parameters, namely, N_r, N_t and L (or $\mathcal{K}$ for SDMA). This is done by compensating m_i with the adequate m_o such that $\frac{m_o}{m_i}$ is kept constant. For instance, consider a network that needs to increase the number of served users $\mathcal{K}$ without compromising the reliability performance of each served user. According to Table 6.1 and Figs. 6.5 and 6.6, this is achieved by keeping $\frac{m_o}{m_i} = c$, where c is a constant, which hence costs the network additional $\lceil \mathcal{K}(c+1) - 1 \rceil$ transmit antennas per BS.

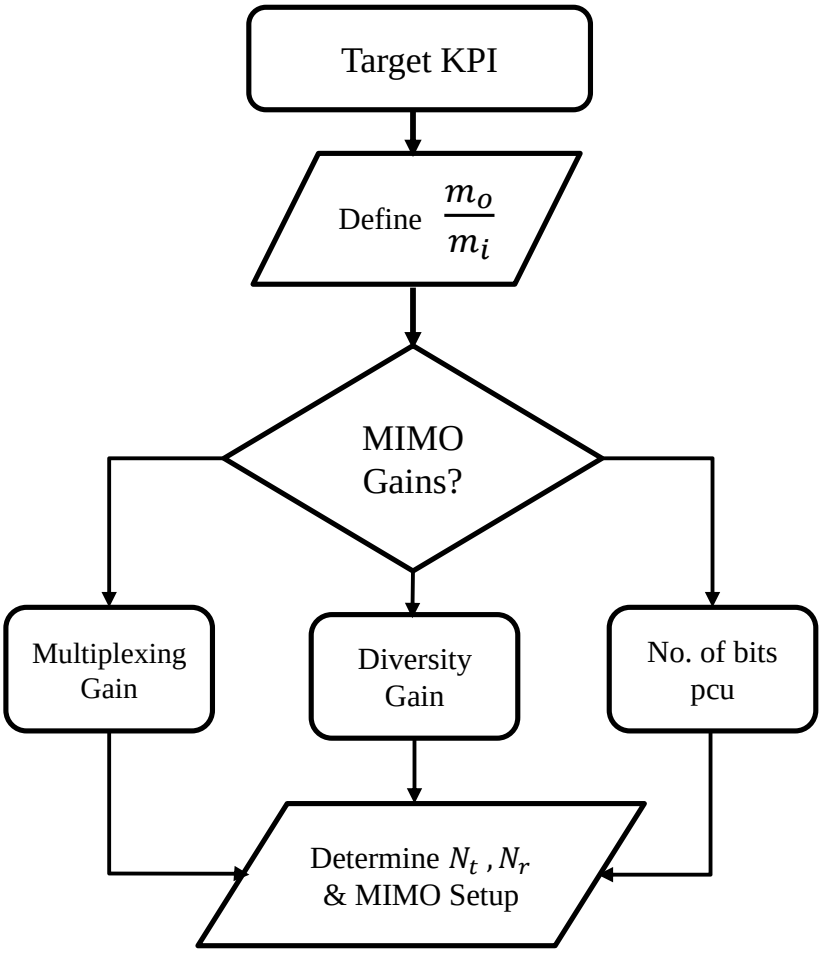

Figure 6.8: Flowchart for MIMO selection in cellular networks

It is worth mentioning that a design based on the ASEP is more tangible as it is sensitive to the used constellation, as opposed to the outage probability as shown in Figs. 6.5 and 6.6, and Table 6.2. Also, note that increasing m_o for a fixed $\frac{m_o}{m_i}$ ratio can slightly vary the outage probability due to the channel hardening effect as shown in Fig 6.7. However, such variation is shown to be negligible for $m_o > 2$. In fact, by direct inspection of eq. (C.1), it is clear that as m_o increases, the value of the summation also increases and therefore, the overall outage performance decreases, since the increase in m_o is interpreted as an enhancement in the desired signal. Nevertheless, if the improvement in the desired signal, i.e., m_o, is compensated by an equivalent in-

crease in the interfering signals, i.e., m_i, the performance eventually saturates and no better performance can be achieved as long as the ratio $\frac{m_o}{m_i}$ is kept constant. Another noteworthy observation is that the second term in (6.10), which corresponds to the $\text{erfc}^2(\cdot)$ term in (6.5), requires threefold nested integrals that involve hypergeometric functions to evaluate the ASEP. Such integration is computationally complex to evaluate and may impose some numerical instability specially for large arguments of m_o and m_i. In order to overcome such complexity and numerical instability, we invoke Jensen's inequality to the $\text{erfc}^2(\cdot)$ term in (6.5). Hence, the ASEP function becomes

$$\text{ASEP}\left(\Upsilon\right) \geq w_1 \mathbb{E}\left[\text{erfc}\left(\sqrt{\beta\Upsilon}\right)\right] + w_2 \mathbb{E}\left[\text{erfc}\left(\sqrt{\beta\Upsilon}\right)\right]^2, \tag{6.15}$$

which reduces one integral from the second term of (6.10). Using Jensen's inequality yields a stable and accurate approximation compared to (6.10) as shown in Figure 6.6, where the red curves represent the numerically unstable ASEP performance as arguments grow, while the black curves represent the Jensen's inequality highly tight upper bounds.

6.7 Chapter Summary and Conclusions

The developed mathematical model presents twofold analysis unification for MIMO cellular networks literature. The unified analysis proposes an equivalent SISO-SINR representation for the per-data stream SINR in MIMO cellular networks. We show that the proposed unification simplifies the analysis without sacrificing the model accuracy. To this end, we discuss the diversity-multiplexing tradeoff imposed by different MIMO schemes. Finally, we propose a unified design methodology to choose the appropriate diversity, multiplexing gain, and number of antennas to meet a certain design objective. In the next chapter, we develop an analogous unified model for the uplink MIMO transmissions.

Chapter 7

Unified Performance Analysis for Uplink MIMO networks

7.1 Introduction

The performance of uplink cellular networks has not be sufficienlty addressed in the literature using Stochastic Geometry analysis. In [83], the outage and ergodic rate for maximum-ratio-combining (MRC) receiver and optimum combining receiver (OC) have been investigated. [120] studies the impact of interference aware fractional power control in SISO uplink heterogeneous cellular networks on the average transmit power, and interference statistics. In order to complement available work in the literature, this chapter presents unified outage, rate and error probability analyses for MIMO uplink cellular networks. Following the downlink transmission analysis concepts presented in Chapter 6, the proposed mathematical framework abstracts the network performance into the channel power gain parameters, namely; m_o and m_i.

7.2 Uplink MIMO System Model

Following the network model depicted in Chapter 3, for the spatial distribution of BSs and UEs over the two-dimensional network, we extend the transmitter/receiver characteristics for a multiple-antenna transmission/reception. The UEs are equipped with N_t colocated antennas. Similarly, BSs operate N_r-antenna receivers. Rayleigh multi-path fading environment is assumed, where each link between a transmitting antenna and a receiving antenna follows an i.i.d complex Gaussian distribution $\mathcal{CN}(0,1)$, which is independent from the transmitter and receiver locations as well

as the other channel gains. Full inversion power control is employed to fully compensate for the path-loss attenuation. An average received signal power ρ is maintained constant at the test receiver. The transmit power of the i^{th} UE is a random variable P_{u_i}. Moreover, UEs have a maximum transmit power constraint of P_U, thus, $P_{u_i} = \min\{\rho D_i^{\eta}, P_U\}$, with D_i is the distance between an active UE and its serving BS. Without loss of generality, the distance D_i has the Rayleigh distribution

$$f_{D_i}(d) = 2\pi\lambda_B\, d e^{-\pi\lambda_B\, d^2}, \qquad 0 \leq d < \infty. \tag{7.1}$$

Consequently, the distance-dependent transmit power is also a random variable with PDF [47]

$$f_{P_{u_i}}(x) = \frac{2\pi\lambda x^{\frac{1}{b}-1} e^{-\pi\lambda\left(\frac{x}{\rho}\right)^{\frac{1}{b}}}}{2b\left(1 - e^{-\pi\lambda\left(\frac{P_U}{\rho}\right)^{\frac{1}{b}}}\right)}, \quad x > 0, \tag{7.2}$$

and j^{th} moment [47]

$$\mathbb{E}_{P_{u_i}}\left[P_{u_i}^{\mathrm{j}}\right] = \frac{\rho^{\mathrm{j}}\ \gamma\left(\mathrm{j}b+1, \pi\lambda\left[\frac{P_U}{\rho}\right]^{\frac{1}{b}}\right)}{(\pi\lambda)^{\mathrm{j}b}\left(1 - e^{-\pi\lambda\left(\frac{P_U}{\rho}\right)^{\frac{1}{b}}}\right)}. \tag{7.3}$$

As has been shown for the downlink transmission in Chapter 6, due to the different MIMO setups, various precoding techniques at the transmitter side and/or combining/equalization techniques at the receiver side are adopted. This renders the equivalent channel gains after being processed, i.e., the SISO-equivalent gains, no longer exponential. The intended and interfering SISO-equivalent gains distributions depend on the adopted MIMO scheme and the number of transmit and receive antennas, namely N_t and N_r.

7.2.1 Uplink MIMO Received Signal Model

Employing full inversion power control in an arbitrary MIMO system setup for Rayleigh fading environment, the complex baseband received signal taking into account arbitrary combining schemes, is expressed as

$$\begin{aligned}\tilde{\mathbf{y}} &= \mathbf{W}_o\mathbf{y} \\ &= \sqrt{\frac{\rho}{N_t}}\,\mathbf{W}_o\mathbf{H}_o\,\mathbf{s} + \sum_{r_i\in\tilde{\Psi}_{u_i}} \sqrt{\frac{P_{u_i}}{N_t}} r_i^{-\frac{\eta}{2}} \mathbf{W}_o\mathbf{H}_i\mathbf{s}_i + \mathbf{W}_o\mathbf{n},\end{aligned} \tag{7.4}$$

where the intended and interfering channels are modeled by independent and identically distributed zero-mean complex Gaussian random variables. The intended channel matrix to the serving BS is denoted by $\mathbf{H}_o \in \mathbb{C}^{N_r\times N_t}$, and the interfering channel matrix from the i^{th} interfering UE to the test BS is denoted by $\mathbf{H}_i \in \mathbb{C}^{N_r\times N_t}$. The intended and interfering transmitted symbols are $\mathbf{s} \in \mathbb{C}^{L\times 1}$ and $\mathbf{s}_i \in \mathbb{C}^{L\times 1}$, respectively, where L is the number of multiplexed data streams. Note that L itself is dictated by the MIMO setting under study.

From the test receiver point of view, and by adopting the Gaussian signaling approximation, the symbols $\mathbf{s}_i$ are approximated by $\tilde{\mathbf{s}}_i \sim \mathcal{CN}(0, \mathbf{I}_L)$, where $\mathbf{I}_L$ is an identity matrix of size L. On the other hand, the exact symbols in $\mathbf{s}$ are taken into account and are independently drawn from an equiprobable two-dimensional constellations with $|s_l|^2 = 1, l = 1, 2, \cdots, L$. The matrix $\mathbf{W}_o \in \mathbb{C}^{L\times N_r}$ is the combining matrix at the test receiving BS and it depends on the corresponding realization of $\mathbf{H}_o$, according to the employed MIMO scheme. Last, $\mathbf{n} \in \mathbb{C}^{N_r\times 1}$ is the zero-mean additive white Gaussian noise vector with covariance matrix $\mathcal{N}_o\mathbf{I}_{N_r}$, where $\mathbf{I}_{N_r}$ is the identity matrix of size N_r. The receiving BS employs a per-symbol maximum likelihood (ML) receiver to decode the received symbols.

It is worth highlighting that considering the case of multi-user MIMO in the uplink is still an open problem as it will require cooperation among the UEs to perform

precoding and is thus not studied in this chapter. Further, it does not necessarily boil down to a single-antenna transmission equivalent representation. However, we refer to multi-user uplink transmission in this chapter as multiple MRC links. That is, for $\mathcal{K}$ single-antenna UEs uniformly distributed across the cell of study, each UE-BS link is seen as single-input-multiple-output link with a maximum-ratio-combining receiver at the BS. Without any loss of generality, we study one UE-BS link out of the $\mathcal{K}$ links.

7.3 Equivalent Uplink SISO-SINR Representation

In this chapter, we mainly focus on orthogonal space time block coding, maximum-ratio combining, and zero-forcing receivers as the studied uplink scenarios. Therefore, combining, and equalization techniques that decode multiplexed symbols from diverse streams, are of interest in the sequel. The received signal model after applying the combining matrix is given by

$$\tilde{y}_l = \sqrt{\frac{\rho}{N_t}} \underbrace{\sum_{k=1}^{L} \overbrace{\bar{\mathbf{w}}_{o,l}^T \mathbf{H}_o}^{[0\ 0 \ldots g_{o,k} \ldots 0\ 0]} s_k}_{g_{o,l} s_l} + \sum_{r_i \in \tilde{\Psi}_{u_i}} \underbrace{\sqrt{\frac{P_{u_i} r_i^{-\eta}}{N_t}} \sum_{k=1}^{L} \overbrace{\bar{\mathbf{w}}_{o,l}^T \mathbf{H}_i}^{a_{l,k}^{(i)}} s_{i,k}}_{I_i} + \bar{\mathbf{w}}_{o,l}^T \mathbf{n}, \tag{7.5}$$

where $\bar{\mathbf{w}}_{o,l}$ is the l^{th} column of matrix $\mathbf{W}_o^T$, $a_{l,k}^{(i)}$, $\forall k$ are the complex random coefficients combining the interfering symbols from the antennas of the i^{th} interfering UE. The coefficients $a_{l,k}^{(i)}$ are therefore functions of realizations of the channel matrices $\mathbf{H}_o$ and $\mathbf{H}_i$.

It is clear that from (7.5), similar to the downlink transmission, that the product $\mathbf{W}_o\mathbf{H}_o$ will also result in an identity matrix with possibly different values on the diagonal, according to the stream being decoded. We use $g_{o,l}$ to denote the l^{th} stream. Note that $|g_{o,l}|^2,\ \forall l \in \{1, \cdots, L\}$ are i.i.d Gamma random variables.

By adopting the Gaussian signaling approach for the interfering symbols, (7.5) is

approximated by

$$y_l \approx \sqrt{\frac{\rho}{N_t}}\, g_{o,l} s_l + \sum_{r_i \in \tilde{\Psi}_{u_i}} \underbrace{\sqrt{\frac{P_{u_i}}{N_t}} r_i^{-\frac{\eta}{2}} \sum_{k=1}^{L} a_{l,k}^{(i)} \tilde{s}_{i,k}}_{I_i} + \bar{\mathbf{w}}_{o,l}^T \mathbf{n}. \tag{7.6}$$

Following Proposition 6.1 in Chapter 6, the uplink SISO-equivalent SINR is expressed as

$$\Upsilon = \frac{\frac{\rho}{N_t} \tilde{g}_o}{\sum_{r_i \in \tilde{\Psi}_{u_i}} \frac{P_{u_i}}{N_t} r_i^{-\eta} \tilde{g}_i + \mathcal{N}_o}, \tag{7.7}$$

where $\tilde{g}_o$ and $\tilde{g}_i$ represent the abstraction of the MIMO setting effect, i.e., combining matrices. Further, $\tilde{g}_o$ and $\tilde{g}_i$ are i.i.d Gamma random variables with shape parameters m_o and m_i, respectively.

7.4 A Unified Uplink Performance Analysis

Building on the notion of the uplink equivalent SISO-SINR, and exploiting the claimed Gamma distributions of $\tilde{g}_o$ and $\tilde{g}_i$ in (8.7), we next focus on the unified Laplace Transform of the PDF of the aggregate interference, $\mathcal{L}_{\mathcal{I}_U}(z) = \exp\{-z\mathcal{I}_U\}$, given in the following lemma.

Lemma 7.1. *In an uplink two-dimensional cellular network, with the intensity of the Poisson distributed interfering UEs is $\lambda = p\lambda_B$, employing full channel inversion power control, under a multiple-antenna transmission scheme, that is abstracted via the equivalent SISO-SINR from* (8.7)*, a UE transmits a vector of length L per channel use (pcu) of complex Gaussian symbols $\tilde{\mathbf{s}}_i \sim \mathcal{CN}(0, \boldsymbol{I}_L)$. Accordingly, the LT of the aggregate interference power at a test receiving BS is given by*

$$\mathcal{L}_{\mathcal{I}_U}(z) = \exp\left\{-\nu(\rho,\lambda)\left[\left({}_2F_1\left(\frac{-1}{b}, m_i; 1-\frac{1}{b}; -z\rho\right) - 1\right)\right]\right\}, \tag{7.8}$$

where ${}_2F_1(\cdot,\cdot;\cdot;\cdot)$ *is the Gauss hypergeometric function [112] and*

$$\nu\left(\rho,\lambda\right)=\frac{\gamma\left(2,\pi\lambda\left[\frac{P_U}{\rho}\right]^{\frac{1}{b}}\right)}{1-e^{-\pi\lambda\left(\frac{P_U}{\rho}\right)^{\frac{1}{b}}}}. \tag{7.9}$$

Proof. Starting from the definition of the LT, we have

$$\begin{aligned}\mathcal{L}_{\mathcal{I}_U}\left(z\right)=&\mathbb{E}\left[\exp\left\{-z\sum_{r_i\in\tilde{\Psi}_{u_i}}P_{u_i}r_i^{-\eta}\tilde{g}_i\right\}\right]\\ &\overset{(a)}{\approx}\exp\left\{-2\pi\lambda\int_t^{\infty}\mathbb{E}\left[1-e^{-zP_{u_i}x^{-\eta}\tilde{g}}\right]x\mathrm{d}x\right\}\\ &\overset{(b)}{=}\exp\left\{-2\pi\lambda\int_t^{\infty}\left[1-\frac{1}{(1+zP_{u_i}x^{-\eta})^{m_i}}\right]x\mathrm{d}x\right\},\\ &\overset{(c)}{=}\exp\left\{-\nu\left(\rho,\lambda\right)\int_0^{1}\left[1-\frac{1}{(1+z\bar{x})^{m_i}}\right]\frac{1}{\bar{x}^{\frac{2}{\eta}+1}}\mathrm{d}\bar{x}\right\},\end{aligned} \tag{7.10}$$

where (a) follows from the probability generating functional (PGFL) [17] of an approximate homogeneous PPP that is constituted by interfering UEs whose average received power at the test BS is less than ρ, i.e., $t=\left(\frac{P_{u_i}}{\rho}\right)^{\frac{1}{\eta}}$, (b) follows from the LT of the gamma distributed channel gains with shape parameter m_i and unity scale parameter, and (c) is obtained from the moment of the transmit power P_{u_i} given in (7.3), and by employing a simple change of variables $\bar{x}=P_{u_i}x^{-\eta}$. By solving the integral in (c), we directly obtain the final expression for the uplink aggregate interference LT in (6.8). □

The uplink MIMO KPIs expressions for cellular networks employing M-QAM modulation scheme and full channel inversion power control are represented in the following theorem.

Theorem 7.1. *Unified Analysis: For an uplink MIMO cellular network with an equivalent SISO-SINR model represented by* (8.7) *under an equiprobable unit-power square quadrature amplitude modulation (M-QAM) scheme, and by approximating the point*

process of the interfering UEs by a homogeneous PPP with intensity $\lambda = p\lambda_B$, then the ASEP for an arbitrary symbol is approximated by

$$\begin{aligned}\mathrm{ASEP}_{\mathrm{UL}} \approx w_1 \left[1 - \frac{\Gamma\left(m_o + \frac{1}{2}\right)}{\Gamma\left(m_o\right)} \frac{2}{\pi} \int_0^{\infty} \frac{1}{\sqrt{z}} e_1^{-z\left(1+\frac{m_o \mathcal{N}_o}{\beta\rho}\right)} F_1\left(1 - m_o; \frac{3}{2}; z\right) \cdot \mathcal{L}_{\mathcal{I}_U}\left(\frac{m_o z}{\beta\rho}\right) \mathrm{d}z\right] \\ + w_2 \left[1 - \frac{4m_o}{\pi} \int_0^{\infty} e^{-z\left(\frac{m_o \mathcal{N}_o}{\beta\rho}\right)} \int_0^{\frac{\pi}{4}} {}_1F_1\left(m_o + 1; 2; \frac{-z}{sin^2\vartheta}\right) \frac{1}{sin^2\vartheta} \cdot \mathcal{L}_{\mathcal{I}_U}\left(\frac{m_o z}{\beta\rho}\right) \mathrm{d}\vartheta \mathrm{d}z\right],\end{aligned} \tag{7.11}$$

with ${}_1F_1(\cdot;\cdot;\cdot)$ defined as the Kummer confluent hypergeometric function [112].

We write the probability that the SIR for an arbitrary symbol goes below a predefined threshold θ as

$$\mathcal{O}_{\mathrm{UL}}\left(\theta\right) \approx 1 - \sum_{j=0}^{m_o - 1} \frac{(-1)^j}{j!} \frac{\mathrm{d}^j}{\mathrm{d}z^j} \left(\frac{\theta}{\rho}\right)^j \mathcal{L}_{\mathcal{I}_U}\left(z\right) \Big|_{z=\frac{\theta}{\rho}}, \tag{7.12}$$

whereas the ergodic capacity for an arbitrary data stream is expressed as

$$\mathcal{R}_{\mathrm{UL}} \approx \int_0^{\infty} \mathcal{L}_{\mathcal{I}_U}\left(\frac{z}{\rho}\right) \left(\frac{1 - (1+z)^{-m_o}}{z}\right) \mathrm{d}z. \tag{7.13}$$

Proof. We build on the AWGN and the Gaussian interference ASEP expressions, given as

$$\mathrm{ASEP}\left(\Upsilon\right) = w_1 \mathbb{E}\left[\mathrm{erfc}\left(\sqrt{\beta\Upsilon}\right)\right] + w_2 \mathbb{E}\left[\mathrm{erfc}^2\left(\sqrt{\beta\Upsilon}\right)\right], \tag{7.14}$$

with $w_1 = 2\frac{\sqrt{M}-1}{\sqrt{M}}, w_2 = -\left(\frac{\sqrt{M}-1}{\sqrt{M}}\right)^2$, and $\beta = \frac{3}{2(M-1)}$ are the constellation-dependent determinstic values. For the complementary metrics to fully quantify the network performance, we follow the outline of the outage and ergodic rate proofs in Appendix C.1, noting that we no longer average over the intended link distance r_o, due to the

full power control compensation. □

Unlike the downlink transmission, where the outage and ergodic rate expressions are exact, the uplink outage and ergodic rate are both approximations due to the PPP assumption of the interfering UEs. Exploiting the proposed unified model, the characterization of the different MIMO setups for the uplink is the similar to the downlink scenario, summarized in Table 7.1.

MIMO Setup	L	$\boldsymbol{m_o}$	$\boldsymbol{m_i}$	Accuracy
MRC	1	N_r	1	Exact
OSTBC	N_s	$N_s N_r$	N_s	Exact
ZF-Rx	N_t	$N_r - N_t + 1$	N_t	Exact

Table 7.1: SISO-equivalent gamma distribution parameters for various uplink MIMO settings.

7.5 Characterizing Uplink MIMO Configurations

7.5.1 Maximum-Ratio-Combining (MRC) receivers

Maximum-ratio-combiners (receive diversity) are considered the optimum linear combiners for mutliple-antenna transmissions under Gaussian interference channels in presence of independent fading channels across antenna elements [121–123]. The MRC vector at the intended BS, dropping the l^{th} stream index for notational convenience, $\bar{\mathbf{w}}_o^T = \mathbf{h}_o^H$, optimally combines the N_r replicas of the received signal at the test BS. Therefore, the received signal is written as

$$\begin{aligned}\tilde{y} &= \bar{\mathbf{w}}_o^T \mathbf{y} \\ &= \sqrt{\frac{\rho}{N_t}}\, \bar{\mathbf{w}}_o^T \mathbf{h}_o\, \mathbf{s} + \sum_{r_i \in \tilde{\Psi}_{u_i}} \sqrt{\frac{P_{u_i}}{N_t}} r_i^{-\frac{\eta}{2}} \bar{\mathbf{w}}_o^T \mathbf{h}_i \mathbf{s}_i + \bar{\mathbf{w}}_o^T \mathbf{n}, \end{aligned} \tag{7.15}$$

where $\mathbf{h}_o$ and $\mathbf{h}_i$ are $N_r \times 1$ complex Gaussian vectors with i.i.d entries. Similar to the SIMO downlink transmission, the abstract fading parameters are $m_o = N_r$, i.e., the diversity gain, and $m_i = 1$, i.e., the number of multiplexed streams.

7.5.2 Orthogonal Space-Time Block Coding (OSTBC)

Exploiting space-time constellations in an uplink multiple-antenna transmission for diversity and mulitplexing gains, the combining matrix $\mathbf{W}_o = \frac{\mathbf{H}_{\text{eff}}^H}{\|\mathbf{H}_o\|_{\text{F}}}$, where $\mathbf{H}_{\text{eff}}$ is the effective channel impulse response that corresponds to the constructed orthogonal space-time code (cf. Chapter 6). Finally, similar to the downlink OSTBC transmission, we have $m_o = N_s \times N_r$ and $m_i = N_r$.

7.5.3 Zero-Forcing beamforming with MLR (ZF-Rx)

Suboptimal zero-forcing receivers are employed to achieve multiplexing gains. Combining matrix $\mathbf{W}_o$ is a function of the uplink channel matrix and is given by $\mathbf{W}_o = \left(\mathbf{H}_o^H \mathbf{H}_o\right)^{-1} \mathbf{H}_o^H$. The diversity gain is thus $m_o = N_r - N_t + 1$ and the multiplexing gain is $m_i = N_t$.

7.6 Numerical and Simulations Results

In order to provide a fair comparison, we compare the uplink MIMO transmissions employing maximum ratio combining (MRC), zero-forcing receiver (ZF-Rx), and orthogonal space time block coding (OSTBC), for a 2×2 MIMO system. Note that for the MRC scheme, $N_t = 1$. The intensity of BSs is $\lambda_B = 4\text{BSs/km}^2$, with an activity factor $p = 1$. The UEs uniformly distributed across the network is $\lambda_U = 8\text{UEs/km}^2$. However, the effective intensity of the interfering UEs is that of the active BSs. The noise power $\mathcal{N}_o = -90$ dBm. The average received power ρ varies to provide the varying average receive SNR $\frac{\rho}{\mathcal{N}_o}$. The path-loss exponent $\eta = 4$. Lines represent theoretical results, while markers represent Monte Carlo simulations.

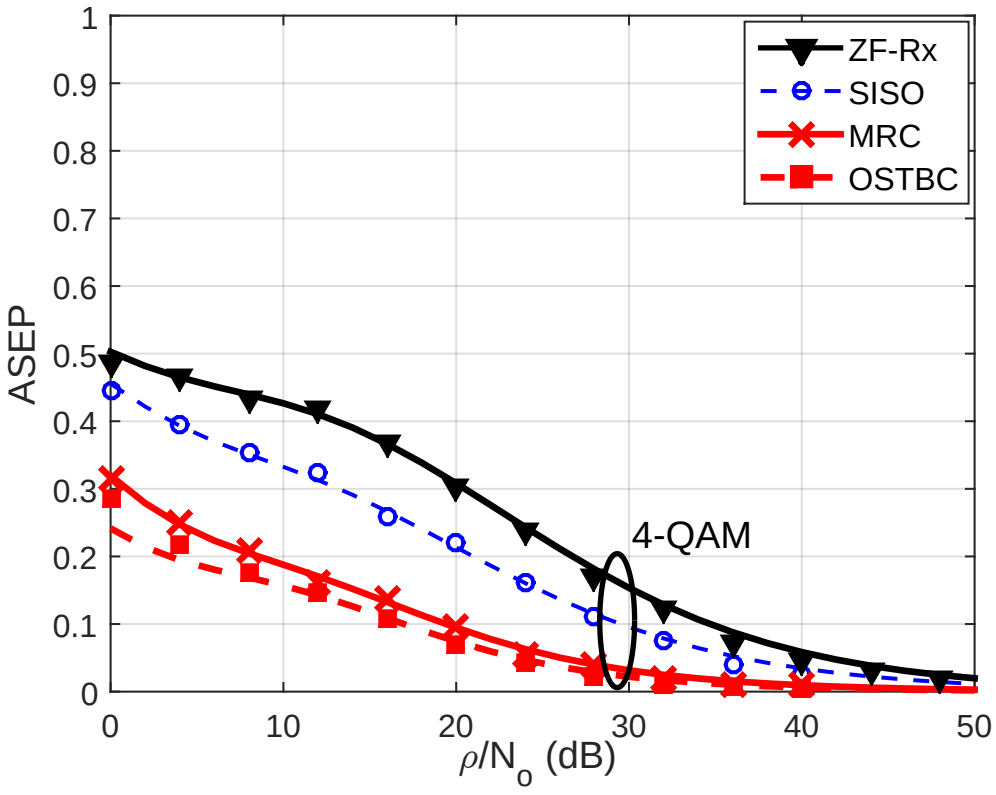

Figure 7.1: ASEP for 4-QAM modulation, for the different MIMO setups using the same number of antennas $N_t = 2$ and $N_r = 2$, at $p = 1$.

In Figs. 7.1 and 7.2 the performance of average symbol error is verified via Monte Carlo simulations. Clearly, the best ASEP and outage performance are achieved by the OSTBC scheme, with $\frac{m_o}{m_i} = 2$, and the least is by the ZF-Rx, with $\frac{m_o}{m_i} = \frac{1}{2}$, since OSTBC provides transmit and receive diversity whereas the ZF-Rx offers multiplexing diversity. MRC provides receive diversity, with $\frac{m_o}{m_i} = 2$ similar to the OSTBC and thus has a very close performance. However, the actual values of m_o and m_i have an impact on the resulting performance, which is in compliance with the observations for the downlink transmission from Chapter 6

The analytic unified uplink MIMO outage probability and ASEP performance results are presented in Figs. 7.3 and 7.4, respecitvely. Obviously, by exploiting Figs. 7.3 and 7.4, we can have a complete network design model for different ρ and/or

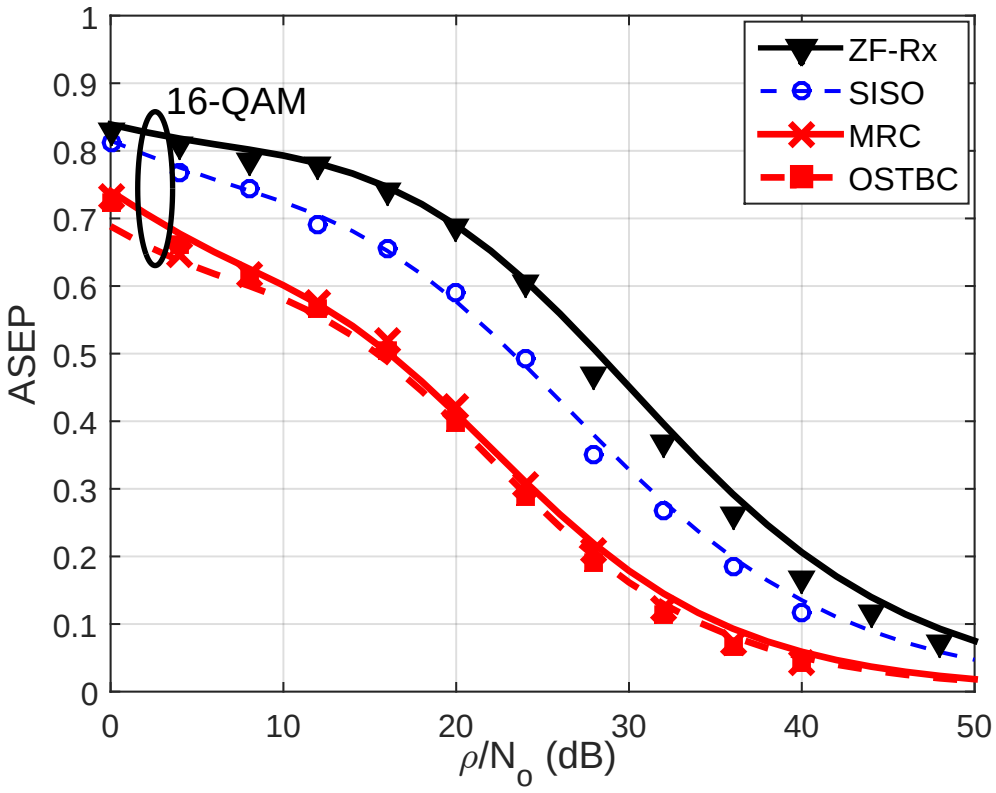

Figure 7.2: ASEP for 16-QAM modulation, for the different MIMO setups using the same number of antennas $N_t = 2$ and $N_r = 2$, at $p = 1$.

θ values. The same network design methodology from Chapter 6 holds for the uplink transmission.

7.7 Chapter Summary and Conclusions

Performance trends of uplink MIMO transmissions are studied in this chapter. Motivated by the unified framework developed in Chapter 6 for the downlink transmissions, this chapter presents a unified paradigm for uplink cellular networks employing full channel inversion power control. The ASEP, outage probability and ergodic rate have been analytically formulated via tractable unified mathematical expressions. Orthogonal space time block coding, zero-forcing receiver, and maximum ratio combiner only have been studied since they were shown to be the uplink MIMO setups that

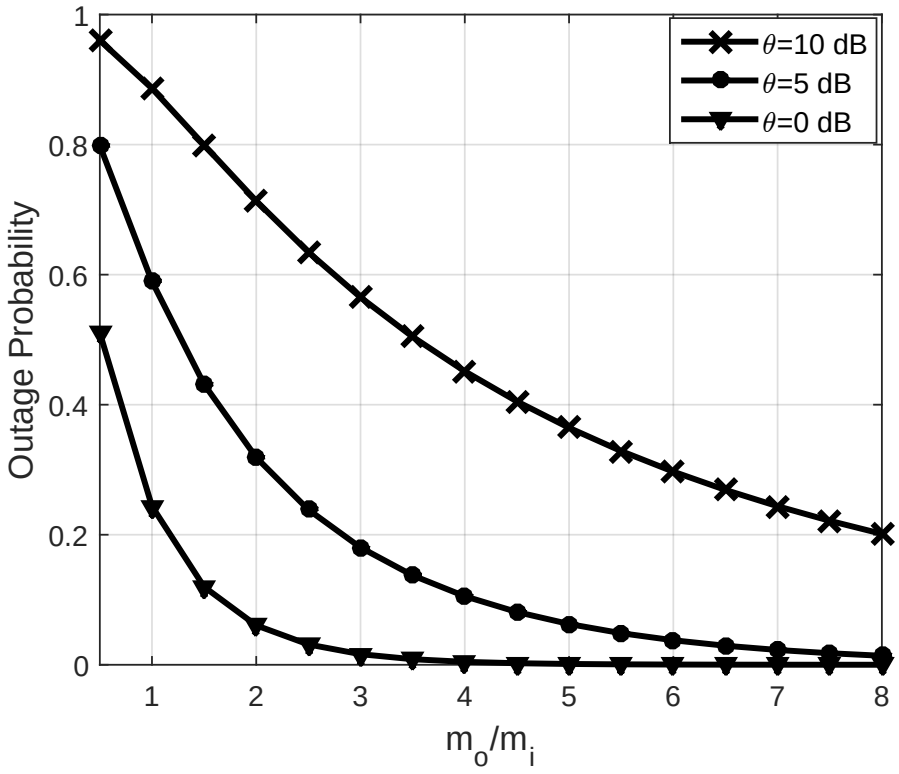

Figure 7.3: Unified Outage performance versus the ratio $\frac{m_o}{m_i}$ for an arbitrary uplink MIMO setup, for $\theta = 0, 5, 10$ dB at $\rho = -70$ dBm.

boil down to a single-antenna transmission equivalent. With the aid of the presented mathematical framework, an uplink design strategy is developed that allows for efficient use of network parameters and resources, e.g., UEs transmit power, number of antennas, and MIMO setting. In the next chapter, we study the impact of interference temporal correlation on retransmissions upon decoding errors performance, in both downlink and uplink scenarios.

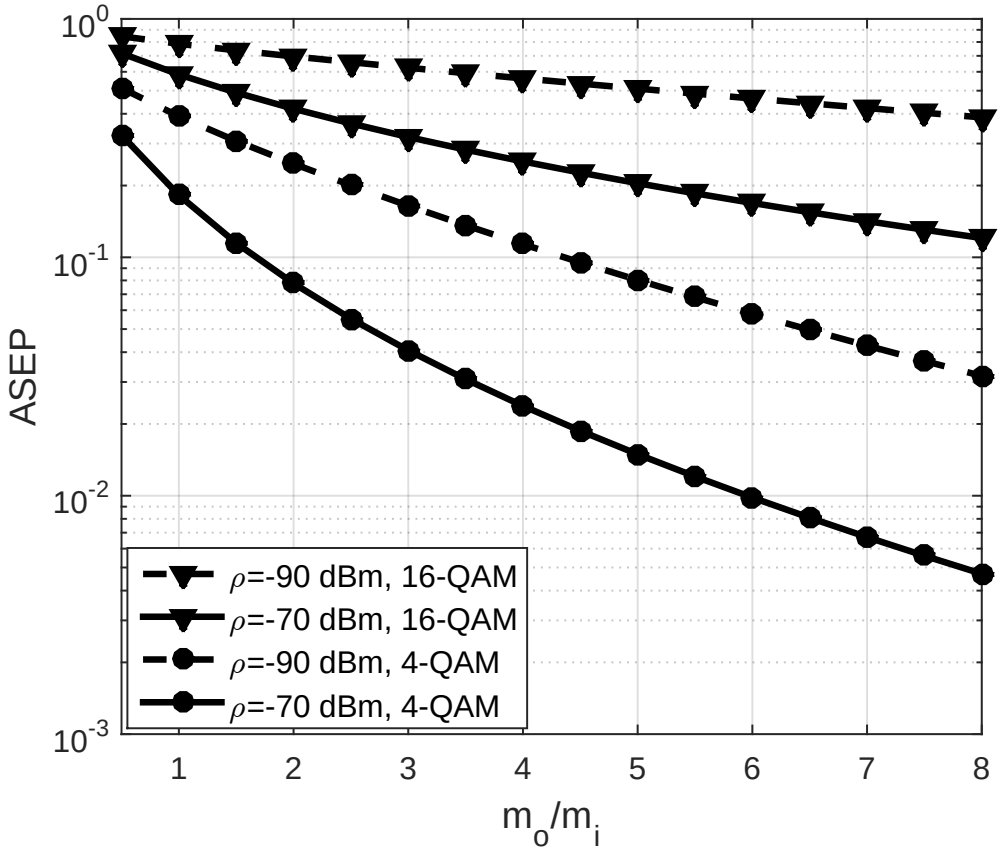

Figure 7.4: Unified ASEP performance versus the ratio $\frac{m_o}{m_i}$ for an arbitrary uplink MIMO setup, for 4-QAM and 16-QAM.

Chapter 8

Effect of Interference Temporal Correlation

8.1 Introduction

Signals retransmissions are used for incorrectly received data in large-scale cellular networks to improve the network performance. Erroeneous signals retransmissions in cellular networks implicitly imply that the randomly chosen test user has encountered decoding errors due to being in a spatial location with poor signal-to-interference-and-noise-ratio (SINR) or signal-to-interference-ratio (SIR) condition. Poor SINR and SIR conditions may imply a poor intended link quality, high interference, or both. Due to the common set of interfering sources, it is shown that the aggregate interference in large-scale cellular networks is correlated over the spatial and time domains [124]. That is to say, interference temporal correlation in cellular networks is an inherent network characteristic which degrades the overall performance.Although we assume that the channel fading independently changes from one time slot to another, the interference at a given location is correlated across time for the same network realization due to the fixed locations of the complete set of BSs and/or UEs. In other words, assuming a static UE, a subset of the interferers at a given time slot might also be interfering in subsequent time slots, which introduces temporal interference correlation that needs to be taken into account. Potential performance gains, specifically time diversity gains, can be realized through erroneous signals retransmissions in both downlink and uplink scenarios. Hence, it is crucial to account for the temporal interference correlation for true assessment of the retransmissions performance [32, 125, 126].

This chapter extends the unified mathematical paradigm proposed in Chapters 5 and 6 to account for signal retransmission upon decoding errors, in which the temporal correlation among the SINRs of the original and retransmitted signals is accounted for. For the downlink setup, the effect of retransmission upon decoding errors on the network performance is only studied for cooperating single-antenna BSs [32], which is different from the case when both BSs and UEs are equipped with multiple antennas and precoding/combining is applied in the downlink. In this chapter, we shed lights on the diversity loss due to the temporal correlation among the SINRs of the original and retransmitted signals in the downlink. For the uplink scenario, power control strategies play a vital role in the achievable retransmission diversity. Thus, this chapter investigates the impact of fractional power control schemes on network-wide coverage probability and quantifies the potential time diversity gains. Full channel inversion is shown to overcome interference correlation and achieve the optimistic independent transmissions performance. Furthermore, several design insights are highlighted for both setups. The uplink system model employed in this study follows the state of the art stochastic geometry models developed in [47, 83, 127] and all the mathematical findings herein are verified via Monte Carlo simulations.

8.2 Temporal Correlation in the Downlink

The downlink network performance with retransmission cannot be directly deduced from Lemma 6.1 and Theorem 6.1 of Chapter 6 due to the temporal interference correlation. In this chapter, we study temporal correlation between two arbitrary time slots at the same spatial location. Based on the interference temporal correlation, we derive the conditional success probability of a retransmission such that an earlier transmission at the same location was unsuccessful. Note that the presented analysis captures the pairwise temporal correlation across any two time slots as long as the spatial location of the test receiver is fixed. This section builds on the same system

model as that described in Chapter 6, where an $N_r \times N_t$ system employing an aribtrary MIMO setting is considered. Let $\tilde{\Psi}^o$ be the set of distances between the interferers to the test receiver, excluding r_o, such that $\tilde{\Psi}^o = \{r_i\}, \forall i$. We assume that p is the independent BSs activity factor in an arbitrary time slot. We study a snapshot of two arbitrary time slots over which a signal retransmission is required to enhance the the SIR performance.

To incorporate the effect of retransmission into the analysis, the temporal correlation of the interference should be characterized via the joint LT of the interferences across different time slots. First, let $\tilde{\Psi}^o_1 \subset \tilde{\Psi}^o$ and $\tilde{\Psi}^o_2 \subset \tilde{\Psi}^o$ be the sets of interfering BSs in the first and second time slots of transmissions, respectively. Exploiting the independent transmission assumption per time slot, $\tilde{\Psi}^o_1$ and $\tilde{\Psi}^o_2$ can be decomposed into the three independent PPPs, that for notational and mathematical convenience are represented by the sets $\{\tilde{\Psi}^o_1 \setminus \tilde{\Psi}^o_2\}$, $\{\tilde{\Psi}^o_2 \setminus \tilde{\Psi}^o_1\}$, and $\{\tilde{\Psi}^o_2 \cap \tilde{\Psi}^o_1\}$, and have the intensities $p(1-p)\lambda_B$, $(1-p)p\lambda_B$, and $p^2\lambda_B$, respectively. The receive SIR at the receiving UE, at a given time slot j, is written as

$$\bar{\Upsilon}^{(j)} = \frac{Pr_o^{-\eta}\tilde{g}_o}{\sum_{r_i \in \tilde{\Psi}^o} Pr_i^{-\eta}\tilde{g}_i}. \tag{8.1}$$

Substituting $p\lambda_B = \lambda$, the joint LT of the two random variables $\mathcal{I}_D^{(1)}$, and $\mathcal{I}_D^{(2)}$ is given by the following lemma.

Lemma 8.1. *Consider a cellular network with MIMO transmission scheme that can be represented via the equivalent SISO-SINR in* (8.1) *and BSs are modeled via a PPP with intensity λ_B and activity factor p, the joint LT of the interferences at a given location at two different time slots, denoted by $\mathcal{I}_D^{(1)}$ and $\mathcal{I}_D^{(2)}$, such that the interfering*

BSs may use different MIMO scheme across time, is given by

$$\mathcal{L}_{\mathcal{I}_D^{(1)},\mathcal{I}_D^{(2)}\big|r_o}(z_1,z_2)=\exp\left\{-\pi\lambda r_o^2\left[p\left(\mathcal{F}_1\left(\frac{-2}{\eta};m_{i,1},m_{i,2};1-\frac{2}{\eta};-z_1r_o^{-\eta},-z_2r_o^{-\eta}\right)+1\right)\right.\right.$$
$$\left.\left.+(1-p)\ \left({}_2F_1\left(\frac{-1}{b},m_{i,2};1-\frac{1}{b};-zPr_o^{-\eta}\right)+{}_2F_1\left(\frac{-1}{b},m_{i,1};1-\frac{1}{b};-zPr_o^{-\eta}\right)\right)-2\right]\right\}, \tag{8.2}$$

where $m_{i,1}$ and $m_{i,2}$ are the parameters of the Gamma distributed equivalent channel gains (given in Table 6.1) corresponding to the employed MIMO scheme at the first and second time slots, respectively, and $\mathcal{F}_1(\cdot;\cdot,\cdot;\cdot;u,v)$ is the Appell Hypergeometric function, which extends the hypergeometric function to two variables u and v [128].

Proof. The joint LT of $\mathcal{I}_D^{(1)}$ and $\mathcal{I}_D^{(2)}$ is given by

$$\begin{aligned}
\mathcal{L}_{\mathcal{I}_D^{(1)},\mathcal{I}_D^{(2)}\big|r_o}(z_1,z_2)&=\mathbb{E}\left[\exp\left\{-z_1\mathcal{I}_D^{(1)}-z_2\mathcal{I}_D^{(2)}\right\}\right]\\
&=\mathbb{E}\left[\exp\left\{-\sum_{r_i\in\tilde{\Psi}_2^o\cap\tilde{\Psi}_1^o}Pr_i^{-\eta}\left(z_1\tilde{g}_i^{(1)}+z_2\tilde{g}_i^{(2)}\right)\right\}\right.\\
&\qquad\left.\times\exp\left\{-z_1\sum_{r_i\in\tilde{\Psi}_1^o\setminus\tilde{\Psi}_2^o}Pr_i^{-\eta}\tilde{g}_i^{(1)}-z_2\sum_{r_i\in\tilde{\Psi}_2^o\setminus\tilde{\Psi}_1^o}Pr_i^{-\eta}\tilde{g}_i^{(2)}\right\}\right]\\
&\overset{(a)}{=}\exp\left\{-2\pi p\lambda\int_{r_o}^{\infty}\mathbb{E}_{\tilde{g}_i^{(1)},\tilde{g}_i^{(2)}}\left[1-e^{-Px^{-\eta}\left(z_1\tilde{g}_i^{(1)}+z_2\tilde{g}_i^{(2)}\right)}\right]x\mathrm{d}x\right\}\\
&\qquad\times\exp\left\{-2\pi(1-p)\lambda\int_{r_o}^{\infty}\mathbb{E}_{\tilde{g}_i^{(1)}}\left[1-e^{-Px^{-\eta}z_1\tilde{g}_i^{(1)}}\right]x\mathrm{d}x\right.\\
&\qquad\left.-2\pi(1-p)\lambda\int_{r_o}^{\infty}\mathbb{E}_{\tilde{g}_i^{(2)}}\left[1-e^{-Px^{-\eta}z_2\tilde{g}_i^{(2)}}\right]x\mathrm{d}x\right\}\\
&\overset{(b)}{=}\exp\left\{-2\pi\lambda\int_{r_o}^{\infty}\left(p\left[1-\frac{1}{\left(1+Px^{-\eta}z_1\right)^{m_{i,1}}}\frac{1}{\left(1+Px^{-\eta}z_2\right)^{m_{i,2}}}\right]\right.\right.\\
&\qquad\left.\left.+(1-p)\left[1-\frac{1}{\left(1+Px^{-\eta}z_1\right)^{m_{i,1}}}\right]+(1-p)\left[1-\frac{1}{\left(1+Px^{-\eta}z_2\right)^{m_{i,2}}}\right]\right)x\mathrm{d}x\right\},
\end{aligned} \tag{8.3}$$

where (a) is obtained from the PGFL and exploiting the independence between the

PPPs represented by the sets $\{\tilde{\Psi}_1^o \setminus \tilde{\Psi}_2^o\}$, $\{\tilde{\Psi}_2^o \setminus \tilde{\Psi}_1^o\}$, and $\{\tilde{\Psi}_2^o \cap \tilde{\Psi}_1^o\}$ [17], and (b) follows from the LT of the two independent gamma distributed random variables $\tilde{g}_i^{(1)}$ and $\tilde{g}_i^{(2)}$. Solving the integral completes the proof.

□

8.2.1 Downlink Coverage Probability Analysis

The average coverage probability (defined as $1 - \mathcal{O}(\theta)$) with retransmissions and independent signal decoding is given by

$$\mathcal{P}_{\text{cov}}^{\text{DL}}(\theta) = \mathbb{P}\left(\bar{\Upsilon}^{(1)} > \theta\right) + \mathbb{P}\left(\bar{\Upsilon}^{(2)} > \theta\right) - \mathbb{P}\left(\bar{\Upsilon}^{(1)} > \theta, \bar{\Upsilon}^{(2)} > \theta\right), \tag{8.4}$$

where $\bar{\Upsilon}^{(1)}$ and $\bar{\Upsilon}^{(2)}$ are the SIRs at the first and second transmissions. Using the joint LT in Lemma 8.1, the average coverage probability with retransmission in MIMO cellular network is given by the following theorem.

Theorem 8.1. *Consider a cellular network with MIMO transmission scheme that can be represented via the equivalent SISO-SINR in* (8.1) *and BSs modeled via a PPP with intensity λ_B, the SIR coverage probability for a generic UE with retransmission such that the serving BS and interfering BSs may use different MIMO schemes across time, is given by*

$$\mathcal{P}_{\text{cov}}^{\text{DL}}(\theta) = \int_0^\infty 2\pi\lambda_B\, x e^{-\pi\lambda_B x^2} \Bigg[- \sum_{j_1=0}^{m_{o,1}-1} \sum_{j_2=0}^{m_{o,2}-1} \frac{(-1)^{j_1+j_2}}{j_1! j_2!} \bar{\theta}^{j_1+j_2} \frac{\partial^{(j_1+j_2)}}{\partial z_1^{j_1} \partial z_2^{j_2}} \mathcal{L}_{\mathcal{I}^{(1)},\mathcal{I}^{(2)}|x}(z_1, z_2)\Big|_{z_1=z_2=\bar{\theta}} + \sum_{j_1=0}^{m_{o,1}-1} \frac{(-1)^{j_1}}{j_1!} \bar{\theta}^{j_1} \frac{\partial^{j_1}}{\partial z_1^{j_1}} \mathcal{L}_{\mathcal{I}^{(1)}|x}(z_1)\Big|_{z_1=\bar{\theta}} + \sum_{j_2=0}^{m_{o,2}-1} \frac{(-1)^{j_2}}{j_2!} \bar{\theta}^{j_2} \frac{\partial^{j_2}}{\partial z_2^{j_2}} \mathcal{L}_{\mathcal{I}^{(2)}|x}(z_2)\Big|_{z_2=\bar{\theta}} \Bigg] \mathrm{d}x, \tag{8.5}$$

where $\bar{\theta} = \frac{\theta x^\eta}{P}$.

Proof. See Appendix D.1. □

8.2.2 Numerical and Simulation Results

In this section, we verify the validity and accuracy of the proposed unified model for the downlink setup, incorporating the effect of temporal correlation of interference. The BSs transmit powers (P) vary while $\mathcal{N}_o$ is kept constant to vary the transmit SNR, the path-loss exponent $\eta = 4$, the noise power $\mathcal{N}_o = -90$ dBm, the BSs intensity $\lambda_B = 10$ BSs/km^2, $\lambda_u = 20$ users/km^2. Lines represent theoretical findings, while markers represent Monte Carlo simulations.

Fig. 8.1 validates Theorem 8.1 for the outage before and after retransmission against Monte Carlo simulations. The figure shows the time diversity loss due to interference temporal correlation when compared to the independent interference scenario. The figure also shows that assuming independent interference across time is too optimistic, since those UEs requiring retransmissions are then biased to ones where there are interferers nearby due to interference temporal correlation. Nevertheless, it is possible for the network operators to exploit more diversity in the second transmission to compensate for the expected degraded retransmission performance. Fig. 8.2, shows the effect of incremental diversity in the second transmission on the outage performance for $m_o = 2$ and $m_i = 2$. The figure shows that adjusting the MIMO configuration such that $m_o = 5$ in the second transmission compensates for the temporal correlation effect and achieves the same performance as independent transmission (e.g., up to 3 dB SIR improvement can be achieved).

8.3 Temporal Correlation in the Uplink

Next, the retransmission performance in uplink cellular networks is investigated. UEs transmit powers define the aggressiveness of the aggregate network interference power, and consequently, impact the effectiveness of signals retransmissions. To this end, power control strategies are being adopted for the effective use of the UEs transmit power as a valuable and limited resource, as well as limiting the interference power.

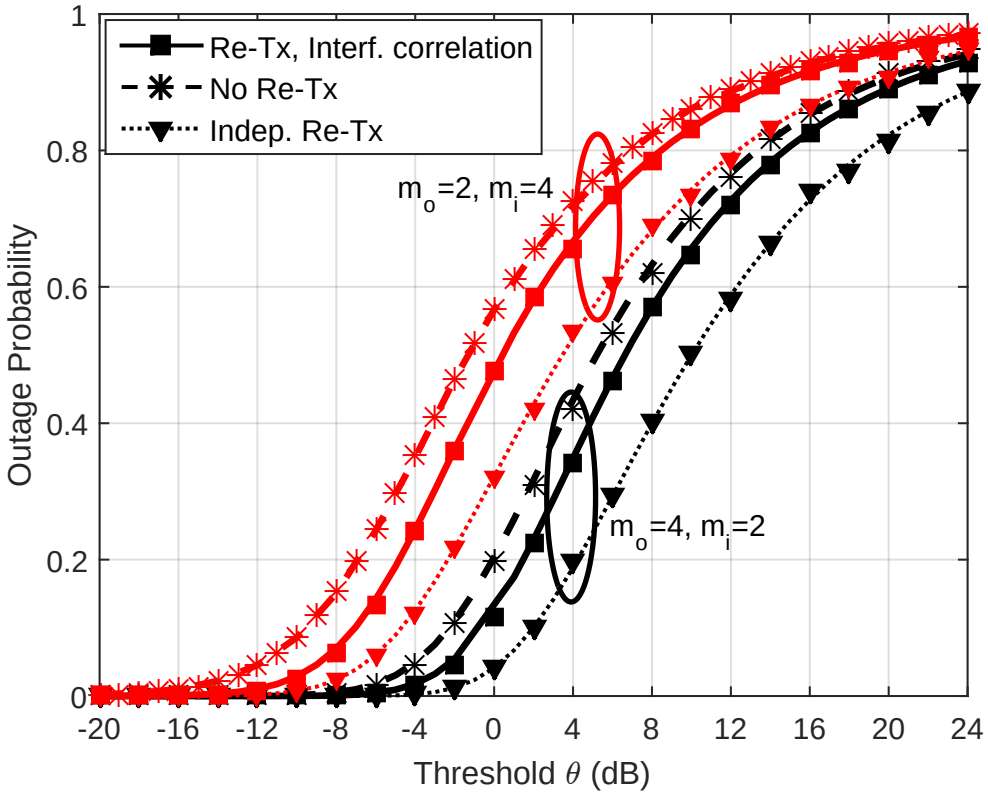

Figure 8.1: The effect of interference correlation for different m_o and m_i.

Specifically, a UE is able to partially compensate for the path-loss attenuation via a fractional power control (FPC) [129, 130] scheme that depends on the distance between the transmitting UE and its intended Base Station (BS) [83,120,127,131]. In the context of cellular networks, the effect of interference correlation is mainly studied for downlink transmission [24, 32, 125, 126]. The effect of temporal SIR correlation in uplink transmission is never addressed. In this section, we study the impact of FPC on interference temporal correlation in uplink cellular networks. We propose a network design methodology based on the power-ramping scheme, for an enhanced performance by adjusting the fractional compensation of the path-loss attenuation during the retransmission slot.

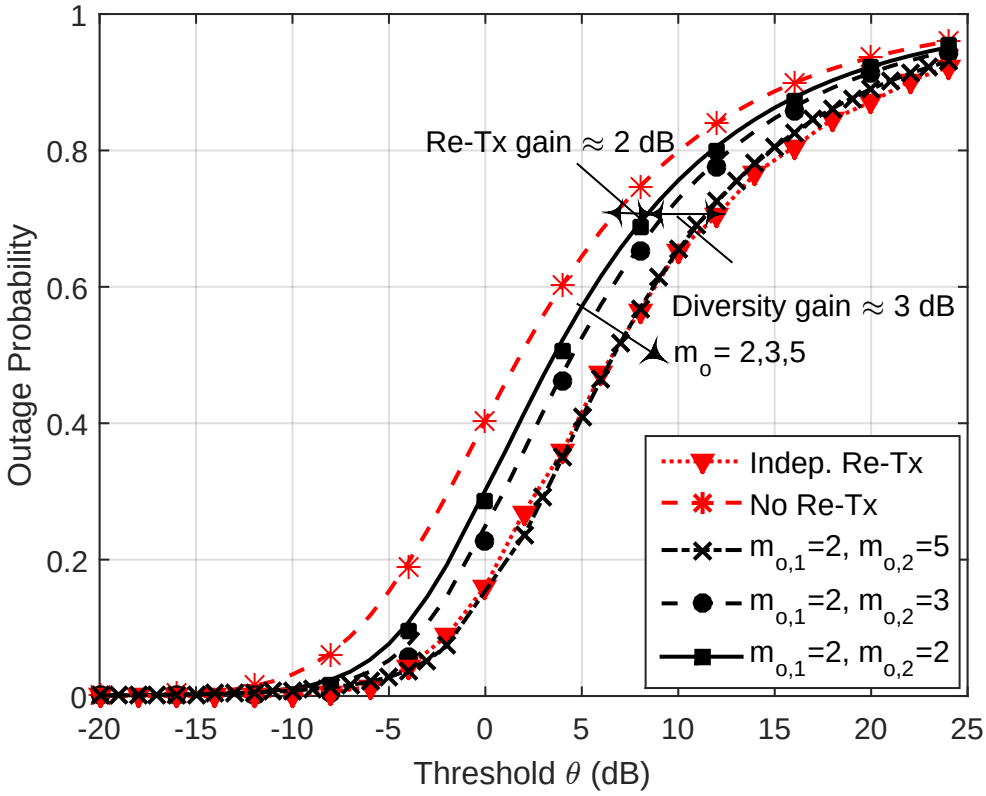

Figure 8.2: Incremental diversity for the same inter-cell interference.

8.3.1 System Model

We study a single-tier single-input-single-output (SISO) uplink cellular network and follow the same network model in Chapter 3 with some modifications, where BSs and UEs locations are modeled by two independent homogeneous PPPs, denoted by ψ_B and ψ_u with intensities λ_B and λ_U, respectively. Although the locations of interfering UEs are correlated, they are identically distributed. However, for tractability, we ignore such dependence and consider the distances between an active UE and its serving BS, denoted as D_i, to be i.i.d Rayleigh distributed random variable. Let r_i be the distance from the interfering UE to the test BS. We follow the system model in [127] to impose the interference protection region analogous to the downlink scenario. Therefore, since $r_i \geq D_i$, the PDF of D_i conditioned on r_i is a truncated

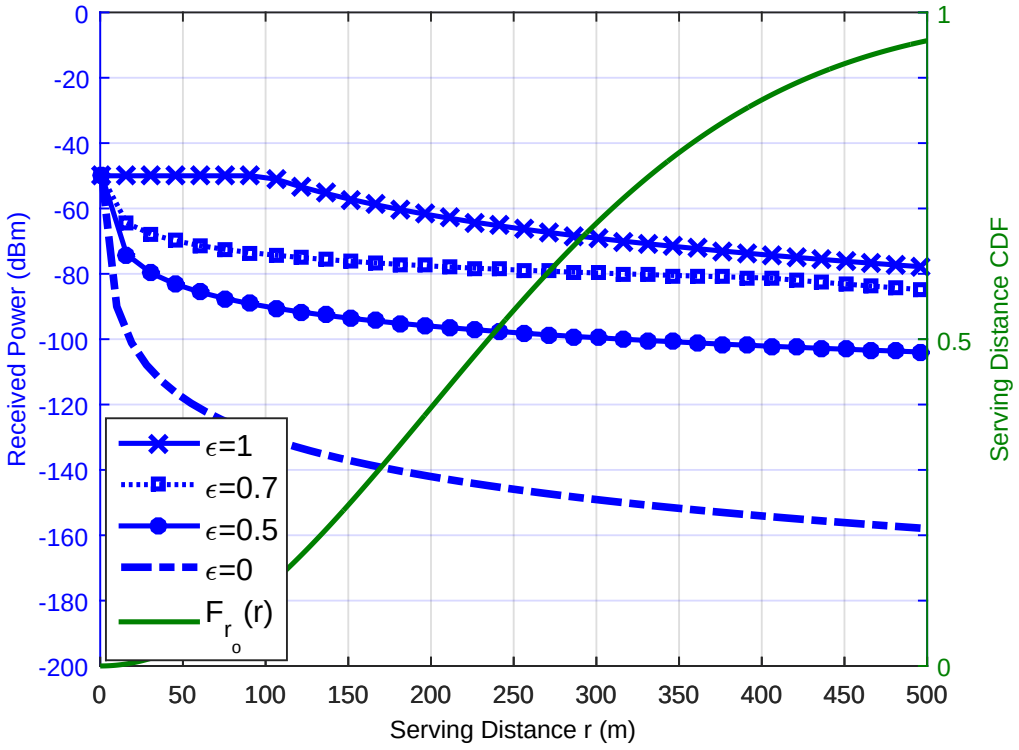

Figure 8.3: Variation of the average received power for the different ϵ values together with the CDF of the serving distance against the serving distance r_o.

Rayleigh distribution [127], where,

$$f_{D_i|r_i}(d|r_i) = \frac{2\pi\lambda_B d e^{-\pi\lambda_B d^2}}{1 - e^{-\pi\lambda_B r^2}}, 0 \leq d \leq r_i. \tag{8.6}$$

Further, interferers observed by the intended BS outisde a disc of radius r from this BS, constitute a non-homogeneous PPP with intensity $\lambda_B \left(1 - e^{-\pi\lambda_B r^2}\right)$. The point process of the actively serving BSs after independent thinning is also a PPP but with intensity $\lambda = p\lambda_B \left(1 - e^{-\pi\lambda_B r^2}\right)$ [17], where p is the independent activity probability for each BS in Ψ_B. Note that, due to the no intra-cell interference assumption, the interfering UEs do not constitute a PPP. However, following [47,110], we approximate the set of interfering UEs by a PPP $\tilde{\psi}_u$ whose effective intensity is that of the active BSs, i.e., λ. Let the set $\tilde{\Psi}_u$ contain the distances between the interferering UEs to the test BS, r_i.

Power-law path-loss attenuation is assumed, such that the signal power attenuates at the rate $d^{-\eta}$ with the distance d, where $\eta > 2$ is the path-loss exponent. A Rayleigh fading environment is considered in which the channel power gains are exponentially distributed with unit mean. Channel gains are independent from each other as well as from the spatial locations of the UEs and BSs. UEs have single antennas and maximum transmit powers of P_U. In addition, UEs employ FPC with parameter $\epsilon \in [0, 1]$ to partially compensate for the path-loss attenuation [83, 127], in which $\epsilon = 0$ and $\epsilon = 1$ correspond, respectively, to the constant transmit power and full channel inversion. At full channel inversion, every UE intends to maintain an average received power of ρ at its serving BS [47]. However, fractional channel inversion may be adopted to mitigate prominent interference induced by UEs located far-away from their serving BSs at the expense of maintaining lower average received powers at their serving BSs. Overall, the transmit power of a typical UE to its intended BS at distance d is $P = \min\{\rho d^{\eta\epsilon}, P_U\}$, which accounts for full inversion, partial inversion, and the maximum transmit power constraint of the UEs. Fig. 8.3 demonstrates the effect of the FPC and the compensation factor on the average received power at the test receiver as well the percentages of UEs that employ a certain FPC scheme based on their distance from their intended BS.

8.3.2 Uplink Coverage Probability Analysis for Retransmissions

Despite that the BSs and UEs constitute independent PPPs, the mutually interfering UEs do not form a PPP because uplink scheduling enforces only one UE per resource block at each Voronoi cell. Furthermore, the association link distances in adjacent cells are correlated because of the correlated sizes of adjacent Voronoi cells. For tractability, we approximate the interfering UEs with a PPP with independent link distances. This approximation is also used in [47, 83, 127] and is verified herein via

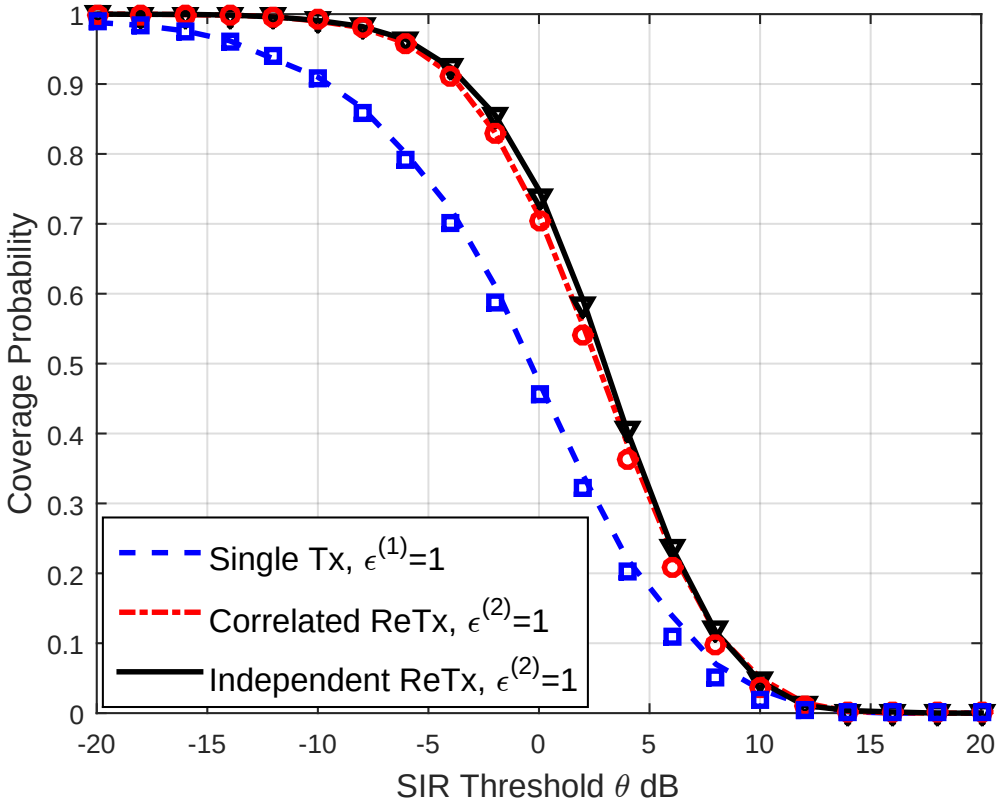

Figure 8.4: Coverage probability for $\epsilon = 1$.

Monte Carlo simulations.

Without loss of generality, we conduct the analysis on a test BS located at an arbitrary origin. Let $\tilde{\Psi} \subset \tilde{\Psi}_u$ be the set of actively interfering UEs and D_i be the i^{th} association link distance (i.e., the distance between the i^{th} interfering UE and the i^{th} BS). The set of UEs that can fulfill the FPC is denoted as $\tilde{\Psi}_{\mathrm{PC}} = \{r_i \in \tilde{\Psi} : D_i < \sqrt[\eta\epsilon_i]{P_m/\rho}\}$, and hence, the set of UEs that transmit at their peak power is $\tilde{\Psi}_{\mathrm{NI}} = \tilde{\Psi} \setminus \tilde{\Psi}_{PC}$. Consequently, the SIR at the j^{th} time slot at the test BS is given by

$$\bar{\Upsilon}^{(j)} = \frac{P_o\, r_o^{-\eta}\, \tilde{g}_o^{(j)}}{\underbrace{\sum_{r_i \in \tilde{\Psi}_{\mathrm{PC}}^{(j)}} \rho D_i^{\eta\epsilon_i} \tilde{g}_i^{(j)} r_i^{-\eta}}_{\triangleq \mathcal{I}_{\mathrm{PC}}^{(j)}} + \underbrace{\sum_{r_i \in \tilde{\Psi}_{\mathrm{NI}}^{(j)}} P_U \tilde{g}_i^{(j)} r_i^{-\eta}}_{\triangleq \mathcal{I}_{\mathrm{NI}}^{(j)}}}, \tag{8.7}$$

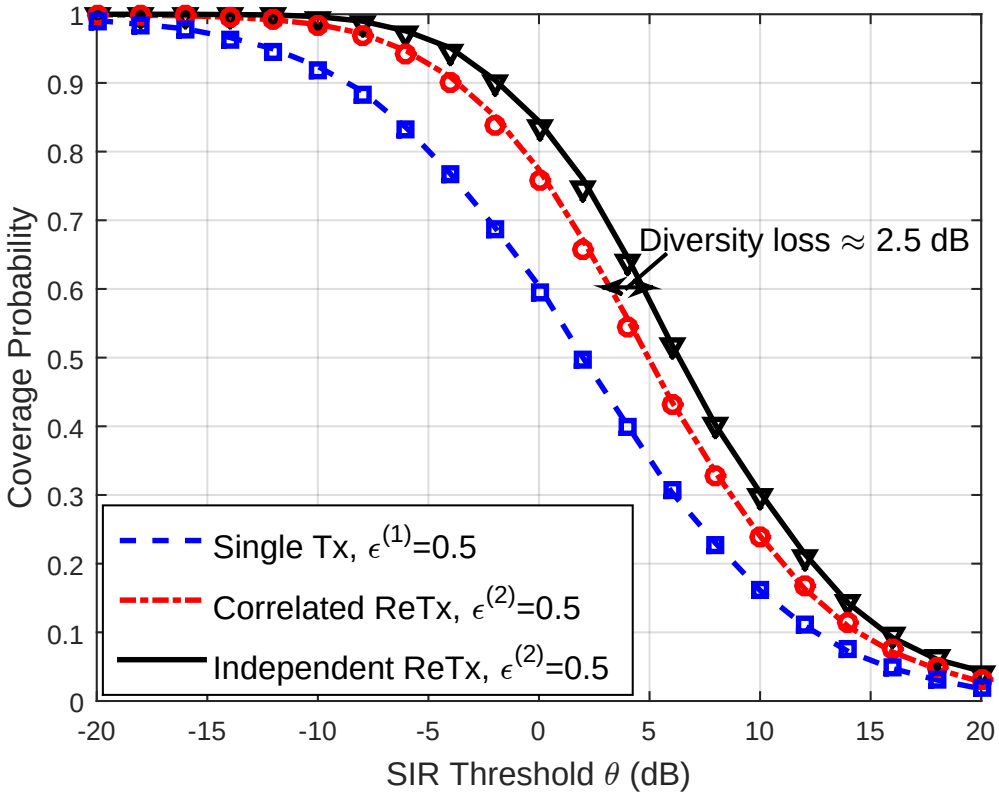

Figure 8.5: Coverage probability for $\epsilon = 0.5$.

where a superscript of $(\cdot)$ denotes the time slot and is only associated to parameters that change with time when conditioned on the network geometry, $P_o = \min\left\{\rho r_o^{\eta\epsilon^{(j)}}, P_U\right\}$ is the test UE's transmit power, r_o is the intended link distance, $\epsilon^{(j)}$ is the power control parameter for the test UE at time slot j, ϵ_i is the power control parameter of the i^{th} UE which is considered fixed across time, $\tilde{g}_o^{(j)}$ and $\tilde{g}_i^{(j)}$ at the intended and interfering channel gains at time slot j, respectively.

Let $\mathcal{C}_\circ^{(j)}$ be the probability that the test UE can satisfy the FPC at the j^{th} time slot. Then, the probability of FPC is fulfilled for the test UE is $\mathcal{C}_\circ^{(j)} = \mathbb{P}\left(\rho r_o^{\eta\epsilon^{(j)}} \leq P_U\right) = 1 - e^{-\pi\lambda_B\left(\frac{P_U}{\rho}\right)^{\frac{2}{\eta\epsilon^{(j)}}}}$. Note that, the test UE may change the FPC parameter upon transmission failure to improve the retransmission performance. On the other hand, the FPC parameter of the interfering UEs is considered fixed for simplicity. Hence, we drop the time index in the probability of FPC fulfillment for the interfering UEs, which

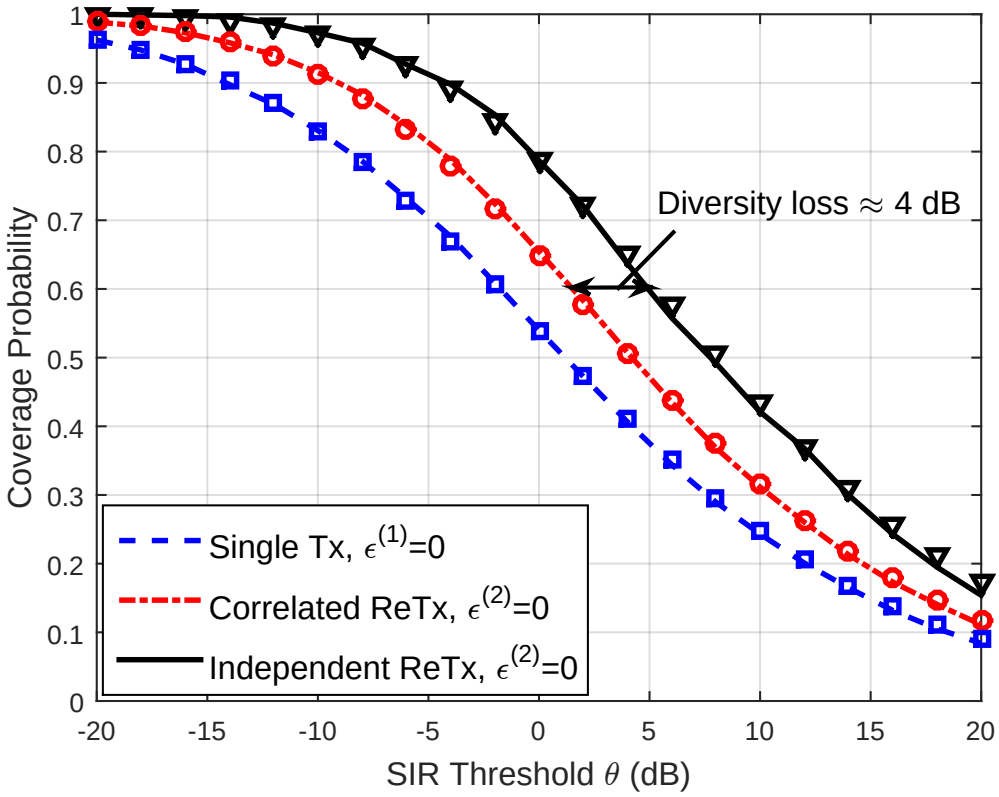

Figure 8.6: Coverage probability for $\epsilon = 0$.

is given by $\mathcal{C}_i = \mathbb{P}\left(\rho D_i^{\eta\epsilon_i} \leq P_U\right) = 1 - e^{-\pi\lambda_B \left(\frac{P_U}{\rho}\right)^{\frac{2}{\eta\epsilon_i}}}$. Let p be the independent activity probability for each BS in Ψ_B, with $0 \leq p \leq 1$. Then, active BSs constitute a PPP, with intensity $\lambda = p\lambda_B \left(1 - e^{-\pi\lambda_B r^2}\right)$ [127]. Exploiting the PPP with independent distance distributions approximation, the PPPs represented by the sets $\tilde{\Psi}_{\mathrm{PC}}^{(j)}$ and $\tilde{\Psi}_{\mathrm{NI}}^{(j)}$, are independent with intensities $\mathcal{C}_i\lambda$ and $(1 - \mathcal{C}_i)\,\lambda$, respectively. This is because $\tilde{\Psi}_{\mathrm{PC}}^{(j)} \cup \tilde{\Psi}_{\mathrm{NI}}^{(j)} = \tilde{\Psi}$ and $\tilde{\Psi}_{\mathrm{PC}}^{(j)} \cap \tilde{\Psi}_{\mathrm{NI}}^{(j)} = \phi$, in which the total intensity is λ due to the one active UE per resource block per Voronoi cell.

To study the joint transmission and retransmission performance, we consider a snapshot of two arbitrary time slots over which the UE of interest is static and thus is associated to the same BS. Let $\mathcal{I}^{(j)} \triangleq \mathcal{I}_{\mathrm{PC}}^{(j)} + \mathcal{I}_{\mathrm{NI}}^{(j)}$ be the total aggregate interference at time slot j. We define the Laplace transforms (LTs) of the marginal and joint PDF of the aggregate interference as $\mathcal{L}_{\mathcal{I}}^{(j)}(z) \triangleq \mathbb{E}\{\exp(-z\mathcal{I}^{(j)})\}$ and $\mathcal{L}_{\mathcal{I}}^{(1,2)}(z_1, z_2) \triangleq$

$\mathbb{E}\{\exp(-z_1\mathcal{I}^{(1)} - z_2\mathcal{I}^{(2)})\}$, respectively. Both LTs are characterized via the following lemmas.

Lemma 8.2. *The LT of the aggregate interference induced by UEs transmitting at their peak powers (i.e., non-inverting UEs), is given by*

$$\mathcal{L}^{\mathrm{NI}}_{\mathcal{I}^{(j)}}(z) = \mathbb{E}\left[e^{-z\sum_{r_i\in\tilde{\Psi}^{(j)}_{\mathrm{NI}}} P_U g_i r_i^{-\eta}}\right]$$
$$= \exp\left\{-2\pi p\lambda_B e^{-\pi\lambda_B\left(\frac{P_U}{\rho}\right)^{\frac{2}{\eta\epsilon_i}}} \times \int_0^\infty (1-e^{-\pi\lambda_B x^2})\left(1-\frac{1}{1+zP_U x^{-\eta}}\right) x\mathrm{d}x\right\}. \quad (8.8)$$

The LT of the aggregate interference resulting from UEs which can apply FPC, is given by

$$\mathcal{L}^{\mathrm{PC}}_{\mathcal{I}^{(j)}}(z) = \mathbb{E}\left[e^{-z\sum_{r_i\in\tilde{\Psi}^{(j)}_{\mathrm{PC}}} \rho D_i^{\eta\epsilon_i} g_i^{(j)} r_i^{-\eta}}\right]$$
$$= \exp\left\{-2\pi p\lambda_B\left(1-e^{-\pi\lambda_B\left(\frac{P_U}{\rho}\right)^{\frac{2}{\eta\epsilon_i}}}\right)\int_0^\infty\int_{d_i=0}^{x} 2\pi\lambda_B d_i e^{-\pi\lambda_B d^2}\left(1-\frac{1}{1+z\rho D_i^{\eta\epsilon_i}x^{-\eta}}\right) x\,\mathrm{d}d_i\,\mathrm{d}x\right\}. \quad (8.9)$$

Finding the joint LT $\mathcal{L}^{(1,2)}_{\mathcal{I}}(z_1, z_2)$ across time is a major contribution of this paper. We focus on the worst case of maximally correlated interference scenario, i.e., $p = 1$. The partially correlated scenario $p < 1$ can be easily obtained by following similar steps but considering the three disjoint sets of interfering UEs $\{\tilde{\Psi}^{(j)} \setminus \tilde{\Psi}^{(k)}\}$, $\{\tilde{\Psi}^{(k)} \setminus \tilde{\Psi}^{(j)}\}$, and $\{\tilde{\Psi}^{(j)} \cap \tilde{\Psi}^{(k)}\}$ with intensities $(1-p)\lambda$, $(1-p)\lambda$, and $p\lambda$, respectively [32, 125]. The joint LT is hence given by the following lemma for $p = 1$.

Lemma 8.3. *Consider a power-ramping scheme, i.e., $\epsilon_1 < \epsilon_2$, in an uplink cellular network with FPC. Then, the joint LT of maximally correlated interference powers $\mathcal{I}^{(1)}_U$ and $\mathcal{I}^{(2)}_U$, i.e., p=1, is given by*

$$\mathcal{L}_{\mathcal{I}_U}^{(1,2)}(z_1,z_2)=\mathbb{E}\left[e^{-\sum_{\tilde{\Psi}_{\mathrm{NI}}^{(j)}}\left(z_1P_Ur_i^{-\eta}\tilde{g}_i^{(1)}+z_2P_Ur_i^{-\eta}\tilde{g}_i^{(2)}\right)}\times e^{-\sum_{\tilde{\Psi}_{\mathrm{PC}}^{(j)}}\left(z_1\rho D_i^{\eta\epsilon_i}r_i^{-\eta}\tilde{g}_i^{(1)}+z_2\rho D_i^{\eta\epsilon_i}r_i^{-\eta}\tilde{g}_i^{(2)}\right)}\right]$$
$$=\exp\left\{-2\pi\int_0^\infty\lambda\left(1-\mathcal{C}_i\right)\left[1-\frac{1}{1+z_1P_Ux^{-\eta}}\frac{1}{1+z_2P_Ux^{-\eta}}\right]x\mathrm{d}x\right\}$$
$$\times\exp\left\{-2\pi\int_0^\infty\int_0^x\lambda\mathcal{C}_i\cdot\frac{2\pi\lambda_Bd_ie^{-\pi\lambda_Bd^2}}{1-e^{-\pi\lambda_Bx^2}}\left[1-\frac{1}{1+z_1\rho d_i^{\eta\epsilon_i}x^{-\eta}}\frac{1}{1+z_2\rho d_i^{\eta\epsilon_i}x^{-\eta}}\right]x\,\mathrm{d}d_i\,\mathrm{d}x\right\}. \tag{8.10}$$

Proof. Due to the independence of $\Psi_{\mathrm{NI}}^{(j)}$ and $\Psi_{\mathrm{PC}}^{(j)}$, and by averaging over the PDF [127],

$$f_{D_i|r_i}(d|r_i)=\frac{2\pi\lambda_Bde^{-\pi\lambda_Bd^2}}{1-e^{-\pi\lambda_Br^2}},\quad 0\le d\le r_i \tag{8.11}$$

equation (8.10) is obtained. □

Exploiting lemmas 8.2 and 8.3, we derive the average coverage probability in the next theorem.

Theorem 8.2. *The coverage probability for a single transmission at an arbitrary time instant j, for predefined SIR threshold θ, is given as*

$$\mathcal{P}_c^{(j)}(\theta)=\mathbb{E}\left[\mathbb{P}\left(\bar{\Upsilon}^{(j)}>\theta\right)\right]$$
$$=\int_0^{\left(\frac{P_U}{\rho}\right)^{\frac{1}{\eta\epsilon^{(j)}}}}2\pi\lambda r_o\,e^{-\pi\lambda r_o^2}\,\mathcal{L}_{\mathcal{I}}^{(j)}\left(\frac{\theta r_o^{\eta(1-\epsilon^{(j)})}}{\rho}\right)+\int_{\left(\frac{P_U}{\rho}\right)^{\frac{1}{\eta\epsilon^{(j)}}}}^\infty 2\pi\lambda r_o\,e^{-\pi\lambda r_o^2}\,\mathcal{L}_{\mathcal{I}}^{(j)}\left(\frac{\theta r_o^\eta}{P_U}\right)\mathrm{d}r_o. \tag{8.12}$$

Further, the average coverage probability upon signal retransmission, given by

$$\mathcal{P}_{cov}^{\mathrm{UL}}(\theta)=\sum_{j=1}^{2}\mathbb{P}\left(\bar{\Upsilon}^{(j)}>\theta\right)-\mathbb{P}\left(\bar{\Upsilon}^{(1)}>\theta,\bar{\Upsilon}^{(2)}>\theta\right). \tag{8.13}$$

where the marginal coverage probabilities are expressed in (8.12) *and the joint coverage probability is given by*

$$\begin{aligned}
&\mathbb{P}\left(\bar{\Upsilon}^{(1)} > \theta, \bar{\Upsilon}^{(2)} > \theta\right) \\
&\quad \approx \int_0^{\mathcal{T}_2} 2\pi\lambda_B r_o \, e^{-\pi\lambda_B r_o^2} \sum_{z_2 \in \mathcal{Z}_2} \mathcal{L}_{\mathcal{I}}^{(1,2)}\left(z_1, z_2\right)\Big|_{z_1=\frac{\theta r_o^{\eta\left(1-\epsilon^{(1)}\right)}}{\rho}} \mathrm{d}r_o \\
&\quad + \int_{\mathcal{T}_1}^{\infty} 2\pi\lambda_B r_o \, e^{-\pi\lambda_B r_o^2} \, \mathcal{L}_{\mathcal{I}}^{(1,2)}\left(z_1, z_2\right)\Big|_{z_1=z_2=\frac{\theta}{P_U r_o^{-\eta}}} \mathrm{d}r_o,
\end{aligned} \tag{8.14}$$

with $\mathcal{T}_1 = \left(\frac{P_U}{\rho}\right)^{\frac{1}{\eta\epsilon^{(1)}}}$, $\mathcal{T}_2 = \left(\frac{P_U}{\rho}\right)^{\frac{1}{\eta\epsilon^{(2)}}}$, *and* $\mathcal{Z}_2 = \left\{\frac{\theta r_o^{\eta\left(1-\epsilon^{(2)}\right)}}{\rho}, \frac{\theta r_o^{\eta}}{P_U}\right\}$.

Proof. Eq. (8.12) follows from the complementary cumulative distribution function (CCDF) of the exponential random variable $\tilde{g}_o^{(j)}$, and by averaging over the PDF of r_o given as $f_{r_o}(r) = 2\pi\lambda_B r e^{-\pi\lambda_B r^2}, r_o > 0$. Eq. (8.13) follows from the law of total probability. Assuming power-ramping (i.e., $\epsilon^{(2)} > \epsilon^{(1)}$), the joint CCDF of $\bar{\Upsilon}^{(1)}$ and $\bar{\Upsilon}^{(2)}$ is approximated by

$$\begin{aligned}
&\mathbb{P}\left(\bar{\Upsilon}^{(1)} > \theta, \bar{\Upsilon}^{(2)} > \theta\right) \\
&\quad \approx \mathbb{E}\left[\mathbb{P}\left(\tilde{g}_o^{(1)} > \frac{\theta\mathcal{I}^{(1)}}{\rho r_o^{\eta(\epsilon^{(1)}-1)}}, \tilde{g}_o^{(2)} > \frac{\theta\mathcal{I}^{(2)}}{\rho r_o^{\eta(\epsilon^{(2)}-1)}}\right)\mathcal{C}_o^{(2)}\right] \\
&\quad + \mathbb{E}\left[\mathbb{P}\left(\tilde{g}_o^{(1)} > \frac{\theta\mathcal{I}^{(1)}}{\rho r_o^{\eta(\epsilon^{(1)}-1)}}, \tilde{g}_o^{(2)} > \frac{\theta\mathcal{I}^{(2)}}{P_U r_o^{-\eta}}\right)\bar{\mathcal{C}}_o^{(2)}\right] \\
&\quad + \mathbb{E}\left[\mathbb{P}\left(\tilde{g}_o^{(1)} > \frac{\theta\mathcal{I}^{(1)}}{P_U r_o^{-\eta}}, \tilde{g}_o^{(2)} > \frac{\theta\mathcal{I}^{(2)}}{P_U r_o^{-\eta}}\right)\bar{\mathcal{C}}_o^{(2)}\right],
\end{aligned} \tag{8.15}$$

and incorporating the CCDFs of the i.i.d. $\tilde{g}_o^{(1)}$ and $\tilde{g}_o^{(2)}$, which leads to (8.14). Finally, the LT of the resulting interference at an arbitrary time instant j, is given as $\mathcal{L}_{\mathcal{I}^{(j)}}(z) = \mathcal{L}_{\mathcal{I}^{(j)}}^{\mathrm{NI}}(z) \times \mathcal{L}_{\mathcal{I}^{(j)}}^{\mathrm{PC}}(z)$. Note that, the case that the intended user transmits at its peak power in the first time slot and fulfills the FPC in the second slot is neglected due to the employed power-ramping scheme. □

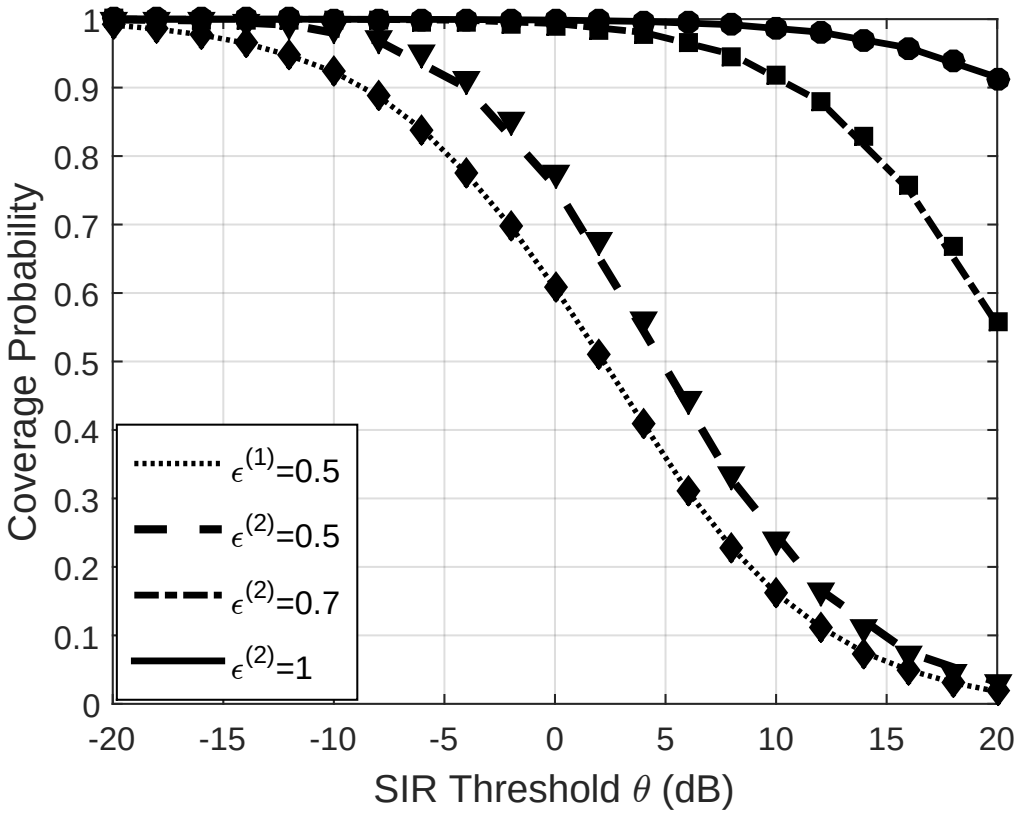

Figure 8.7: Coverage probability for hybrid compensation factors.

8.4 Non-binding Transmit Power Constraint

The case of non-binding maximum power constraint is of special interest as it is th typical scenario in dense cellular environments. Following [47], such scenario is captured by setting $P_U = \infty$. The following lemmas characterize the LT of the aggregate network interference where all UEs are always capable of inverting their path-loss effect, in which $\mathcal{L}^{\mathrm{NI}}_{\mathcal{I}^{(j)}} = 1$ and $\mathcal{C}^{(j)}_o = \mathcal{C}_i = 1$. For notational convenience, we define the following functions,

$$\mathcal{H}_1(z,u,v) = \int_0^{\infty}\int_0^{v} 2\pi p\lambda_B u e^{-\pi\lambda_B u^2}\left(1 - \frac{1}{1+z\rho\, u^{\eta\epsilon_i} v^{-\eta}}\right) v\mathrm{d}u\mathrm{d}v, \tag{8.16}$$

and,

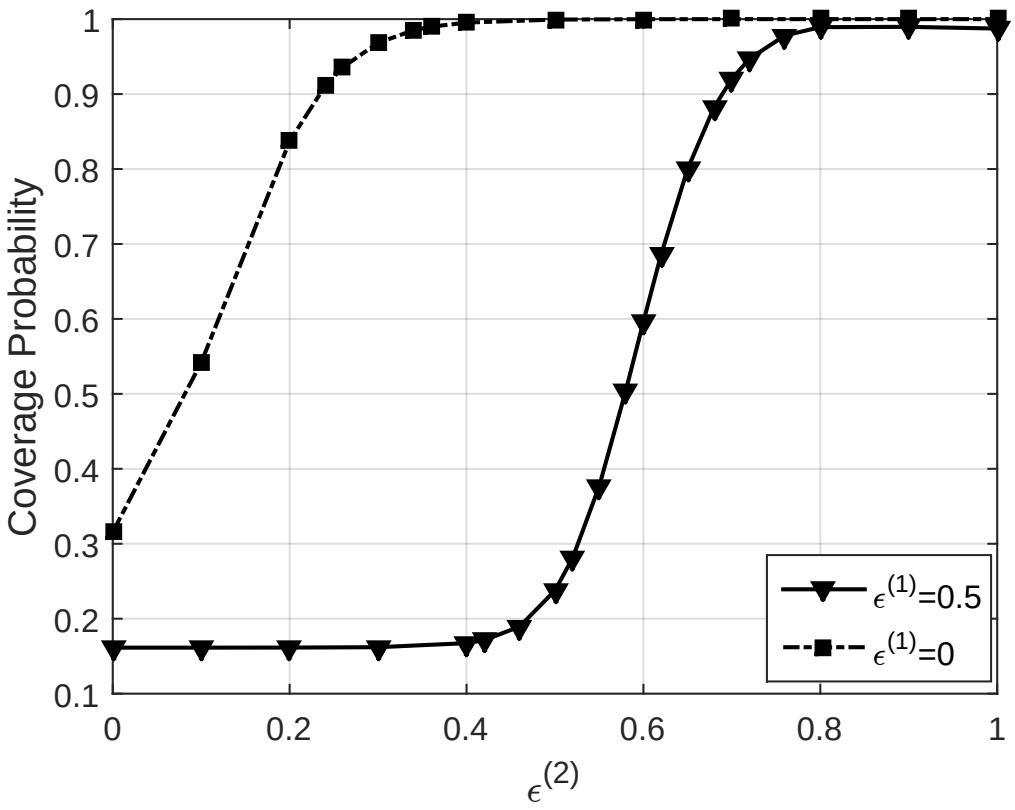

Figure 8.8: Analytic coverage probability versus $\epsilon^{(2)}$ employing power-ramping scheme at $\theta = 10$ dB.

$$\mathcal{H}_2\left(z_1, z_2, u, v\right) = \int_0^{\infty}\int_0^{v} 2\pi p\lambda_B u e^{-\pi\lambda_B u^2}\left[1 - \frac{1}{\left(1 + z_1\rho\, u^{\eta\epsilon_i} v^{-\eta}\right)}\frac{1}{1 + \left(z_2\rho\, u^{\eta\epsilon_i} v^{-\eta}\right)}\right] v\mathrm{d}u\mathrm{d}v. \tag{8.17}$$

The Laplace transform of the interference for the non-binding power constraint is given by the following two lemmas.

Lemma 8.4. *Consider an uplink cellular network employing FPC with $P_U = \infty$, the LT of the interference power at an arbitrary time instant j at the intended BS is given by*

$$\begin{aligned}\mathcal{L}_{\mathcal{I}_U^{(j)}}(z) &= \mathbb{E}\left[\exp\left\{-z\sum_{r_i\in\Psi}\rho D_i^{\eta\epsilon_i}\tilde{g}_i^{(j)} r_i^{-\eta}\right\}\right] \\ &= \exp\left\{-2\pi p\lambda_B\mathcal{H}_1(z, d_i, x)\right\}. \end{aligned}\tag{8.18}$$

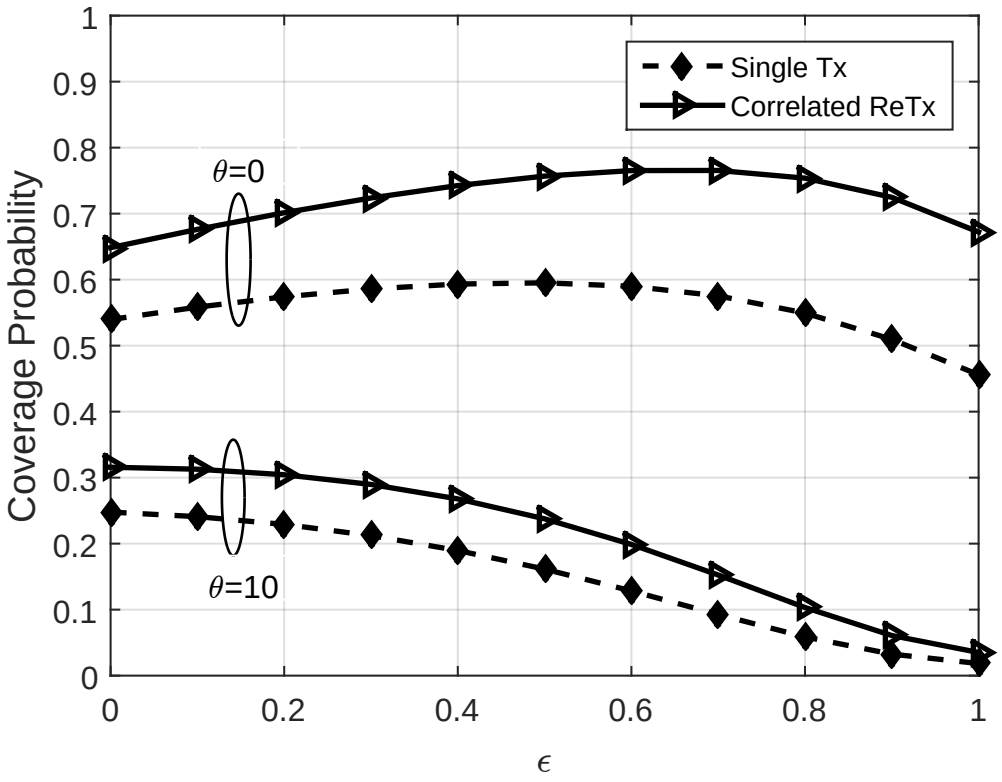

Figure 8.9: Analytic coverage probability versus ϵ employing for $P_U = \infty$ at $\theta = 0, 10$ dB.

Proof. Following the steps in Lemma 8.2, such that the special function defined in (8.16) is exploited, eq. (8.18) is obtained. □

Lemma 8.5. *For the depicted system model with FPC, the joint LT of the interferences at a given location at two different time slots, denoted by* $\mathcal{I}^{(1)}$ *and* $\mathcal{I}^{(2)}$*, for an arbitrary activity factor* $0 \leq p \leq 1$*, is computed as*

$$\mathcal{L}_{\mathcal{I}_U}^{(1,2)}(z_1, z_2) = \exp\left\{-2\pi p^2 \lambda_B \mathcal{H}_2(z_1, z_2, d_i, x) - 2\pi p(1-p)\lambda_B \mathcal{H}_1(z_1, d_i, x) - 2\pi p(1-p)\lambda_B \mathcal{H}_1(z_2, d_i, x)\right\}. \tag{8.19}$$

Proof. Following [125, Lemma 2], we exploit the MGF of $\tilde{g}_i^{(1)}$ and $\tilde{g}_i^{(2)}$, together with the PGFL of the PPPs. Finally, we average over the PDF $f_{D_i|r_i}(d|r_i)$, and utilize the special functions in (8.16) and (8.17), then, (8.19) is obtained.

The coverage probability for the non-binding scenario is similar to Theorem 8.2, but using the LTs from Lemmas 8.4 and 8.5. □

8.5 Numerical and Simulations Results

We first verify the accuracy of the proposed mathematical model via Monte Carlo simulations. Unless otherwise stated, the simulations setup is as follows. The maximum average received power at the receivers $\rho = -50$ dBm, the path-loss exponent $\eta = 4$, the BSs intensity $\lambda_B = 4$ BSs/km^2, $\lambda_u = 8$ users/km^2, $P_U = 1$ W, and finally the activity factor $p = 1$, which implies maximum interference temporal correlation. In all figures, theoretical results and Monte Carlo simulations are represented by lines and markers, respectively.

Fig. 8.9 shows the coverage performance for the single transmission, retransmission with correlated SIRs, and retransmission assuming independent SIRs for $\epsilon^{(1)} = \epsilon^{(2)} = \epsilon$ with non-binding transmit power constraint ($P_U = \infty$). The figure manifests the effect of temporal SIR correlation and confirms that assuming independent SIRs result in an optimistic performance assessment. Interestingly, the figure shows that increasing the amount of path-loss compensation mitigates the effect of temporal correlations, which is due to mitigating the impact of path-loss on the SIR correlation. The full power inversion shown in Fig. 8.4 almost achieves the independent transmission performance, i.e., full diversity, as it completely eliminates the intended link path-loss. Since the interference is maximally correlated across time, i.e., $p = 1$, it is concluded that the path-loss effect is much more prominent for SIR temporal correlation than the interference.

In light of Fig. 8.4 insights, we advocate adjusting the FPC compensation parameter during the second time slot as shown in Fig. 8.7. The figure is plotted for $\epsilon^{(1)} = 0.5$ in which $\epsilon^{(2)}$ is increased in the retransmission to improve the temporal diversity gain due to the power-ramping, (i.e., $\epsilon^{(2)} > \epsilon^{(1)}$). As evident from the figure,

$\approx 90\%$ diversity gain is achieved at $\theta = 20$ dB, by employing full channel inversion in the retransmission slot. Fig. 8.8 shows that retransmission performance can only be improved by increasing ϵ. For instance, for $\epsilon^{(1)} = 0$, full coverage can be obtained by adjusting $\epsilon^{(2)} = 0.4$, while for $\epsilon^{(1)} = 0.5$, full coverage is achieved by setting $\epsilon^{(2)} = 0.8$. Consequently, a lower ϵ at the first time slot can immensely save the retransmission power. Fig. 8.9 demonstrates the optimum operational ϵ in both time slots under non-binding transmit power constraint.

8.6 Chapter Summary and Conclusions

This chapter proposes an extension for the developed paradigm in Chapters 5 and 6 to study the coverage probability after signal retransmission upon decoding errors in a MIMO downlink cellular network, and a SISO uplink cellular network. For the downlink scenario, we shed lights on the diversity loss due to temporal interference correlation and discuss the diversity-multiplexing tradeoff imposed by MIMO configurations. In addition, this chapter studys the effect of fractional power control on temporal transmission diversity performance for uplink cellular networks. It is shown that the path-loss has more prominent effect than interference on the SIR correlation and that completely inverting the path-loss almost achieves full temporal diversity. A Hybrid fractional power control scheme via increased path-loss compensation is advocated to improve the retransmission performance. Finally, the proposed model provides an insightful design methodology to choose the appropriate diversity, multiplexing, number of antennas in the downlink, and compensation factor in the uplink, to meet a certain design objective.

Chapter 9

Interference Management

9.1 Introduction

In this chapter, we extend the proposed framework in Chapter 5 to study the effect of different interference management techniques in downlink cellular networks. In the context of interference management, [132] provides a tractable analysis for successive interference cancellation (SIC) in downlink OFDM-based heterogeneous cellular networks. In [30], the authors investigate the improvement in coverage under BSs coordinated multi-point transmission (CoMP) in downlink communication to deal with the increase in inter-cell interference in heterogeneous networks. Moreover, in [29] the performance in a location-aware two-tier CoMP scheme is quantified. SINR characterization via its cumulative distribution function (CDF), i.e., outage probability, is a common factor in the aforementioned literature.

In this work, we take advantage of the proposed unified framework, to quantify the effect of interference management on the ASEP performance in downlink cellular systems. Particularly, we take into account the effect of interference management techniques, namely; frequency reuse and BS coordination, on the ASEP performance.

9.2 System Model

We consider the single-tier downlink cellular network depicted in Chapter 3. In addition, signals experience unit mean (i.i.d.) Nakagmai-m channel power gains, where m is assumed to be an integer. Therefore, the analysis is valid for various

fading environments, as Nakagami-m can approximate several fading models.

For the purpose of interference management, BSs coordination and frequency reuse are considered. Note that traditional hexagonal grid tailored frequency reuse schemes cannot be employed due to the random network structure. Instead, the available spectrum is divided into Δ sub-bands and each BS selects one of the sub-bands for transmission. Fractional frequency reuse (FFR) is the most commonly studied interference management technique in the literature, since it achieves balance between the cell-edge users performance and cell-center users performance [87, 133, 134]. For mathematical convenience, we analyze two sub-band selection schemes, namely, simple random frequency reuse [14, 87] and coordinated frequency reuse schemes. In the random frequency reuse scheme, each BS selects one of the Δ sub-bands with equal probability Δ^{-1}. On the other hand, the coordinated frequency reuse scheme necessitates that the BSs coordinate together such that the Δ-closest neighboring BS use different frequencies[1]. Furthermore, it is assumed that the test receiver has perfect intended link CSI and is unaware of the inter-cell interference.

9.3 Impact of Interference Management on ASEP performance

In this section, we study the ASEP performance under inter-cell interference management. As mentioned before, we consider two main frequency reuse schemes with Δ sub-bands. In the first, denoted as coordinated frequency reuse scheme, each BS chooses a sub-band not used by its $(\Delta-1)$ neighboring BSs. In the second, denoted as random frequency reuse scheme, each BS randomly and independently chooses one of the sub-bands with probability $\frac{1}{\Delta}$. For the sake of comparison, we study BS coordination without frequency reuse, in which the test BS avoids or cancels the interference from the $(\Delta - 1)$ neighboring BSs only.

[1]The Δ-closest BSs are with respect to the UE not the BS.

9.3.1 Random Frequency Reuse

The random frequency reuse scheme is easy to incorporate into the analysis due to the independent and random selection of the frequency sub-band. As shown in [14], in the random frequency reuse scheme, interfering BSs constitute a PPP thinned by the factor Δ^{-1}. As a consequence, the LT of the residual downlink interference under random frequency reuse, denoted as $\hat{\mathcal{I}}_D$ is given as

$$\mathcal{L}^{\text{RFR}}_{\hat{\mathcal{I}}_D|r_o}(z) = \exp\left\{-\pi\frac{\lambda}{\Delta}r_o^2\left[\left({}_2F_1\left(\frac{-2}{\eta}, m_i; 1-\frac{2}{\eta}; -z\Omega_i P r_o^{-\eta}\right)-1\right)\right]\right\}, \tag{9.1}$$

where ${}_2F_1(\cdot,\cdot;\cdot;\cdot)$ is the Gauss hypergeometric function [112]. Note that, this is similar to (5.7), but with intensity $\frac{\lambda}{\Delta}$.

9.3.2 Coordinated Frequency Reuse

On the other hand, the analysis of the coordinated frequency reuse scheme is more involved for two reasons. The first is that the sub-band selection scheme introduces correlations, in the form of repulsion, between the set of BSs using the same frequency. Hence, the interfering BSs (excluding the origin) do not constitute a PPP. Secondly, we have to find the joint distribution between the distance to the serving BS and the distance to the $\Delta^{th}-1$ neighbor to estimate the interference protection imposed by the BS coordination. Let the distance between the test UE to its n^{th} neighbor interfering BS be denoted as $\|x_n\|$. The conditional and joint distributions between the distance to the serving BS r_o and the distance to the n^{th} neighboring BS are given by the following lemma.

Lemma 9.1. *The conditional PDF of the distance between a user, located r_o meters away from its serving BS, to the n^{th} neighbor interfering BS is given by*

$$f_{\|x_n\|\big|r_o}(\mathrm{x}_n|r_o) = \frac{2(\pi\lambda)^n \mathrm{x}_n(\mathrm{x}_n^2-r_o^2)^{n-1}e^{-\pi\lambda(\mathrm{x}_n^2-r_o^2)}}{\Gamma(n)}, \tag{9.2}$$

where $r_o < x_n < \infty$. The joint PDF of $\|x_n\|$ and r_o is given as

$$f_{\|x_n\|,r_o}(\mathrm{x}_n, r) = \frac{4(\pi\lambda)^{n+1} r \mathrm{x}_n (\mathrm{x}_n^2 - r_o^2)^{n-1} e^{-\pi\lambda \mathrm{x}_n^2}}{\Gamma(n)}, \tag{9.3}$$

where $r < \mathrm{x}_n < \infty$, where $0 \leq r \leq \infty$.

Proof. See Appendix E.1. □

For the sake of simple presentation, we focus on the special case of $\eta = 4$ and Rayleigh fading with $m = m_o = 1$ in the rest of the chapter. For analytical tractability, we approximate the set of interfering BSs, in the coordinated frequency reuse scheme, with a PPP with intensity $\frac{\lambda}{\Delta}$. It is well known that approximating a point process with repulsion with an equi-dense PPP gives an accurate estimate for the interference if the exclusion distance around the test receiver is well estimated [13, 46, 47, 135, 136]. Exploiting the equi-dense PPP approximation and the interference exclusion distance estimated in Lemma 9.1, the LT of the downlink aggregate interference $\hat{\mathcal{I}}_D$ in the case of coordinated frequency reuse scheme is given by the following lemma.

Lemma 9.2. *Let $\mathcal{D}_\Delta$ be the set of dominant interferers up to the nearest $\Delta^{th} - 1$ interferer. Thus, conditioned on r_o, the LT of $\hat{\mathcal{I}}_D$ under coordinated frequency reuse is given by*

$$\begin{aligned}\mathcal{L}^{\mathrm{CFR}}_{\hat{\mathcal{I}}_D\big|r_o}(z) &= \int_{r_o}^{\infty} \frac{2(\pi\lambda)^{\Delta-1}\mathrm{x}_n(\mathrm{x}_n^2 - r_o^2)^{\Delta-2} e^{-\pi\lambda(\mathrm{x}_n^2 - r_o^2)}}{\Gamma(\Delta-1)} \\ &\quad \times \exp\left\{-\pi\frac{\lambda}{\Delta}x_n^2\left[{}_2F_1\left(\frac{-2}{\eta}, m_i; 1 - \frac{2}{\eta}; \frac{-zP\Omega_i}{x_n^\eta}\right) - 1\right]\right\}\mathrm{dx}_n \\ &\overset{\eta=4, m_i=1, \Omega_i=1}{=} \int_{r_o}^{\infty} \frac{2(\pi\lambda)^{\Delta-1}\mathrm{x}_n(\mathrm{x}_n^2 - r_o^2)^{\Delta-2} e^{-\pi\lambda(\mathrm{x}_n^2 - r_o^2)}}{\Gamma(\Delta-1)} \exp\left\{-\pi\frac{\lambda}{\Delta} r_o^2 \sqrt{zP}\arctan\left(\frac{\sqrt{zP}}{x_n^2}\right)\right\}\mathrm{dx}_n\end{aligned} \tag{9.4}$$

Proof. See Appendix E.2. □

The ASEP under interference management is consequently expressed as

$$\begin{aligned}\mathrm{ASEP}_{\mathrm{DL}}^{\mathrm{IM}} \approx w_1 \Bigg[1 - \frac{\Gamma\left(m_o+\frac{1}{2}\right)}{\Gamma\left(m_o\right)}\frac{2}{\pi}\int_0^{\infty}\int_0^{\infty} 2\pi\lambda r e^{-\pi\lambda r^2}\frac{1}{\sqrt{z}}e^{-z\left(1+\frac{m_o\mathcal{N}_o r^{\eta}}{\Omega_o\beta P}\right)}\,{}_1F_1\left(1-m_o;\frac{3}{2};z\right)\cdot\mathcal{L}_{\hat{\mathcal{I}}_D|r}\left(\frac{m_o z r^{\eta}}{\Omega_o\beta P}\right)\mathrm{d}r\mathrm{d}z\Bigg] \\ + w_2\Bigg[1-\frac{4m_o}{\pi}\int_0^{\infty}\int_0^{\infty}2\pi\lambda r e^{-\pi\lambda r^2}e^{-z\left(\frac{m_o\mathcal{N}_o r^{\eta}}{\Omega_o\beta P}\right)}\int_0^{\frac{\pi}{4}}{}_1F_1\left(m_o+1;2;\frac{-z}{\sin^2\vartheta}\right)\frac{1}{\sin^2\vartheta}\cdot\mathcal{L}_{\hat{\mathcal{I}}_D|r}\left(\frac{m_o z r^{\eta}}{\Omega_o\beta P}\right)\mathrm{d}\vartheta\mathrm{d}r\mathrm{d}z\Bigg],\end{aligned} \tag{9.5}$$

where $\mathcal{L}_{\hat{\mathcal{I}}_D|r}(z)$ is replaced with $\mathcal{L}^{\mathrm{CFR}}_{\hat{\mathcal{I}}_D\big|r_o}$ or $\mathcal{L}^{\mathrm{RFR}}_{\hat{\mathcal{I}}_D\big|r_o}$ according to the employed interference management technique.

As shown in (9.5), the interference protection imposed by the coordinated frequency reuse scheme highly complicates the ASEP expression. Nevertheless, the integrals in (9.5) can be numerically evaluated by Matlab and the results can be used to draw design insights. For the BS coordination only (i.e., without frequency reuse), the exact ASEP is similar to the expression given in (9.5) without the intensity thinning factor Δ^{-1} in the first term in the exponent of (9.4).

9.4 Simulation Results

In this section, we verify the proposed analysis, for the depicted downlink scenario, via Monte Carlo simulations and against the EiD approach, which is denoted as *"Exact"* in the figures. We vary the BS transmit powers P, while keeping $\mathcal{N}_o$ constant. Unless otherwise stated, the path-loss exponent $\eta = 4$, the noise power $\mathcal{N}_o = -90$ dBm, the users intensity $\lambda_u = 30$ UEs/km^2, the BSs intensity $\lambda = 10$ BSs/km^2, Rayleigh fading is assumed with unity mean channel (power) gain. The desired and interfering symbols are modulated using square quadrature amplitude modulation (QAM) scheme, with a constellation size $M \in \{4, 16\}$. For illustration purposes, we consider the intended and the interfering signals to be modulated via the same modulation scheme.

Figs. 9.1 and 9.2 quantify the performance of the ASEP under coordinated fre-

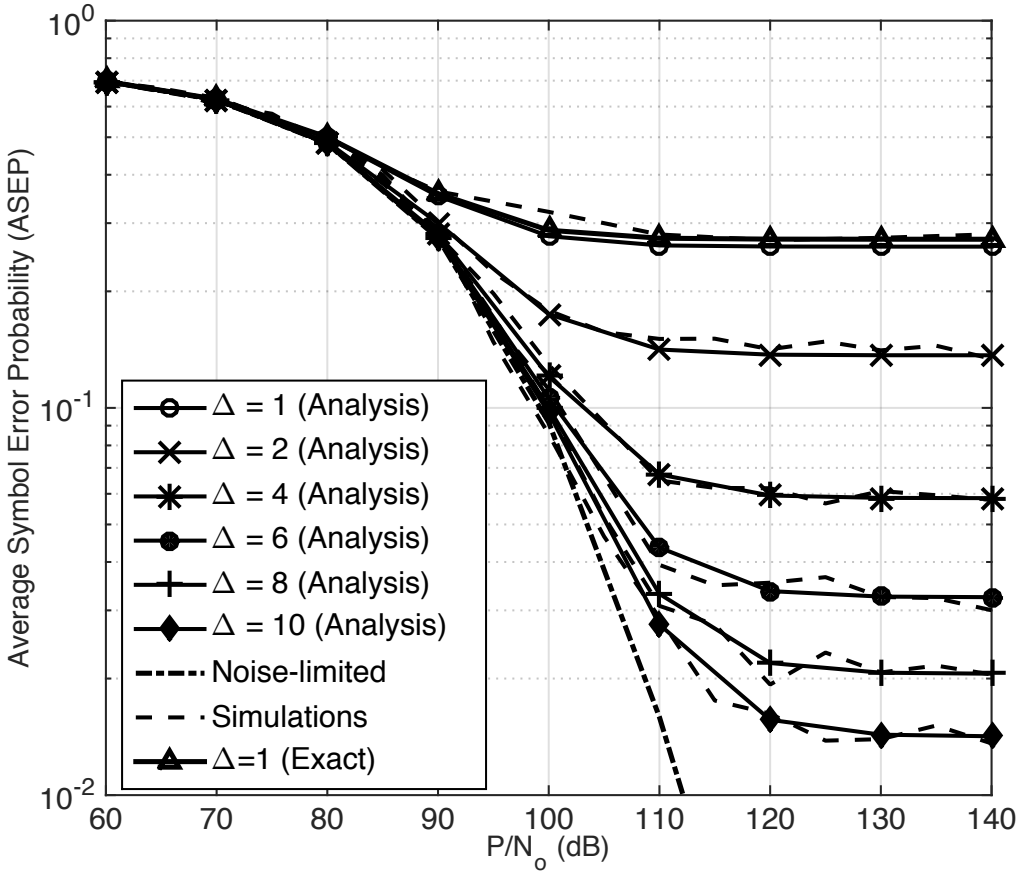

Figure 9.1: The effect of coordinated frequency reuse on the average symbol error probability in the downlink scenario for 4-QAM modulated signals.

quency reuse for different values of Δ, for 4-QAM and 16-QAM modulated signals, respectively. The figures show a close match between simulations and the proposed Gaussian codebook approximation for all values of Δ, which validates our analysis. We also plot the EiD approach, which is denoted as *"Exact"* in the figures, for $\Delta = 1$ case to demonstrate that the exact EiD analysis highly matches the proposed analysis. Extensions of the EiD approach for higher values of Δ are not investigated due to tractability issues.

In Figs. 9.1 and 9.2, we plot the aggressive frequency reuse scheme ($\Delta = 1$) and the noise-limited downlink performance to benchmark the frequency reuse performance. The performance gap between the noise-limited and the derived expressions

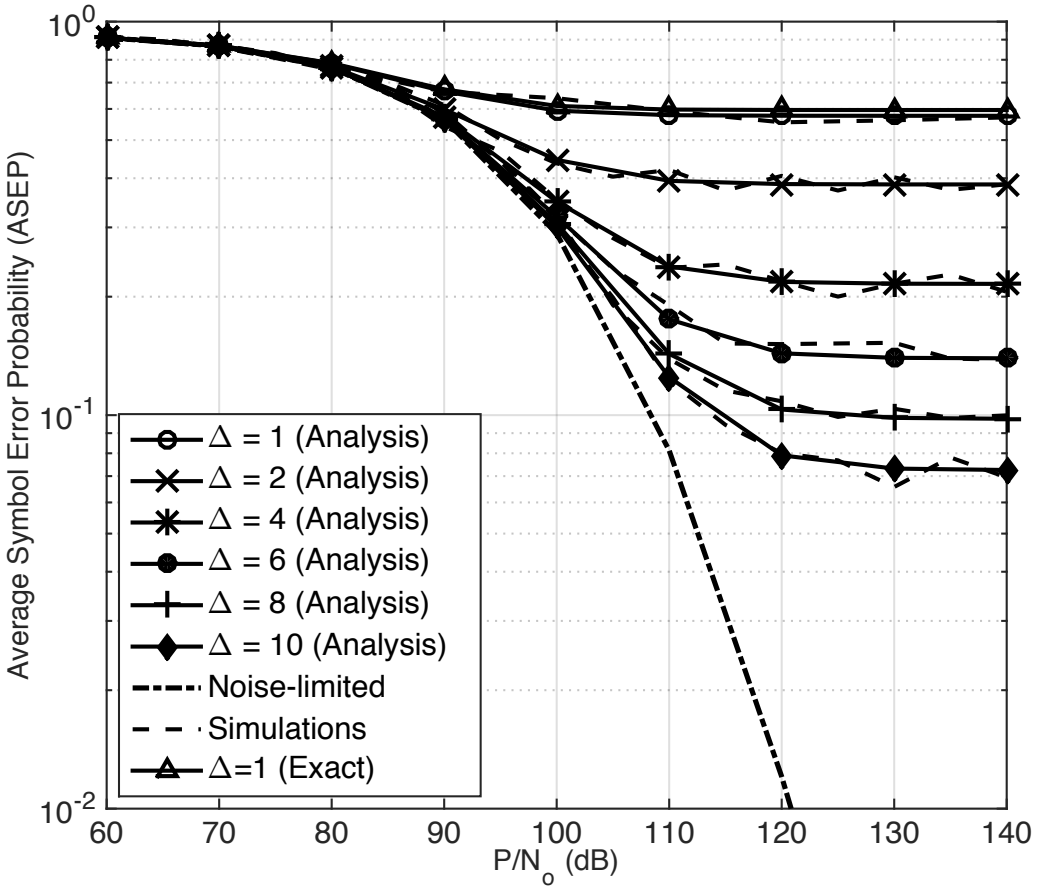

Figure 9.2: The effect of coordinated frequency reuse on the average symbol error probability in the downlink scenario for 16-QAM modulated signals.

for the ASEP represents the performance degradation of the MLR due to aggregate network interference. Hence, the figures clearly show the penalty of interference. That is, while the ASEP in the noise-limited case monotonically decreases with the transmitted power, the ASEP in downlink network saturates at a certain power, due to the transition to the interference-limited operation. This saturation is due to the fact that the noise term becomes negligible as P increases and therefore the increase in the serving BS transmit power is canceled by the increase in interference signals. No matter how much interferers are avoided with coordinated frequency reuse, the ASEP performance will be interference-limited at a certain transmit power. However, the transition point from the noise-limited operation to the interference-limited operation

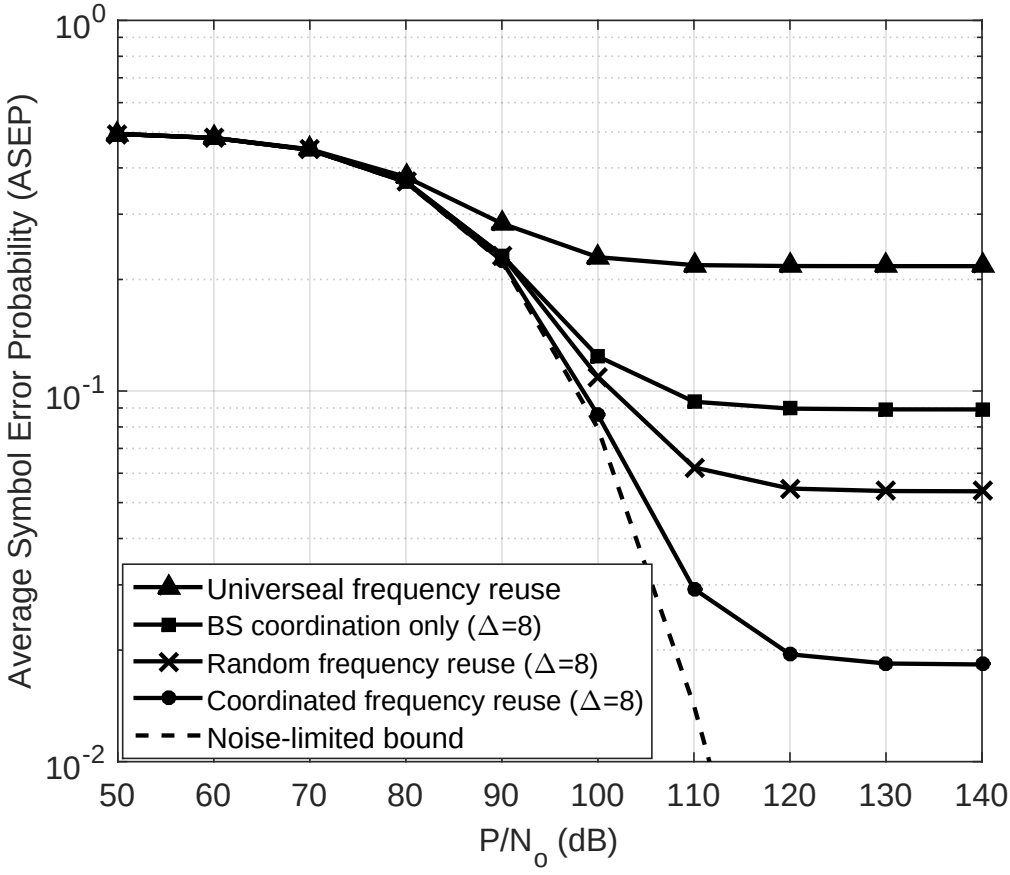

Figure 9.3: The effect of coordination and frequency reuse on average symbol error probability in the downlink scenario for 4-QAM modulated signals with $\Delta = 8$.

depends on the frequency reuse scheme. The figures also show the additional gain acquired by increasing Δ. It is worth noting that these results may be exploited to design the transmit power of the cellular network such that a noise-limited operation is always guaranteed. This is because any increase in the transmit power after the transition to the interference-limited operation is wasted.

In Figs. 9.3 and 9.4, the impact of the different interference management techniques, namely, BSs coordination, random frequency reuse, and coordinated frequency reuse on the ASEP performance improvement is investigated. The figures also show the degraded ASEP performance due to the aggressive universal frequency reuse for $\Delta = 1$. Hence, interference management is essential for adequate network opera-

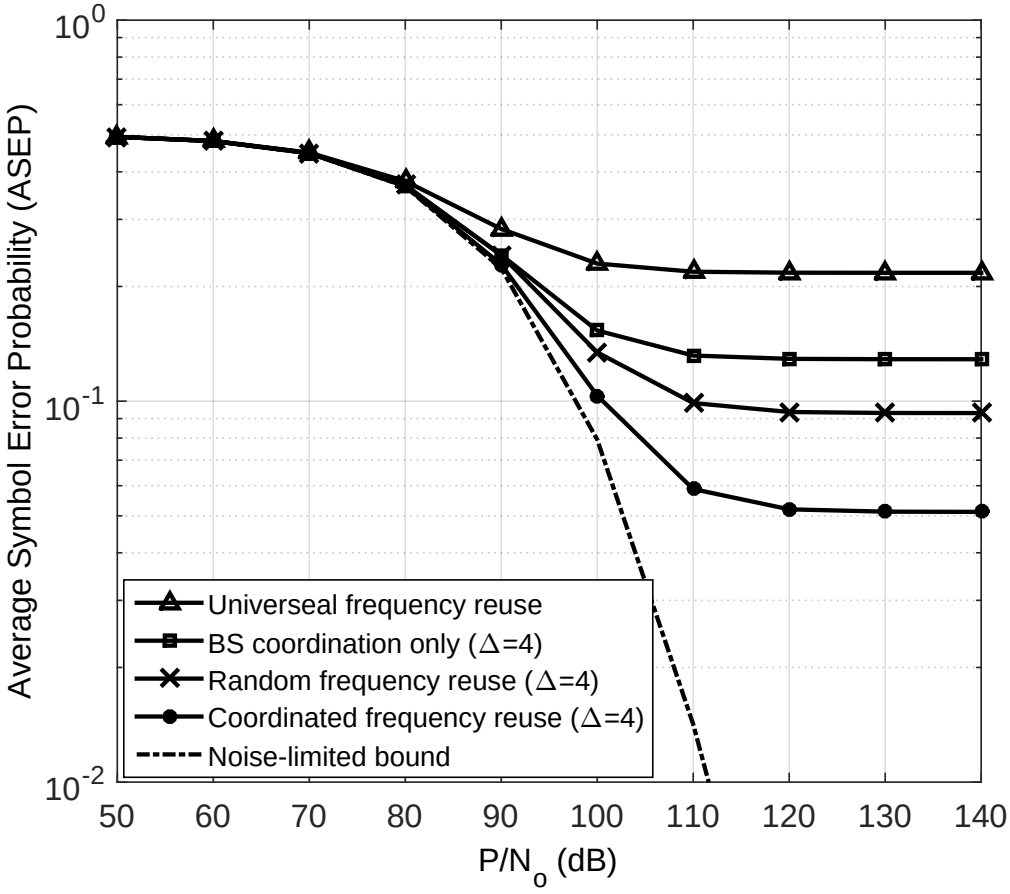

Figure 9.4: The effect of coordination and frequency reuse on average symbol error probability in the downlink scenario for 4-QAM modulated signals with $\Delta = 4$.

tion. While it is obvious that the coordinated frequency reuse scheme achieves the best ASEP performance, it is not intuitive that the random frequency reuse scheme outperforms the BS coordination. Hence, it can be concluded that the interferers intensity have more prominent effect than the interference boundaries in cellular networks. This is because the UEs are already protected in the downlink via the association strategy from arbitrary nearby interferers. Fig. 9.3 also shows that coordinated frequency reuse provides an additional 35% and 80% reduction in the ASEP over, respectively, the random frequency reuse, and BS coordination.

9.5 Chapter Summary and Conclusions

In this chapter, we analyze the average symbol error performance with interference management in downlink cellular networks, through a simple unified framework. The proposed approach characterizes the parametric ASEP in realistic interference environments and captures several key network parameters. We investigate different interference management techniques for the purpose of enhancing the ASEP performance. We observe that coordinated frequency reuse provides 35% reduction in the ASEP compared to the random frequency reuse. Also, we show that random frequency reuse outperforms BSs coordination only by up to 40% lower ASEP.

Chapter 10

Concluding Remarks and Future Directions

10.1 Conclusion

Models exploiting tools from Stochastic Geometry have been proposed to capture several sources of randomness that govern large-scale interference and study spatially averaged network-wide performance. Basically, in this thesis, the developed framework is based on the homogeneous spatial point processes abstraction model from stochastic geometry theory, such that the aggregate network interference is represented as a Poisson point process (PPP). To this end, a stochastic geometric model is utilized to study the exact aggregate network interference in a simple single-input-single-output (SISO) network setup in Chapter 4. The error performance of a sinlge-tier and a multi-tier uplink cellular network with power control has been investigated. Following the recently proposed Equivalent-in-Disrtibution (EiD) methodology for aggregate interference characterization, single integral expressions have been derived to compute the ASEP in realistic interference environments. Furthermore, the performance of the commonly used Gaussian interference power approximation has been shown to be highly optimistic when compared to the performance of the interference characterization derived following the EiD approach. Thus, such Gaussian power approximation does not provide true network performance assessment. With the analysis being inevitably involved due to statistically accounting for each interferer's signal, we then exploit the Gaussian signaling approximation in Chapter 5. Using Gaussian codebooks the distribution of the out-of-cell aggregate interference signal is

represented by a conditionally Gaussian distribution, when conditioning on the network geometry. Hence, the ASEP expressions for AWGN channels are legitimate to be exploited. Such approximation circumvents the complexity of the EiD approach by abstracting unnecessary system details (i.e., the interferers transmitted symbols) without compromising the performance accuracy. Moreover, it is directly extended to different fading environments in both uplink and downlink cellular networks. In Chapter 6, we go beyond the simplistic network model, and study more complex system setups employing various MIMO transmission schemes. We develop a unified analysis that is based on an equivalent SISO representation for the per-data stream SINR in downlink MIMO cellular networks. In addition, we present a single comprehensive study that bridges the gap between error probability, outage probability, and ergodic rate analysis. Hence, it is possible to look at all three performance metrics within a single study in order to efficiently shed lights on design guidelines and optimize the network performance. Further, we discuss the diversity-multiplexing tradeoff imposed by different MIMO schemes. Since the uplink MIMO networks are not sufficiently addressed in the literature, Chapter 7 investigates the performance of decoding error probability, outage and ergodic rate under a full channel inversion power control scheme. Similar to the downlink transmission scenario, a novel network design methodology is proposed.

Chaper 8 quanitfys the time diversity loss due to the temporal correlation among the SIRs of the original and retransmitted signals when compared to the independent interference scenario. It studies the retransmission performance in MIMO downlink cellular networks, in addition to SISO uplink cellular networks with fractional channel inversion power control. Then, we advocate proper adjustment of different network parameters in the retransmission slot, to improve retransmission diversity. Specifically, in the MIMO downlink scenario, appropriate choice of the diverstity gain in the retransmission time slot achieves a higher temporal diversity gain in the retransmis-

sion performance. On the other hand, for the uplink scenario, the power control compensation parameter is adjusted in the second time slot to achieve enhanced coverage probability. Furthermore, it has been shown that full channel inversion power control scheme has the potential to completely eliminate the intereference temporal correlation effect, and achieves the optimistic independent retransmissions performance. Therefore, the developed model provides a design strategy that has the potential to suggest modified network operational parameters in order to achieve the optimistic independent transmissions scenario.

In addition, characterizing the aggregate network interference in large-scale networks opens the road for applying interference management techniques in order to enhance the network performance. The effect of interference management techniques, namely; frequency reuse and BS coordination, on the ASEP performance has been studied in Chapter 9.

The proposed framework throughout this thesis has been verified against the exact EiD approach, and intensive Monte Carlo simulations, demonstrating high accuracy as well as significantly reduced computational complexity.

10.2 Future Directions

10.2.1 Impact of imperfect Channel state information (CSI)

The proposed model throughout the thesis relies on the assumption of perfect channel state information (CSI) availability. However, in practical scenarios, channel information is prone to estimation errors during pilot-aided transmissions. Channel estimation errors in MIMO setups will introduce another type of interference to the network in addition to the typical inter-cell interference. Specifically, intra-cell interference will represent a non-negligible portion of the aggregate network interference. Moreover, the new channel estimates distributions will be location-dependent, which is expected to complicate the analysis. Therefore, the network geometry has a

strong impact on the estimation errors and hence it is essential to quantify the effect of the introduced intra-cell interference in a realistic scenario on the network-wide performance.

10.2.2 Extension to Massive MIMO Setup

Massive MIMO systems are envisioned as one of the promising solutions for meeting existing and future challenges in emerging wireless demands. Specifically, massive MIMO is considered an enabler for next-generation 5G wireless networks. By employing a huge number of antennas at the BSs, spectacular potential gains are expected to be achieved. However, deploying massive MIMO technology in future heterogeneous networks is still an open research direction in order to tackle the encountered technical challenges. To name a few, the effect of pilot contamination on the aggregate interference, the need for efficient interference management strategies, as well as achieving energy efficient operation. In [137, 138] the pilot contamination effect on the aggregate network inetrference has been quantified. In [139], optimal energy efficiency performance in massive MIMO networks has been studied by joint optimization of several system parameters. Utilizing the proposed unified model, it is possible to take the model some steps further to quantify the effect of pilot contamination, deploying more BSs versus adding more antennas to the BSs and/or served users to the network on the energy consumption requirements coupled with other tangible performance metrics.

REFERENCES

[1] Dave Evans, "The Internet of things: How the next evolution of the Internet is changing everything," *CISCO White Paper*, April 2011.

[2] Ericsson White Paper, "More than 50 billion connected devices," *Tech. Rep*, pp. 284 23–3149, Feb. 2011.

[3] Ericsson, "3GPP tech. rep. 25.820,," *v. 8.2.0*, Sept 2008.

[4] P. Lin, J. Zhang, Y. Chen, and Q. Zhang, "Macro-femto heterogeneous network deployment and management: from business models to technical solutions," *IEEE Wireless Communications*, vol. 18, no. 3, pp. 64–70, June 2011.

[5] E. Hossain, M. Rasti, H. Tabassum, and A. Abdelnasser, "Evolution toward 5G multi-tier cellular wireless networks: An interference management perspective," *IEEE Wireless Communications*, vol. 21, no. 3, pp. 118–127, June 2014.

[6] C. B. Papadias H. Huang and S. Venkatesan, *MIMO Communication for Cellular Networks*, Springer, 2012.

[7] C. Oestges and B. Clerckx, *MIMO Wireless Communications: From Real-World Propagation to Space-Time Code Design*, Elsevier Science, 2010.

[8] E. Larsson and P. Stoica, *Space-Time Block Coding for Wireless Communications*, Cambridge University Press, Cambridge, UK, 2003.

[9] Ericsson, "5G radio access, research and vision," *White Paper*, 2013.

[10] Metis, "Scenarios, requirements and kpis for 5G mobile and wireless system," *ICT-317669 METIS project*, May 2013.

[11] C. X. Wang, F. Haider, X. Gao, X. H. You, Y. Yang, D. Yuan, H. M. Aggoune, H. Haas, S. Fletcher, and E. Hepsaydir, "Cellular architecture and key technologies for 5G wireless communication networks," *IEEE Communications Magazine*, vol. 52, no. 2, pp. 122–130, February 2014.

[12] J. Silvester and L. Kleinrock, "On the capacity of multihop slotted aloha networks with regular structure," *IEEE Transactions on Communications*, vol. 31, no. 8, pp. 974–982, Aug 1983.

[13] H. ElSawy, E. Hossain, and M. Haenggi, "Stochastic geometry for modeling, analysis, and design of multi-tier and cognitive cellular wireless networks: A survey," *IEEE Communications Surveys & Tutorials*, vol. 15, no. 3, pp. 996–1019, 2013.

[14] J. G. Andrews, F. Baccelli, and R. K. Ganti, "A tractable approach to coverage and rate in cellular networks," *IEEE Transactions on Communications*, vol. 59, no. 11, pp. 3122–3134, Nov. 2011.

[15] François Baccelli, Maurice Klein, Marc Lebourges, and Sergei Zuyev, "Stochastic geometry and architecture of communication networks," *Telecommunication Systems*, vol. 7, no. 1, pp. 209–227, 1997.

[16] B. Boots A. Okabe and K. Sugihara, *Spatial Tessellations: Concepts and Applications of Voronoi Diagrams*, John Wiley,, 1992.

[17] M. Haenggi, *Stochastic Geometry for Wireless Networks*, Cambridge University Press, 2012.

[18] M. Z. Win, P. C. Pinto, and L. A. Shepp, "A mathematical theory of network interference and its applications," *Proceedings of the IEEE*, vol. 97, no. 2, pp. 205–230, Feb 2009.

[19] F. Baccelli and B. Baszczyszyn, *Stochastic Geometry and Wireless Networks, Volume I – Theory*, NoW Publishers, 2009.

[20] F. Baccelli and B. Baszczyszyn, *Stochastic Geometry and Wireless Networks, Volume II – Applications*, NoW Publishers, 2009.

[21] M. Haenggi, J. G. Andrews, F. Baccelli, O. Dousse, and M. Franceschetti, "Stochastic geometry and random graphs for the analysis and design of wireless networks," *IEEE Journal on Selected Areas in Communications*, vol. 27, no. 7, pp. 1029–1046, September 2009.

[22] Matthias Wildemeersch, "Statistical modeling and analysis of interference in wireless networks," 2013.

[23] H. S. Dhillon, R. K. Ganti, F. Baccelli, and J. G. Andrews, "Coverage and ergodic rate in k-tier downlink heterogeneous cellular networks," in *Communication, Control, and Computing (Allerton), 2011 49th Annual Allerton Conference on*, Sept. 2011, pp. 1627–1632.

[24] R. Tanbourgi, H. S. Dhillon, and F. K. Jondral, "Analysis of joint transmit-receive diversity in downlink MIMO heterogeneous cellular networks," *IEEE Transactions on Wireless Communications*, accepted 2015.

[25] R. Tanbourgi and F. K. Jondral, "Downlink MIMO diversity with maximal-ratio combining in heterogeneous cellular networks," in *IEEE International Conference on Communications (ICC)*, June 2015, pp. 1831–1837.

[26] T. M. Nguyen, Y. Jeong, T.Q.S. Quek, W. P. Tay, and H. Shin, "Interference alignment in a Poisson field of MIMO femtocells," *IEEE Transactions on Wireless Communications*, vol. 12, no. 6, pp. 2633–2645, Jun. 2013.

[27] A. Adhikary, H. S. Dhillon, and G. Caire, "Massive-MIMO meets HetNet: Interference coordination through spatial blanking," *IEEE Journal on Selected Areas in Communications*, accepted 2015.

[28] N. Lee, D. M.-Jimenez, A. Lozano, and R.W. Heath, "Spectral efficiency of dynamic coordinated beamforming: A stochastic geometry approach," *IEEE Transactions on Wireless Communications*, vol. 14, no. 1, pp. 230–241, Jan. 2015.

[29] A.H. Sakr and E. Hossain, "Location-aware cross-tier coordinated multipoint transmission in two-tier cellular networks," *Wireless Communications, IEEE Transactions on*, vol. 13, no. 11, pp. 6311–6325, Nov 2014.

[30] G. Nigam, P. Minero, and M. Haenggi, "Coordinated multipoint joint transmission in heterogeneous networks," *Communications, IEEE Transactions on*, vol. 62, no. 11, pp. 4134–4146, Nov 2014.

[31] X. Zhang and M. Haenggi, "A stochastic geometry analysis of inter-cell interference coordination and intra-cell diversity," *IEEE Transactions on Wireless Communications*, vol. 13, no. 12, pp. 6655–6669, Dec. 2014.

[32] G. Nigam, P. Minero, and M. Haenggi, "Spatiotemporal cooperation in heterogeneous cellular networks," *IEEE Journal on Selected Areas in Communications*, vol. 33, no. 6, pp. 1253–1265, June 2015.

[33] R. Tanbourgi, S. Singh, J. G. Andrews, and F. K. Jondral, "A tractable model for noncoherent joint-transmission base station cooperation," *IEEE Transactions on Wireless Communications*, vol. 13, no. 9, pp. 4959–4973, Sept 2014.

[34] H. S. Dhillon, M. Kountouris, and J. G. Andrews, "Downlink MIMO HetNets: Modeling, ordering results and performance analysis," *IEEE Transactions on Wireless Communications*, vol. 12, no. 10, pp. 5208–5222, Oct. 2013.

[35] A. K. Gupta, H. S. Dhillon, S. Vishwanath, and J. G. Andrews, "Downlink multi-antenna heterogeneous cellular network with load balancing," *IEEE Transactions on Communications*, vol. 62, no. 11, pp. 4052–4067, Nov. 2014.

[36] M. Di Renzo and W. Lu, "Stochastic geometry modeling and performance evaluation of mimo cellular networks using the equivalent-in-distribution (eid)-based approach," *IEEE Transactions on Communications*, vol. 63, no. 3, pp. 977–996, March 2015.

[37] M. Di Renzo and W. Lu, "Stochastic geometry modeling and performance evaluation of MIMO cellular networks using the equivalent-in-distribution (EiD)-based approach," *IEEE Transactions on Communications*, vol. 63, no. 3, pp. 977–996, Mar. 2015.

[38] M. Di Renzo and Peng Guan, "A mathematical framework to the computation of the error probability of downlink MIMO cellular networks by using stochastic geometry," *IEEE Transactions on Communications*, vol. 62, no. 8, pp. 2860–2879, Aug. 2014.

[39] Hesham ElSawy, Ahmed Kamal Sultan-Salem, Mohamed-Slim Alouini, and Moe Z. Win, "Modeling and analysis of cellular networks using stochastic geometry: A tutorial," *CoRR*, vol. abs/1604.03689, 2016.

[40] K. A. Hamdi, "A useful technique for interference analysis in nakagami fading," *IEEE Transactions on Communications*, vol. 55, no. 6, pp. 1120–1124, 2007.

[41] A. Giorgetti and M. Chiani, ," .

[42] M. Haenggi and R. K. Ganti, "Interference in large wireless networks," *NOW: Foundations and Trends in Networking,*, 2009.

[43] P. C. Pinto and M. Z. Win, "Communication in a poisson field of interferers–Part I: Interference distribution and error probability," *IEEE Transactions on Wireless Communications*, vol. 9, no. 7, pp. 2176–2186, July 2010.

[44] A. Guo and M. Haenggi, "Spatial stochastic models and metrics for the structure of base stations in cellular networks," *IEEE Transactions on Wireless Communications*, vol. 12, no. 11, pp. 5800–5812, Nov. 2013.

[45] M. Di Renzo, C. Merola, A. Guidotti, F. Santucci, and G. E. Corazza, "Error performance of multi-antenna receivers in a poisson field of interferers: A stochastic geometry approach," *IEEE Transactions on Communications*, vol. 61, no. 5, pp. 2025–2047, May 2013.

[46] H. ElSawy and E. Hossain, "Two-tier HetNets with cognitive femtocells: Downlink performance modeling and analysis in a multichannel environment," *IEEE Transactions on Mobile Computing*, vol. 13, no. 3, pp. 649–663, Mar. 2014.

[47] H. ElSawy and E. Hossain, "On stochastic geometry modeling of cellular uplink transmission with truncated channel inversion power control," *IEEE Transactions on Wireless Communications*, vol. 13, no. 8, pp. 4454–4469, Aug. 2014.

[48] Savo G. Glisic, *Advanced Wireless Communications and Internet: Future Evolving Technologies*, Wiley Publishing, 3rd edition, 2011.

[49] T. Hou and V. Li, "Transmission range control in multihop packet radio networks," *IEEE Trans. Commun*, vol. 34, no. 1, pp. 38–44, Jan. 1986.

[50] L. Kleinrock and J. A. Silvester, "Optimum transmission radii for packet radio networks or why six is a magic number," *in ConferenceRecord: National Telecommunication Conference*, pp. 4.3.1–4.3.5, Dec. 1978.

[51] E. S. Sousa, "Optimum transmission range in a direct-sequence spread spectrum multihop packet radio network," *IEEE J. Sel. Areas Commun.*, vol. 8, no. 15, year=1990, pages=762–771,.

[52] B. Baszczyszyn, M. K. Karray, and H. P. Keeler, "Using poisson processes to model lattice cellular networks," in *INFOCOM, 2013 Proceedings IEEE*, April 2013, pp. 773–781.

[53] Wei Lu and Marco Di Renzo, "Stochastic geometry modeling of cellular networks: Analysis, simulation and experimental validation," *CoRR*, vol. abs/1506.03857, 2015.

[54] M. Haenggi, "The mean interference-to-signal ratio and its key role in cellular and amorphous networks," *IEEE Wireless Communications Letters*, vol. 3, no. 6, pp. 597–600, Dec 2014.

[55] H. Wei, N. Deng, W. Zhou, and M. Haenggi, "Approximate sir analysis in general heterogeneous cellular networks," *IEEE Transactions on Communications*, vol. 64, no. 3, pp. 1259–1273, March 2016.

[56] R. K. Ganti and M. Haenggi, "Asymptotics and approximation of the sir distribution in general cellular networks," *IEEE Transactions on Wireless Communications*, vol. 15, no. 3, pp. 2130–2143, March 2016.

[57] S. B. Lowen and M. C. Teich, "Power-law shot noise," *IEEE Transactions on Information Theory*, vol. 36, no. 6, pp. 1302–1318, Nov 1990.

[58] J. Ilow and D. Hatzinakos, "Analytic alpha-stable noise modeling in a poisson field of interferers or scatterers," *IEEE Transactions on Signal Processing*, vol. 46, no. 6, pp. 1601–1611, Jun 1998.

[59] T. X. Brown, "Cellular performance bounds via shotgun cellular systems," *IEEE Journal on Selected Areas in Communications*, vol. 18, no. 11, pp. 2443–2455, Nov 2000.

[60] A. Guo and M. Haenggi, "Spatial stochastic models and metrics for the structure of base stations in cellular networks," *IEEE Transactions on Wireless Communications*, vol. 12, no. 11, pp. 5800–5812, November 2013.

[61] B. Baszczyszyn, M. K. Karray, and H. P. Keeler, "Using poisson processes to model lattice cellular networks," in *INFOCOM, 2013 Proceedings IEEE*, April 2013, pp. 773–781.

[62] A. Rabbachin, T. Q. S. Quek, P. C. Pinto, I. Oppermann, and M. Z. Win, "Non-coherent uwb communication in the presence of multiple narrowband interferers," *IEEE Transactions on Wireless Communications*, vol. 9, no. 11, pp. 3365–3379, November 2010.

[63] S. Govindasamy, D. W. Bliss, and D. H. Staelin, "Asymptotic spectral efficiency of the uplink in spatially distributed wireless networks with multi-antenna base stations," *IEEE Transactions on Communications*, vol. 61, no. 7, pp. 100–112, July 2013.

[64] H. ElSawy, E. Hossain, and Dong In Kim, "Hetnets with cognitive small cells: user offloading and distributed channel access techniques," *IEEE Communications Magazine*, vol. 51, no. 6, pp. 28–36, June 2013.

[65] P. Madhusudhanan, J. G. Restrepo, Y. Liu, T. X. Brown, and K. R. Baker, "Downlink performance analysis for a generalized shotgun cellular system," *IEEE Transactions on Wireless Communications*, vol. 13, no. 12, pp. 6684–6696, Dec 2014.

[66] R. W. Heath, M. Kountouris, and T. Bai, "Modeling heterogeneous network interference using poisson point processes," *IEEE Transactions on Signal Processing*, vol. 61, no. 16, pp. 4114–4126, Aug 2013.

[67] S. Mukherjee, "Distribution of downlink sinr in heterogeneous cellular networks," *IEEE Journal on Selected Areas in Communications*, vol. 30, no. 3, pp. 575–585, April 2012.

[68] T. Bai and R. W. Heath, "Location-specific coverage in heterogeneous networks," *IEEE Signal Processing Letters*, vol. 20, no. 9, pp. 873–876, Sept 2013.

[69] M. D. Renzo, A. Guidotti, and G. E. Corazza, "Average rate of downlink heterogeneous cellular networks over generalized fading channels: A stochastic geometry approach," *IEEE Transactions on Communications*, vol. 61, no. 7, pp. 3050–3071, July 2013.

[70] Y. J. Chun, M. O. Hasna, and A. Ghrayeb, "Modeling heterogeneous cellular networks interference using poisson cluster processes," *IEEE Journal on Selected Areas in Communications*, vol. 33, no. 10, pp. 2182–2195, Oct 2015.

[71] T. D. Novlan, H. S. Dhillon, and J. G. Andrews, "Analytical modeling of uplink cellular networks," *IEEE Transactions on Wireless Communications*, vol. 12, no. 6, pp. 2669–2679, June 2013.

[72] A. AlAmmouri, H. ElSawy, and M. S. Alouini, "Load-aware modeling for uplink cellular networks in a multi-channel environment," in *2014 IEEE 25th Annual International Symposium on Personal, Indoor, and Mobile Radio Communication (PIMRC)*, Sept 2014, pp. 1591–1596.

[73] H. Y. Lee, Y. J. Sang, and K. S. Kim, "On the uplink SIR distributions in heterogeneous cellular networks," *IEEE Communications Letters*, vol. 18, no. 12, pp. 2145–2148, Dec 2014.

[74] Z. Zeinalpour-Yazdi and S. Jalali, "Outage analysis of uplink two-tier networks," *IEEE Transactions on Communications*, vol. 62, no. 9, pp. 3351–3362, Sept 2014.

[75] Y. Wen, S. Loyka, and A. Yongacoglu, "Asymptotic analysis of interference in cognitive radio networks," *IEEE Journal on Selected Areas in Communications*, vol. 30, no. 10, pp. 2040–2052, November 2012.

[76] S. Singh, F. Baccelli, and J. G. Andrews, "On association cells in random heterogeneous networks," *IEEE Wireless Communications Letters*, vol. 3, no. 1, pp. 70–73, February 2014.

[77] Matthias Wildemeersch, Tony QS Quek, Marios Kountouris, and Cornelis H Slump, "Successive interference cancellation in uplink cellular networks," in *2013 IEEE 14th Workshop on Signal Processing Advances in Wireless Communications (SPAWC)*. IEEE, 2013, pp. 310–314.

[78] Hongguang Sun, Min Sheng, Matthias Wildemeersch, and Tony QS Quek, "Modeling of d2d enhanced two-tier dynamic tdd heterogeneous cellular networks," in *2014 IEEE/CIC International Conference on Communications in China (ICCC)*. IEEE, 2014, pp. 609–614.

[79] Matthias Wildemeersch, Tony QS Quek, Alberto Rabbachin, Cornelis H Slump, and Aiping Huang, "Energy efficient design of cognitive small cells," in *2013 IEEE International Conference on Communications (ICC)*. IEEE, 2013, pp. 2701–2706.

[80] C. Li, J. Zhang, J. G. Andrews, and K. B. Letaief, "Success probability and area spectral efficiency in multiuser MIMO HetNets," *IEEE Transactions on Communications*, vol. 64, no. 4, pp. 1544–1556, April 2016.

[81] R. Tanbourgi, H. S. Dhillon, J. G. Andrews, and F. K. Jondral, "Effect of spatial interference correlation on the performance of maximum ratio combining," *IEEE Transactions on Wireless Communications*, vol. 13, no. 6, pp. 3307–3316, June 2014.

[82] R. Tanbourgi, H. S. Dhillon, J. G. Andrews, and F. K. Jondral, "Dual-branch MRC receivers under spatial interference correlation and Nakagami fading," *IEEE Transactions on Communications*, vol. 62, no. 6, pp. 1830–1844, June 2014.

[83] M. Di Renzo and P. Guan, "Stochastic geometry modeling and system-level analysis of uplink heterogeneous cellular networks with multi-antenna base sta-

tions," *IEEE Transactions on Communications*, vol. 64, no. 6, pp. 2453–2476, June 2016.

[84] K. Hosseini, W. Yu, and R. S. Adve, "A stochastic analysis of network mimo systems," *IEEE Transactions on Signal Processing*, vol. 64, no. 16, pp. 4113–4126, Aug 2016.

[85] C. Zhu and W. Yu, "Stochastic analysis of user-centric network mimo," in *2016 IEEE 17th International Workshop on Signal Processing Advances in Wireless Communications (SPAWC)*, July 2016, pp. 1–5.

[86] Y. Lin and W. Yu, "Ergodic capacity analysis of downlink distributed antenna systems using stochastic geometry," in *2013 IEEE International Conference on Communications (ICC)*, June 2013, pp. 3338–3343.

[87] Yicheng Lin and W. Yu, "Optimizing user association and frequency reuse for heterogeneous network under stochastic model," in *2013 IEEE Global Communications Conference (GLOBECOM)*, Dec 2013, pp. 2045–2050.

[88] Marco Di Renzo, Wei Lu, and Peng Guan, "The intensity matching approach: A tractable stochastic geometry approximation to system-level analysis of cellular networks," *CoRR*, vol. abs/1604.02683, 2016.

[89] H. Inaltekin, "Gaussian approximation for the wireless multi-access interference distribution," *IEEE Transactions on Signal Processing*, vol. 60, no. 11, pp. 6114–6120, Nov 2012.

[90] M. Aljuaid and H. Yanikomeroglu, "Investigating the gaussian convergence of the distribution of the aggregate interference power in large wireless networks," *IEEE Transactions on Vehicular Technology*, vol. 59, no. 9, pp. 4418–4424, Nov 2010.

[91] M. Z. Win, P. C. Pinto, and L. A. Shepp, "A mathematical theory of network interference and its applications," *Proceedings of the IEEE*, vol. 97, no. 2, pp. 205–230, Feb. 2009.

[92] Gennady Samorodnitsky and Murad S. Taqqu, *Stable non-Gaussian random processes : stochastic models with infinite variance*, Stochastic modeling. Chapman & Hall, New York, 1994, Rimpr. par CRC Press : 2000.

[93] Xueshi Yang and A. P. Petropulu, "Co-channel interference modeling and analysis in a poisson field of interferers in wireless communications," *IEEE Transactions on Signal Processing*, vol. 51, no. 1, pp. 64–76, Jan 2003.

[94] Chrysostomos L. Nikias and Min Shao, *Signal Processing with Alpha-stable Distributions and Applications*, Wiley-Interscience, New York, NY, USA, 1995.

[95] M. Shao and C. L. Nikias, "Signal processing with fractional lower order moments: stable processes and their applications," *Proceedings of the IEEE*, vol. 81, no. 7, pp. 986–1010, Jul 1993.

[96] K. Gulati, B. L. Evans, J. G. Andrews, and K. R. Tinsley, "Statistics of co-channel interference in a field of poisson and poisson-poisson clustered interferers," *IEEE Transactions on Signal Processing*, vol. 58, no. 12, pp. 6207–6222, Dec 2010.

[97] K. Gulati, B. L. Evans, and K. R. Tinsley, "Statistical modeling of co-channel interference in a field of poisson distributed interferers," in *2010 IEEE International Conference on Acoustics, Speech and Signal Processing*, March 2010, pp. 3490–3493.

[98] M. K. Simon and M.-S. Alouini, *Digital Communication over Fading Channels*, vol. 95, Wiley-Interscience, 2005.

[99] R.J. Marks, G.L. Wise, D.G. Haldeman, and J.L. Whited, "Detection in Laplace noise," *IEEE Trans. on Aerosp. Electron. Syst.*, vol. AES-14, no. 6, pp. 866–872, Nov 1978.

[100] S. Jiang and N.C. Beaulieu, "Precise ber computation for binary data detection in bandlimited white laplace noise," *IEEE Transactions on Communications*, vol. 59, no. 6, pp. 1570–1579, June 2011.

[101] H. Soury, F. Yilmaz, and M. S. Alouini, "Error rates of m-pam and m-qam in generalized fading and generalized gaussian noise environments," *IEEE Communications Letters*, vol. 17, no. 10, pp. 1932–1935, October 2013.

[102] L. H. Afify, H. ElSawy, T. Y. Al-Naffouri, and M. S. Alouini, "The influence of gaussian signaling approximation on error performance in cellular networks," *IEEE Communications Letters*, vol. 19, no. 12, pp. 2202–2205, Dec 2015.

[103] L. H. Afify, H. ElSawy, T. Y. Al-Naffouri, and M.-S. Alouini, "Unified tractable model for downlink mimo cellular networks using stochastic geometry," in *2016 IEEE International Conference on Communications (ICC)*, May 2016, pp. 1–7.

[104] L. H. Afify, H. ElSawy, T. Y. Al-Naffouri, and M.-S. Alouini, "A unified stochastic geometry model for MIMO cellular networks with retransmissions," *IEEE Transaction on Wireless Communications, to appear.*

[105] R. Vaze and R. W. Heath, "Transmission capacity of ad-hoc networks with multiple antennas using transmit stream adaptation and interference cancellation," *IEEE Transactions on Information Theory*, vol. 58, no. 2, pp. 780–792, Feb 2012.

[106] A. M. Hunter, J. G. Andrews, and S. Weber, "Transmission capacity of ad hoc networks with spatial diversity," December 2008, vol. 7, pp. 5058–5071.

[107] W. Choi, N. Himayat, S. Talwar, and M. Ho, "The effects of co-channel interference on spatial diversity techniques," in *Wireless Communications and Networking Conference, 2007.WCNC 2007. IEEE*, March 2007, pp. 1936–1941.

[108] H. ElSawy and E. Hossain, "On cognitive small cells in two-tier heterogeneous networks," in *Proc. of the 9th International Workshop on Spatial Stochastic Models for Wireless Networks (SpaSWiN'2013)*, Tsukuba Science City, Japan, May 2013.

[109] H.S. Dhillon, R.K. Ganti, and J.G. Andrews, "Load-aware heterogeneous cellular networks: Modeling and sir distribution," in *Global Communications Conference (GLOBECOM), 2012 IEEE*, Dec 2012, pp. 4314–4319.

[110] T. D. Novlan, H. S. Dhillon, and J. G. Andrews, "Analytical modeling of uplink cellular networks," *IEEE Transactions on Wireless Communications*, vol. 12, no. 6, pp. 2669–2679, June 2013.

[111] H. Holma and A. Toskala, *LTE Advanced: 3GPP Solution for IMT-Advanced*, John Wiley & Sons, 2012.

[112] M. Abramowitz and I. A. Stegun, Eds., *Handbook of Mathematical Functions, Tenth Printing*, Dover Publications, Dec. 1972.

[113] L. H. Afify, H. ElSawy, T. Al-Naffouri, and M.-S. Alouini, "Error performance analysis in K-tier uplink cellular networks using a stochastic geometric approach," in *Proc. of the IEEE ICC 4th International Workshop on Small Cell and 5G Networks (SmallNets)*, London, UK, Jun. 2015.

[114] Y. M. Shobowale and K. A. Hamdi, "A unified model for interference analysis in unlicensed frequency bands," *IEEE Transactions on Wireless Communications*, vol. 8, no. 8, pp. 4004–4013, Aug. 2009.

[115] X. Cheng, C. X. Wang, H. Wang, X. Gao, X. H. You, D. Yuan, B. Ai, Q. Huo, L. Y. Song, and B. L. Jiao, "Cooperative mimo channel modeling and multi-link spatial correlation properties," *IEEE Journal on Selected Areas in Communications*, vol. 30, no. 2, pp. 388–396, February 2012.

[116] M. Di Renzo and P. Guan, "Stochastic geometry modeling of coverage and rate of cellular networks using the gil-pelaez inversion theorem," *IEEE Communications Letters*, vol. 18, no. 9, pp. 1575–1578, Sept 2014.

[117] H. Alzer, "On some inequalities for the incomplete gamma function," *Mathematics of Computation*, vol. 66, no. 218.

[118] K. Huang, R. W. Heath, and J. G. Andrews, "Space division multiple access with a sum feedback rate constraint," *IEEE Transactions on Signal Processing*, vol. 55, no. 7, pp. 3879–3891, July 2007.

[119] Andrea Goldsmith, *Wireless Communications*, Cambridge University Press, New York, NY, USA, 2005.

[120] F. J. Martin-Vega, G. Gomez, M. C. Aguayo-Torres, and M. Di Renzo, "Analytical modeling of interference aware power control for the uplink of heterogeneous cellular networks," *IEEE Transactions on Wireless Communications*, vol. PP, no. 99, pp. 1–1, 2016.

[121] J. H. Winters, "Optimum combining in digital mobile radio with cochannel interference," *IEEE Transactions on Vehicular Technology*, vol. 33, no. 3, pp. 144–155, Aug 1984.

[122] R. Tanbourgi, H. S. Dhillon, J. G. Andrews, and F. K. Jondral, "Effect of spatial interference correlation on the performance of maximum ratio combining," *IEEE Transactions on Wireless Communications*, vol. 13, no. 6, pp. 3307–3316, June 2014.

[123] D. G. Brennan, "Linear diversity combining techniques," *Proceedings of the IRE*, vol. 47, no. 6, pp. 1075–1102, June 1959.

[124] R. K. Ganti and M. Haenggi, "Spatial and temporal correlation of the interference in ALOHA ad hoc networks," *IEEE Communications Letters*, vol. 13, no. 9, pp. 631–633, Sep 2009.

[125] L. H. Afify, H. ElSawy, T. Y. Al-Naffouri, and M. S. Alouini, "A unified stochastic geometry model for MIMO cellular networks with retransmissions," *IEEE Transactions on Wireless Communications*, vol. 15, no. 12, pp. 8595–8609, Dec 2016.

[126] Shankar Krishnan and Harpreet S. Dhillon, "Spatio-temporal interference correlation and joint coverage in cellular networks," *CoRR*, vol. abs/1606.05332, 2016.

[127] S. Singh, X. Zhang, and J. G. Andrews, "Joint rate and SINR coverage analysis for decoupled uplink-downlink biased cell associations in hetnets," *IEEE Transactions on Wireless Communications*, vol. 14, no. 10, pp. 5360–5373, Oct 2015.

[128] F. Olver, *NIST handbook of mathematical functions*, Cambridge University Press, 2010.

[129] LTE Evolved Universal Terrestrial Radio Access (E-UTRA), "Physical layer procedures," in *RTS/TSGR-0136213v880, 3GPP TS 36.213. Version 8.8.0, Release 8.*

[130] A. Simonsson and A. Furuskar, "Uplink power control in LTE - overview and performance,," in *Vehicular Technology Conference, 2008. VTC 2008-Fall. IEEE 68th*, Sept 2008, pp. 1–5.

[131] N. Jindal, S. Weber, and J. G. Andrews, "Fractional power control for decentralized wireless networks," *IEEE Transactions on Wireless Communications*, vol. 7, no. 12, pp. 5482–5492, December 2008.

[132] Xinchen Zhang and M. Haenggi, "Successive interference cancellation in downlink heterogeneous cellular networks," in *Globecom Workshops (GC Wkshps), 2013 IEEE*, Dec 2013, pp. 730–735.

[133] T. D. Novlan, R. K. Ganti, J. G. Andrews, and A. Ghosh, "A new model for coverage with fractional frequency reuse in ofdma cellular networks," in *2011 IEEE Global Telecommunications Conference - GLOBECOM 2011*, Dec 2011, pp. 1–5.

[134] T. D. Novlan, R. K. Ganti, A. Ghosh, and J. G. Andrews, "Analytical evaluation of fractional frequency reuse for heterogeneous cellular networks," *IEEE Transactions on Communications*, vol. 60, no. 7, pp. 2029–2039, July 2012.

[135] M. Haenggi, "Mean Interference in Hard-Core Wireless Networks," *IEEE Communications Letters*, vol. 15, no. 8, pp. 792–794, Aug. 2011, Available at `http://www.nd.edu/~mhaenggi/pubs/cl11.pdf`.

[136] H.Q. Nguyen, F. Baccelli, and D. Kofman, "A stochastic geometry analysis of dense IEEE 802.11 networks," in *In Proc. of the 26th IEEE International Conference on Computer Communications, INFOCOM 2007.*, May 2007, pp. 1199–1207.

[137] Tianyang Bai and Robert W Heath Jr, "Analyzing uplink sir and rate in massive MIMO systems using stochastic geometry," *arXiv preprint arXiv:1510.02538*, 2015.

[138] N. Liang, W. Zhang, and C. Shen, "An uplink interference analysis for massive MIMO systems with mrc and zf receivers," in *2015 IEEE Wireless Communications and Networking Conference (WCNC)*, March 2015, pp. 310–315.

[139] E. Bjornson, L. Sanguinetti, and M. Kountouris, "Deploying dense networks for maximal energy efficiency: Small cells meet massive MIMO," *IEEE Journal on Selected Areas in Communications*, vol. 34, no. 4, pp. 832–847, April 2016.

[140] S. Kotz K.-T. Fang and K. W. Ng, *Symmetric Multivariate and Related Distributions*, London, U.K.: Chapman and Hall, 1990.

[141] I. S. Gradshteyn and I. M. Ryzhik, *Table of Integrals, Series, and Products, Seventh Edition*, Academic Press, 2007.

[142] K. A. Hamdi, "A useful lemma for capacity analysis of fading interference channels," *IEEE Transactions on Communications*, vol. 58, no. 2, pp. 411–416, 2010.

[143] B. Hassibi and B. M. Hochwald, "High-rate codes that are linear in space and time," *IEEE Transactions on Information Theory*, vol. 48, no. 7, pp. 1804–1824, July 2002.

[144] R. Nabar A. Paulraj and D. Gore., *Introduction to Space-Time Wireless Communications*, Cambridge University Press, Cambridge, UK, 2003.

APPENDICES

Appendix A

A.1 Proof of Lemma 4.1

Let $z_i = s_i g_i$. Based on the assumed Rayleigh distribution of g_i, then z_i is a spherically symmetric (SS) random variable [36]. That is, its distribution is rotationally invariant [140]. As a consequence, I_{agg} which can be represented as

$$\begin{aligned} I_{agg} &= \sum_{r_i \in \tilde{\Psi}_u} \sqrt{P_{u_i}} r_i^{-b} g_i s_i \\ &= \sum_{r_i \in \tilde{\Psi}_u} \sqrt{P_{u_i}} r_i^{-b} z_i, \end{aligned} \tag{A.1}$$

is also an SS random variable. Now recall that, the characteristic function of an SS random variable is a function of $|\boldsymbol{\omega}|^2$. Accordingly, the characteristic function of the aggregate interference is given by

$$\Phi_{I_{agg}}(|\boldsymbol{\omega}|) = \mathbb{E}\left[e^{\jmath|\boldsymbol{\omega}| I_{agg}}\right] = \mathbb{E}\left[e^{\jmath|\boldsymbol{\omega}| \sum_{r_i \in \tilde{\Psi}_u} \sqrt{P_{u_i}} z_i r_i^{-b}}\right]. \tag{A.2}$$

Owing to the fact that P_{u_i} is a random variable with PDF given in (4.3), then,

$$\begin{aligned} \Phi_{I_{agg}}(|\boldsymbol{\omega}|) &= \mathbb{E}_{P_{u_i}, z_i, \tilde{\Psi}_u}\left[\prod_{i \in \tilde{\Psi}_u} e^{\jmath|\boldsymbol{\omega}| \sqrt{P_{u_i}} z_i r_i^{-b}}\right] \\ &\approx \exp\left\{-2\pi\lambda \int_t^{\infty} \mathbb{E}_{P_{u_i}, z_i}\left[1 - e^{\jmath|\boldsymbol{\omega}| \sqrt{P_{u_i}} z_i x_i^{-b}}\right] x \mathrm{d}x\right\}, \end{aligned} \tag{A.3}$$

where $t = \sqrt{(\frac{P_{u_i}}{\rho})^{\frac{1}{b}}}$. The approximation in (A.3) follows from approximating $\tilde{\Psi}_u$ (i.e., the set of interfering users) with a PPP and using the probability generating functional (PGFL) of the PPP [17], while the limits of the integral follow from the constraint on the received power at the intended BS, where $P_{u_i} r_i^{-\eta} < \rho$. Let $u = |\boldsymbol{\omega}| x^{-b}$, and $\hat{z}_i = \mathrm{Re}\{z_i\}$. Using properties of the SS random variable [140] where $\Phi_X(\boldsymbol{\omega}) = \Phi_{\mathrm{Re}\{X\}}(\boldsymbol{\omega})$ and $\Phi_X(\boldsymbol{\omega}) = \mathrm{Re}\{\Phi_X(\boldsymbol{\omega})\}$, we can write

$$\begin{aligned}
\Phi_{I_{agg}}(|\boldsymbol{\omega}|) &\approx \exp\left\{ \frac{-2\pi\lambda}{b}\, \mathbb{E}_{P_{u_i}} \left[\int_0^{|\boldsymbol{\omega}|\sqrt{\frac{\rho}{P_{u_i}}}} \mathbb{E}_{\hat{z}_i} \left[1 - \cos(\sqrt{P_{u_i}} \hat{z}_i u \right] u^{-1-\frac{2}{b}} \mathrm{d}u \right] \right\} \\
&\overset{(a)}{=} \exp\left\{ -\pi\lambda \left(\frac{P_{u_i}}{\rho}\right)^{\frac{1}{b}} \left[{}_1F_2\left(\frac{-1}{b}; \frac{1}{2}, 1 - \frac{1}{b}; \frac{-|\boldsymbol{\omega}|^2 \rho \hat{z}_i^2}{4} \right) - 1 \right] \right\} \\
&\overset{(b)}{=} \exp\left\{ \mathbb{E}_{P_{u_i}} \left[-\pi\lambda \left(\frac{P_{u_i}}{\rho}\right)^{\frac{1}{b}} \mathbb{E}_{\hat{z}_i} \left(\sum_{q=1}^{\infty} \tau_q \left[\frac{-|\boldsymbol{\omega}|^2 \rho \hat{z}_i^2}{4} \right]^q \right) \right] \right\} \\
&\overset{(c)}{=} \exp\left\{ \nu(\rho, \lambda) \left(\sum_{q=1}^{\infty} \mathbb{E}_{\hat{z}_i} \left[\hat{z}_i^{2q} \right] \tau_q \left[\frac{-|\boldsymbol{\omega}|^2 \rho}{4} \right]^q \right) \right\}, \qquad \text{(A.4)}
\end{aligned}$$

where $\nu(\rho, \lambda)$ is defined in (4.6) and τ_q in (4.7).

We use the following steps in arriving at (A.4), (a) follows from [141, equation 3.771.4], (b) results from the series representation of the generalized hypergeometric function ${}_1F_2(\cdot;\cdot,\cdot;\cdot)$ [112], while (c) follows from the independence of P_{u_i} and $\hat{z}_i$. It remains to compute $\mathbb{E}_{\hat{z}_i}\left[\hat{z}_i^{2q}\right]$. To do so, we derive the moments of the random variable $w = \cos^2(\varphi_i + \phi_i)$. We can show that, $\mathbb{E}_{\phi_i}[w^q] = \frac{\Gamma\left(q+\frac{1}{2}\right)}{\sqrt{\pi}\Gamma(q+1)}$. Consequently,

$$\begin{aligned}
\mathbb{E}_{\hat{z}_i}\left[\hat{z}_i^{2q}\right] &= \mathbb{E}\left[\alpha^{2q}\right] \mathbb{E}\left[|s|^{2q}\right] \mathbb{E}\left[w^q\right] \\
&= \Omega_i^q \sum_{\kappa=1}^{M} \frac{1}{M} \left|s^{(\kappa)}\right|^{2q} \frac{\Gamma\left(q+\frac{1}{2}\right)}{\sqrt{\pi}\Gamma\left(q+1\right)}. \qquad \text{(A.5)}
\end{aligned}$$

Substituting (A.5) in (A.4) completes the proof.

A.2 Proof of Lemma 4.2

Let $\zeta = \frac{\rho}{\mathcal{N}_o}\left[1+\sum_{q=1}^{\infty}\frac{\mathcal{B}_q\sigma_q^2}{\mathcal{N}_o}\right]^{-1}$. Then,

$$\begin{aligned} F_{\Upsilon}\left(\mathrm{y}\right) &= \mathbb{P}\left\{\zeta\alpha_o^2 < \mathrm{y}\right\} \overset{(d)}{=} \mathbb{E}_{\mathcal{B}_q}\left[1-e^{-\frac{\mathrm{y}}{\zeta\Omega_i}}\right] \\ &= \mathbb{E}_{\mathcal{B}_q}\left[1-e^{-\frac{y\mathcal{N}_o}{\rho\Omega_i}\left(1+\sum_{q=1}^{\infty}\frac{\mathcal{B}_q\sigma_q^2}{\mathcal{N}_o}\right)}\right] \\ &\overset{(e)}{=} 1-e^{-\frac{\mathrm{y}\mathcal{N}_o}{\Omega_i\rho}}\left(\prod_{q=1}^{\infty}e^{-\frac{\sigma_q^{2q}\mathrm{y}^q}{\Omega-i^q\rho^q}}\right) \\ &= 1-e^{-\frac{\mathrm{y}\mathcal{N}_o}{\Omega_i\rho}}\left[e^{-\sum_{q=1}^{\infty}\frac{\sigma_q^{2q}\mathrm{y}^q}{\Omega_i^q\rho^q}}\right], \end{aligned} \tag{A.6}$$

where (d) follows from the Rayleigh fading assumption and (e) from $\mathcal{M}_{\mathcal{B}_q}(s) = \exp\{s^q\}$. Let

$$\Delta(\mathrm{y}) = \sum_{q=1}^{\infty}\frac{\sigma_q^{2q}\mathrm{y}^q}{\Omega_i^q\rho^q}. \tag{A.7}$$

The SINR CDF expression then follows by substituting σ_q^2 from equation (4.7) in (A.7).

A.3 Proof of Theorem 4.1

The ASEP expression in (4.17) directly follows from (4.13) and the definition of $\mathcal{J}_{\Upsilon}(\mu,\beta)$. The integral $\mathcal{J}_{\Upsilon}(\mu,\beta)$ is computed as follows

$$\mathcal{J}_{\Upsilon}(\mu,\beta) = \int_o^{\mu}\frac{\beta}{\sin^2\vartheta}\int_o^{\infty}e^{\left(-\frac{\beta}{\sin^2\vartheta}\right)}F_{\Upsilon}(\mathrm{y})\mathrm{d}\mathrm{y}\mathrm{d}\vartheta. \tag{A.8}$$

By interchanging the two integrals, applying a change of variables to the integral $\int_o^{\mu} \frac{\beta}{\sin^2\vartheta} e^{\left(-\frac{\beta}{\sin^2\vartheta}\right)} \mathrm{d}\vartheta$ and making use of the integral

$$\int \frac{e^{-a\mathfrak{m}}}{\sqrt{\mathfrak{m}-1}} \mathrm{d}\mathfrak{m} = \frac{\sqrt{\pi} e^{-a} \mathrm{erf}(\sqrt{a(\mathfrak{m}-1)})}{\sqrt{a}}, \tag{A.9}$$

we get

$$\mathcal{J}_{\Upsilon}(\mu, \beta) = \mu - \int_o^{\infty} \beta \mathcal{Y}(\beta \mathrm{y}) \overline{F}_{\Upsilon}(\mathrm{y}) \mathrm{dy}, \tag{A.10}$$

where $\overline{F}_{\Upsilon}(\mathrm{y}) = 1 - F_{\Upsilon}(\mathrm{y})$ and $\mathcal{Y}(\beta \mathrm{y})$ is defined in (4.19). Direct substitution in (A.10) yields the result of Theorem 4.1.

A.4 Proof of Lemma 4.3

By following the same steps as Appendix A.1, and letting $z_{i,k} = s_{i,k} g_{i,k}$, where $z_{i,k}$ is a spherically symmetric (SS) random variable [36]. Then the inter-cell interference from tier k, I_k, is given by

$$I_k = \sum_{i \in \tilde{\Psi}_{u,k}} \sqrt{P_{u_i,k}} r_{i,k}^{-b} g_{i,k} s_{i,k} = \sum_{i \in \tilde{\Psi}_{u,k}} \sqrt{P_{u_i,k}} r_{i,k}^{-b} z_{i,k}, \tag{A.11}$$

which is also found to be an SS random variable. Next, similar to Appendix A.1, we need to derive the characteristic function of the CF of the inter-cell intereference as an SS random variable, which is expressed as

$$\Phi_{I_k}(|\boldsymbol{\omega}|) = \mathbb{E}\left[e^{\jmath|\boldsymbol{\omega}| I_k}\right] = \mathbb{E}\left[e^{\jmath|\boldsymbol{\omega}| \sum_{i \in \tilde{\Psi}_{u,k}} \sqrt{P_{u_i,k}} z_{i,k} r_{i,k}^{-b}}\right]. \tag{A.12}$$

Note that, the UE transmit power of a generic UE in the k^{th} tier, $P_{u_i,k}$, is a random variable with PDF given in (4.20), then,

$$\begin{aligned}\Phi_{I_k}(|\boldsymbol{\omega}|) = \mathbb{E}\left[\prod_{i\in\tilde{\Psi}_{u,k}} e^{\jmath|\boldsymbol{\omega}|\sqrt{P_{u_i,k}}z_{i,k}r_{i,k}^{-b}}\right] \\ \approx \exp\left\{-2\pi\lambda_k\int_t^{\infty}\mathbb{E}_{P_{u_i,k},z}\left[1-e^{\jmath|\boldsymbol{\omega}|\sqrt{P_{u_i,k}}zx^{-b}}\right]x\mathrm{d}x\right\},\end{aligned} \tag{A.13}$$

such that $t=\sqrt{(\frac{P_{u_i,k}}{\rho_k})^{\frac{1}{b}}}$. As shown in Appendix A.1, the set of interfering users, $\tilde{\Psi}_{u,k}$, is approximated by a PPP. The limits of the integral follow from the constraint on the received power at the intended BS in tier k, where $P_{u_i,k}r_k^{-\eta}<\rho_k$. By following the proof steps in Appendix A.1, we have

$$\begin{aligned}\Phi_{I_k}(|\boldsymbol{\omega}|) &\approx \exp\left\{\frac{-2\pi\lambda_k}{b}\,\mathbb{E}_{P_{u_i,k}}\left[\int_0^{|\boldsymbol{\omega}|\sqrt{\frac{\rho_k}{P_{u_i,k}}}}\mathbb{E}_{\hat{z}}\left[1-\cos(\sqrt{P_{u_i,k}}\hat{z}u)\right]u^{-1-\frac{2}{b}}\mathrm{d}u\right]\right\} \\ &= \exp\left\{-\pi\lambda_k\left(\frac{P_{u_i,k}}{\rho_k}\right)^{\frac{1}{b}}\left[{}_1F_2\left(\frac{-1}{b};\frac{1}{2},1-\frac{1}{b};\frac{-|\boldsymbol{\omega}|^2\rho_k\hat{z}^2}{4}\right)-1\right]\right\} \\ &= \exp\left\{\mathbb{E}_{P_{u_i,k}}\left[-\pi\lambda_k\left(\frac{P_{u_i,k}}{\rho_k}\right)^{\frac{1}{b}}\mathbb{E}_{\hat{z}}\left(\sum_{q=1}^{\infty}\tau_q\left[\frac{-|\boldsymbol{\omega}|^2\rho_k\hat{z}^2}{4}\right]^q\right)\right]\right\} \\ &= \exp\left\{-\nu(\rho_k,\lambda_k)\left(\sum_{q=1}^{\infty}\mathbb{E}_{\hat{z}}\left[\hat{z}^{2q}\right]\tau_q\left[\frac{-|\boldsymbol{\omega}|^2\rho_k}{4}\right]^q\right)\right\},\end{aligned} \tag{A.14}$$

where $\nu\left(\rho_k,\lambda_k\right)$ is defined in (4.23) and τ_q is given as in (4.7)

The moments of $\hat{z}$ are computed like in Appendix A.1, and accordingly,

$$\begin{aligned}\mathbb{E}_{\hat{z}}\left[\hat{z}^{2q}\right] &= \mathbb{E}\left[\alpha^{2q}\right]\mathbb{E}\left[|s|^{2q}\right]\mathbb{E}\left[w^q\right] \\ &= \Omega_k^q\sum_{\kappa=1}^{M}\frac{1}{M}\left|s^{(\kappa)}\right|^{2q}\frac{\Gamma\left(q+\frac{1}{2}\right)}{\sqrt{\pi}\Gamma\left(q+1\right)}.\end{aligned} \tag{A.15}$$

Then, the lemma is obtained by substituting (A.15) in (A.14).

A.5 Proof of Lemma 4.4

As shown in Appendix A.2, we derive the CDF of the SINR at the test UE in tier j. First, let $\zeta_j = \frac{\rho_j}{\mathcal{N}_o}\left[1+\sum_{k=1}^{K}\sum_{q=1}^{\infty}\frac{\mathcal{B}_{q,k}\sigma_{q,k}^2}{\mathcal{N}_o}\right]^{-1}$. Then,

$$\begin{aligned} F_{\Upsilon_j}(\mathrm{y}) &= \mathbb{P}\left\{\zeta_j\alpha_j^2 < \mathrm{y}\right\} = \mathbb{E}_{\mathcal{B}_{q,k}}\left[1-e^{-\frac{\mathrm{y}}{\zeta_j\Omega_j}}\right] \\ &= \mathbb{E}_{\mathcal{B}_{q,k}}\left[1-e^{-\frac{\mathrm{y}\mathcal{N}_o}{\rho_j\Omega_j}\left(1+\sum_{k=1}^{K}\sum_{q=1}^{\infty}\frac{\mathcal{B}_{q,k}\sigma_{q,k}^2}{\mathcal{N}_o}\right)}\right] \\ &= 1-e^{-\frac{\mathrm{y}\mathcal{N}_o}{\Omega_j\rho_j}}\left(\prod_{k=1}^{K}\prod_{q=1}^{\infty}e^{-\frac{\sigma_{q,k}^{2q}\mathrm{y}^q}{\Omega_k^q\rho_k^q}}\right) \\ &= 1-e^{-\frac{\mathrm{y}\mathcal{N}_o}{\Omega_j\rho_j}}\left[e^{-\sum_{k=1}^{K}\sum_{q=1}^{\infty}\frac{\sigma_{q,k}^{2q}\mathrm{y}^q}{\Omega_k^q\rho_k^q}}\right], \end{aligned} \tag{A.16}$$

We let $\Delta(\mathrm{y},k) = \sum_{q=1}^{\infty}\frac{\sigma_{q,k}^{2q}\mathrm{y}^q}{\Omega_k^q\rho_k^q}$, then SINR CDF expression then follows by substituting $\sigma_{q,k}^2$ from equation (4.25) in $\Delta(y,k)$ to conclude the proof.

A.6 Proof of Theorem 4.2

Theorem 4.2 is proved directly as in Appendix A.3, by substituting Υ with Υ_j, and therefore,

$$\mathcal{J}_{\Upsilon_j}(\mu,\beta) = \mu - \int_o^{\infty}\beta\mathcal{Y}(\beta\mathrm{y})\,\overline{F}_{\Upsilon_j}(\mathrm{y})\mathrm{dy}, \tag{A.17}$$

Direct substitution in (A.17) yields the result of Theorem 4.2.

Appendix B

B.1 Proof of Lemma 5.1

Conditioned on r_o, the LT of $\mathcal{I}_D$ is given by

$$\begin{aligned}\mathcal{L}_{\mathcal{I}_D|r_o}(z) &\overset{(a)}{=} \exp\left\{\frac{-2\pi\lambda_B}{\eta} r_o^2 \int_0^1 \left[1-\left(\frac{1}{1+z\Omega_i y}\right)^{m_i}\right] \frac{1}{y^{\frac{2}{\eta}+1}} \mathrm{d}y\right\} \\ &\overset{(b)}{=} \exp\left\{-\pi\lambda_B r_o^2 \left[{}_2F_1\left(\frac{-2}{\eta}, m_i; 1-\frac{2}{\eta}; -z\Omega_i\right)-1\right]\right\} \end{aligned} \tag{B.1}$$

where (a) follows from the gamma distribution of g_i with shape and scale parameters m_i and Ω_i, respectively, and (b) is obtained from a simple change of variables $y = x^{-\eta} r_o^{\eta}$ and evaluating the integral using [141].

B.2 Proof of Lemma 5.2

The LT of the uplink interference power is expressed as

$$\begin{aligned}\mathcal{L}_{\mathcal{I}_U}(z) &\overset{(c)}{\approx} \exp\left\{-2\pi\lambda_B \int_t^{\infty} \mathbb{E}_{P,g}\left[1-e^{-zP_{u_i}x^{-\eta}g}\right] x\mathrm{d}x\right\} \\ &\overset{(d)}{=} \exp\left\{-\nu\left(\rho,\lambda_B\right) \int_0^1 \left[1-\left(\frac{1}{1+z\Omega_i y}\right)^{m_i}\right] \frac{1}{y^{\frac{2}{\eta}+1}} \mathrm{d}y\right\} \end{aligned} \tag{B.2}$$

where the approximation of (c) follows from the PPP assumption of the active UEs, (d) follows by the independence of P_{u_i} and g_i, incorporating the LT of the gamma random variable g_i, and the change of variables $y = x^{-\eta}P$. Solving the integral as in

Appendix B.1 and substituting using (4.3) such that

$$\mathbb{E}\left[P^{\frac{2}{\eta}}\right] = \frac{1}{\pi\lambda_B} \frac{\rho^{\frac{2}{\eta}}\gamma\left(2, \pi\lambda_B\left(\frac{P_u}{\rho}\right)^{\frac{2}{\eta}}\right)}{1 - e^{-\pi\lambda_B\left(\frac{P_u}{\rho}\right)^{\frac{2}{\eta}}}} \tag{B.3}$$

from (4.4) (cf. [47]) completes the proof.

Appendix C

C.1 Proof of Theorem 6.1

The ASEP expression in (6.10) is obtained by taking the expectation over Υ and then using expressions from [114, eq. (11), (21)] as has been detailed in Chapter 5.
For the outage probability, conditioned on r_o, we have

$$\begin{aligned}\mathcal{O}_{\mathrm{DL}}\left(r_o,\theta\right) &= \mathbb{E}\left[\mathbb{P}\left(\tilde{g}_o < \frac{\theta\mathcal{I}}{Pr_o^{-\eta}}\right)\right] \\ &\overset{(e)}{=} \mathbb{E}\left[1-\sum_{j=0}^{m_o-1}\frac{1}{j!}\left(\frac{\theta\mathcal{I}}{Pr_o^{-\eta}}\right)^j \exp\left\{\frac{-\theta\mathcal{I}}{Pr_o^{-\eta}}\right\}\right], \end{aligned} \tag{C.1}$$

where (e) follows from the CDF of the gamma distribution. The expression of (6.11) is finally obtained using the rules of differentiation of the LT, together with averaging over the PDF of r_o.

The ergodic rate expression in (6.12) follows from [142, Lemma 1] which represents the ergodic capacity as

$$\mathbb{E}\left[\ln\left(1+\frac{Y}{X+C}\right)\right] = \int_0^\infty \frac{\mathcal{L}_X\left(z\right)-\mathcal{L}_{X,Y}\left(z\right)}{z}\exp\left(-zC\right)\mathrm{d}z \tag{C.2}$$

Now set $Y = Pr_o^{-\eta}\tilde{g}_o$, $X = \sum_{r_i\in\tilde{\Psi}^o} Pr_i^{-\eta}\tilde{g}_i$ in an interference-limited scenario ($C = \mathcal{N}_o = 0$), and exploit the independence between the useful and interfering signals, as well as incorporating the CDF of the gamma random variable, to obtain the ergodic capacity exprssion in (6.12).

C.2 Equivalent SISO model for different MIMO configurations

C.2.1 Proof of Lemma 6.2

In SIMO transmission, by applying MRC at the receiver side, for $\bar{\mathbf{w}}_o^T = \mathbf{h}_o^H$, the post-processed signal is written as

$$\begin{aligned}\tilde{y} &= \bar{\mathbf{w}}_o^T \mathbf{y} \\ &= \sqrt{P} r_o^{-\frac{\eta}{2}} \|\mathbf{h}_o\|^2 \, s_o + \sum_{r_i \in \tilde{\Psi}^o} \sqrt{P} r_i^{-\frac{\eta}{2}} \mathbf{h}_o^H \mathbf{h}_i \tilde{s}_i + \mathbf{h}_o^H \mathbf{n}. \end{aligned} \tag{C.3}$$

We start with computing the effective noise variance since a post-processor is applied. The noise power is expressed as

$$\mathrm{Var}_{\mathbf{n}} \left[\mathbf{h}_o^H \mathbf{n} \right] = \mathcal{N}_o \|\mathbf{h}_o\|^2. \tag{C.4}$$

Therefore, the random variable $\varepsilon = \|\mathbf{h}_o\|^2$, is used to normalize the resultant interference power. The effective interference variance conditioned on the network geometry and the intended channel gains with respect to $\tilde{s}_i$ is given by

$$\mathcal{I}_D = \frac{1}{\varepsilon} \mathrm{Var}_{\tilde{s}_i} \left[\sum_{r_i \in \tilde{\Psi}^o} \sqrt{P} r_i^{-\frac{\eta}{2}} \, \mathbf{h}_o^H \mathbf{h}_i \tilde{s}_i \right] = \sum_{r_i \in \tilde{\Psi}^o} P r_i^{-\eta} \frac{|\mathbf{h}_o^H \mathbf{h}_i|^2}{\|\mathbf{h}_o\|^2}. \tag{C.5}$$

By inspection of the interference variance, it is clear that $\left\{ \breve{\mathbf{H}} \right\} = \{\mathbf{H}_o\}$. Also, we notice that there exists only one coefficient $a_l^{(i)} = \frac{\mathbf{h}_o^H \mathbf{h}_i}{\|\mathbf{h}_o\|}$. Recall that the number of independent coefficients $a_{l,k}^{(i)}$ depends on the number of independent transmitted streams, which is equal to one in the SIMO case. Accordingly, $\tilde{g}_i = \left| a_l^{(i)} \right|^2 \sim \mathrm{Gamma}\left(m_i, 1\right)$, with $m_i = 1$. Similarly, conditioned on the intended and interfering channel gains,

the received signal power, with respect to the transmitted signal, can be shown to be

$$\mathcal{S} = \frac{1}{\varepsilon}\mathrm{Var}_{s_o}\left[\sqrt{P}r_o^{-\frac{\eta}{2}}\|\mathbf{h}_o\|^2 s_o\right] = Pr_o^{-\eta}\|\mathbf{h}_o\|^2. \tag{C.6}$$

Therefore, $\tilde{g}_o = \|\mathbf{h}_o\|^2 \sim \text{Gamma}\,(m_o, 1)$ where $m_o = N_r$.

C.2.2 Proof of Lemma 6.3

Employing OSTBC, the received vector at a typical user at time instant $\tau, N_t \leq \tau \leq T$, is given by

$$\mathbf{y}\,(\tau) = \sqrt{P}r_o^{-\frac{\eta}{2}}\mathbf{H}_o\mathbf{s} + \sum_{r_i \in \tilde{\Psi}^o} \sqrt{P}r_i^{-\frac{\eta}{2}}\mathbf{H}_i\tilde{\mathbf{s}}_i + \mathbf{n}\,(\tau)\,. \tag{C.7}$$

Let $\boldsymbol{\mathcal{Y}}$ be the stacked vector of received symbols over T intervals, and let $L = N_t$, such that,

$$\boldsymbol{\mathcal{Y}} = \sqrt{P}r_o^{-\frac{\eta}{2}}\mathbf{H}_{\text{eff}}\,\mathbf{s} + \mathbf{i}_{\text{agg}} + \mathbf{n}. \tag{C.8}$$

where $\boldsymbol{\mathcal{Y}} \in \mathbb{C}^{T\cdot N_r \times 1}$, and $\mathbf{i}_{\text{agg}}$ is the concatinated aggregate interference $T\cdot N_r \times 1$ vector. The effective channel matrix $\mathbf{H}_{\text{eff}} \in \mathbb{C}^{T\cdot N_r \times N_t}$ is expressed as a linear combination of the set of dispersion matrices $\mathcal{A}$ and $\mathcal{B}$ chosen according to the adopted orthogonal space-time code as follows [8, 143],

$$\mathbf{H}_{\text{eff}} = \sum_{j=1}^{N_r}\sum_{\mathfrak{q}=1}^{N_t} \alpha_{j\mathfrak{q}}\mathcal{A}_{j\mathfrak{q}} + \jmath\beta_{j\mathfrak{q}}\mathcal{B}_{j\mathfrak{q}}, \tag{C.9}$$

where $h_{j\mathfrak{q}} = \alpha_{j\mathfrak{q}} + \jmath\beta_{j\mathfrak{q}}$. Moreover, $\mathbf{H}_{\text{eff}}^H\mathbf{H}_{\text{eff}} = \|\mathbf{H}_o\|_{\text{F}}^2\mathbf{I}$ where $\|\mathbf{H}_o\|_{\text{F}}^2 = \sum_{j=1}^{N_r}\sum_{\mathfrak{q}=1}^{N_t}|h_{j\mathfrak{q}}|^2$ is the squared Frobenius norm of the intended channel matrix. Hence, $\|\mathbf{H}_o\|_{\text{F}}^2 \sim$

$\frac{1}{2}\chi^2\left(2N_sN_r\right)$ [144]. Moreover, the aggregate interfering signals are expressed as

$$\mathbf{i}_{\text{agg}} = \sum_{r_i \in \tilde{\Psi}^o} \sqrt{P} r_i^{-\frac{\eta}{2}} \mathbf{H}_{i,\text{eff}}\, \tilde{\mathbf{s}}_i, \tag{C.10}$$

such that $\mathbf{H}_{i,\text{eff}}$ is defined similar to (C.9). For detection, we equalize the effective channel matrix at the receiver side by $\mathbf{W}_o$. Hence, the received vector $\tilde{\boldsymbol{\mathcal{Y}}}$ is written as

$$\begin{aligned}\tilde{\boldsymbol{\mathcal{Y}}} &= \mathbf{W}_o \boldsymbol{\mathcal{Y}} \\ &= \sqrt{P} r_o^{-\frac{\eta}{2}} \|\mathbf{H}_o\|_{\text{F}}\, \mathbf{s} + \sum_{r_i \in \tilde{\Psi}^o} \sqrt{P} r_i^{-\frac{\eta}{2}} \mathbf{A}_i \tilde{\mathbf{s}}_i + \mathbf{w},\end{aligned} \tag{C.11}$$

such that $\mathbf{w} = \mathbf{W}_o\mathbf{n}$ and $\mathbf{A}_i = \mathbf{W}_o\mathbf{H}_{i,\text{eff}}$ with elements $a_{l,k}^{(i)}$ as defined in (6.2). Without loss of generality, let us consider the detection of the l^{th} arbitrary symbol from the received vector $\tilde{\boldsymbol{\mathcal{Y}}}$. Due to the adopted Gaussian signaling scheme, we lump interfernce with noise, and thus it is essential to obtain the interference variance. First, let us define $\boldsymbol{q}_k$ as the k^{th} column of the matrix $\mathbf{H}_{\text{eff}}$, similarly, $\boldsymbol{q}_{i,k}$ is the k^{th} column of the matrix $\mathbf{H}_{i,\text{eff}}$. Then, the received interference variance for the l^{th} symbol denoted as $\mathcal{I}_l$, computed with respect to the interfering symbols $\tilde{\mathbf{s}}_i$ can be derived as

$$\mathcal{I}_l = \text{Var}_{\tilde{\mathbf{s}}_i}\left[\sum_{r_i \in \tilde{\Psi}^o} \sum_{k=1}^{N_s} \sqrt{P} r_i^{-\frac{\eta}{2}} \frac{\boldsymbol{q}_l^H \boldsymbol{q}_{i,k}}{\|\mathbf{H}_o\|_{\mathbf{F}}} s_{i,k}\right] = \sum_{r_i \in \tilde{\Psi}^o} \sum_{k=1}^{N_s} P r_i^{-\eta} \frac{\left|\boldsymbol{q}_l^H \boldsymbol{q}_{i,k}\right|^2}{\|\mathbf{H}_o\|_{\mathbf{F}}^2}, \tag{C.12}$$

where the summation is over the N_s active antennas per transmission. Note that, conditioned on $\left\{\breve{\mathbf{H}}\right\} = \{\mathbf{H}_o\}$, $a_{l,k}^{(i)} = \frac{\boldsymbol{q}_l^H \boldsymbol{q}_{i,k}}{\|\mathbf{H}_o\|_{\mathbf{F}}}$ is a normalized and independently weighted sum of complex Gaussian random variables, thus $a_{l,k}^{(i)} \sim \mathcal{CN}\left(0,1\right)$. Although a post-processor is applied, the noise power is maintained to be $\mathcal{N}_o$. Thus, $\tilde{g}_i \sim (m_i, \Omega_i)$

with $m_i = N_s$ and $\Omega_i = 1$. Similarly, the received signal power is found to be

$$\mathcal{S} = \mathrm{Var}_{\mathbf{s}}\left[\sqrt{P} r_o^{-\frac{\eta}{2}} \|\mathbf{H}_o\|_{\mathrm{F}}\right] = P r_o^{-\eta} \|\mathbf{H}_o\|_{\mathrm{F}}^2, \tag{C.13}$$

where $\tilde{g}_o \sim \mathrm{Gamma}\left(m_o, \Omega_o\right)$ with $m_o = N_s N_r$ and $\Omega_o = 1$.

C.2.3 Proof of Lemma 6.4

Applying a ZF-Rx, without loss of generality, we focus on the detection of an arbitrary symbol l from the received vector $\tilde{\mathbf{y}} = \mathbf{W}_o \mathbf{y}$, given by

$$\tilde{y}_l = \sqrt{P} r_o^{-\frac{\eta}{2}} \, s_l + \sum_{r_i \in \tilde{\Psi}^o} \sqrt{P} r_i^{-\frac{\eta}{2}} \bar{\mathbf{w}}_{o,l}^T \mathbf{H}_i \tilde{\mathbf{s}}_i + \bar{\mathbf{w}}_{o,l}^T \mathbf{n}, \tag{C.14}$$

which is similar to (6.2). First we need to to obtain the received noise variance since a post-processing matrix is applied and thus the noise variance is scaled. Conditioned on $\mathbf{H}_o$, the received noise power is defined as

$$\begin{aligned} \mathrm{Var}_{\mathbf{n}}\left[\bar{\mathbf{w}}_{o,l}^T \mathbf{n}\right] &= \bar{\mathbf{w}}_{o,l}^T \mathbb{E}\left[\mathbf{n}\mathbf{n}^H\right] \bar{\mathbf{w}}_{o,l}^* \\ &= \mathcal{N}_o \left(\mathbf{W}_o \mathbf{W}_o^H\right)_{ll} \\ &= \mathcal{N}_o \left(\mathbf{H}_o \mathbf{H}_o^H\right)_{ll}^{-1}. \end{aligned} \tag{C.15}$$

Then, the scaling random variable is $\varepsilon = \left(\mathbf{H}_o \mathbf{H}_o^H\right)_{ll}^{-1}$. Next, we obtain the effective interference variance from the l^{th} received symbol as

$$\begin{aligned}\mathcal{I}_l &= \frac{1}{\varepsilon}\mathrm{Var}_{\tilde{\mathbf{s}}_i}\left[\sum_{r_i\in\tilde{\Psi}^o}\sqrt{P}r_i^{-\frac{\eta}{2}}\bar{\mathbf{w}}_{o,l}^T\mathbf{H}_i\tilde{\mathbf{s}}_i\right]\\ &= \frac{1}{\varepsilon}\sum_{r_i\in\tilde{\Psi}^o}Pr_i^{-\eta}\left(\mathbf{W}_o\mathbf{W}_o^H\right)_{ll}\left(\mathbf{H}_i\mathbf{H}_i^H\right)_{ll}\\ &= \sum_{r_i\in\tilde{\Psi}^o}Pr_i^{-\eta}\left(\mathbf{H}_i\mathbf{H}_i^H\right)_{ll}. \end{aligned} \tag{C.16}$$

In this case, the processing resulting interference channel set $\left\{\breve{\mathbf{H}}\right\} = \emptyset$. Therefore, $a_{l,k}^{(i)} = \left(\mathbf{H}_i\mathbf{H}_i^H\right)_{ll}$ and $\tilde{g}_i \sim (m_i, \Omega_i)$, with $m_i = N_t$ and $\Omega_i = 1$. The received signal power is similarly computed as

$$\mathcal{S} = \frac{1}{\varepsilon}\mathrm{Var}_{\mathbf{s}}\left[\sqrt{P}r_o^{-\frac{\eta}{2}}s_l\right] = \frac{Pr_o^{-\eta}}{\left(\mathbf{H}_o\mathbf{H}_o^H\right)_{ll}^{-1}}. \tag{C.17}$$

Since $g_w = \left(\mathbf{H}_o\mathbf{H}_o^H\right)_{ll}^{-1} \sim \text{Inv-Gamma}\left(N_r - N_t + 1, 1\right)$ [144]. Then, we can let $\frac{1}{g_w} = \tilde{g}_o \sim \text{Gamma}\left(m_o, \Omega_o\right)$, where $m_o = N_r - N_t + 1$ and $\Omega_o = 1$.

C.2.4 Proof of Lemma 6.5

In a multi-user MIMO setting, we introduce a slight abuse of notation for the intended and interfering channel matrices such that they are of dimensions $\mathcal{K}\times N_t$. The received interference power at user l where $1 \le l \le \mathcal{K}$, averaged over the interfering symbols $\tilde{\boldsymbol{s}}_{\boldsymbol{i}}$ is given by

$$\mathcal{I}_l = \mathrm{Var}_{\tilde{\boldsymbol{s}}_{\boldsymbol{i}}}\left[\sum_{r_i\in\tilde{\Psi}^o}\sqrt{P}r_i^{-\frac{\eta}{2}}\mathbf{h}_{i,l}\mathbf{V}_i\tilde{\boldsymbol{s}}_{\boldsymbol{i}}\right] = \sum_{r_i\in\tilde{\Psi}^o}Pr_i^{-\eta}\|\mathbf{h}_{i,l}\mathbf{V}_i\|^2, \tag{C.18}$$

where $\mathbf{h}_{i,l}$ is the l^{th} row of $\mathbf{H}_i$ and $\left\{\breve{\mathbf{H}}\right\} = \{\mathbf{V}_i\}$. Also, $\|\mathbf{h}_{i,l}\mathbf{V}_i\|^2 = \sum_{l=1}^{\mathcal{K}}|a_{l,k}^{(i)}|^2$. However, the column vectors of $\mathbf{V}_i$ are *not* independent. Therefore, conditioned on $\mathbf{v}_{i,l}$, the linear combination $\sum_{l=1}^{\mathcal{K}}\left|a_{l,k}^{(i)}\right|^2$ does not follow a Gamma distribution. Neverthe-

less, for tractability we *approximate* this summation by a Gamma distribution. Thus, $\tilde{g}_i \sim \text{Gamma}\,(m_i, \Omega_i)$, where $m_i = \mathcal{K}$ and $\Omega_i = 1$ by assuming such independence. This renders the aggregate interference power distribution at user l an *approximation*. Similarly, the useful signal power at user l is straightforward to be obtained, after appropriate diagonalization, as $\mathcal{S} = \frac{1}{\|\mathbf{v}_l\|^2} \sim \text{Gamma}\,(m_o, \Omega_o)$, with $m_o = N_t - \mathcal{K} + 1$ and $\Omega_o = 1$ [6]. This can also be interpreted as having the precoding matrix nulling out $\mathcal{K} - 1$ directions out of the N_t subspace at the transmitter side.

C.2.5 Proof of Lemma 6.6

Since, there are N_t distinct multiplexed symbols to be transmitted, we will study the pairwise error probability (PEP) of two distinct transmitted codewords, denoted as $\text{PEP} = \mathbb{P}\left\{\tilde{\mathbf{s}} = \mathbf{s}_1 | \mathbf{s}_o\right\}$. For ease of notaion, let $\delta = \sqrt{P} r_o^{-\frac{\eta}{2}}$. Therefore,

$$\|\mathbf{y} - \delta \mathbf{H}_o \mathbf{s}_o\|^2 \underset{\mathbf{s}_o}{\overset{\mathbf{s}_1}{\gtrless}} \|\mathbf{y} - \delta \mathbf{H}_o \mathbf{s}_1\|^2. \tag{C.19}$$

Using some mathematical manipulations, and assuming $\mathbf{s}_o$ was the actual transmitted symbols, it can be shown that

$$\text{PEP}\,(\mathbf{e}) = \mathbb{P}\left\{ \left[\mathbf{I}_{\text{agg}}^{\text{H}} + \mathbf{n}^{\text{H}}\right] \mathbf{H}_{\text{o}} \mathbf{e} + \mathbf{e}^{\text{H}} \mathbf{H}_{\text{o}}^{\text{H}} \left[\mathbf{I}_{\text{agg}} + \mathbf{n}\right] > \delta \mathbf{e}^{\text{H}} \mathbf{H}_{\text{o}}^{\text{H}} \mathbf{H}_{\text{o}} \mathbf{e} \right\}, \tag{C.20}$$

where $\mathbf{I}_{\text{agg}} = \sum_{r_i \in \tilde{\Psi}^o} I_i$. Conditioned on the channel matrices $\mathbf{H}_o$ and $\mathbf{H}_i$, and considering the Gaussian signaling approximation, the L.H.S of the above inequality represents the interference-plus-noise power and is a Gaussian random variable, denoted as $\mathcal{V}$ with zero-mean and variance $\sigma_{\mathcal{V}}^2$, thus, $\text{PEP}\,(\mathbf{e}) = \frac{1}{2}\text{erfc}\left(\frac{\delta\, \mathbf{e}^{\text{H}} \mathbf{H}_{\text{o}}^{\text{H}} \mathbf{H}_{\text{o}} \mathbf{e}}{\sqrt{2\sigma_{\mathcal{V}}^2}}\right)$, where the variance $\sigma_{\mathcal{V}}^2$ is given by

$$\sigma_{\mathcal{V}}^2 = 2\left[\, \mathbf{e}^H \mathbf{H}_o^H \mathbf{H}_o \mathbf{e}\right] \left(\mathcal{N}_o + \sum_{r_i \in \tilde{\Psi}^o} P r_i^{-\eta} \sum_{k=1}^{N_t} \frac{\left| \left(\mathbf{H}_o \mathbf{e}\right)^H \mathbf{h}_{i,k} \right|^2}{\|\mathbf{H}_o \mathbf{e}\|_2^2} \right). \tag{C.21}$$

By following the same convention used in this thesis, it is clear that the interference power is represented as

$$\mathcal{I}_D = \sum_{r_i \in \tilde{\Psi}^o} P r_i^{-\eta} \sum_{k=1}^{N_t} \frac{|\left(\mathbf{H}_o \mathbf{e}\right)^H \mathbf{h}_{i,k}|^2}{\|\mathbf{H}_o \mathbf{e}\|^2}, \tag{C.22}$$

and thus we see that $\left\{\breve{\mathbf{H}}\right\} = \{\mathbf{H}_o\}$ and $a_{l,k}^{(i)} = \frac{(\mathbf{H}_o \mathbf{e})^H \mathbf{h}_{i,k}}{\|\mathbf{H}_o \mathbf{e}\|}$. Conditioned on $\mathbf{H}_o$, $\tilde{g}_i \sim \text{Gamma}\left(N_t, 1\right)$. Furthermore, let $\mathcal{S} = \mathbf{e}^H \mathbf{H}_o^H \mathbf{H}_o \mathbf{e} \overset{d}{=} \|\mathbf{e}\|^2 \left(\mathbf{H}_o^H \mathbf{H}_o\right)_{ll}$, hence it is starightforward to see that $\left(\mathbf{H}_o^H \mathbf{H}_o\right)_{ll}$ has a $\chi^2\left(N_r\right)$ distribution. Thus, $\tilde{g}_o = \left(\mathbf{H}_o^H \mathbf{H}_o\right)_{ll} \sim \text{Gamma}\left(m_o, \Omega_o\right)$, with $m_o = N_r$ and $\Omega_o = 1$. Then, the conditional pairwise error probability is expressed by

$$\text{PEP}\left(\mathbf{e}\right) = \frac{1}{2}\text{erfc}\left(\sqrt{\frac{P r_o^{-\eta} \|\mathbf{e}\|^2 \tilde{g}_o}{4\ \left(\mathcal{N}_o + \sum_{r_i \in \tilde{\Psi}^o} P r_i^{-\eta} \tilde{g}_i\right)}}\right). \tag{C.23}$$

Appendix D

D.1 Proof of Theorem 8.1

The joint CCDF of $\bar{\Upsilon}^{(1)}$ and $\bar{\Upsilon}^{(2)}$ is given by

$$\begin{aligned}
\mathbb{P}\left(\bar{\Upsilon}^{(1)}>\theta,\bar{\Upsilon}^{(2)}>\theta\right) &= \mathbb{E}\left[\mathbb{P}\left(\tilde{g}_o^{(1)}>\frac{\theta\mathcal{I}^{(1)}}{Pr_o^{-\eta}},\ \ \tilde{g}_o^{(2)}>\frac{\theta\mathcal{I}^{(2)}}{Pr_o^{-\eta}}\right)\right] \\
&\overset{(i)}{=} \mathbb{E}\left[\sum_{j_1=0}^{m_{o,1}-1}\sum_{j_2=0}^{m_{o,2}-1}\frac{1}{j_1!j_2!}\left(\frac{-\theta}{Pr_o^{-\eta}}\right)^{j_1+j_2}\left(\left(\mathcal{I}^{(1)}\right)^{j_1}\left(\mathcal{I}^{(2)}\right)^{j_2}\right)\exp\left\{\frac{-\theta\left(\mathcal{I}^{(1)}+\mathcal{I}^{(2)}\right)}{Pr_o^{-\eta}}\right\}\right] \\
&\overset{(ii)}{=} \mathbb{E}\left[\sum_{j_1=0}^{m_{o,1}-1}\sum_{j_2=0}^{m_{o,2}-1}\frac{1}{j_1!j_2!}\left(\frac{-\theta}{Pr_o^{-\eta}}\right)^{j_1+j_2}\frac{\partial^{(j_1+j_2)}}{\partial z_1^{j_1}\partial z_2^{j_2}}\mathcal{L}_{\mathcal{I}^{(1)},\mathcal{I}^{(2)}|r_o}\left(z_1,z_2\right)\Big|_{z_1=z_2=\frac{\theta}{Pr_o^{-\eta}}}\right],
\end{aligned} \tag{D.1}$$

such that (i) follows from the independence of $\tilde{g}_o^{(1)}$ and $\tilde{g}_o^{(2)}$ along with the CCDF of their Gamma distributions. (ii) is obtained by utilizing the LT identity $t_1^a t_2^b f(t_1,t_2) \Leftrightarrow \frac{\partial^{(a+b)}}{\partial z_1^a \partial z_2^b}\mathcal{L}_{t_1,t_2}(z_1,z_2)$, which can be proved as follows. First, we write the joint Laplace Transform of two variables t_1 and t_2 as

$$\mathcal{L}_{t_1,t_2}\left(z_1,z_2\right) = \int_0^\infty\int_0^\infty f(t_1,t_2)e^{-z_1t_1}e^{-z_2t_2}\mathrm{d}t_1\mathrm{d}t_2, \tag{D.2}$$

then,

$$\begin{aligned}
\frac{\partial^{j_1+j_2}\mathcal{L}_{t_1,t_2}\left(z_1,z_2\right)}{\partial z_1^{j_1}\partial z_2^{j_2}} &= \frac{\partial^{j_1+j_2}}{\partial z_1^{j_1}\partial z_2^{j_2}}\int_0^\infty\int_0^\infty f(t_1,t_2)e^{-z_1t_1}e^{-z_2t_2}\mathrm{d}t_1\mathrm{d}t_2 \\
&= \int_0^\infty\int_0^\infty(-1)^{j_1+j_2}\left(t_1\right)^{j_1}\left(t_2\right)^{j_2}f(t_1,t_2)e^{-z_1t_1}e^{-z_2t_2}\mathrm{d}t_1\mathrm{d}t_2,
\end{aligned} \tag{D.3}$$

where the second equality follows by Leibniz rule and applying the rules of partial differentiation, which proves the identity.

Appendix E

E.1 Proof of Lemma 9.1

Since the number of points in disjoint regions are independent, the conditional CDF for the distance to the n^{th} neighboring BS can be written as

$$\mathbb{P}\left\{\|x_n\| < r|\ r_o\right\} = 1 - \sum_{j=0}^{\mathrm{n}-1} \frac{\pi\lambda\left(\mathrm{x}_n^2 - r_o^2\right)^j e^{-\pi\lambda(\mathrm{x}_n^2 - r_o^2)}}{j!}. \tag{E.1}$$

By differentiating (E.1), the conditional PDF is given by

$$f_{\|x_\mathrm{n}\|\big|\, r_o}\left(\mathrm{x}_n|\ r_o\right) = 2\pi\lambda\,\mathrm{x}_n\, e^{-\pi\lambda\,(\mathrm{x}_n^2 - r_o^2)} \left(\sum_{j=0}^{\mathrm{n}-1} \frac{\pi\lambda(\mathrm{x}_n^2 - r_o^2)^j}{j!} - 1_{\{\mathrm{n}>2\}} \sum_{j=0}^{\mathrm{n}-2} \frac{\pi\lambda(\mathrm{x}_n^2 - r_o^2)^j}{j!}\right) \tag{E.2}$$

which can be further simplified to the form of (9.2). Then, multiplying (9.2) by the PDF of r_o, the joint PDF of $\|x_n\|$ and r_o is given as in (9.3).

E.2 Proof of Lemma 9.2

Let $\mathrm{n}=\Delta-1$. Since the distance of the interferers $\|x_i\|>\|x_{\mathrm{n}}\|$, then the LT of the residual conditional interference is obtained from

$$\begin{aligned}
\mathcal{L}_{\hat{\mathcal{I}}_D\left|x_n,r_o\right.}(z) &= \mathbb{E}\left[\prod_{r_i\in\Psi^o\setminus\mathcal{D}_\Delta} e^{-zPr_i^{-\eta}g_i}\right] \\
&\overset{(a)}{=} \exp\left\{-2\pi\frac{\lambda}{\Delta}\int_{\|x_{\mathrm{n}}\|}^{\infty}\mathbb{E}\left[1-e^{-zPr_i^{-\eta}g_i}\right]x\mathrm{d}x\right\} \\
&\overset{(b)}{=} \exp\left\{\frac{-2\pi\lambda}{\Delta\eta}x_{\mathrm{n}}^2\int_0^1\left[1-\left(\frac{1}{1+zP\Omega_i y x_{\mathrm{n}}^{-\eta}}\right)^{m_i}\right]\frac{1}{y^{\frac{2}{\eta}+1}}\mathrm{d}y\right\} \\
&\overset{(c)}{=} \exp\left\{-\pi\frac{\lambda}{\Delta}\|x_{\mathrm{n}}\|^2\left[{}_2F_1\left(\frac{-2}{\eta},m_i;1-\frac{2}{\eta};\frac{-zP\Omega_i}{x_{\mathrm{n}}^{\eta}}\right)-1\right]\right\} \\
&\overset{(\eta=4,m_i=1,\Omega_i=1)}{=} \exp\left\{-\pi\frac{\lambda}{\Delta}r_o^2\sqrt{zP}\arctan\left(\frac{\sqrt{zP}}{x_{\mathrm{n}}^2}\right)\right\}
\end{aligned} \tag{E.3}$$

where (a) is obtained by utilizing the PGFL of the interfering BSs that are *approximated* by a PPP [17], (b) follows from the MGF of the gamma distribution of g_i with parameters m_i,Ω_i, along with a simple change of variables $y=\frac{\|x_{\mathrm{n}}\|^\eta}{x^\eta}$ and (c) is obtained by solving the integral using [141] where ${}_2F_1(\mathrm{a},\mathrm{b};\mathrm{c};z)=\sum_{q=0}^{\infty}\frac{(\mathrm{a})_k(\mathrm{b})_k}{(\mathrm{c})_k k!}z^k$ is the Gauss hypergeometric function [112]. Then, we average over the conditional distribution of $\|x_n\|$ given r_o, and apply the change of variables $r=\frac{\|x_n\|}{r_o}$ to get (9.4).

Appendix F

F.1 Journal Publications

1. Laila Hesham Afify, H. ElSawy, T. Y. Al-Naffouri and M.–S. Alouini, "Insights into the Effect of Uplink Power Control on Retransmissions Performance," submitted to IEEE Communications Letters.

2. Laila Hesham Afify, H. ElSawy, T. Y. Al-Naffouri and M.–S. Alouini, "Unified Stochastic Geometry Model for MIMO Cellular Networks with Retransmissions," IEEE Transactions on Wireless Communications, vol. 15, no. 12, pp. 8595–8608. Dec. 2016.

3. Laila Hesham Afify, H. ElSawy, T. Y. Al-Naffouri and M.–S. Alouini, "The Influence of Gaussian Signaling Approximation on Error Performance in Cellular Networks," IEEE Communications Letters, vol. 19, pp. 2202–2205, Dec. 2015.

4. Laila Hesham Afify, H. ElSawy, T. Y. Al-Naffouri and M.–S. Alouini, "Per-link performance of Uplink MIMO Cellular Networks using Stochastic Geometry," in preparation.

5. Laila Hesham Afify, H. ElSawy, T. Y. Al-Naffouri and M.–S. Alouini, "Impact of Imperfect Channel State Information on the Performance of MIMO Uplink Cellular Networks: Stochastic Geometry Approach," in preparation.

6. M. Masood, **Laila Hesham Afify** and T. Y. Al-Naffouri, "Efficient Coordinated Recovery of Sparse Channels in Massive MIMO," in IEEE Transactions on Signal Processing, vol. 63, no. 1, pp. 104-118, Jan.1, 2015.

F.2 Conference Publications

1. Laila Hesham Afify, H. ElSawy, T. Y. Al-Naffouri and M.–S. Alouini, "Unified Tractable Model for Downlink MIMO Cellular Networks using Stochastic Geometry," IEEE International Conference on Communications (ICC), May 2016.

2. Laila Hesham Afify, H. ElSawy, T. Y. Al-Naffouri and M.–S. Alouini, "Error performance analysis in K-tier uplink cellular networks using a stochastic geometric approach," Proc. of the IEEE ICC 4th International Workshop on Small Cell and 5G Networks (SmallNets), London, UK, June, 2016. **(Best Paper Award)**

3. Laila Hesham Afify, H. ElSawy, T. Y. Al-Naffouri and M.–S. Alouini, "Error performance analysis in downlink cellular networks with interference management", IEEE 13th International Symposium on Modeling and Optimization in Mobile, Ad Hoc, and Wireless Networks (WiOpt), pp. 591-596, Mumbai, May 2015

4. M. Masood, **Laila Hesham Afify** and T. Y. Al-Naffouri, "Efficient collaborative sparse channel estimation in massive MIMO," 2015 IEEE International Conference on Acoustics, Speech and Signal Processing (ICASSP), South Brisbane, QLD, 2015, pp. 2924-2928.